UNIVERSITÀ POLITECNICA DELLE MARCHE

FACOLTÀ DI INGEGNERIA

Corso di Laurea Magistrale in Ingegneria Civile

Interpretation of dynamic characterization tests performed during the final proof test of bridges

L'interpretazione di prove di caratterizzazione dinamica eseguite nelle fasi di collaudo dei ponti

Relatore:

Dott. Ing. Sandro Carbonari

Tesi di Laurea di:

Stefano Orselli

Correlatore:

Prof. Ing. Fabrizio Gara

Anno accademico 2019/2020

Summary

Sommario

Il collaudo di una struttura è l'insieme delle operazioni necessarie per verificarne il corretto funzionamento prima della sua messa in esercizio. È un'operazione essenziale nella realizzazione di una costruzione perché il suo superamento attesta che le prestazioni sono e saranno conformi a quelle previste in fase di progettazione.

Con riferimento ai ponti, è obbligatorio eseguire una prova di carico statica (legge n.1086 / 71), le cui direttive per l'esecuzione sono riportate nella Sezione 9 delle Nuove Norme Tecniche per le Costruzioni (NTC 2018), mentre le prove dinamiche sono obbligatorie solo per ponti stradali e ferroviari di significativa importanza. In particolare, il periodo fondamentale determinato sperimentalmente deve essere confrontabile con quello previsto in fase di progettazione.

Tuttavia, in territorio ad alto rischio sismico come quello italiano, il comportamento dinamico di una costruzione acquista notevole rilevanza e i test dinamici, il cui scopo è quello di identificare i parametri dinamici di una struttura, stanno prendendo campo nelle opere civili, specialmente con riferimento ai ponti.

La caratterizzazione dinamica delle costruzioni, fornisce al progettista uno strumento di controllo dei metodi e degli strumenti di progetto; il confronto tra i parametri modali identificati e quelli del modello numerico fornisce infatti una utile informazione circa l'attendibilità di quest'ultimo, incluse le ipotesi semplificative adottate. Se i risultati attesi provenienti dal modello numerico sono congrui ai parametri effettivi, allora il modello è efficiente e ben calibrato. In caso contrario, una discrepanza potrebbe portare il progettista a concludere che la struttura è più deformabile di quanto aveva previsto in fase di progettazione, il che, nel caso dei ponti, potrebbe pregiudicare l'esito della prova di collaudo dinamica.

Quando i test dinamici devono essere eseguiti su un ponte, l'Operative Modal Analysis (OMA) è una soluzione veloce, economica ed efficiente perché la caratterizzazione dinamica è basata sulla risposta alle vibrazioni ambientali, a cui una struttura è sempre soggetta. Questa prova si presta spesso per essere eseguita anche su costruzioni che richiedono un elevato livello di energia per innescare l'oscillazione e che sarebbe impossibile eccitare con mezzi artificiali. Per ottenere test affidabili, sono necessarie una

serie di competenze e abilità ingegneristiche durante la loro pianificazione, esecuzione e successiva analisi e interpretazione dei dati.

Per dare coerenza ai risultati e garantire la validità del modello, sempre più frequentemente queste prove dinamiche sono eseguite in occorrenza del collaudo statico e della relativa prova di carico. Le prove dinamiche in genere sono eseguite nella giornata del collaudo statico sia sul ponte scarico che sul ponte carico. Le prove sul ponte carico in genere offrono la possibilità di valutare la dinamica della struttura soggetta ad una differente distribuzione (nota) di massa rispetta a quella che compete ai carichi permanenti.

I carichi sono solitamente costituiti da autocarri pesanti distribuiti su una o più file sia longitudinalmente che trasversalmente rispetto alla campata del ponte. Il loro peso può arrivare fino a 50 tonnellate e può modificare in modo significativo il comportamento dinamico del ponte.

Nel modello numerico, i camion utilizzati per le prove statiche sono generalmente modellati soltanto in termini di masse aggiunte sul ponte. Questo metodo non considera che il sistema dinamico costituito dal camion, gli ammortizzatori e gli pneumatici, interagendo con il sistema dinamico costituito dal ponte, ne possa cambiare anche significativamente la risposta modale, in altre parole si trascura il fatto che la massa dei camion agisce per il tramite di un sistema cedevole. Non tenere conto dell'interazione camion-ponte, e dei relativi effetti sulle frequenze di vibrazione, potrebbe portare ad un'errata interpretazione dell'esito del test dinamico, e conseguentemente dell'esito del collaudo.

Nell'ambito di questa tesi, si è dapprima indagata l'effettiva importanza dei fenomeni di interazione camion-ponte, attraverso una adeguata modellazione della struttura e degli autocarri, e successivamente si è studiato il problema in termini parametrici concentrandosi sugli effetti della suddetta interazione sulla prime frequenze flessionali dell'impalcato.

All'inizio lo studio si è limitato a modelli analitici semplici, in cui il ponte e il camion erano ridotti entrambi ad un sistema 1DOF. Spinti dalle osservazioni fatte su questi modelli semplificati, è stata eseguita una modellazione agli elementi finiti di un ponte su cui sono presenti gli autocarri.

Il modello a “masse aggiunte” è costituito da una molla, la cui rigidezza simula quella del ponte, e da una massa, il cui valore è la somma delle masse del ponte e dell'autocarro.

Il modello più semplice, attraverso il quale sono stati indagati qualitativamente i fenomeni, è un modello 2DOF in cui due molle in serie descrivono il ponte ed il camion, ognuno con la propria massa e rigidezza. L'analisi modale, condotta su entrambi i sistemi (1DOF e 2DOF), ha permesso di ricavarne le frequenze naturali, che si sono studiate al variare della rigidezza del camion.

La Figura 1 mostra, al variare del rapporto tra la frequenza del camion e del ponte scarico, il valore delle due frequenze naturali del sistema 2DOF, normalizzate rispetto alla frequenza del ponte scarico.

Nel caso di camion con bassa rigidezza, il periodo fondamentale del ponte è il secondo periodo del sistema 2DOF, mentre quando la rigidezza del camion è elevata, il primo periodo del sistema 2DOF è anche il periodo fondamentale del ponte.

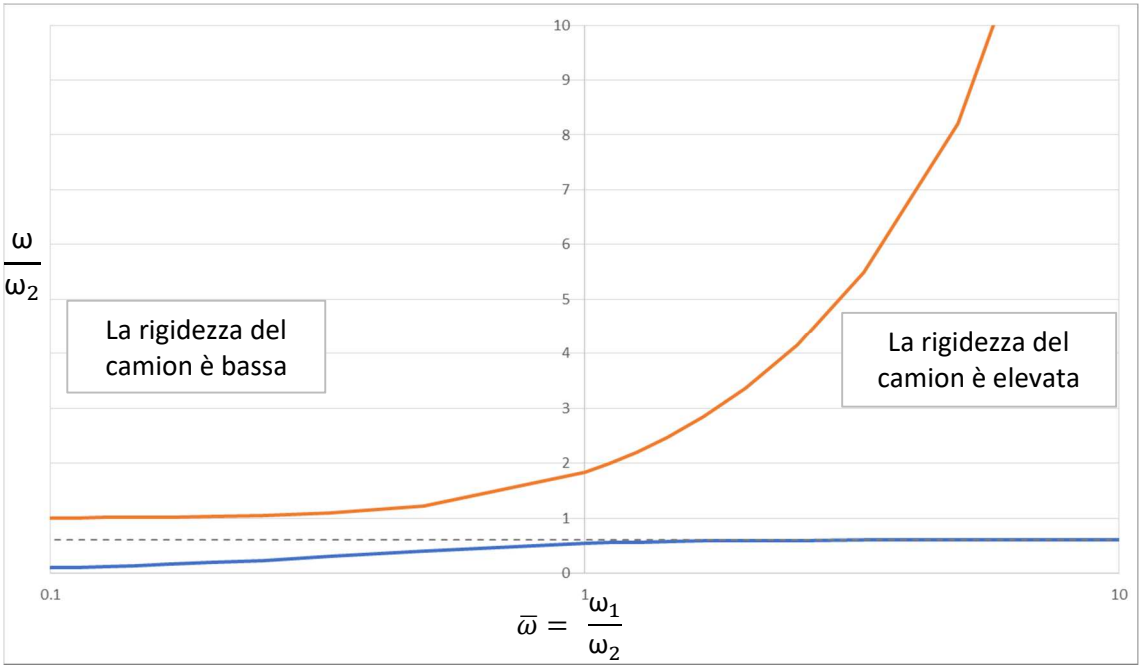

Figura 1: Le due frequenze naturali del sistema 2DOF per diversi valori del rapporto tra le frequenze del camion e del ponte.

La prima frequenza naturale del ponte nei due modelli, risulta molto diversa per quei casi in cui le frequenze proprie del ponte e del camion sono simili.

Per valori di $\bar{\omega}$ (definito come il rapporto tra la frequenza del camion e la frequenza del ponte) vicini all’unità avviene un'interazione ponte-camion, in quanto quest'ultimo si

comporta come un Tuned Mass Damper, modificando il comportamento dinamico del ponte: non solo ne riduce l'ampiezza delle vibrazioni meccaniche, ma ne modifica anche le frequenze.

In questi casi, l'uso di un modello a masse aggiunte, che non è in grado di cogliere questa interazione, porta a un'errata interpretazione dell'OMA.

In seguito, lo studio è stato condotto su ponti a campata unica di diverse lunghezze, modellati con gli elementi finiti. L'obiettivo era monitorare la variazione della frequenza fondamentale del ponte al variare di alcuni parametri, quali:

- La rigidezza del camion;
- La configurazione di carico, intesa come il numero di autocarri disposti longitudinalmente e nella sezione trasversale;
- Il rapporto $\bar{L} = \frac{L_{caricata}}{L_{Campata}}$;
- Il rapporto $\bar{m} = \frac{m_{camion}}{m_{Area\ caricata}}$;

In Figura 2 sono rappresentate le frequenze dei primi due modi di vibrare di un ponte (che si trova in determinate condizioni di carico: $\bar{m} = 0{,}2$, $\bar{L} = 0{,}5$, sono presenti 4 camion longitudinalmente ed uno trasversalmente), normalizzate rispetto alla frequenza fondamentale del ponte scarico.

È stato osservato che quando i camion sono molto flessibili, le frequenze fondamentali dei ponti scarichi o in presenza degli autocarri sono molto simili. Viceversa, quando i camion hanno una rigidezza paragonabile a quella del ponte, la frequenza fondamentale del ponte caricato cambia notevolmente rispetto a quella del ponte nella configurazione scarica. In particolare, in corrispondenza della discontinuità di salto, il rapporto tra queste due frequenze raggiunge valori massimi di circa 1,3 e valori minimi di circa 0,5.

Questa differenza è tanto più pronunciata quanto più alto è il rapporto$\bar{L}$ ed $\bar{m}$. Inoltre, all'aumentare del valore di questi due parametri, la gamma di frequenze per le quali il camion si comporta come un TMD è più ampia. È stato riscontrato che l'aumento del numero di masse nella sezione trasversale fa sì che il camion si comporti come un TMD per valori più alti di $\bar{\omega}$, ovvero quando questo è più rigido del ponte. Infine, la disposizione di più camion lungo il ponte, se avviene in modo simmetrico, ha un effetto

limitatamente alle frequenze del secondo modo di vibrare, per il quale valgono tutte le conclusioni precedenti.

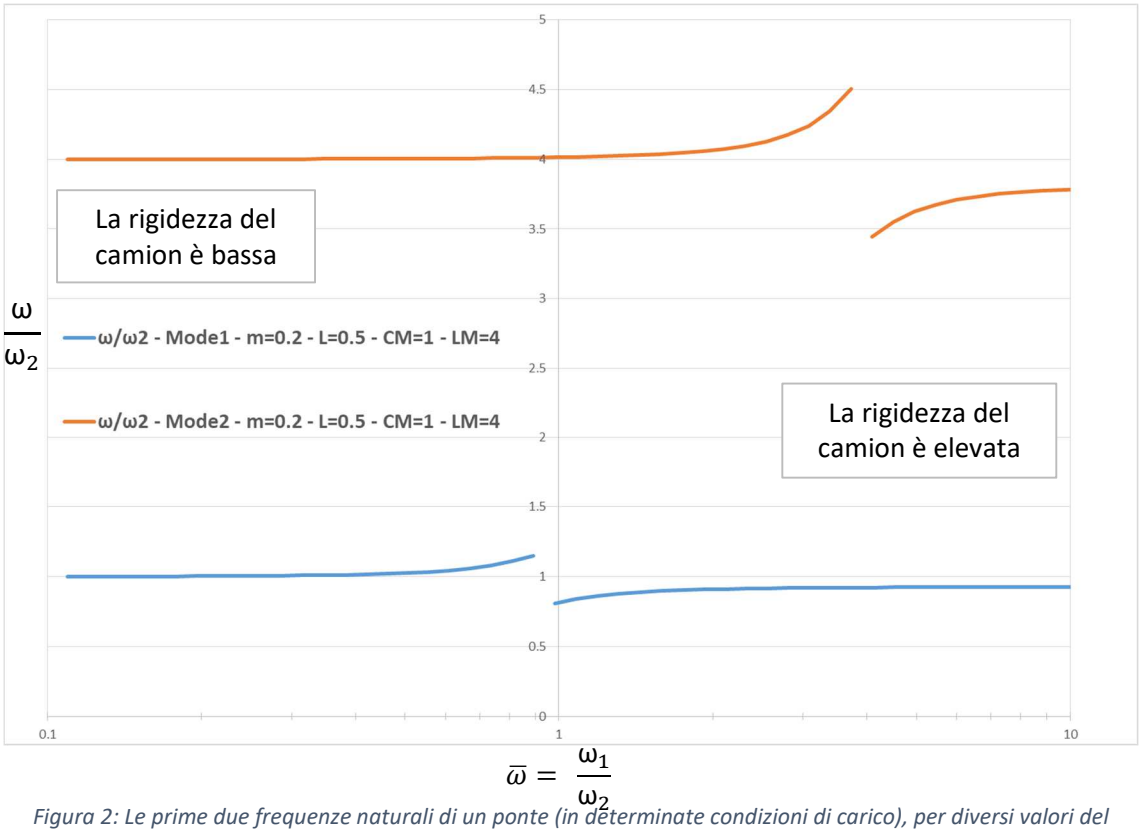

Figura 2: Le prime due frequenze naturali di un ponte (in determinate condizioni di carico), per diversi valori del rapporto tra le frequenze del camion e del ponte.

Introduction

The testing of a structure is the set of operations necessary to verify its correct functioning before putting it into operation. It is an essential operation in the construction of a building because exceeding it certifies that the performances are and will conform to those expected in the design phase.

With reference to the bridges, it is mandatory to perform a static load test (law n.1086 / 71), the directives for which are reported in Section 9 of the New Technical Standards for Construction (NTC 2018), while the dynamic tests they are mandatory only for road and rail bridges of significant importance. In particular, the fundamental period determined experimentally must be comparable with that foreseen in the design phase.

However, in areas with a high seismic risk such as the Italian one, the dynamic behaviour of a building acquires considerable importance and the dynamic tests, whose purpose is to identify the dynamic parameters of a structure, are taking place in civil works, especially with reference to bridges.

The dynamic characterization of buildings provides the designer with a tool for controlling the methods and design tools; the comparison between the identified modal parameters and those of the numerical model provides in fact useful information about the reliability of the latter, including the simplified hypotheses adopted. If the expected results from the numerical model are congruent with the actual parameters, then the model is efficient and well calibrated. Otherwise, a discrepancy could lead the designer to conclude that the structure is more deformable than he had foreseen in the design phase, which, in the case of bridges, could jeopardize the outcome of the dynamic acceptance test.

When dynamic tests have to be performed on a bridge, Operative Modal Analysis (OMA) is a fast, cheap and efficient solution because the dynamic characterization is based on the response to environmental vibrations to which a structure is always subject. This test is often suitable to be performed also on constructions that require a high level of energy to trigger the oscillation and which would be impossible to excite by artificial means. To obtain reliable tests, a set of engineering skills and abilities are required during their planning, execution and subsequent analysis and interpretation of the data.

In order to give consistency to the results and guarantee the validity of the model, these dynamic tests are carried out more and more frequently in the case of the static test and the relative load test. The dynamic tests are generally performed on the day of the static test both on the unloading deck and on the loading deck. The tests on the loaded bridge generally offer the possibility of evaluating the dynamics of the structure subject to a different (known) mass distribution compared to that of the permanent loads.

The loads are usually made up of heavy trucks distributed in one or more rows both longitudinally and transversely to the bridge span. Their weight can be up to 50 tons and can significantly change the dynamic behaviour of the bridge.

In the numerical model, trucks used for static tests are generally modelled only in terms of added masses on the bridge.

This method does not consider that the dynamic system consisting of the truck, the shock absorbers and the tires, interacting with the dynamic system constituted by the bridge, can also significantly change its modal response. In other words, the fact that the mass of the trucks acts through a flexible system is neglected.

In particular, when the frequencies of the bridge and those of the trucks are similar, the latter behave as a tuned mass damper. Not only they reduce the amplitude of mechanical vibrations on the bridge, but they also change its frequencies.

Not taking into account the truck-bridge interaction, and the related effects on vibration frequencies, could lead to an incorrect interpretation of the dynamic test result, and consequently the test result.

As part of this thesis, the effective importance of the truck-bridge interaction phenomena was first investigated, through an adequate modelling of the structure and trucks, and subsequently the problem was studied in parametric terms, focusing on the effects of the aforementioned interaction on first bending frequencies of the deck.

At the beginning the study was limited to simple analytical models, in which the bridge and the truck were both reduced to a 1DOF system. Driven by the observations made on these simplified models, a finite element modelling of a bridge on which the trucks are present was performed.

To have a measure of the effect of the bridge-truck interaction, the variations of the frequencies and the participating mass factors of the first two modes of vibrating of the

bridge were monitored. In order for the results to be of practical interest, the study was conducted on realistic case studies obtained taking into account four parameters. These are the ratio between the mass of the trucks and the mass of the loaded portion of the bridge; the ratio between the loaded length and the length of the bridge; the number of trucks present in the longitudinal direction; the number of trucks present in the cross section.

Chapter 1

The operative modal analysis

During the past year, the use of experimental dynamic testing has become more and more widespread. The aim of this type of testing is to identify the dynamic parameters of a structure: the frequencies of the natural modes of vibration, its mode shapes and an estimation of the damping ratio.

These parameters are correlated to the intrinsic features of the structure, such as the rigidity of the components or the degree of constraints, and they are not dependent on the type of testing.

The methods of modal analysis can be divided in two categories. The Experimental Modal Analysis (EMA) involve the excitation of a structure through artificial vibrations, which can be generated by dynamic shakers or impact hammers, whose great advantage would be the possibility to measure input and output at the same time. However, when monitoring or performing a dynamic test on a bridge, providing enough artificial energy in the frequency range of interest is difficult, if not impossible.

It is in those cases that the Operative Modal Analysis (OMA) is adopted. The OMA, which uses environmental vibrations to which a structure is always subject to, can also be carried out on construction projects that require a high level of energy in order to ignite oscillation, and that it would be impossible to excite through artificial means.

In order to get reliable tests, a set of engineering competences and skills are required during their planning, execution, and subsequent analysis and data interpretation.

A network of sensors measuring the vibration of a certain physical quantity in time is installed on a structure subject to environmental vibrations. The input is identified in an amount of stress that can provide the structure with enough energy in the frequency range of interest. The sensors will then measure the time history of the physical quantity (e.g. of the acceleration, in the case of accelerometers). The signal coming from the network of sensors is then elaborated - in order to increase the signal and noise ratio, remove

unnecessary frequency ranges, etc…- and acquired. Afterwards, the dynamics of the structure is obtained through different analysis techniques.

1.1. Some applications of OMA

Knowledge of modal parameters can serve as a useful tool in different moments of the life of the construction project, starting from its first construction phases.

According to the current legislation – NTC 2018 –, dynamic testing and the identification of the fundamental period for road and railway bridges is mandatory when these are "construction projects of significant importance". From articles 9.2.2 and 9.2.3:

"For construction projects of significant importance, static tests must be integrated with dynamic tests that will measure the bridge response to dynamic excitation, while ensuring that the experimental fundamental period corresponds to the one expected according to the project".

Dynamic testing can be performed though different types of tests, whose aim is to identify the dynamic parameters of a structure, which are of fundamental interest for forecasting the response of a structure subject to seismic input. These parameters are related to the intrinsic properties of the structure, and they are not dependent on the type of testing. By performing the dynamic testing at the moment of construction, its digital fingerprint can be obtained. This can be used as a reference for future testing. By monitoring dynamic parameters over time through measurements that are continuous, planned or single – e.g. as a result of exceptional events – it is possible to estimate possible damages on the structure, or to monitor the degree of deterioration, since a variation of the parameters would be detected (a loss in rigidity would translate in an increase of the fundamental period of vibration).

By performing dynamic tests during construction, the designer can ensure the truthfulness of his or her hypothesis, by comparing experimental parameters to analytical ones. If the expected results coming from the FEM model are congruous to the actual parameters, then the model is efficient and well-balanced. Otherwise, it could be necessary to reconsider some hypothesis and perform model updating, a process of re-calibration of the model.

This is executed by modifying the parameters that influence the dynamics of the model from time to time (elastic models, the distribution of masses, the meshing, the constraints,

the geometry, etc…), so that it gets closer and closer to reality at every iteration. In the event that it was impossible to calibrate the model, the reason could be in the imperfect realization of the construction project or in the possibility that it was inadequate.

Models of existing structure which need to be adjusted or improved can be calibrated by dynamic testing as well. This way, it is possible to plan optimal intervention and – after the construction - to verify its success with an additional dynamic test.

Regarding OMA, it is important to point out that the measurements are carried out on the actual operative conditions of the structure. Therefore, the dynamic parameters are representative of the dynamic behaviour of the structure in its actual conditions of use. Additionally, the test does not interfere with the operation of the structure.

1.2. Environmental vibrations

In order to obtain the dynamic response of a structure it is necessary to ignite oscillation. To this end, it is possible to provide either artificial or environmental vibrations. The UNI 10985 provides a classification:

Table 1: classification of dynamic analysis methods according toUNI 10985.

Natura delle sorgente di eccitazione	Sorgente di eccitazione	Andamento temporale delle vibrazioni
Artificiale	Vibrodina meccanica Vibratore elettroidraulico Vibratore elettrodinamico Rilascio improvviso di una forza impressa Urti (di massa)	Sinusoidale Sinusoidale/random Sinusoidale/random Transitorio Impulsivo
Ambientale	Microsisma Traffico Vento Sisma	Random Transitorio/random Transitorio/random Transitorio

Systems that use artificial vibrations are called input-output systems. These vibrations are provided with specific equipment whose intensity is possible to measure and control. The driving force – i.e., the input supplied to the structure – can be either impulsive, sinusoidal, or random and it is known at every moment.

The methodology of dynamic analysis for the identification of an input-output system is the EMA, Experimental Modal Analisys,

The limit connected to the artificial exciting techniques is the impossibility of introducing enough energy in large-scale structures, so as to considerably excite all vibration modes.

Moreover, these tests resort to one or more punctual driving forces which does not make the excitation of vibration modes that require forcing functions on different points simple.

One the other hand, the sources of environmental vibrations are the wind, microseisms and traffic, which are random forcing functions and are not possible to control or foresee. Therefore, systems using this type of forcing are output-only systems, and the analysis identifying the dynamic parameters of the system is the OMA, the Operational Modal analysis.

Measuring the actual dynamic load produced by the wind it is in fact impossible, because of the distribution of the load itself on the exposed surfaces, so much so that the excitation can only be described on a static basis. Microseisms are a basically permanent random excitation for the structure. However, the oscillation provided to the structure is limited, therefore needing high sensitivity equipment. Moreover, the output signal can be easily be interfered with by background noise, a certain degree of thoughtfulness is therefore needed when acquiring the signal. Traffic generates a dynamic response of significant extent and easily measurable, and it is easy to be used for operating structures. It is possible to use conveniently planned traffic, for example, having a single vehicle with known properties go through. Alternatively, ordinary traffic can be used.

Every civil structure is always subject to excitement by environmental forcing functions. Their availability allows both a simplification of the execution of the test and consistent cost savings. The peculiarity of these vibrations is that they succeed in excite even large structures which would otherwise be impossible to excite. Moreover, their energy is distributed in a broad frequency band and they can excite many of the structure modes.

The OMA allows to obtain the dynamic properties of the structure subject to environmental forcing functions, as long as the input is comparable to white noise. In order for this to be true, the length of the time histories and the period of measurement are of paramount importance.

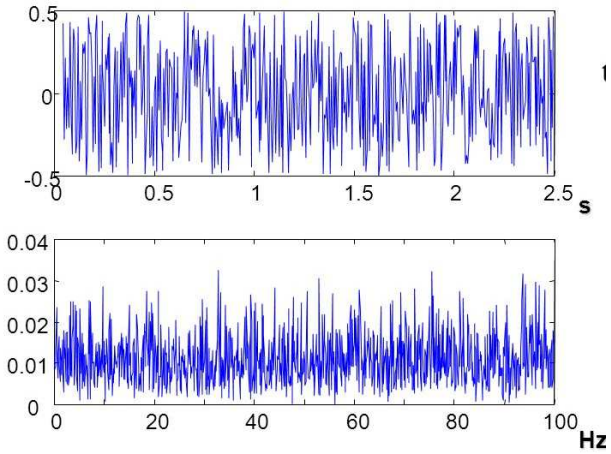

Picture 3: Time history and frequency spectrum curve of white noise excitation.

The minimum duration of measurement is recommended to be around 1000 or 2000 times the first natural period of the structure. In order to have a flat spectrum in the frequency domain, a sufficient number of time histories are to be mediated. In some cases, the level of environmental excitation available can be quite low and the available data could be limited - that is, they were not mediated for enough time. The results could be affected by noise and the modal parameters resulting from the analysis could be uncertain. This occurrence cannot happen in the EMA with artificial forcing, where the advantage lays in the control one has over the level of forcing and the energy entering the structure.

1.3.Equipment to acquire data

In order to convert a physical phenomenon to digital data that can be used in an analysis it is necessary to prepare a measurement chain. The starting element is the sensor, which is connected to a data acquisition system. The sensor converts a physical quantity into an electrical signal, which - through the wiring network or a wireless system - reaches the air conditioning system which modifies the signal to make it easier to acquire or to facilitate subsequent reading. The conditioning system transmits the signal via cables or wirelessly to the acquisition system, which is the system that converts the analog data into digital. Finally, the data is recorded and saved on the hardware memory.

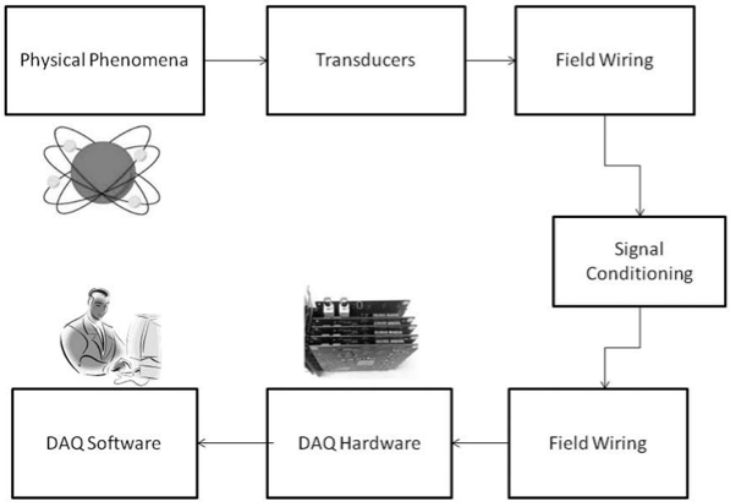

Picture 4: The steps of the measurement chain of a physical phenomenon.

This measurement chain must be designed before starting the tests, in order to choose the appropriate tools.

During the design phase of the experimental tests, as much information as possible on the structure is to be acquired, such as the geometry, the type and characteristics of the materials, the type of constraints and foundations, in order to be able to make predictions on the dynamic behaviour thanks to analytical or numerical models (based on the degree of complexity of the structure to be analysed). With these starting assumptions and considering the size of the structure, the input, number and type of sensors are chosen, as well as their positioning, which must be such as to capture the vibration modes of the structure.

1.3.1. Measurement sensors and their positioning in the case of bridges

A sensor is an instrument that converts a physical quantity into an electrical signal. Their classification is provided by UNI 10985.

"… They are transducers capable of measuring physical quantities (whether they are kinematic, mechanical or other) both in the static and in the dynamic range. Generally, the transducer is connected to an electronic conditioning circuit capable of supplying an electrical signal linked to the quantity to be measured; this signal can be acquired and recorded for the necessary processing.

The most commonly used sensors can be classified:

a) Based on the quantities to be detected:
- *Accelerometers*
- *Velocimeters*
- *Seismometers*
- *Displacement transducers*
- *Strain gauges*
- *Inclinometers*
- *Load cells*
- *others (anemometers, traffic detectors, counters and frequency meters, etc.)*

b) based on the physical principle of operation:
- *Resistive transducers;*
- *Capacitive transducers;*
- *Inductive transducers;*
- *Piezoelectric instruments;*
- *Optical measurements,*

c) Based on the type of reference (relative or absolute) with respect to which the measurement is made, three different families can be identified (classification that takes its cue from the standard, but does not exactly adhere to it):
- *reference and measurement point both belonging to the structure (e.g. strain gauges)*
- *external reference to the structure and measuring point belonging to the structure (e.g. optical transducers or wire potentiometers);*
- *absolute reference (within the body of the instrument it is possible to identify a point considered to be stationary or the operating principle of the transducer provides absolute quantities as in the case of accelerometers);*

d) based on the the time spent on site and the duration of the survey:
- *for temporary applications aimed at dynamic characterizations or occasional checks (one-time or systematic but with time intervals of one or more years);*
- *sensors for continuous or periodic monitoring. ... "*

The most widely used sensors are piezoelectric accelerometers, which use the properties of quartz. The piezoelectric material is on the one hand connected to the inertial mass of

the sensor, and on the other to the base of the sensor. When this is subjected to vibrations, the quartz is compressed and develops an electric charge on its surface proportional to the force (and therefore to the acceleration) imprinted on the crystal.

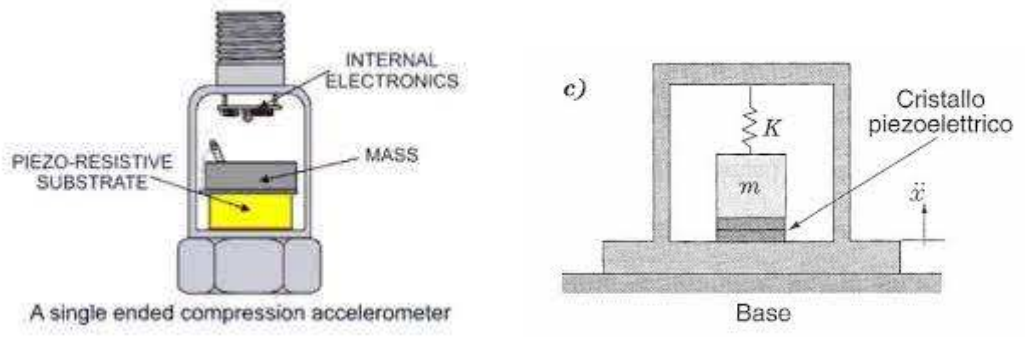

Picture 5: On the left an example of a piezoelectric accelerometer, on the right its mechanical schematization.

The piezoelectric accelerometer consists of a mass connected to the casing with an elastic element and submerged in a liquid. Its mechanical scheme is therefore similar to that of a damped one degree of freedom oscillator, in which the rigidity k is provided by the piezoelectric material and the damping by the liquid in which the mass is submerged.

The main properties of the sensors are:

- *Sensitivity*: it is the minimum measurable variation of the measured physical quantity, expressed by the relationship Volt / physical quantity (for example, mV/g). With the same physical quantity, the greater the measurable voltage variation, the higher the sensitivity;
- *Frequency range*: this is the operating range of the instrument. The sensor installed on the structure behaves like a spring in series, therefore the outgoing signal will be subject to a certain phase shift and a certain value of the amplification function. Both of these parameters depend on the damping value of the sensor and the relationship between the frequencies of the structure and the accelerometer. In particular, it is important that this ratio is far from one, value for which the amplification function is maximum. For a damping value of 0.65, the amplification function is constant if the frequency ratio varies between 0.05 and 0.6. Lastly, it must be taken into account that the fixing system acts as an additional spring in series with the accelerometer and affects its resonance frequency. If the rigidity of the support is high, the sensitivity deviation of the sensor occurs for very high frequencies;

- P*eak value*: is the maximum value that the instrument can measure, it depends on both the sensor and the conditioning system;
- *Minimum resolution*: it is the minimum value that the instrument is able to capture and depends on the background noise of the instrument;

In light of these characteristics, the appropriate sensor must be chosen based on the type of analysis that takes place. The artificial vibrations used for the EMAs are an input of medium or high intensity and require a sensitivity of 0.1-1 Volt/g, with a frequency range that varies from 1 to 1000 Hz and a minimum resolution of 0.1-1mg. For AOM more sensitive sensors are used, with a sensitivity in the range of 1-10 Volt/g due to the low intensity of the environmental input, the frequency range varies from 0.1 to 100 Hz and the minimum resolution is between 1 and 10 μg .

The number and position of the sensors must be such as to allow the reconstruction of the modal forms, therefore they must not be arranged in those measuring points where it is not possible to observe the modal forms, or the null points of the modal forms.

The number and position of the sensors must be such as to allow the reconstruction of the modal forms, therefore they must not be arranged in those measuring points where it is not possible to observe the modal forms, or the null points of the modal forms.

When dynamic tests are carried out on viaducts, different configurations of the measuring systems are required. The transverse modes are usually coupled with the flexural-torsional ones, to capture them it is sufficient to arrange transversely an array of sensors, being careful to avoid the shoulders of the bridge, as they are fixed points. Generally, the bending and torsional modes are coupled together, therefore the sensors must be arranged in such a way as to capture both modes simultaneously. To grasp the bending modes, an array of accelerometers sensitive to vertical accelerations must be arranged longitudinally, placing two in each measurement section, one on the right side and one on the left side of the deck, it is also possible to evaluate the torsional modes.

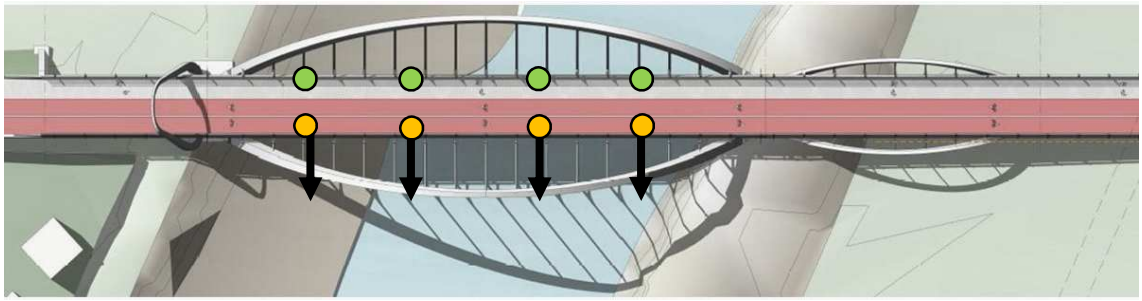

Picture 6: The sensors layout on a bridge. The black arrows the are sensors for the transverse modes, the green and the orange ones are the ones for the flexural and torsional modes.

Among the various set-ups it is useful to keep some measurement positions unchanged, in order to have a fixed reference that allows you to check the measurements obtained and overlap the results, effectively increasing the number of points useful for the reproduction of the vibrating modes.

1.3.2. The data acquisition system and signal processing

Sensors convert a measured quantity into an analog electrical signal. The analog/digital acquisition cards transform the electrical signal into a digital one, with the aim of collecting time histories in hardware memories for future analysis. The first step in analysing the signal is its conversion from analog to digital formats, in this way the collected data is processed in the form of discrete values and not continuous functions.

In this first phase of conversion, different types of problems are identified in the data acquisition method and in the signal transformation method: these problems are related to the insurgence of aliasing and leakage errors.

The number of bits used to represent the analog signal defines the resolution of the card. An 8-bit card divides the measurement range of the analog signal into 2^8=256 points, while a 24-bit card uses a range of 4069 points. Typically, A/D converters have a resolution of 10-24 bits.

The measurement range is the minimum and maximum voltage value that the card is able to acquire, generally from 0 to 10 Volts or from -5 to 5 Volts. In order to measure the signal with the highest possible resolution, the range of the card must be adapted to the range of the signal, which must not exceed the limits of the acquisition card, because it would lead to an overload and subsequent cutting of the signal.

Before digitizing the signal, some amplification or attenuation operations of the signal are performed, to adapt it to the measurement range of the card and fully use its resolution. The operations of amplification or attenuation of the signal are the gain of the card. Amplification is an operation that increases the signal-to-noise ratio (SNR), the digital signal must be amplified before noise occurs, therefore immediately after its acquisition by the sensor, because even the passage of the signal in the cables causes noise .

The conversion of the analog signal takes place by sampling it with a certain sampling $f_s = \frac{1}{\Delta t}$, where Δt is the time interval between the samples. According to Nyquist's theorem, in order for an analog signal of maximum frequency f_M to be uniquely reconstructed starting from samples of frequency, f_s must be $2f_M > f_s$.

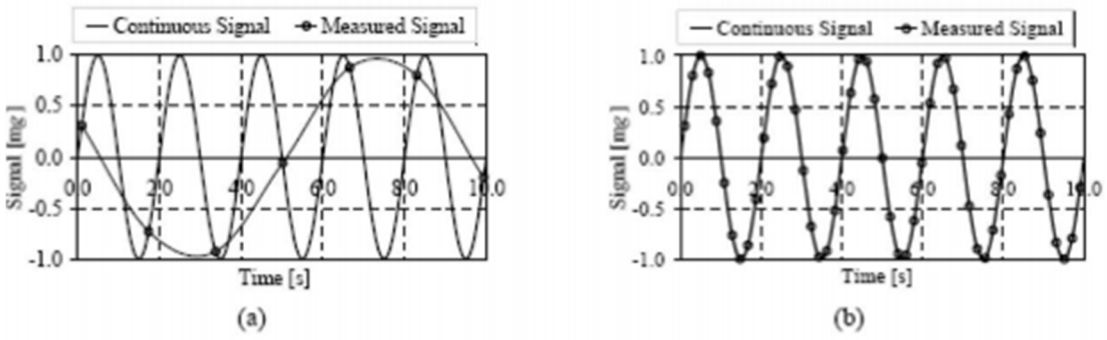

Picture 7: Importance of the sampling frequency of a continuous signal. On the left a signal reconstructed following a undersampling, while on the right a signal reconstructed with an adequate sampling.

The sampling frequency of the card must be at least double the frequency f_M of the signal, otherwise it would be undersampling and it would be possible for the reconstructed signal to be different from the real one. This phenomenon is called aliasing and can no longer be corrected after the A/D conversion, so an anti-aliasing filter must always be placed before the A/D conversion.

The anti-aliasing filter is a low pass filter with a cut-off frequency equal to half the sample rate. This way, only signals that can be uniquely defined can be transformed into digital signals.

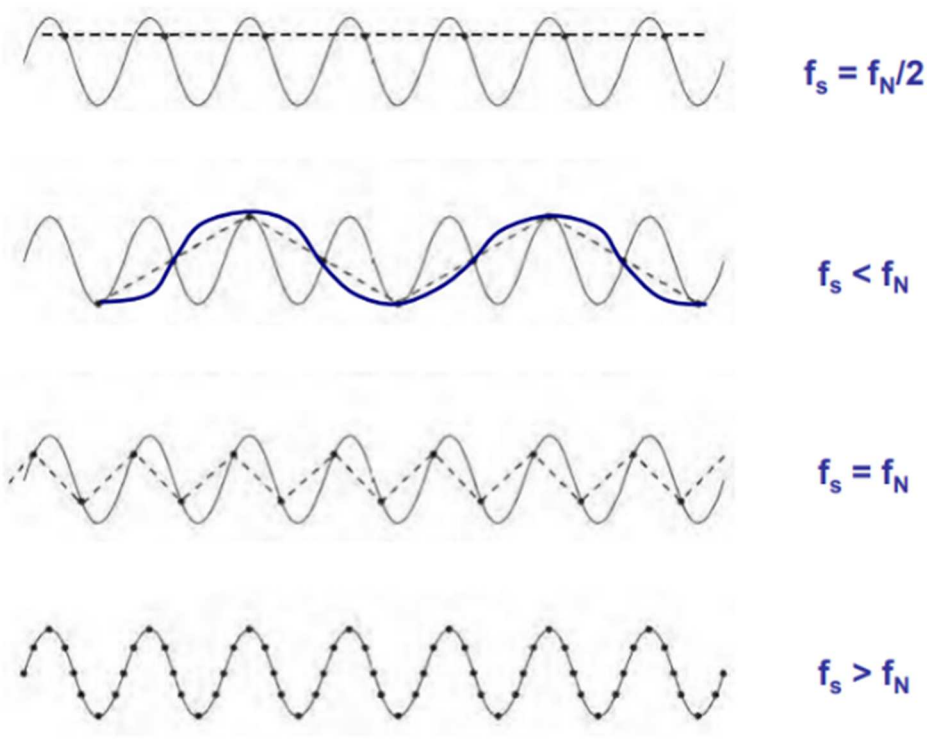

Picture 8: Examples of subsampling.

To reduce the memory occupation of the signals to be acquired, a decimation operation can be used. The digital signal is resampled, with a decimation frequency $f_s^{dec} > 2f_c$. This operation is analogous to applying a low pass filter. By using the appropriate decimation factor, Nyquist's theorem is respected, and no information on the original signal is lost.

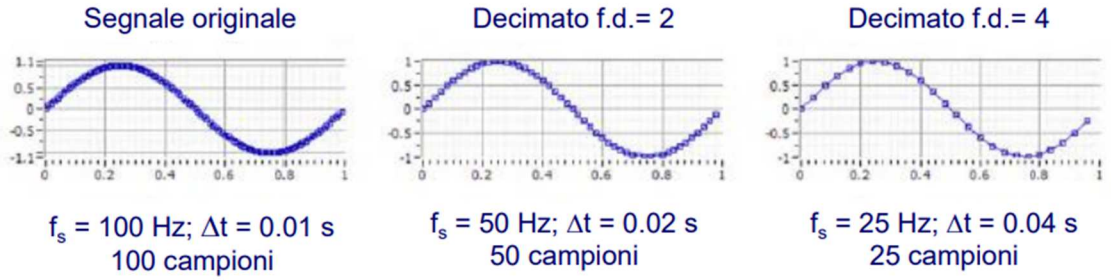

Picture 9: Example of decimation of a signal. With the decimation the number of samples decreases, but the information on the signal is equivalent.

Normally, acquired signals (such as acceleration, displacement or forces) are functions in the time domain, while the most common methods of analysis process data in the frequency domain. The transition from the time domain to that of frequencies occurs with

the use of the Fourier transform. Leakage is a problem related to the length of the time history, which is finite in size, associated with the assumption of signal periodicity.

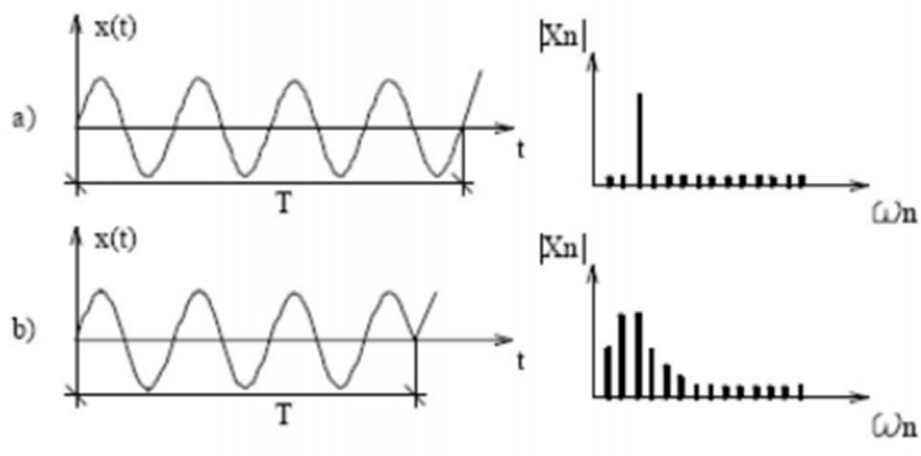

Picture 10: Example of leakage. In graph b) the signal does not stop at a full cycle. Consequently, the Fourier transform uses more harmonic series to reconstruct the signal and the resulting spectrum is misleading.

If we consider a segment of signal with length T equal to an integer multiple of the signal itself, there is no problem. Otherwise, the assumption of periodicity is not strictly valid, especially near the ends of the interval, this entails a dispersion of spectral energy. Leakage can be reduced with windowing techniques which consist in filtering the x(t) signal with a W(t) filter function. The product between these two functions in the time domain returns the function x'(t), the Fourier transform of this function has a lower dispersion of power in the frequency domain.

Sometimes the time domain signal can have peaks due to external sources or signal processing, not representative of the behaviour of the structure.

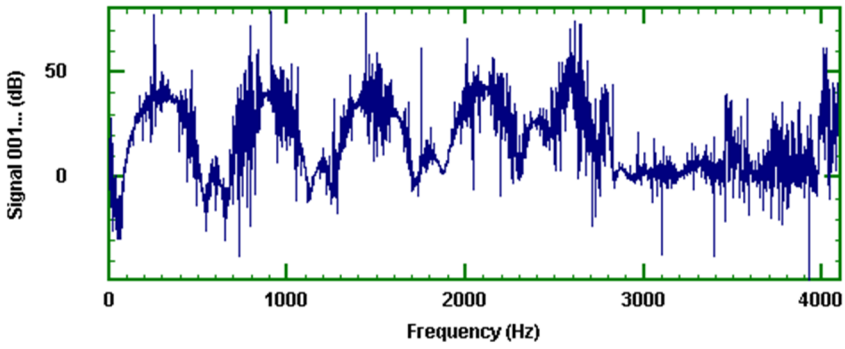

Picture 11: The spectrum of a signal before spectral smoothing.

To alleviate the problem, spectral smoothing is used. The signal in the time domain is subdivided into segments, the segment is then windowed and mediated to then be Fourier

transformed. TDFs obtained on segments of the same length are usually overlapped to improve accuracy. This way, the frequency resolution of the TDF is lower and the curve is smoother.

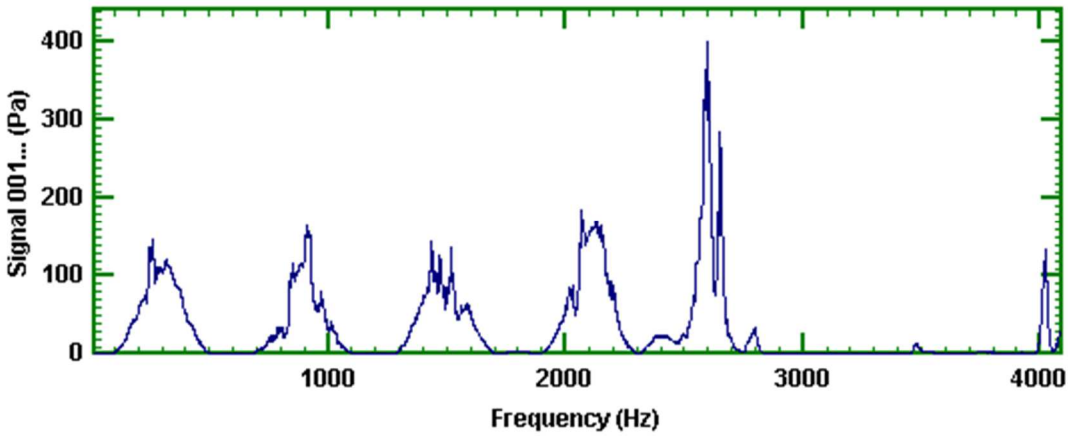

Picture 12: The spectrum of a signal after being smoothed.

1.4. Signal analysis

The data collected during the course of the test must be processed to extract the modal parameters that describe the structure. Analysis techniques can use the time domain or the frequency domain.

In practice, a Multiple Degree Of Freedom (MDOF) model is used, which describes any system as a set of masses, springs and dampers with varying degrees of freedom.

The time domain techniques are based on the solutions of the following system of differential equations, which describes the MDOF system:

$$M\ddot{x}(t) + C\dot{x}(t) + Fx(t) = F(t)$$

in which:

- M is the mass matrix;

- C is the damping matrix;

- K is the stiffness matrix;

- $x(t)$ is the vector that describes the displacements of the degrees of freedom;

- $F(t)$ is the driving force of the system.

The methods that use the frequency domain use the same model, but, going from the time domain to that of frequencies by exploiting the functional transformation known as the Fourier transform. In this way, the system of ordinary differential equations becomes a system of algebraic equations of simpler resolution:

$$(-\mathrm{M}\omega\ 2 + i\mathrm{C}\omega + \mathrm{K}) \cdot X(\omega) = F(\omega)$$

in which:

- ω is the natural frequency of the system;

- (ω) are the degrees of freedom;

- (ω) is the driving force.

The starting point of EMA or OMA analyses are the measured frequency response functions (FRFs). In general, FRFs are the ratio between a quantity such as displacement, velocity or acceleration and the driving force in the frequency domain.

$$H(\omega) = \frac{X(\omega)}{F(\omega)};\ \ H(\omega) = \frac{V(\omega)}{F(\omega)};\ \ H(\omega) = \frac{A(\omega)}{F(\omega)}$$

An FRF (indicated as H (ω)) is the receptance, expressed as the ratio between the Fourier transforms of the displacements (X) of a system due to a driving force (F) and the force itself:

$$H(\omega)\ = \frac{X(\omega)}{F(\omega)}\ \ = (-M\omega\ 2\ +\ iC\omega\ +\ K)^{-1}$$

If N are the degrees of freedom of the system, the reception matrix is a symmetric matrix, of dimensions NxN. The element $H_{ij}(\omega)$ of the matrix represents the response in the degree of freedom i due to the driving force in j. Thanks to its symmetry, the reciprocal theorem is valid for the matrix H(ω), so that $H_{ij}(\omega) = H_{ji}(\omega)$. By exploiting this property, it is possible to know all the components of the matrix starting from the knowledge of a row or a column. Knowing a row of the matrix, means measuring in the same station (fixed output) by varying the position of the input. The knowledge of a column is obtained by changing the measurement point and leaving the point of application of the driving force fixed.

The following equation show the relation between the FRF and the modal parameters:

$$H_{ij}(\omega) = H_{ji}(\omega) = \sum_{r=1}^{N} \frac{\varphi_{ir}\varphi_{jr}}{(\omega_r^2 - \omega^2) + \frac{i\omega c_r}{m_r}}$$

In which φ_{ir} and φ_{jr} are respectively the l'i-th and the j-the element of the r-th eigenvector φ_r. c_r and m_r are respectively the viscosity and mass matrices orthogonalized pre-multiplying and post multiplying by the matrix of eigenvectors.

This equation highlights a direct correlation between the modal properties and the FRF. From a practical point of view, it suggests that there may be a means to determine the modal properties of a system starting from the FRF, which can be derived from direct measurements only in the case of EMA.

Various similar representations of the FRF contain the same amount of information. The properties of the structure can be derived more easily, sometimes from one and sometimes from the other:

- Bode diagram: modulus and phase of the transfer function as a function of frequency;
- Nyquist diagram or polar diagram: imaginary part as a function of the real part;
- Cartesian diagram: real and imaginary part of the FFT as a function of frequency

In the Bode diagram the modes of vibration can be identified as peaks of the FRF, the relative frequency of these peaks is one of the system's natural frequencies. The height of the peak is indicative of the amplification that the excitation signal undergoes at the point of measurement, while its more or less tapered shape indicates low or high damping.

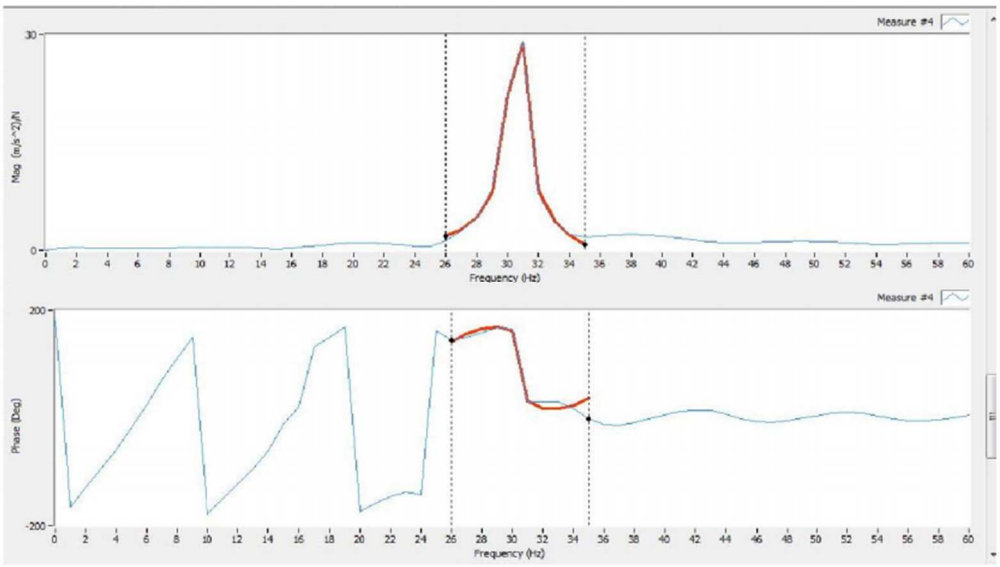

Picture 13: The Bode diagram consists of a FRF-Frequency graph, at the top, and a Phase-Frequency graph, at the bottom.

It should be noted that in the EMA case, for which both the input and the structural response are known, the measured FRFs are available. OMAs allow dynamic identification even in the case where the input is not measurable, as long as this is comparable to white noise, that is a Gaussian background noise with a null average value. It is not possible to find the previously proposed FRFs, since they require the knowledge of the driving force.

The OMA methods allow tracing the modal parameters of the structure by analyzing the Power Spectral Density, PSD. The first step of the analysis consists in performing an FFT on the data in the time domain to obtain – for each series of measurements performed – the acceleration spectral density matrices $G_{yy}(\omega)$ which contain all the dynamic informations.

Given the signal $y_i(t)$:

$$FFT(y_i) = \int_{-\infty}^{+\infty} y_i(t) \cdot e^{-i\omega t}\, dt$$

The PSD is:

$$G_{yiyi}(\omega) = \frac{FFT(y_i) \cdot FFT(y_i)}{\Delta f}$$

$$G_{yy}(\omega)_i = \begin{bmatrix} G_{11}(\omega) & \dots & G_{1N}(\omega) \\ \dots & \dots & \dots \\ G_{N1}(\omega) & \dots & G_{NN}(\omega) \end{bmatrix}$$

The dimension of the matrix $G_{yy}(\omega)$ is NxN, being N the number of transducers. Each element of the matrix $G_{yy}(\omega)$ is a function of the spectral density of the acceleration $\left(\frac{g^2}{\text{Hz}}\right)$. Self-spectra, the elements in the main diagonal of the matrix, are a measure of the magnitudes of the PSD between a response and itself. The cross-spectra, the off-diagonal elements, are the crossed spectral densities between different responses.

Once the PSD matrix has been defined, through the FDD (frequency domain decomposition) method the modes can be estimated from the PSDs, under the assumptions of white noise as input and weakly damped structure. The non-parametric technique identifies the modal characteristics using the Singular Value Decomposition (SVD) of each of the spectral density matrices. This decomposition corresponds to the identification of a Single Degree of Freedom (SDOF) of the system for each single value. The correctness of the results provided by the OMA can be affected if a non-random excitation is superimposed on the white noise, since this would produce peaks in PSDs that cannot be correlated with the properties of the system.

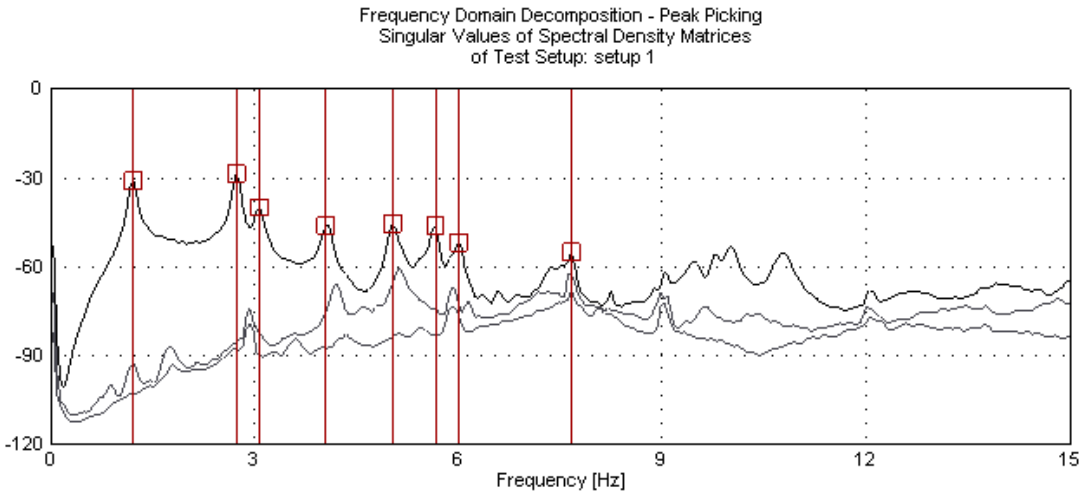

Picture 14: The FDD technique involves the application of the Peak picking methodology on the SV of the PSDs.

The FFD method also exists in its "enhanced" version, the Enhanced FDD (EFFD) which allows you to more accurately evaluate the natural frequencies of the system and to obtain an estimation of the damping value. Basically, the first step of the EFDD method is to identify the useful band of the SVD with the Modal Assurance Criterion (MAC) among the modal forms close to a frequency.

$$MAC(i,j) = \frac{\left|\varphi_i^T \varphi_j\right|^2}{(\varphi_i^T \varphi_i)(\varphi_j^T \varphi_j)}$$

where φ_i and φ_j are the vectors of the i-th and j-th modal forms. The coefficient is the closer to one the more the compared modes are similar to each other. It is the closer to zero the more the modes are orthogonal to each other.

The estimate of frequency values and damping coefficients are calculated through the application of the inverse function FFT (IFFT) of each spectral density function for each vibrational mode. The self-correlation response function obtained is a typical response of a system to a single degree of freedom in free vibrations.

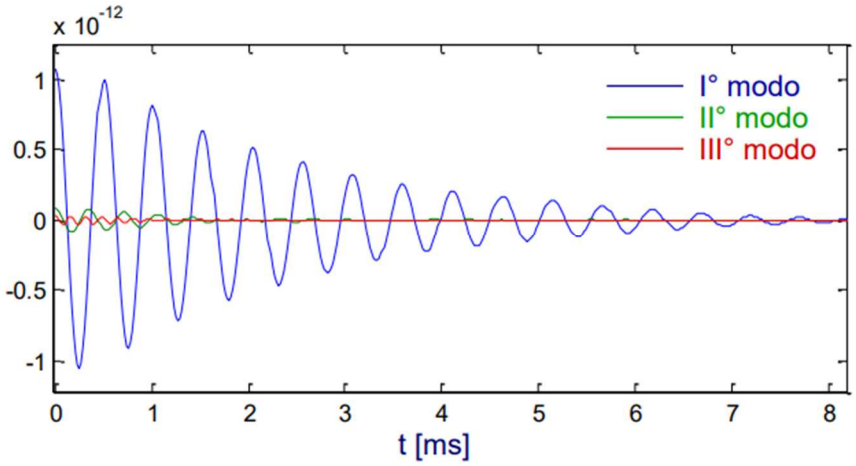

Picture 15: The IFFT of a PSD returns time histories similar to those of a damped SDOF oscillator free to vibrate.

The intersection with the abscissa axis gives the natural frequencies for each system and the damping coefficients are estimated through logarithmic decreases.

Chapter 2
Truck-bridge dynamic interaction through a 2DOF system

When dynamic testing is to be performed on a bridge, the OMA are a fast, cheap and efficient solution. When running an OMA on an unloaded bridge, by following the precautions set out in the previous chapter, the analysis should lead to results that are easy to interpret. To give consistency to the results and ensure that the model is valid, the test might also be carried on the loaded bridge. The loading configuration of the static test turns out to be a good opportunity to perform these further tests, since the structure is under the action of loads whose position and intensity are known.
The loads usually consist of heavy trucks deployed in one or multiple rows both longitudinally and transversely with respect of the bridge span, their weight can reach up to 50 tons and can change significantly the dynamic behaviour of the bridge. They are usually modelled on the FEM model as added masses on a bridge span.

This chapter shows how this modelling can lead to very different results from the experimental ones, implying in some cases a negative judgment of the final dynamic test. A more in-depth modelling consists in describing each truck as a dynamic system composed of a mass connected to the bridge deck by a deformable element, a spring whose stiffness represents the tires and shock absorbers system. In this way, the model takes into account the dynamic interaction that occurs between the trucks and the bridge. The problem is studied comparing the dynamic behaviour of three simple systems, the unloaded bridge is reduced to a 1DOF system, the modelling with added masses is represented again with a 1DOF system, and eventually a 2DOF system is used to study the dynamic interaction.

2.1. Modal analysis for the 1DOF systems

To study the dynamic behaviour of the unloaded bridge, it is reduced to a 1DOF system, The mass of the oscillator is equal to the mass of the bridge while its stiffness is equal to the stiffness of the bridge.

To reproduce the modelling of the trucks on the bridge during the loaded configuration as added masses, the mass of the system has to be equal to the sum of the mass of the bridge and the mass of the trucks, keeping the stiffness constant.

Picture 16: Mechanical schemes of the 1DOF systems.

A system with 1-DOF has only one natural frequency ω, its value is simply the square root of the ratio between the stiffness and the mass:

$$\omega_2 = \sqrt{\frac{k_2}{m_2}}$$

$$\tilde{\omega} = \sqrt{\frac{k_2}{m_1 + m_2}} = \sqrt{\frac{k_2}{m_2\left(1 + \frac{m_1}{m_2}\right)}} = \omega_2 \sqrt{\frac{1}{\left(1 + \frac{1}{\bar{m}}\right)}} = \omega_2 \sqrt{\frac{\bar{m}}{(1 + \bar{m})}}$$

2.2. Modal analysis for the 2DOF system

Indeed, from a dynamic point of view considering the system composed of the trucks and the bridge as a two-coupled spring-mass system would be more rigorous. The bridge and the truck are reduced to a 2DOF system and modelled as two coupled spring-mass system not subject to damping. The truck is linked to the bridge by means of a spring whose stiffness is k_1 , that represents the tires and shock absorbers system.

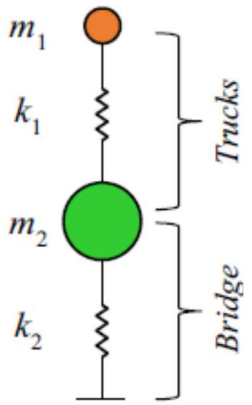

Picture 17: mechanical scheme of the 2DOF system.

Being k_1 and m_1 respectively the stiffness and the mass of the truck, and being k_2 and m_2 respectively the stiffness and the mass of the bridge, the dynamic equation for the system in matrix form is:

$$\begin{bmatrix} m_1 & 0 \\ 0 & m_2 \end{bmatrix} \begin{bmatrix} \ddot{u}_1^2 \\ \ddot{u}_2^2 \end{bmatrix} + \begin{bmatrix} k_1 & -k_1 \\ -k_1 & k_1 + k_2 \end{bmatrix} \begin{bmatrix} u_1 \\ u_2 \end{bmatrix} = 0$$

Which can be written in the frequency domain as:

$$\begin{bmatrix} k_1 & -k_1 \\ -k_1 & k_1 + k_2 \end{bmatrix} \begin{bmatrix} u_1 \\ u_2 \end{bmatrix} - \omega^2 \begin{bmatrix} m_1 & 0 \\ 0 & m_2 \end{bmatrix} \begin{bmatrix} u_1 \\ u_2 \end{bmatrix} = 0$$

The displacements are a common term and can be collected:

$$\left\{ \begin{bmatrix} k_1 & -k_1 \\ -k_1 & k_1 + k_2 \end{bmatrix} - \omega^2 \begin{bmatrix} m_1 & 0 \\ 0 & m_2 \end{bmatrix} \right\} \begin{bmatrix} u_1 \\ u_2 \end{bmatrix} = 0$$

Performing some substitutions it is possible to obtain problem depending on two parameters, $\frac{\omega_2}{\omega_1} = \hat{\omega}$ and $\frac{m_2}{m_1} = \hat{m}$.

First it is necessary to divide by k_1:

$$\left\{ \begin{bmatrix} 1 & -1 \\ -1 & 1 + \frac{k_2}{k_1} \end{bmatrix} - \omega^2 \begin{bmatrix} \frac{m_1}{k_1} & 0 \\ 0 & \frac{m_2}{k_1} \end{bmatrix} \right\} \begin{bmatrix} u_1 \\ u_2 \end{bmatrix} = 0$$

Using the relations $\omega^2 = \frac{k}{m}$ and collecting ω_1^2 from the second term:

$$\left\{ \begin{bmatrix} 1 & -1 \\ -1 & 1 + \frac{m_2 \omega_2^2}{m_1 \omega_1^2} \end{bmatrix} - \frac{\omega^2}{\omega_1^2} \begin{bmatrix} 1 & 0 \\ 0 & \frac{m_2}{m_1} \end{bmatrix} \right\} \begin{bmatrix} u_1 \\ u_2 \end{bmatrix} = 0$$

Eventually, the system can be written as:

$$\left\{ \begin{bmatrix} 1 & -1 \\ -1 & 1 + \hat{m}\hat{\omega}^2 \end{bmatrix} - \frac{\omega^2}{\omega_1^2} \begin{bmatrix} 1 & 0 \\ 0 & \hat{m} \end{bmatrix} \right\} \begin{bmatrix} u_1 \\ u_2 \end{bmatrix} = 0$$

A two degree of freedom system has two normal modes of vibration corresponding to two natural frequencies. In order to find the modal parameter, the eigenvalue problem must be solved:

$$det \left\{ \begin{bmatrix} 1 & -1 \\ -1 & 1 + \hat{m}\hat{\omega}^2 \end{bmatrix} - \frac{\omega^2}{\omega_1^2} \begin{bmatrix} 1 & 0 \\ 0 & \hat{m} \end{bmatrix} \right\} = 0$$

The determinant of the matrix is calculated:

$$\left(1-\frac{\omega^2}{\omega_1^2}\right)\left(1+\hat{m}\hat{\omega}^2-\frac{\omega^2}{\omega_1^2}\hat{m}\right)-1=0$$

Carrying out the multiplications and rearranging the equation:

$$\left(\frac{\omega^2}{\omega_1^2}\right)^2\hat{m}+\frac{\omega^2}{\omega_1^2}(-\hat{m}-1-\hat{m}\hat{\omega}^2)+\hat{m}\hat{\omega}^2=0$$

Calling $\frac{\omega^2}{\omega_1^2}=\lambda$ it is possible to find the eigenvalues by solving the equation of the characteristic polynomial:

$$\lambda^2\hat{m}+\lambda(-\hat{m}-1-\hat{m}\hat{\omega}^2)+\hat{m}\hat{\omega}^2=0$$

Which after some calculations leads to:

$$\lambda_{1-2}=\frac{1+\hat{m}(1+\hat{\omega}^2)\pm\sqrt{\left(1+\hat{m}(1+\hat{\omega}^2)\right)^2-4\hat{m}^2\hat{\omega}^2}}{2\hat{m}}$$

The two circular frequencies of the 2DOF system can be expressed as:

$$\frac{\omega}{\omega_1}=\sqrt{\frac{1+\hat{m}(1+\hat{\omega}^2)\pm\sqrt{\left(1+\hat{m}(1+\hat{\omega}^2)\right)^2-4\hat{m}^2\hat{\omega}^2}}{2\hat{m}}}$$

2.3. Comparison between the 1DOF and the 2DOF systems

Picture 18 plots $\frac{\omega}{\omega_2}=\frac{\omega}{\omega_1}\frac{1}{\hat{\omega}}$ for a fixed value of $\hat{m}=0.6$. The grey line represents the frequency of the 1-DOF system with m=m1+m2, which is a constant value lower than one. The blue line is the first circular frequency of the 2DOF system and the orange line represents the second one. For low values of the ratio $\frac{\omega_1}{\omega_2}$ the value of the first circular frequency of the system approaches to zero, while the value of the second circular frequency tends to 1.

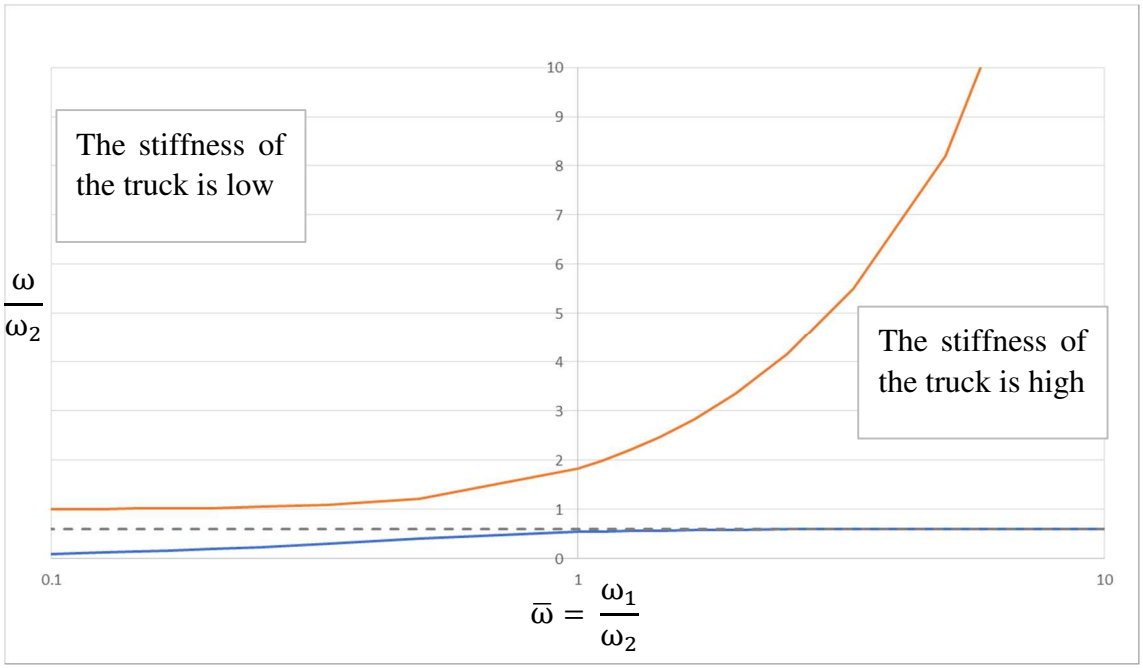

Picture 18: Frequencies of the 2-DOF system.

For a fixed mass ratio, when the $\frac{\omega_1}{\omega_2}$ ratio is low, the frequency of the truck is much lower than the one of the bridge and so is its stiffness compared to the one of the bridge. In this system, the first mode of vibrating, relative to the first circular frequency, sees both masses moving in a concordant direction, but due to the low stiffness of the truck the vibration period is high and ω tends to zero. The second vibrational mode in a 2-DOF system sees the masses moving in opposite directions, if $\frac{\omega}{\omega_2}$ tends to one it means that the system vibrates with the same frequency as the bridge without the truck would vibrate. For high values of the $\frac{\omega}{\omega_2}$ ratio, the first circular frequency of the system tends to the same value obtained with the 1-DOF modelling. In fact, when the stiffness of the truck increases it tends to be integral with the bridge. The second circular frequency growing fast with respect of ω_2 is related to the second way of vibrating, which sees the truck oscillating very quickly and the bridge moving very little.

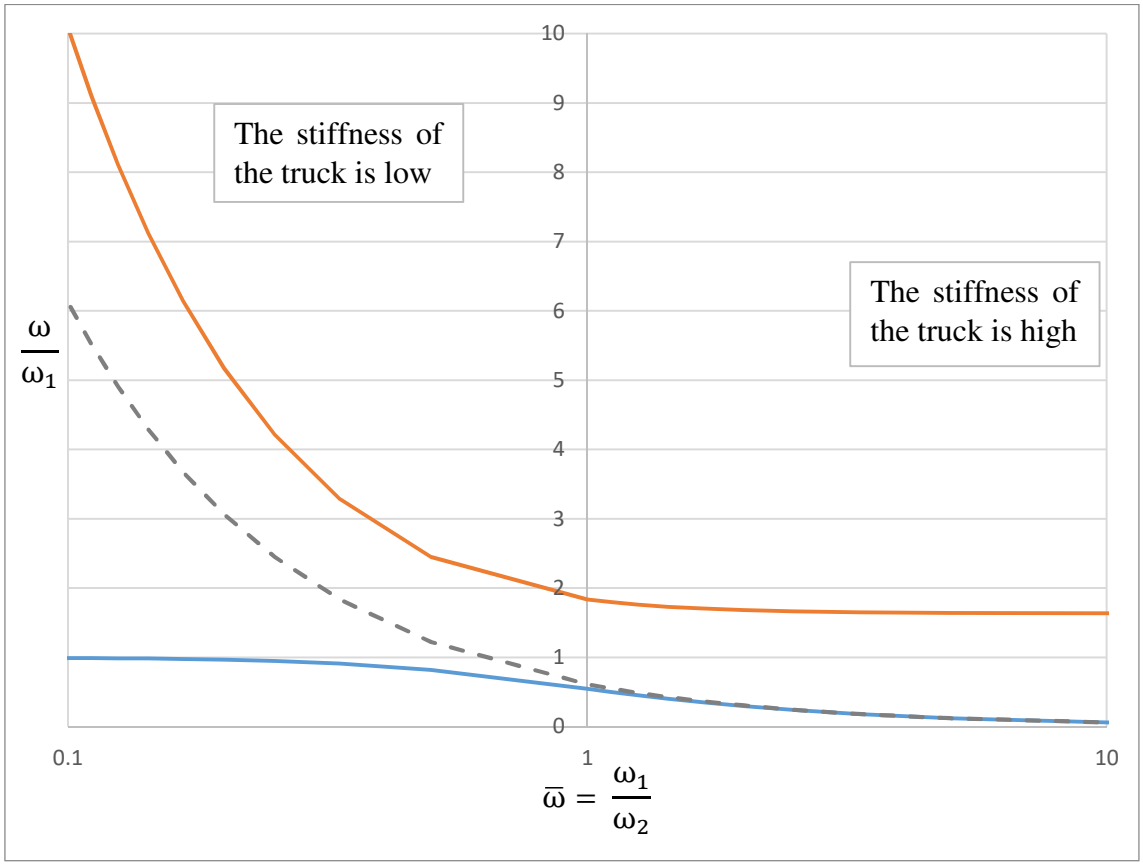

Picture 19: Frequencies of the 2-DOF system.

These results can be more easily comprehended from the Picture 19, that plots $\frac{\omega}{\omega_2}$. In conclusion, for low values of the ratio $\frac{\omega_1}{\omega_2}$, the first circular frequency of the 2DOF system tends to the frequency of the truck alone, while the second circular frequency of the system tends to the one of the bridge alone. For high values of the ratio $\frac{\omega_1}{\omega_2}$, the first circular frequency of the 2DOF system tends to the frequency 1-DOF system.

The influence of the mass ratio $\hat{m}$ can be seen from Picture 20, which compares the case of m equal to 0.5 and that of m equal to 1.7. The green and the red curve are the frequencies of a system with $\hat{m} = 5$, while the orange and the blue ones to a system with $\hat{m} = 0.6$. As the mass of the truck increases, the range of frequencies for which it behaves as a TMD is wider

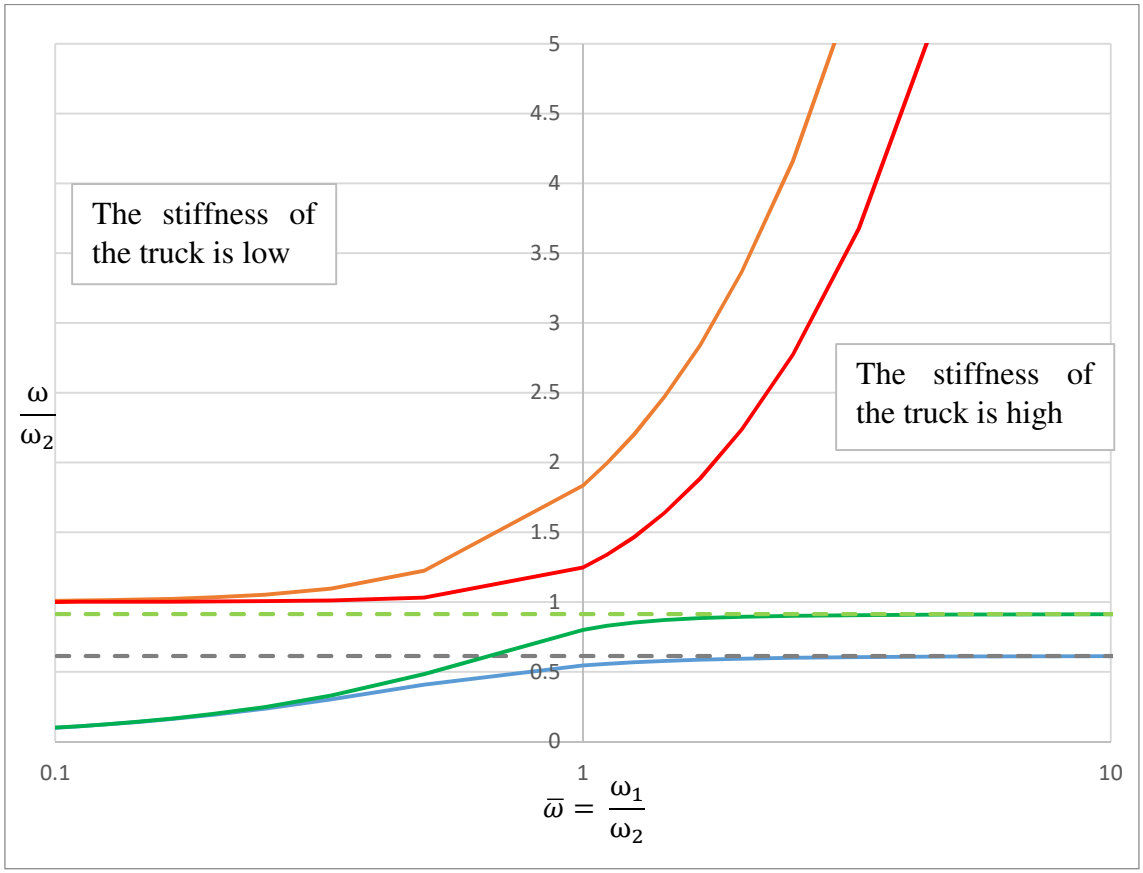

Picture 20: Comparison of the frequencies of two 2-DOF systems with different mass ratio.

2.4. The FRFs of the 2-DOF system

To better understand the dynamic interaction, it is useful to observe the FRFs of the displacements of the systems shown in Picture 21 and Picture 22. The FRFs for three different $\bar{\omega}$ ratios have been obtained by applying a steady state unit displacement at the base.

The blue line is the FRF of the bridge in the unloaded condition, the grey line represents the modelling with added masses, while the yellow, red and green lines represent the displacements of the system measured from the deck for different ration of $\bar{\omega}$.

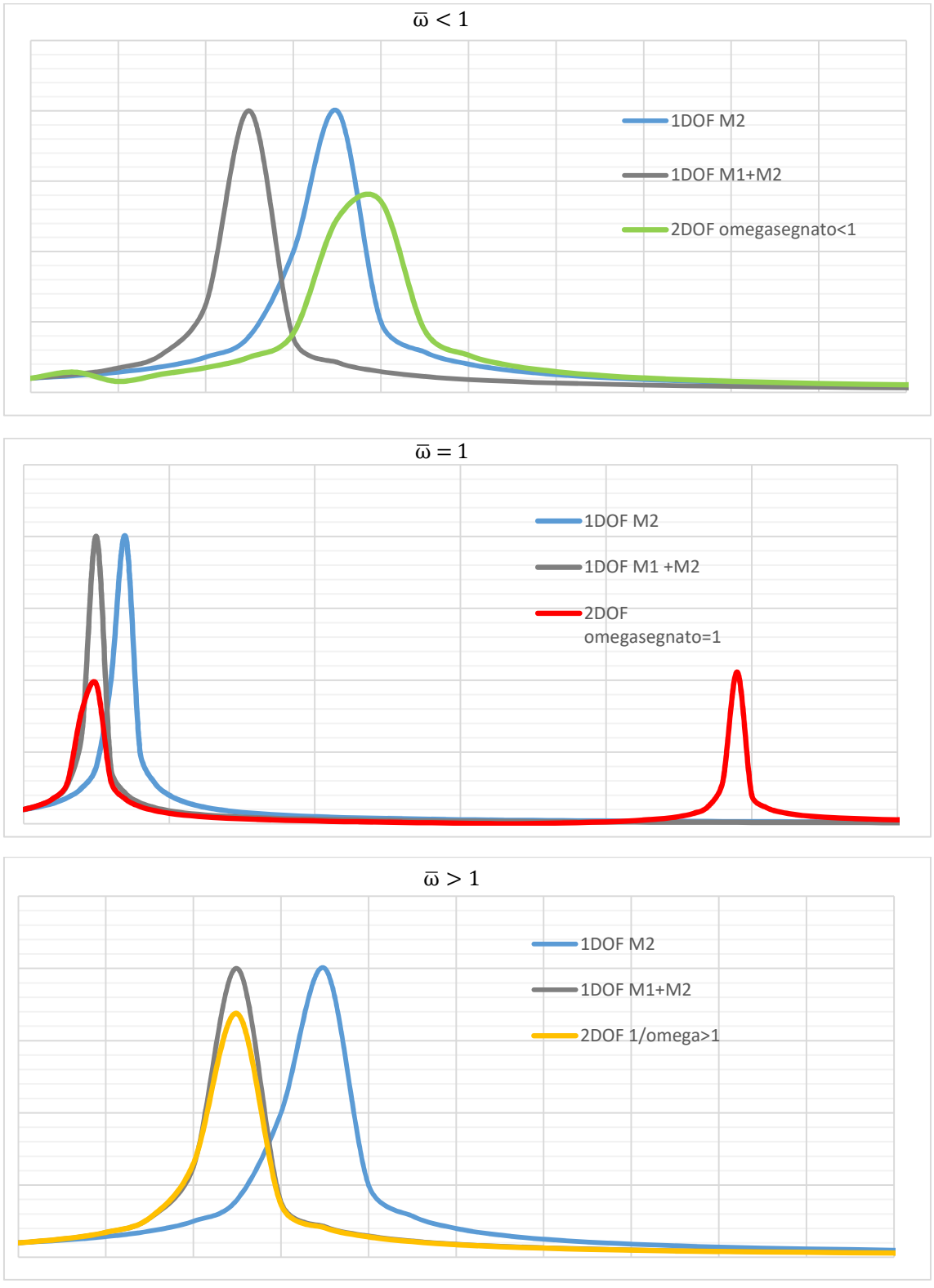

Picture 21: The FRFs of the 2 DOF system for different ratios $\frac{1}{\bar{\omega}}$.

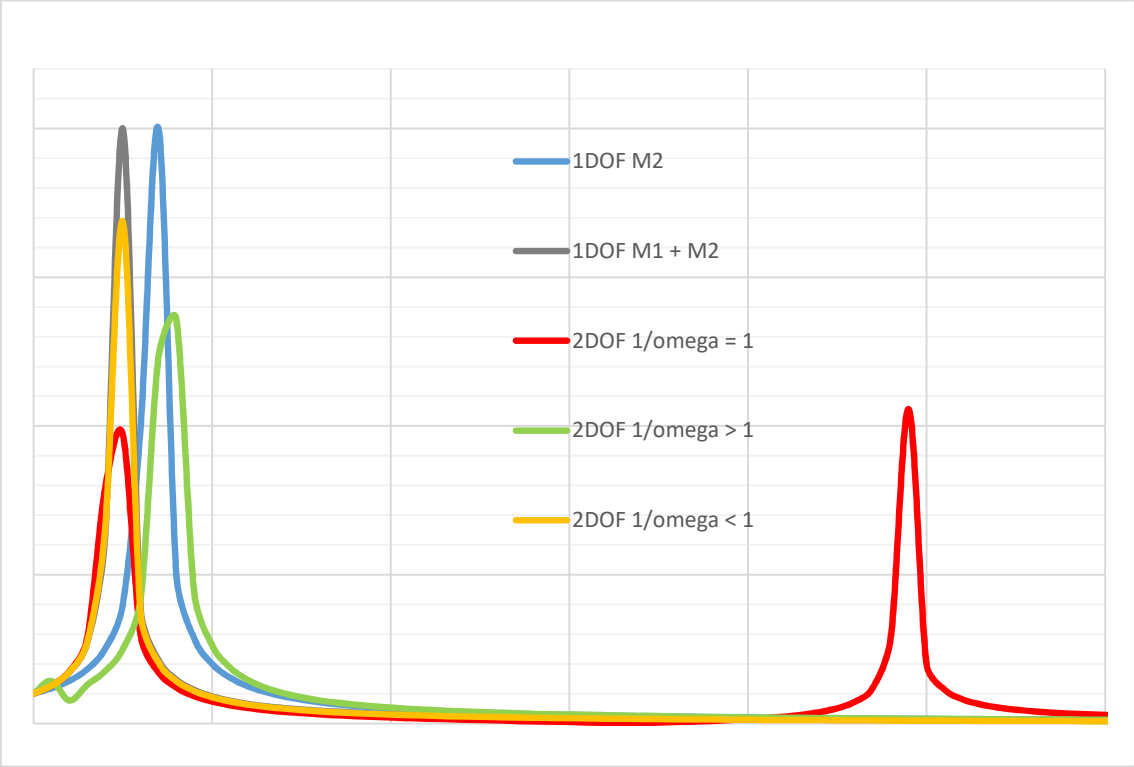

Picture 22: FRF of the five systems compared

For $\bar{\omega} < 1$, the peak of the grey curve occurs for lower frequencies compared to the green curve, therefore the 1-DOF system underestimates the fundamental frequency of the bridge. There is a discrepancy between the results obtained by the 1DOF model and the experimental data that would be obtained with an OMA, which could lead the designer to conclude that the structure is more deformable than he had foreseen from the FE model. This would lead to a failure of the dynamic test. Notice that for this scenario the first frequency of the system, which is the first peak of the FRF, cannot be considered the fundamental frequency of the bridge. In fact, this is a frequency for which the truck is more excited and consequently it produces a small perturbation on the bridge, which results in a peak of the FRF. This is in accordance with the conclusions drawn in the previous section, namely that in this situation the first frequency of the system is the same as that of the truck and the second frequency of the system corresponds to that of the bridge alone. It can be concluded that for these cases the second frequency of the 2DOF system must be compared with the fundamental frequency obtained from the OMA. The simplest case occurs when $\bar{\omega} > 1$, in this case the highest peak of the FRF is also the first to occur, meaning that the first frequency of the 2DOF system is the one that must be compared to the results from OMA.

However, in the transition from the first to the second situation, the intensity of the first peak must increase and that of the second must decrease. This means that there is a range of values of $\bar{\omega}$ for which the two peaks have a comparable intensity and both mode shapes of the system may be of interest. For values of $\bar{\omega} \approx 1$ the two peaks of similar intensity occurs because of the truck behaving as a tuned mass damper for the bridge, vibrating in opposition with the excitation and counteracting it. As a result, the vibration on the bridge with the truck are lower than the vibration of the bridge alone.

2.5. Conclusions

The comparison between the three different systems allows us to conclude that the model with added masses does not correctly identify the fundamental frequency of the structure. This modelling underestimates the first frequency when the stiffness of the truck is low, while it overestimates it when the truck is very stiff. There are intermediate cases in which the tuned mass damper phenomenon occurs, the truck works as a damper and it creates a trough in the frequency response with practically no response at damper inherent frequency.

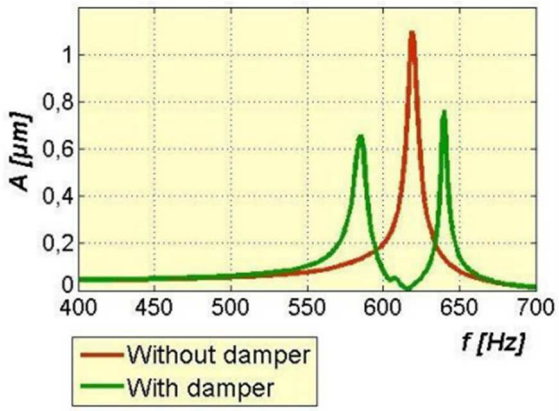

Picture 23: FRF of a system with and without a mass damper.

For these cases, the frequency calculated with the added mass model is significantly different from that of the 2DOF model, since this neglects the effect of the damper.

The 2DOF system allows you to easily identify the fundamental frequency of the bridge when the truck is not very rigid or very rigid. In both cases it can be assumed as the frequency at which the FRF has the highest peak. If the truck is very flexible this will happen for the second peak of the FRF, while if the truck stiffens the first peak of the curve is also the highest one. By increasing the stiffness of the truck, the first peak of the

curve grows until it reaches the intensity of the second peak, this occurs when the truck behaves as a damper. There are two modes of the system which both have the properties of the first mode of vibrating, the same shape and comparable amplitudes. This problem is dealt with more fully in the next chapters, using finite element model in which a simply supported beam represents the bridge, while masses connected to the beam by means of springs simulate the presence of trucks. The study is conducted for different mass ratios, different load configurations, and different loaded length over bridge length ratios.

Chapter 3
Definition of the parametric investigation

The purpose of the study conducted in this thesis work is to monitor the frequencies of a set of bridges with different properties under typical load configurations of static tests. Only single-span bridges with a constant section are considered.

Generally the trucks used for the static test have a weight ranging from 30 to 50 tons, a length of about 8.5 meters and are arranged about one meter from each other. It is reasonable to assume a model truck representative of those used during testing as one with a weight of 40 tons and a length of 10 meters.

The Picture 24 shows the load configurations generally used during a static load test. One, two or four trucks are set longitudinally, while one to three trucks are set crosswise.

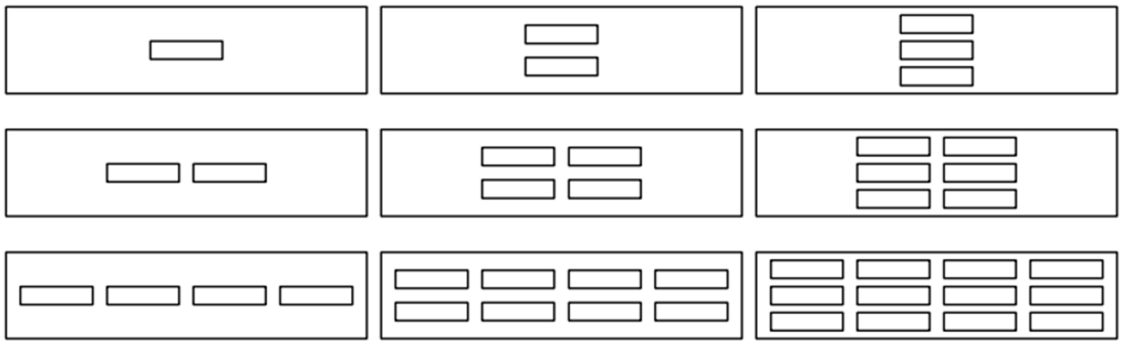

Picture 24: Loading configurations for static load tests

Three parameters regulate the problem. One is the lengths ratio $\bar{L}$, defined as the ratio between the loaded deck length and the total length of the deck, three values of $\bar{L}$ have been chosen for which to carry out the subsequent analyses: $\bar{L} = 0{,}25$, $\bar{L} = 0{,}50$ and $\bar{L} = 0{,}75$. Table 1 shows the 9 lengths of the deck obtained. It was decided to conduct the analyses on single-span bridges of various lengths, with spans ranging from 10 to 160 meters.

Table 2: Lenghts of the decks.

One truck longitudinally		Two trucks longitudinally		Four trucks longitudinally	
L_{loaded} / L_{deck}	L_{deck}	L_{loaded} / L_{deck}	L_{deck}	L_{loaded} / L_{deck}	L_{deck}
[/]	[m]	[/]	[m]	[/]	[m]
0.25	40.00	0.25	80.00	0.25	160.00
0.50	20.00	0.50	40.00	0.50	80.00
0.75	13.33	0.75	26.67	0.75	53.33

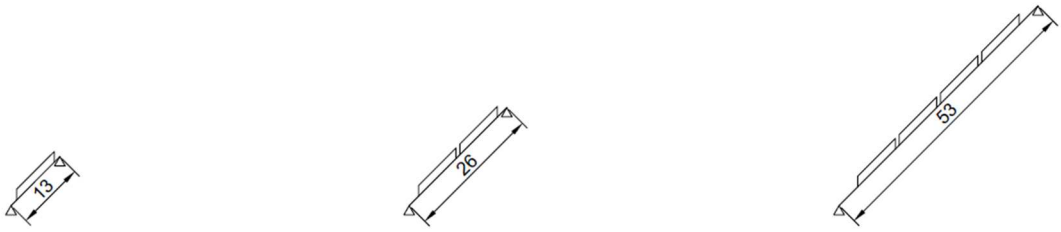

Picture 25: Bridges lengths for $\bar{L}$=0.75

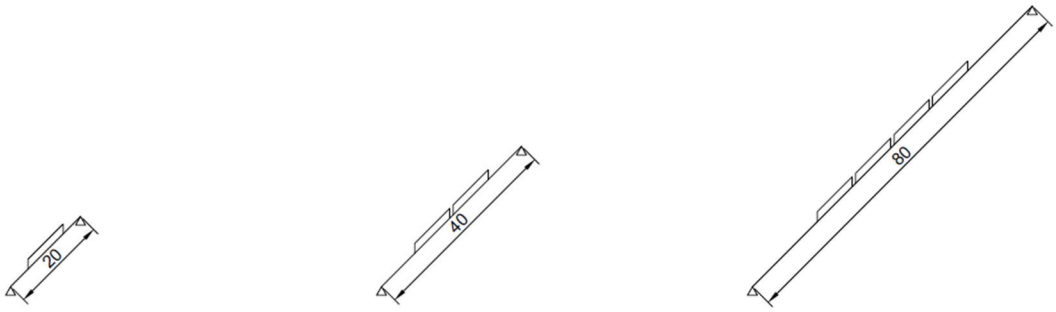

Picture 26: Bridges lengths for $\bar{L}$=0.50

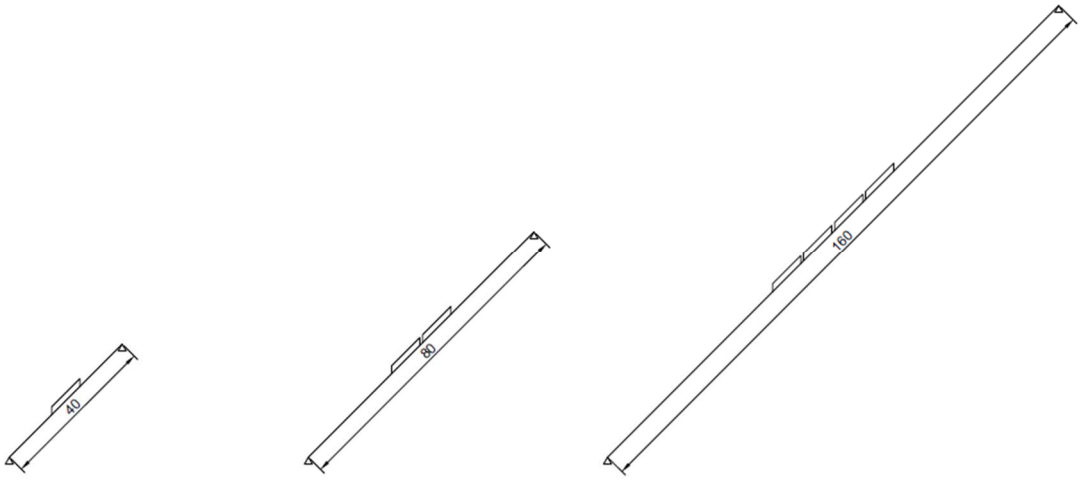

Picture 27: Bridges lengths for $\bar{L}$=0.25

The comparison of the curves obtained from two simple systems with 2-DOF with different mass ratios, it emerged that this is a key parameter. The mass ratio for the finite element analysis is defined as the ratio between the mass of the truck and the mass of the loaded deck area, $\overline{m} = \frac{M_{truck}}{M_{loaded\ deck}}$. Since the mass of the truck is set to 40 tons, $\overline{m}$ changes with respect to the number of transverse trucks and the section properties of the deck. To find the range of interest of the mass ratios, four different types of sections are considered for the deck.

3.1. Mass ratios for steel-concrete composite sections

Composite sections are a popular choice in the realization of a bridge, since they combine some advantages of steel bridges with some key factors of concrete bridges. The steel main structure is much easier to erect if compared to the construction of a concrete girder and the final structure is light, which imposes smaller loads on piers and foundations, allowing for economy.

The main types of sections used for continuous decks on one span can be traced back to the two layouts of double steel beam and box section.

The double steel beam section, consisting of two I-beams, is the one most used, for simplicity and economy. A bridge section is composed of the metallic carpentry, the concrete slab and finally the road pavement.

The box section is obtained with a metal beam open at the top, on which is casted a concrete slab. It is generally heavier than the previous one, and more complex to manufacture, since the metal carpentry is entirely made in the workshop.

In calculating the mass ratios, a deck width of 12 meters and a thickness of the concrete slab of 25 cm with a density of 25 kN/m^3 are chosen. The road pavement has a thickness of 12 cm and a density of 20 kN/m^3. The weight of the metal structure depends on the length of the span, from the graph in Picture 28 it is possible estimate its weight once the length of the deck has been chosen. The Table 3 and Table 4 show the results of the calculation.

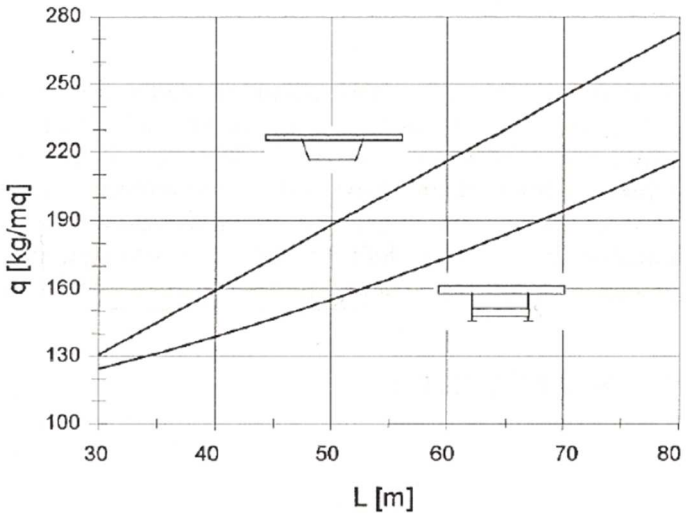

Picture 28: Weight of the metallic carpentry for two-I and box composite beams

Table 3: Mass ratios for Two-I composite beams

Two-I composite beam					
Weight of the metallic carpentry			From the graph		
Slab thickness			0.25 meters		
Concrete density			25.00 kN/m^3		
Road pavement thickness			0.12 meters		
Road pavement density			20.00 kN/m^3		
Weight/meter concrete+pavement			103.80 kN/ml		
Tons/ml concrete+pavement			10.38 t/ml		
Longitudinal number of trucks		1	$\bar{m} = \frac{M_{truck}}{M_{loaded\ deck}}$		
			Number of trucks in the cross section		
$\bar{L}$	L_{deck}	$\frac{Bridge\ weight}{1\ meter}$	1.00	2.00	3.00
[-]	[m]	[t/ml]	[-]	[-]	[-]
0.25	40.00	12.00	0.33	0.67	1.00
0.50	20.00	11.76	0.34	0.68	1.02
0.75	13.33	11.68	0.34	0.68	1.03
Longitudinal number of trucks		2	$\bar{m} = \frac{M_{truck}}{M_{loaded\ deck}}$		
			Number of trucks in the cross section		
$\bar{L}$	L_{deck}	$\frac{Bridge\ weight}{1\ meter}$	1.00	2.00	3.00
[-]	[m]	[t/ml]	[-]	[-]	[-]
0.25	80.00	12.48	0.32	0.64	0.96
0.50	40.00	12.00	0.33	0.67	1.00
0.75	26.67	11.84	0.34	0.68	1.01
Longitudinal number of trucks		4	$\bar{m} = \frac{M_{truck}}{M_{loaded\ deck}}$		
			Number of trucks in the cross section		
$\bar{L}$	L_{deck}	$\frac{Bridge\ weight}{1\ meter}$	1.00	2.00	3.00
[-]	[m]	[t/ml]	[-]	[-]	[-]
0.25	160.00	13.44	0.30	0.60	0.89
0.50	80.00	12.48	0.32	0.64	0.96
0.75	53.33	12.16	0.33	0.66	0.99

Table 4:Mass ratios for Box section composite Beam

Box section					
Weight of the metallic carpentry		From the graph			
Slab thickness		0.25 meters			
Concrete density		25.00 kN/m^3			
Road pavement thickness		0.12 meters			
Road pavement density		20.00 kN/m^3			
Weight/meter concrete+pavement		103.80 kN/ml			
Tons/ml concrete+pavement		10.38 t/ml			
Longitudinal number of trucks	1	$\bar{m} = \frac{M_{truck}}{M_{loaded\ deck}}$			
			Number of trucks in the cross section		
$\bar{L}$	L_{deck}	$\frac{Bridge\ weight}{1\ meter}$	1.00	2.00	3.00
[-]	[m]	[t/ml]	[-]	[-]	[-]
0.25	40.00	12.30	0.33	0.65	0.98
0.50	20.00	11.58	0.35	0.69	1.04
0.75	13.33	11.34	0.35	0.71	1.06
Longitudinal number of trucks	2	$\bar{m} = \frac{M_{truck}}{M_{loaded\ deck}}$			
			Number of trucks in the cross section		
$\bar{L}$	L_{deck}	$\frac{Bridge\ weight}{1\ meter}$	1.00	2.00	3.00
[-]	[m]	[t/ml]	[-]	[-]	[-]
0.25	80.00	12.48	0.32	0.64	0.96
0.50	40.00	12.00	0.33	0.67	1.00
0.75	26.67	11.84	0.34	0.68	1.01
Longitudinal number of trucks	4	$\bar{m} = \frac{M_{truck}}{M_{loaded\ deck}}$			
			Number of trucks in the cross section		
$\bar{L}$	L_{deck}	$\frac{Bridge\ weight}{1\ meter}$	1.00	2.00	3.00
[-]	[m]	[t/ml]	[-]	[-]	[-]
0.25	160.00	13.44	0.30	0.60	0.89
0.50	80.00	12.48	0.32	0.64	0.96
0.75	53.33	12.16	0.33	0.66	0.99

3.2. Mass ratios for sections in prestressed concrete

Concrete is the most popular structural material for bridges, and prestressed concrete is frequently adopted. The advantages of this type of bridge over more traditional designs is that it is quicker to install, more economical and longer-lasting. Compared with simple reinforced concrete, prestressed concrete improved performance can allow for longer

spans, reduced structural thicknesses, and material savings. In short-span bridges of around 10 to 40 metres, prestressing is commonly employed in the form of precast pre-tensioned girder. Medium-length structures of around 40 to 200 metres, typically use precast-segmental, in-situ balanced-cantilever and incrementally-launched designs. For the longest bridges, prestressed concrete deck structures often form an integral part of cable-stayed designs.

The main types of sections used for continuous decks on one span can be traced back to the two layouts of multiple beams and box section.

The section height grows as the length of the span increases. For the calculation of $\bar{m}$, the ratio L/H for a box section is equal to 18, while for a section with multiple beams the is 16. The other parameters of the section, such as the deck width, the thickness of the concrete slab and density of 25 kN/m^3 are the same of the ones adopted for the composite sections. The Table 3 and Table 4 show the results of the calculation.

Table 5: Mass ratios for box section beams in PC

Box section in prestressed concrete							
Ratio L/H					18.00		
Concrete density					25.00 kN/m^3		
Longitudinal number of trucks				1	$\bar{m} = \frac{M_{truck}}{M_{loaded\ deck}}$		
					Number of trucks in the cross		
$\bar{L}$	L_{deck}	$H_{section}$	Section Area	$\frac{Bridge\ weight}{1\ meter}$	1.00	2.00	3.00
[-]	[m]	[m]	[m^2]	[t/ml]	[-]	[-]	[-]
0.25	40.00	2.22	6.29	15.73	0.25	0.51	0.76
0.50	20.00	1.11	5.20	13.00	0.31	0.62	0.92
0.75	13.33	0.74	4.80	12.01	0.33	0.67	1.00
Longitudinal number of trucks				2	$\bar{m} = \frac{M_{truck}}{M_{loaded\ deck}}$		
					Number of trucks in the cross		
$\bar{L}$	L_{deck}	$H_{section}$	Section Area	$\frac{Bridge\ weight}{1\ meter}$	1.00	2.00	3.00
[-]	[m]	[m]	[m^2]	[t/ml]	[-]	[-]	[-]
0.25	80.00	4.44	8.48	21.20	0.19	0.38	0.57
0.50	40.00	2.22	6.29	15.73	0.25	0.51	0.76
0.75	26.67	1.48	5.56	13.91	0.29	0.58	0.86
Longitudinal number of trucks				4	$\bar{m} = \frac{M_{truck}}{M_{loaded\ deck}}$		
					Number of trucks in the cross		
$\bar{L}$	L_{deck}	$H_{section}$	Section Area	$\frac{Bridge\ weight}{1\ meter}$	1.00	2.00	3.00
[-]	[m]	[m]	[m^2]	[t/ml]	[-]	[-]	[-]
0.25	160.00	8.89	12.86	32.16	0.12	0.25	0.37
0.50	80.00	4.44	8.48	21.20	0.19	0.38	0.57
0.75	53.33	2.96	7.02	17.55	0.23	0.46	0.68

Table 6: Mass ratios for multiple beams section in PC

Multiple beams section in prestressed concrete							
Ratio L/H					16.00		
Concrete density					25.00 kN/m³		
Longitudinal number of trucks				1	$\bar{m} = \frac{M_{truck}}{M_{loaded\ deck}}$		
					Number of trucks in the cross		
$\bar{L}$	L_{deck}	$H_{section}$	Section Area	$\frac{Bridge\ weight}{1\ meter}$	1.00	2.00	3.00
[-]	[m]	[m]	[m²]	[t/ml]	[-]	[-]	[-]
0.25	40.00	2.50	5.04	12.59	0.32	0.64	0.95
0.50	20.00	1.25	4.04	10.09	0.40	0.79	1.19
0.75	13.33	0.83	3.70	9.25	0.43	0.86	1.30
Longitudinal number of trucks				2	$\bar{m} = \frac{M_{truck}}{M_{loaded\ deck}}$		
					Number of trucks in the cross		
$\bar{L}$	L_{deck}	$H_{section}$	Section Area	$\frac{Bridge\ weight}{1\ meter}$	1.00	2.00	3.00
[-]	[m]	[m]	[m²]	[t/ml]	[-]	[-]	[-]
0.25	80.00	5.00	8.48	21.20	0.19	0.38	0.57
0.50	40.00	2.50	5.04	12.59	0.32	0.64	0.95
0.75	26.67	1.67	4.37	10.93	0.37	0.73	1.10
Longitudinal number of trucks				4	$\bar{m} = \frac{M_{truck}}{M_{loaded\ deck}}$		
					Number of trucks in the cross		
$\bar{L}$	L_{deck}	$H_{section}$	Section Area	$\frac{Bridge\ weight}{1\ meter}$	1.00	2.00	3.00
[-]	[m]	[m]	[m²]	[t/ml]	[-]	[-]	[-]
0.50	80.00	5.00	8.48	21.20	0.19	0.38	0.57
0.75	53.33	3.33	5.70	14.25	0.28	0.56	0.84

Therefore the range of $\bar{m}$ goes from 0.2 to 1.4.

3.3. Conclusions

The set of cases object of the study includes nine different load configurations for which three length ratios have been chosen. In addition, from the previous tables has been evaluated a range for the mass ratio values that goes from 0.2 to 1.4. The Table 7 recaps all the parameters taken into account. The set of studies in this work includes 189 different cases.

Table 7: Set of cases object of study

Longitudinal number of trucks	Number of trucks in the cross section	$\bar{L}$	$\bar{m}$
1	1	0.25, 0.50, 0.75	0.2-0.4-0.6-0.8-1-1.2-1.4
	2	0.25, 0.50, 0.75	0.2-0.4-0.6-0.8-1-1.2-1.4
	3	0.25, 0.50, 0.75	0.2-0.4-0.6-0.8-1-1.2-1.4
2	1	0.25, 0.50, 0.75	0.2-0.4-0.6-0.8-1-1.2-1.4
	2	0.25, 0.50, 0.75	0.2-0.4-0.6-0.8-1-1.2-1.4
	3	0.25, 0.50, 0.75	0.2-0.4-0.6-0.8-1-1.2-1.4
4	1	0.25, 0.50, 0.75	0.2-0.4-0.6-0.8-1-1.2-1.4
	2	0.25, 0.50, 0.75	0.2-0.4-0.6-0.8-1-1.2-1.4
	3	0.25, 0.50, 0.75	0.2-0.4-0.6-0.8-1-1.2-1.4

Chapter 4

The FEM model

The numerical model is developed using the finite elements method.

The trucks on the bridge are modelled as single masses linked to the bridge by means of a singular spring positioned in the second end of the beam. This allows placing the trucks in any part of the beam. Therefore, the bridge is modelled as a succession of FEs consisting of a beam that presents a spring with a mass attached in the final extremity.

The FE method allows finding the displacement field in the continuum $\mathbf{u}(\omega, z)$ starting from the minimum total potential energy principle for a dynamic system, which can be written using the D'Alambert principle. Hereafter it is possible to move on the discrete problem, in which the solution $\mathbf{u}(\omega, z)$ is known starting from $\mathbf{u}_{el}$, which are the displacements of the degrees of freedom, that is a discrete number of parameters.

4.1. Definitions

The displacements for a point in the beam centreline:

$$\mathbf{u}(\omega, z) = [u_2(\omega, z) \quad u_3(\omega, z)]^T$$

The mass relative displacements:

$$\mathbf{v}(\omega) = [v_2 \quad v_3]^T$$

$\mathcal{D}$ is the differential operator for the beam strain calculation:

$$\mathcal{D}\mathbf{u}(\omega, z) = \left[-\frac{\partial^2 u_2}{\partial z^2} \quad \frac{\partial u_3}{\partial z}\right]^T$$

The beam mass matrix:

$$\mathbf{m} = \rho A \begin{bmatrix} 1 & 0 \\ 0 & 1 \end{bmatrix}$$

Beam sectional stiffness matrix:

$$\mathbf{k}(\omega, z) = \mathrm{E} \begin{bmatrix} I & 0 \\ 0 & A \end{bmatrix}$$

Stress on the beam:

$$\mathbf{s}(\omega, z) = \mathbf{k}\mathcal{D}\mathbf{u}(\omega, z)$$

The mass matrix for a truck**:**

$$\bar{\mathbf{m}} = \begin{bmatrix} m_v & 0 \\ 0 & m_o \end{bmatrix}$$

The stiffness matrix for a truck:

$$\bar{\mathbf{k}} = \begin{bmatrix} k_v & 0 \\ 0 & k_o \end{bmatrix}$$

4.2. The dynamic equilibrium for the mass

The dynamic equilibrium in the frequency domain for the mass on the spring, is analogous to the equilibrium for a simple harmonic oscillator, written neglecting viscosity:

$$\ddot{\mathbf{v}}(t) = -\omega^2 \mathbf{v}(\omega) \qquad \ddot{\mathbf{u}}(L, \mathrm{t}) = -\omega^2 \mathbf{u}(L, \omega)$$

$$-\omega^2 \bar{\mathbf{m}}\mathbf{v}(\omega) + \bar{\mathbf{k}}\mathrm{v}(\omega) = \omega^2 \bar{\mathbf{m}}\mathbf{u}(L, \omega)$$

$$\left(\bar{\boldsymbol{k}} - \omega^2 \bar{\mathbf{m}}\right)\mathbf{v}(\omega) = \omega^2 \bar{\mathbf{m}}\mathbf{u}(L, \omega)$$

$$\bar{\mathbf{k}}\mathbf{v}(\omega) - \omega^2 \bar{\mathbf{m}}\left(\mathbf{v}(\omega) + \mathbf{u}(L, \omega)\right) = 0$$

$$\mathbf{v}(\omega) = \omega^2 \left(\bar{\boldsymbol{k}} - \omega^2 \bar{\mathbf{m}}\right)^{-1} \bar{\mathbf{m}}\mathbf{u}(L, \omega)$$

4.3. The weak formulation – Lagrange and D'Alembert principle

The weak form for this element is obtained using the principle of virtual work that equates the work of the internal stresses to the work of external actions for each virtual admissible variations $\hat{\mathbf{u}}$ and $\hat{\mathbf{v}}$. In addition, D'Alembert principle states that for a dynamic problem, for each state of motion, the mechanical equilibrium can be studied introducing

appropriate inertial forces. This means that it is possible to study a static equivalent condition introducing inertial forces.

The internal work of the beam is:

$$\int_0^L \mathbf{k}\mathcal{D}\mathbf{u}(\omega, z) \cdot \mathcal{D}\hat{\mathbf{u}}(z)dz$$

The external elastic work of the spring is:

$$\bar{\mathbf{k}}\mathbf{v}(\omega) \cdot \hat{\mathbf{u}}(L) + \bar{\mathbf{k}}\mathbf{v}(\omega) \cdot \hat{\mathbf{v}}$$

The kinetic energy of the beam is:

$$-\omega^2 \int_0^L \mathbf{m}\mathbf{u}(\omega, z) \cdot \hat{\mathbf{u}}(z)dz$$

The total inertial work of the mass is:

$$-\omega^2 \bar{\mathbf{m}}\big(\mathbf{v}(\omega) + \mathbf{u}(L, \omega)\big) \cdot \hat{\mathbf{v}}$$

Therefore the energetic equilibrium is:

$$\int_0^L \mathbf{k}\mathcal{D}\mathbf{u}(\omega, z) \cdot \mathcal{D}\hat{\mathbf{u}}(z)dz - \omega^2 \int_0^L \mathbf{m}\mathbf{u}(\omega, z) \cdot \hat{\mathbf{u}}(z)dz - \bar{\mathbf{k}}\mathbf{v}(\omega) \cdot \hat{\mathbf{u}}(L) + \big(\bar{\mathbf{k}} - \omega^2\bar{\mathbf{m}}\big)\mathbf{v}(\omega) \cdot \hat{\mathbf{v}} - \omega^2\bar{\mathbf{m}}\mathbf{u}(L, \omega) \cdot \hat{\mathbf{v}} = 0 \quad \forall \hat{\mathbf{u}}(z), \forall \hat{\mathbf{v}}$$

Being $\mathbf{d}(\omega, z)$ the vector that collects the displacements of the beam and the relative displacements of the mass: $(\omega, z) = \begin{bmatrix} \mathbf{u}(\omega, z) \\ \mathbf{v}(\omega) \end{bmatrix}$, and being $\mathbf{a}_u$ and $\mathbf{a}_v$ the matrices that extract the subvectors from $\mathbf{d}(\omega, z)$:

$$\mathbf{a}_u = \begin{bmatrix} 1 & 0 & 0 & 0 \\ 0 & 1 & 0 & 0 \end{bmatrix} \text{ or } \mathbf{a}_u = [\mathbf{1} \quad \mathbf{0}] \qquad \text{and} \qquad \mathbf{a}_v = \begin{bmatrix} 0 & 0 & 1 & 0 \\ 0 & 0 & 0 & 1 \end{bmatrix} \text{ or } \mathbf{a}_v = [\mathbf{0} \quad \mathbf{1}]$$

It is possible to substitute $\mathbf{u} = \mathbf{a}_u\mathbf{d}$ and $\mathbf{v} = \mathbf{a}_v\mathbf{d}$:

$$\int_0^L \mathbf{k}\mathcal{D}\mathbf{a}_u\mathbf{d}(\omega, z) \cdot \mathcal{D}\mathbf{a}_u\hat{\mathbf{d}}(z)dz - \omega^2 \int_0^L \mathbf{m}\mathbf{a}_u\mathbf{d}(\omega, z) \cdot \mathbf{a}_u\hat{\mathbf{d}}(z)dz - \bar{\mathbf{k}}\mathbf{a}_v\mathbf{d}(\omega, z) \cdot \mathbf{a}_u\hat{\mathbf{d}}(z) + \big(\bar{\mathbf{k}} - \omega^2\bar{\mathbf{m}}\big)\mathbf{a}_v\mathbf{d}(\omega, z) \cdot \mathbf{a}_v\hat{\mathbf{d}}(z) - \omega^2\bar{\mathbf{m}}\mathbf{a}_u\mathbf{d}(\omega, z) \cdot \mathbf{a}_v\hat{\mathbf{d}}(z) = 0 \quad \forall \hat{\mathbf{d}}$$

$$\int_0^L \mathbf{k}\mathbf{a}_u\mathcal{D}\mathbf{d}(\omega, z) \cdot \mathbf{a}_u\mathcal{D}\hat{\mathbf{d}}(z)dz - \omega^2 \int_0^L \mathbf{m}\mathbf{a}_u\mathbf{d}(\omega, z) \cdot \mathbf{a}_u\hat{\mathbf{d}}(z)dz - \bar{\mathbf{k}}\mathbf{a}_v\mathbf{d}(\omega, z) \cdot \mathbf{a}_u\hat{\mathbf{d}}(z) + \big(\bar{\mathbf{k}} - \omega^2\bar{\mathbf{m}}\big)\mathbf{a}_v\mathbf{d}(\omega, z) \cdot \mathbf{a}_v\hat{\mathbf{d}}(z) - \omega^2\bar{\mathbf{m}}\mathbf{a}_u\mathbf{d}(\omega, z) \cdot \mathbf{a}_v\hat{\mathbf{d}}(z) = 0 \quad \forall \hat{\mathbf{d}}$$

4.4.The finite element formulation

The finite element method expresses the solution for the beam in terms of displacements starting from the displacements of some arbitrary points, for example the ends of the beam. The vector $\mathbf{d}^e(\omega)$ is the collection of the displacements in the ends of the beam, being *i* the beginning and *j* the end:

$$\mathbf{d}^e(\omega) = [u_{2i} \quad u_{3i} \quad \varphi_i \quad u_{2j} \quad u_{3j} \quad \varphi_j \quad v_2 \quad v_3]^T$$

The solution $\mathbf{d}(\omega, z)$ is found thanks to the shape functions $n(z)$, which "dose" the discrete solutions at each point to find the exact solution.

$$\mathbf{d}(\omega, z) \cong \mathbf{N}^e(z)\mathbf{d}^e(\omega)$$

As many shape functions $n_i(z)$ as the degrees of freedom of the beam are required.

$$n_1(z) = \left(1 - \frac{3z^2}{L^2} + \frac{2z^3}{L^3}\right);\ n_2(z) = L\left(\frac{z}{L} - \frac{2z^2}{L^2} + \frac{z^3}{L^3}\right);\ n_3(z) = \left(\frac{3z^2}{L^2} - \frac{2z^3}{L^3}\right);$$

$$n_4(z) = L\left(-\frac{z^2}{L^2} + \frac{z^3}{L^3}\right);\ n_5(z) = \left(1 - \frac{z}{L}\right);\ n_6(z) = \left(\frac{z}{L}\right)$$

The matrix $\mathbf{N}^e$ has this form:

$$\mathbf{N}^e = \begin{bmatrix} n_1(z) & 0 & -n_2(z) & n_3(z) & 0 & -n_4(z) & 0 & 0 \\ 0 & n_5(z) & 0 & 0 & n_6(z) & 0 & 0 & 0 \\ 0 & 0 & 0 & 0 & 0 & 0 & 1 & 0 \\ 0 & 0 & 0 & 0 & 0 & 0 & 0 & 1 \end{bmatrix}$$

It is possible to notice that there are two ones in the matrix; in fact, since the mass displacements already are discrete points, they do not need to be described by shape functions.

The energetic equilibrium for the discrete formulation is:

$$\int_0^L \mathbf{k}\mathbf{a}_u\left(\mathcal{D}\mathbf{N}^e(z)\right)\mathbf{d}^e(\omega) \cdot \mathbf{a}_u\left(\mathcal{D}\mathbf{N}^e(z)\right)\hat{\mathbf{d}}^e(\omega)dz - \omega^2 \int_0^L \mathbf{m}\mathbf{a}_u\mathbf{N}^e(z)\mathbf{d}^e(\omega) \cdot \mathbf{a}_u\mathbf{N}^e(z)\hat{\mathbf{d}}^e(\omega)dz - \bar{\mathbf{k}}\mathbf{a}_v\mathbf{N}^e(L)\mathbf{d}^e(\omega)$$
$$\cdot \mathbf{a}_u\mathbf{N}^e(L)\hat{\mathbf{d}}^e + \left(\bar{\mathbf{k}} - \omega^2\bar{\mathbf{m}}\right)\mathbf{a}_v\mathbf{N}^e(L)\mathbf{d}^e(\omega) \cdot \mathbf{a}_v\mathbf{N}^e(L)\hat{\mathbf{d}}^e(\omega) - \omega^2\bar{\mathbf{m}}\mathbf{a}_u\mathbf{N}^e(L)\mathbf{d}^e(\omega)$$
$$\cdot \mathbf{a}_v\mathbf{N}^e(L)\hat{\mathbf{d}}^e(\omega) = 0 \quad \forall\hat{\mathbf{d}}$$

It is possible to simplify the equation and write it in a compact form using the matrixes properties that follow:

$$\mathbf{Aa} \cdot \mathbf{Bb} = \mathbf{B}^T\mathbf{Aa} \cdot \mathbf{b}$$

$$(\mathbf{AB})^T = \mathbf{B}^T\mathbf{A}^T$$

$$\int_0^L \left(\mathcal{D}\mathbf{N}^e(z)\right)^T \mathbf{a}_u^T \mathbf{k} \mathbf{a}_u \left(\mathcal{D}\mathbf{N}^e(z)\right) \mathbf{d}^e(\omega) \cdot \hat{\mathbf{d}}^e(\omega) dz - \omega^2 \int_0^L \left(\mathbf{N}^e(z)\right)^T \mathbf{a}_u^T \mathbf{m} \mathbf{a}_u \mathbf{N}^e(z) \mathbf{d}^e(\omega)$$
$$\cdot \hat{\mathbf{d}}^e(\omega) dz - \left(\mathbf{N}^e(L)\right)^T \mathbf{a}_u^T \bar{\mathbf{k}} \mathbf{a}_v \mathbf{N}^e(L) \mathbf{d}^e(\omega) \cdot \hat{\mathbf{d}}^e(\omega)$$
$$+ \left(\mathbf{N}^e(L)\right)^T \mathbf{a}_v^T \left(\bar{\mathbf{k}} - \omega^2 \bar{\mathbf{m}}\right) \mathbf{a}_v \mathbf{N}^e(L) \mathbf{d}^e(\omega) \cdot \hat{\mathbf{d}}^e(\omega)$$
$$- \omega^2 \left(\mathbf{N}^e(L)\right)^T \mathbf{a}_v^T \bar{\mathbf{m}} \mathbf{a}_u \mathbf{N}^e(L) \mathbf{d}^e(\omega) \cdot \hat{\mathbf{d}}^e(\omega) = 0 \quad \forall \hat{\mathbf{d}}$$

4.5. The stiffness matrix for the finite element

To proceed with the assembly of the dynamic stiffness matrix for the entire beam it is first necessary to derive the dynamic stiffness matrix for a single FE, which can be done writing the previous equation in matrix form. Every term of the equation is considered separately.

The internal work of the beam can be rewritten as:

$$\int_0^L \left(\mathcal{D}\mathbf{N}^e(z)\right)^T \mathbf{a}_u^T \mathbf{k} \mathbf{a}_u \left(\mathcal{D}\mathbf{N}^e(z)\right) \mathbf{d}^e(\omega) \cdot \hat{\mathbf{d}}^e(\omega) dz$$
$$= \int_0^L \begin{bmatrix} \left(\mathcal{D}\mathbf{N}_t^e(z)\right)^T \mathbf{k} \mathcal{D}\mathbf{N}_t^e(z) & \mathbf{0} \\ \mathbf{0} & \mathbf{0} \end{bmatrix} \begin{bmatrix} \mathbf{d}_t^e(\omega) \\ \mathbf{d}_l^e(\omega) \end{bmatrix} \cdot \hat{\mathbf{d}}^e(\omega) dz$$

Where $\begin{bmatrix} \left(\mathcal{D}\mathbf{N}_t^e(z)\right)^T \mathbf{k} \mathcal{D}\mathbf{N}_t^e(z) & \mathbf{0} \\ \mathbf{0} & \mathbf{0} \end{bmatrix}$ is an 8x8 matrix and $\left(\mathcal{D}\mathbf{N}_t^e(z)\right)^T \mathbf{k} \mathcal{D}\mathbf{N}_t^e(z)$ is a 6x6 matrix, they have been obtained with the following calculations:

$$\left(\mathcal{D}\mathbf{N}^e(z)\right)^T \mathbf{a}_u^T \mathbf{k} \mathbf{a}_u \left(\mathcal{D}\mathbf{N}^e(z)\right) \mathbf{d}^e = \begin{bmatrix} \mathcal{D}\mathbf{N}_t^e(z) & \mathbf{0} \\ \mathbf{0} & \mathbf{0} \end{bmatrix}^T \begin{bmatrix} \mathbf{1} \\ \mathbf{0} \end{bmatrix} \mathbf{k} \begin{bmatrix} \mathbf{1} & \mathbf{0} \end{bmatrix} \begin{bmatrix} \mathcal{D}\mathbf{N}_t^e(z) & \mathbf{0} \\ \mathbf{0} & \mathbf{0} \end{bmatrix} \begin{bmatrix} \mathbf{d}_t^e(\omega) \\ \mathbf{d}_l^e(\omega) \end{bmatrix}$$

$$\left(\mathcal{D}\mathbf{N}^e(z)\right)^T \mathbf{a}_u^T \mathbf{k} \mathbf{a}_u \left(\mathcal{D}\mathbf{N}^e(z)\right) \mathbf{d}^e(\omega) = \begin{bmatrix} \mathcal{D}\mathbf{N}_t^e(z) & \mathbf{0} \\ \mathbf{0} & \mathbf{1} \end{bmatrix}^T \begin{bmatrix} \mathbf{1} \\ \mathbf{0} \end{bmatrix} \mathbf{k} \begin{bmatrix} \mathcal{D}\mathbf{N}_t^e(z) & \mathbf{0} \end{bmatrix} \begin{bmatrix} \mathbf{d}_t^e(\omega) \\ \mathbf{d}_l^e(\omega) \end{bmatrix}$$

$$\left(\mathcal{D}\mathbf{N}^e(z)\right)^T \mathbf{a}_u^T \mathbf{k} \mathbf{a}_u \left(\mathcal{D}\mathbf{N}^e(z)\right) \mathbf{d}^e(\omega) = \begin{bmatrix} \mathcal{D}\mathbf{N}_t^e(z) & \mathbf{0} \\ \mathbf{0} & \mathbf{1} \end{bmatrix}^T \begin{bmatrix} \mathbf{1} \\ \mathbf{0} \end{bmatrix} \begin{bmatrix} \mathbf{k} \mathcal{D}\mathbf{N}_t^e(z) & \mathbf{0} \end{bmatrix} \begin{bmatrix} \mathbf{d}_t^e(\omega) \\ \mathbf{d}_l^e(\omega) \end{bmatrix}$$

$$\left(\mathcal{D}\mathbf{N}^e(z)\right)^T \mathbf{a}_u^T \mathbf{k} \mathbf{a}_u \left(\mathcal{D}\mathbf{N}^e(z)\right) \mathbf{d}^e(\omega) = \begin{bmatrix} \mathcal{D}\mathbf{N}_t^e(z) & \mathbf{0} \\ \mathbf{0} & \mathbf{1} \end{bmatrix}^T \begin{bmatrix} \mathbf{k} \mathcal{D}\mathbf{N}_t^e(z) & \mathbf{0} \\ \mathbf{0} & \mathbf{0} \end{bmatrix} \begin{bmatrix} \mathbf{d}_t^e(\omega) \\ \mathbf{d}_l^e(\omega) \end{bmatrix}$$

$$\left(\mathcal{D}\mathbf{N}^e(z)\right)^T\mathbf{a}_u^T\mathbf{k}\mathbf{a}_u\left(\mathcal{D}\mathbf{N}^e(z)\right)\mathbf{d}^e(\omega)=\begin{bmatrix}\left(\mathcal{D}\mathbf{N}_t^e(z)\right)^T\mathbf{k}\mathcal{D}\mathbf{N}_t^e(z) & \mathbf{0}\\ \mathbf{0} & \mathbf{0}\end{bmatrix}\begin{bmatrix}\mathbf{d}_t^e(\omega)\\ \mathbf{d}_l^e(\omega)\end{bmatrix}$$

The kinetic energy of the beam can be rewritten as:

$$\omega^2\int_0^L\left(\mathbf{N}^e(z)\right)^T\mathbf{a}_u^T\mathbf{m}\mathbf{a}_u\mathbf{N}^e(z)\mathbf{d}^e(\omega)\cdot\hat{\mathbf{d}}^e(\omega)dz$$

$$=\omega^2\int_0^L\begin{bmatrix}\left(\mathbf{N}_t^e(z)\right)^T\mathbf{m}\mathbf{N}_t^e(z) & \mathbf{0}\\ \mathbf{0} & \mathbf{0}\end{bmatrix}\begin{bmatrix}\mathbf{d}_t^e(\omega)\\ \mathbf{d}_l^e(\omega)\end{bmatrix}\cdot\hat{\mathbf{d}}^e(\omega)dz$$

Where $\begin{bmatrix}\left(\mathbf{N}_t^e(z)\right)^T\mathbf{m}\mathbf{N}_t^e & \mathbf{0}\\ \mathbf{0} & \mathbf{0}\end{bmatrix}$ is an 8x8 matrix and $(\mathbf{N}_t^e)^T\mathbf{m}\mathbf{N}_t^e$ is a 6x6 matrix, they have been obtained with the following calculations:

$$\left(\mathbf{N}^e(z)\right)^T\mathbf{a}_u^T\mathbf{m}\mathbf{a}_u\mathbf{N}^e(z)\mathbf{d}^e(\omega)=\begin{bmatrix}\mathbf{N}_t^e(z) & \mathbf{0}\\ \mathbf{0} & \mathbf{1}\end{bmatrix}^T\begin{bmatrix}\mathbf{1}\\ \mathbf{0}\end{bmatrix}\mathbf{m}\begin{bmatrix}\mathbf{1} & \mathbf{0}\end{bmatrix}\begin{bmatrix}\mathbf{N}_t^e(z) & \mathbf{0}\\ \mathbf{0} & \mathbf{1}\end{bmatrix}\begin{bmatrix}\mathbf{d}_t^e(\omega)\\ \mathbf{d}_l^e(\omega)\end{bmatrix}$$

$$\left(\mathbf{N}^e(z)\right)^T\mathbf{a}_u^T\mathbf{m}\mathbf{a}_u\mathbf{N}^e(z)\mathbf{d}^e(\omega)=\begin{bmatrix}\left(\mathbf{N}_t^e(z)\right)^T\mathbf{m}\mathbf{N}_t^e(z) & \mathbf{0}\\ \mathbf{0} & \mathbf{0}\end{bmatrix}\begin{bmatrix}\mathbf{d}_t^e(\omega)\\ \mathbf{d}_l^e(\omega)\end{bmatrix}$$

The part of the external elastic work and of the inertial work of the mass that are multiplied for the relative displacements of the mass, can be rewritten as:

$$\left(\mathbf{N}^e(L)\right)^T\mathbf{a}_v^T\left(\bar{\mathbf{k}}-\omega^2\bar{\mathbf{m}}\right)\mathbf{a}_v\mathbf{N}^e(L)\mathbf{d}^e(\omega)\cdot\hat{\mathbf{d}}^e(\omega)=\begin{bmatrix}\mathbf{0} & \mathbf{0}\\ \mathbf{0} & \left(\bar{\mathbf{k}}-\omega^2\bar{\mathbf{m}}\right)\end{bmatrix}\begin{bmatrix}\mathbf{d}_t^e(\omega)\\ \mathbf{d}_l^e(\omega)\end{bmatrix}\cdot\hat{\mathbf{d}}^e(\omega)$$

Where $\begin{bmatrix}\mathbf{0} & \mathbf{0}\\ \mathbf{0} & \left(\bar{\mathbf{k}}-\omega^2\bar{\mathbf{m}}\right)\end{bmatrix}$ is an 8x8 matrix and $\left(\bar{\mathbf{k}}-\omega^2\bar{\mathbf{m}}\right)$ is a 2x2 matrix, they have been obtained with the following calculations:

$$\left(\mathbf{N}^e(L)\right)^T\mathbf{a}_v^T\left(\bar{\mathbf{k}}-\omega^2\bar{\mathbf{m}}\right)\mathbf{a}_v\mathbf{N}^e(L)\mathbf{d}^e(\omega)$$

$$=\begin{bmatrix}\mathbf{N}_t^e(L) & \mathbf{0}\\ \mathbf{0} & \mathbf{1}\end{bmatrix}^T\begin{bmatrix}\mathbf{0}\\ \mathbf{1}\end{bmatrix}\left(\bar{\mathbf{k}}-\omega^2\bar{\mathbf{m}}\right)\begin{bmatrix}\mathbf{0} & \mathbf{1}\end{bmatrix}\begin{bmatrix}\mathbf{N}_t^e(L) & \mathbf{0}\\ \mathbf{0} & \mathbf{1}\end{bmatrix}\begin{bmatrix}\mathbf{d}_t^e(\omega)\\ \mathbf{d}_l^e(\omega)\end{bmatrix}$$

$$\left(\mathbf{N}^e(L)\right)^T\mathbf{a}_v^T\left(\bar{\mathbf{k}}-\omega^2\bar{\mathbf{m}}\right)\mathbf{a}_v\mathbf{N}^e(L)\mathbf{d}^e(\omega)$$

$$=\begin{bmatrix}\mathbf{N}_t^e(L) & \mathbf{0}\\ \mathbf{0} & \mathbf{1}\end{bmatrix}^T\begin{bmatrix}\mathbf{0}\\ \mathbf{1}\end{bmatrix}\left(\bar{\mathbf{k}}-\omega^2\bar{\mathbf{m}}\right)\begin{bmatrix}\mathbf{0} & \mathbf{1}\end{bmatrix}\begin{bmatrix}\mathbf{d}_t^e(\omega)\\ \mathbf{d}_l^e(\omega)\end{bmatrix}$$

$$\left(\mathbf{N}^e(L)\right)^T\mathbf{a}_v^T\left(\bar{\mathbf{k}}-\omega^2\bar{\mathbf{m}}\right)\mathbf{a}_v\mathbf{N}^e(L)\mathbf{d}^e(\omega)=\begin{bmatrix}\mathbf{N}_t^e(L) & \mathbf{0}\\ \mathbf{0} & \mathbf{1}\end{bmatrix}^T\begin{bmatrix}\mathbf{0}\\ \mathbf{1}\end{bmatrix}\begin{bmatrix}\mathbf{0} & \left(\bar{\mathbf{k}}-\omega^2\bar{\mathbf{m}}\right)\end{bmatrix}\begin{bmatrix}\mathbf{d}_t^e(\omega)\\ \mathbf{d}_l^e(\omega)\end{bmatrix}$$

$$\left(\mathbf{N}^e(L)\right)^T\mathbf{a}_v^T\left(\bar{\mathbf{k}}-\omega^2\bar{\mathbf{m}}\right)\mathbf{a}_v\mathbf{N}^e(L)\mathbf{d}^e(\omega)=\begin{bmatrix}\mathbf{N}_t^e(L) & \mathbf{0}\\ \mathbf{0} & \mathbf{1}\end{bmatrix}^T\begin{bmatrix}\mathbf{0} & \mathbf{0}\\ \mathbf{0} & \left(\bar{\mathbf{k}}-\omega^2\bar{\mathbf{m}}\right)\end{bmatrix}\begin{bmatrix}\mathbf{d}_t^e(\omega)\\ \mathbf{d}_l^e(\omega)\end{bmatrix}$$

$$\left(\mathbf{N}^e(L)\right)^T \mathbf{a}_v^T \left(\bar{\mathbf{k}} - \omega^2 \bar{\mathbf{m}}\right) \mathbf{a}_v \mathbf{N}^e(L) \mathbf{d}^e(\omega) = \begin{bmatrix} \mathbf{0} & \mathbf{0} \\ \mathbf{0} & \left(\bar{\mathbf{k}} - \omega^2 \bar{\mathbf{m}}\right) \end{bmatrix} \begin{bmatrix} \mathbf{d}_t^e(\omega) \\ \mathbf{d}_l^e(\omega) \end{bmatrix}$$

The inertial work of the mass done for the displacements of the beam can be simplified as:

$$\omega^2 \left(\mathbf{N}^e(L)\right)^T \mathbf{a}_v^T \bar{\mathbf{m}} \mathbf{a}_u \mathbf{N}^e(L) \mathbf{d}^e(\omega) \cdot \hat{\mathbf{d}}^e(\omega) = \omega^2 \begin{bmatrix} \mathbf{0} & \mathbf{0} \\ \bar{\mathbf{m}} \mathbf{N}_t^e(L) & \mathbf{0} \end{bmatrix} \begin{bmatrix} \mathbf{d}_t^e(\omega) \\ \mathbf{d}_l^e(\omega) \end{bmatrix} \cdot \hat{\mathbf{d}}^e(\omega)$$

Where $\begin{bmatrix} \mathbf{0} & \mathbf{0} \\ \bar{\mathbf{m}} \mathbf{N}_t^e(L) & \mathbf{0} \end{bmatrix}$ is an 8x8 matrix and $\bar{\mathbf{m}} \mathbf{N}_t^e(L)$ is a 2x6 matrix, they have been obtained with the following calculations:

$$\left(\mathbf{N}^e(L)\right)^T \mathbf{a}_v^T \bar{\mathbf{m}} \mathbf{a}_u \mathbf{N}^e(L) \mathbf{d}^e(\omega) = \begin{bmatrix} \mathbf{N}_t^e(L) & \mathbf{0} \\ \mathbf{0} & \mathbf{1} \end{bmatrix}^T \begin{bmatrix} \mathbf{0} \\ \mathbf{1} \end{bmatrix} \bar{\mathbf{m}} \begin{bmatrix} \mathbf{N}_t^e(L) & \mathbf{0} \end{bmatrix} \begin{bmatrix} \mathbf{d}_t^e(\omega) \\ \mathbf{d}_l^e(\omega) \end{bmatrix}$$

$$\left(\mathbf{N}^e(L)\right)^T \mathbf{a}_v^T \bar{\mathbf{m}} \mathbf{a}_u \mathbf{N}^e(L) \mathbf{d}^e(\omega) = \begin{bmatrix} \mathbf{N}_t^e(L) & \mathbf{0} \\ \mathbf{0} & \mathbf{1} \end{bmatrix}^T \begin{bmatrix} \mathbf{0} \\ \mathbf{1} \end{bmatrix} \begin{bmatrix} \bar{\mathbf{m}} \mathbf{N}_t^e(L) & \mathbf{0} \end{bmatrix} \begin{bmatrix} \mathbf{d}_t^e(\omega) \\ \mathbf{d}_l^e(\omega) \end{bmatrix}$$

$$\left(\mathbf{N}^e(L)\right)^T \mathbf{a}_v^T \bar{\mathbf{m}} \mathbf{a}_u \mathbf{N}^e(L) \mathbf{d}^e(\omega) = \begin{bmatrix} \mathbf{N}_t^e(L) & \mathbf{0} \\ \mathbf{0} & \mathbf{1} \end{bmatrix}^T \begin{bmatrix} \mathbf{0} & \mathbf{0} \\ \bar{\mathbf{m}} \mathbf{N}_t^e(L) & \mathbf{0} \end{bmatrix} \begin{bmatrix} \mathbf{d}_t^e(\omega) \\ \mathbf{d}_l^e(\omega) \end{bmatrix}$$

$$\left(\mathbf{N}^e(L)\right)^T \mathbf{a}_v^T \bar{\mathbf{m}} \mathbf{a}_u \mathbf{N}^e(L) \mathbf{d}^e(\omega) = \begin{bmatrix} \mathbf{0} & \mathbf{0} \\ \bar{\mathbf{m}} \mathbf{N}_t^e(L) & \mathbf{0} \end{bmatrix} \begin{bmatrix} \mathbf{d}_t^e(\omega) \\ \mathbf{d}_l^e(\omega) \end{bmatrix}$$

The elastic work of the mass done for the displacements of the beam can be simplified as:

$$\left(\mathbf{N}^e(L)\right)^T \mathbf{a}_u^T \bar{\mathbf{k}} \mathbf{a}_v \mathbf{N}^e(L) \mathbf{d}^e(\omega) \cdot \hat{\mathbf{d}}^e(\omega) = \begin{bmatrix} \mathbf{0} & \mathbf{0} \\ \mathbf{0} & \bar{\mathbf{k}} \\ \mathbf{0} & \mathbf{0} \end{bmatrix} \begin{bmatrix} \mathbf{d}_t^e(\omega) \\ \mathbf{d}_l^e(\omega) \end{bmatrix} \cdot \hat{\mathbf{d}}^e(\omega)$$

Where $\begin{bmatrix} \mathbf{0} & -\left(\mathbf{N}_t^e(L)\right)^T \bar{\mathbf{k}} \\ \mathbf{0} & \mathbf{0} \end{bmatrix}^T$ is an 8x8 matrix and $-\left(\mathbf{N}_t^e(L)\right)^T \bar{\mathbf{k}}$ is a 6x2 matrix, they have been obtained with the following calculations:

$$\left(\mathbf{N}^e(L)\right)^T \mathbf{a}_u^T \bar{\mathbf{k}} \mathbf{a}_v \mathbf{N}^e(L) \mathbf{d}^e(\omega) = \begin{bmatrix} \mathbf{N}_t^e(L) & \mathbf{0} \\ \mathbf{0} & \mathbf{1} \end{bmatrix}^T \begin{bmatrix} \mathbf{1} \\ \mathbf{0} \end{bmatrix} \bar{\mathbf{k}} \begin{bmatrix} \mathbf{0} & \mathbf{1} \end{bmatrix} \begin{bmatrix} \mathbf{d}_t^e(\omega) \\ \mathbf{d}_l^e(\omega) \end{bmatrix}$$

$$\left(\mathbf{N}^e(L)\right)^T \mathbf{a}_u^T \bar{\mathbf{k}} \mathbf{a}_v \mathbf{N}^e(L) \mathbf{d}^e(\omega) = \begin{bmatrix} \mathbf{N}_t^e(L) & \mathbf{0} \\ \mathbf{0} & \mathbf{1} \end{bmatrix}^T \begin{bmatrix} \mathbf{1} \\ \mathbf{0} \end{bmatrix} \begin{bmatrix} \mathbf{0} & \bar{\mathbf{k}} \end{bmatrix} \begin{bmatrix} \mathbf{d}_t^e(\omega) \\ \mathbf{d}_l^e(\omega) \end{bmatrix}$$

$$\left(\mathbf{N}^e(L)\right)^T \mathbf{a}_u^T \bar{\mathbf{k}} \mathbf{a}_v \mathbf{N}^e(L) \mathbf{d}^e(\omega) = \begin{bmatrix} \mathbf{N}_t^e(L) & \mathbf{0} \\ \mathbf{0} & \mathbf{1} \end{bmatrix}^T \begin{bmatrix} \mathbf{0} & \bar{\mathbf{k}} \\ \mathbf{0} & \mathbf{0} \end{bmatrix} \begin{bmatrix} \mathbf{d}_t^e(\omega) \\ \mathbf{d}_l^e(\omega) \end{bmatrix}$$

$$\left(\mathbf{N}^e(L)\right)^T \mathbf{a}_u^T \bar{\mathbf{k}} \mathbf{a}_v \mathbf{N}^e(L) \mathbf{d}^e(\omega) = \begin{bmatrix} \mathbf{0} & -\left(\mathbf{N}_t^e(L)\right)^T \bar{\mathbf{k}} \\ \mathbf{0} & \mathbf{0} \end{bmatrix}^T \begin{bmatrix} \mathbf{d}_t^e(\omega) \\ \mathbf{d}_l^e(\omega) \end{bmatrix} = \begin{bmatrix} \mathbf{0} & \mathbf{0} \\ \mathbf{0} & \bar{\mathbf{k}} \\ \mathbf{0} & \mathbf{0} \end{bmatrix} \begin{bmatrix} \mathbf{d}_t^e(\omega) \\ \mathbf{d}_l^e(\omega) \end{bmatrix}$$

Eventually, the energetic equilibrium can be written as:

$$\begin{bmatrix} \mathbf{K}_{ii}^e & \mathbf{K}_{ij}^e & \mathbf{0} \\ \mathbf{K}_{ij}^e & \mathbf{K}_{jj}^e & \mathbf{0} \\ \mathbf{0} & \mathbf{0} & \mathbf{0} \end{bmatrix} \begin{bmatrix} \mathbf{d}_i^e(\omega) \\ \mathbf{d}_j^e(\omega) \\ \mathbf{v}(\omega) \end{bmatrix} + \begin{bmatrix} \mathbf{0} & \mathbf{0} & \mathbf{0} \\ \mathbf{0} & \mathbf{0} & \bar{\mathbf{k}} \\ \mathbf{0} & \mathbf{0} & \mathbf{0} \end{bmatrix} \begin{bmatrix} \mathbf{d}_i^e(\omega) \\ \mathbf{d}_j^e(\omega) \\ \mathbf{v}(\omega) \end{bmatrix} - \omega^2 \begin{bmatrix} \mathbf{M}_{ii}^e & \mathbf{M}_{ij}^e & \mathbf{0} \\ \mathbf{M}_{ij}^e & \mathbf{M}_{jj}^e & \mathbf{0} \\ \mathbf{0} & \mathbf{0} & \mathbf{0} \end{bmatrix} \begin{bmatrix} \mathbf{d}_i^e(\omega) \\ \mathbf{d}_j^e(\omega) \\ \mathbf{v}(\omega) \end{bmatrix}$$
$$+ \left(\begin{bmatrix} \mathbf{0} & \mathbf{0} & \mathbf{0} \\ \mathbf{0} & \mathbf{0} & \mathbf{0} \\ \mathbf{0} & \mathbf{0} & \bar{\mathbf{k}} \end{bmatrix} - \omega^2 \begin{bmatrix} \mathbf{0} & \mathbf{0} & \mathbf{0} \\ \mathbf{0} & \mathbf{0} & \mathbf{0} \\ \mathbf{0} & \mathbf{0} & \bar{\mathbf{m}} \end{bmatrix} \right) \begin{bmatrix} \mathbf{d}_i^e(\omega) \\ \mathbf{d}_j^e(\omega) \\ \mathbf{v}(\omega) \end{bmatrix} - \omega^2 \begin{bmatrix} \mathbf{0} & \mathbf{0} & \mathbf{0} \\ \mathbf{0} & \bar{\mathbf{m}} & \mathbf{0} \\ \mathbf{0} & \mathbf{0} & \mathbf{0} \end{bmatrix} \begin{bmatrix} \mathbf{d}_i^e(\omega) \\ \mathbf{d}_j^e(\omega) \\ \mathbf{v}(\omega) \end{bmatrix}$$

It is possible to collect the vector in common $\mathbf{d}^e$:

$$\begin{bmatrix} \mathbf{K}_{ii}^e & \mathbf{K}_{ij}^e & \mathbf{0} \\ \mathbf{K}_{ij}^e & \mathbf{K}_{jj}^e & -\bar{\mathbf{k}} \\ \mathbf{0} & \mathbf{0} & \bar{\mathbf{k}} \end{bmatrix} \begin{bmatrix} \mathbf{d}_i^e(\omega) \\ \mathbf{d}_j^e(\omega) \\ \mathbf{v}(\omega) \end{bmatrix} - \omega^2 \begin{bmatrix} \mathbf{M}_{ii}^e & \mathbf{M}_{ij}^e & \mathbf{0} \\ \mathbf{M}_{ij}^e & \mathbf{M}_{jj}^e & \mathbf{0} \\ \mathbf{0} & \bar{\mathbf{m}} & \bar{\mathbf{m}} \end{bmatrix} \begin{bmatrix} \mathbf{d}_i^e(\omega) \\ \mathbf{d}_j^e(\omega) \\ \mathbf{v}(\omega) \end{bmatrix} = \mathbf{0}$$

$$\left(\begin{bmatrix} \mathbf{K}_{ii}^e & \mathbf{K}_{ij}^e & \mathbf{0} \\ \mathbf{K}_{ij}^e & \mathbf{K}_{jj}^e & -\bar{\mathbf{k}} \\ \mathbf{0} & \mathbf{0} & \bar{\mathbf{k}} \end{bmatrix} - \omega^2 \begin{bmatrix} \mathbf{M}_{ii}^e & \mathbf{M}_{ij}^e & \mathbf{0} \\ \mathbf{M}_{ij}^e & \mathbf{M}_{jj}^e & \mathbf{0} \\ \mathbf{0} & \bar{\mathbf{m}} & \bar{\mathbf{m}} \end{bmatrix} \right) \begin{bmatrix} \mathbf{d}_i^e(\omega) \\ \mathbf{d}_j^e(\omega) \\ \mathbf{v}(\omega) \end{bmatrix} = \mathbf{0}$$

The dynamic stiffness matrix for a finite element is:

$$\begin{bmatrix} \tilde{\mathbf{K}}_{ii}^e & \tilde{\mathbf{K}}_{ij}^e & \mathbf{0} \\ \tilde{\mathbf{K}}_{ij}^e & \tilde{\mathbf{K}}_{jj}^e & -\bar{\mathbf{k}} \\ \mathbf{0} & \mathbf{0} & \tilde{\mathbf{k}} \end{bmatrix} \begin{bmatrix} \mathbf{d}_i^e(\omega) \\ \mathbf{d}_j^e(\omega) \\ \mathbf{v}(\omega) \end{bmatrix} = \mathbf{0}$$

4.6. Finite element assembly

The stiffness matrix of the structure can be easily obtained. In fact, every final node *j* of a FE *h* corresponds to the starting node *i* of the following FE *h+1* with exception of the very first and very last point of the structure. To ensure greater order, the stiffness matrix is written by rearranging the displacement vector $\mathbf{d}^e$ so that it first contains the movements of the degrees of freedom of the beam and then those of the masses on the springs. Doing so, the stiffness *h* of the springs is in positions *NDoF+h,NDoF+h* and *h+1,NDoF+h*.

$$\begin{bmatrix} \widetilde{\mathbf{K}}_{ii}^{1} & \widetilde{\mathbf{K}}_{ij}^{1} & \cdots & \mathbf{0} & \mathbf{0} & \cdots & \mathbf{0} & \cdots & \mathbf{0} & \cdots & \mathbf{0} \\ \widetilde{\mathbf{K}}_{ij}^{1} & \widetilde{\mathbf{K}}_{jj}^{1}+\widetilde{\mathbf{K}}_{ii}^{2} & \cdots & \mathbf{0} & \mathbf{0} & \cdots & -\bar{\mathbf{k}}^{1} & \cdots & \mathbf{0} & & \mathbf{0} \\ \vdots & \vdots & & \vdots & \vdots & & \vdots & & \vdots & & \vdots \\ \mathbf{0} & \mathbf{0} & \cdots & \widetilde{\mathbf{K}}_{jj}^{h-1}+\widetilde{\mathbf{K}}_{ii}^{h} & \widetilde{\mathbf{K}}_{ij}^{h} & \cdots & \mathbf{0} & \cdots & \mathbf{0} & \cdots & \mathbf{0} \\ \mathbf{0} & \mathbf{0} & \cdots & \widetilde{\mathbf{K}}_{ij}^{h} & \widetilde{\mathbf{K}}_{jj}^{h}+\widetilde{\mathbf{K}}_{ii}^{h+1} & \cdots & \mathbf{0} & \cdots & -\bar{\mathbf{k}}^{h} & \cdots & \mathbf{0} \\ \vdots & \vdots & & \vdots & \vdots & & \vdots & & \vdots & & \vdots \\ \mathbf{0} & \mathbf{0} & \cdots & \mathbf{0} & \mathbf{0} & \cdots & \tilde{\mathbf{k}}^{1} & \cdots & \mathbf{0} & \cdots & \mathbf{0} \\ \vdots & \vdots & & \vdots & \vdots & & \vdots & & \vdots & & \vdots \\ \mathbf{0} & \mathbf{0} & \cdots & \mathbf{0} & \mathbf{0} & \cdots & \mathbf{0} & \cdots & \tilde{\mathbf{k}}^{h} & \cdots & \mathbf{0} \\ \vdots & \vdots & & \vdots & \vdots & & \vdots & & \vdots & & \vdots \\ \mathbf{0} & \mathbf{0} & \cdots & \mathbf{0} & \mathbf{0} & \cdots & \mathbf{0} & \cdots & \mathbf{0} & \cdots & \tilde{\mathbf{k}}^{n} \end{bmatrix} \begin{bmatrix} \mathbf{d}_{i}^{1}(\omega) \\ \mathbf{d}_{j}^{1}(\omega) \\ \vdots \\ \mathbf{d}_{i}^{h}(\omega) \\ \mathbf{d}_{j}^{h}(\omega) \\ \vdots \\ \mathbf{v}^{1}(\omega) \\ \vdots \\ \mathbf{v}^{h}(\omega) \\ \vdots \\ \mathbf{v}^{n}(\omega) \end{bmatrix}$$

Chapter 5
Truck-bridge dynamic interaction

From the study of the 2DOF model, the graphs of the FRF and the two circular frequencies of the system were obtained. In particular, when taking into account the flexibility of the truck, it was found that:

- For low values of $\bar{\omega}$ (i.e. the truck is not very stiff), the second frequency of the model is the fundamental frequency of the bridge;
- For high values of $\bar{\omega}$ (i.e. the truck is very stiff), the first frequency of the system is also the fundamental frequency of the bridge;
- There are values of $\bar{\omega}$ for which the truck is a mass damper;

In this chapter we want to monitor the trends of the first two frequencies and the mass participation factors (MPF) of a bridge on which there are trucks. The natural frequencies are obtained through the modal analysis of the system, however some of the frequencies obtained are not of interest as they hardly excite the bridge, being frequencies that mainly concern the vibration of the trucks on the bridge. Therefore, it is necessary to uniquely identify the first two frequencies of the bridge. To that end, it was decided to use the FRF of the displacements of the beam. By applying a vertical driving force in the centreline of the beam, and measuring the displacement in a point in a centreline, the peak of the FRF occurs for the most excited frequency from this driving force. As the driving force has been chosen, this frequency turns out to be that of the first way of vibrating. The second frequency of the bridge is deducted using the same principle. In this case, two hemi-symmetric forces act at one quarter and three quarters of the beam. The FRF of the displacements is measured at one quarter of the beam.

5.1. Dynamic behaviour of a simply supported beam

The dynamic solution of the simply supported beam is known. Only the bending modes are considered and the damping is neglected.

The beam has infinite modes of vibrating, the frequencies of which are expressed by the relation:

$$\omega_k = \left(\frac{k\pi}{L}\right)^2 \sqrt{\frac{EJ_y}{m}}$$

The value of the second frequency of the beam is the quadruple of the first. The Picture 29 shows the shape of the first three ways of vibrating.

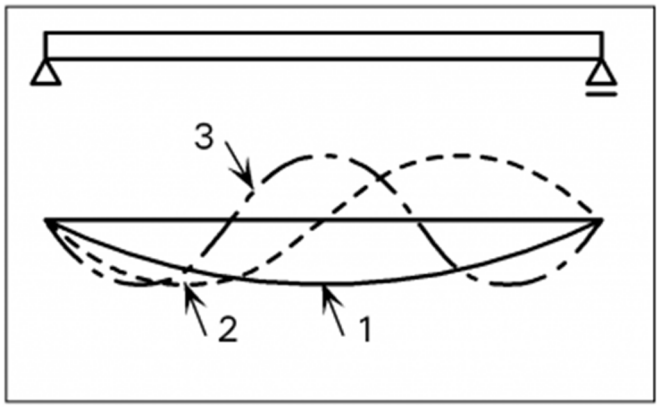

Picture 29: First 3 vibrational shapes for the simply supported beam.

The FRF for a point in the centreline presents a peak for $\omega = \omega_1$ and a value that tends to 0 for $\omega = \omega_2$. The FRF for a point at one quarter of the length of the beam, presents several peaks. Among those peaks the one that has the highest values occurs when $\omega = \omega_2$.

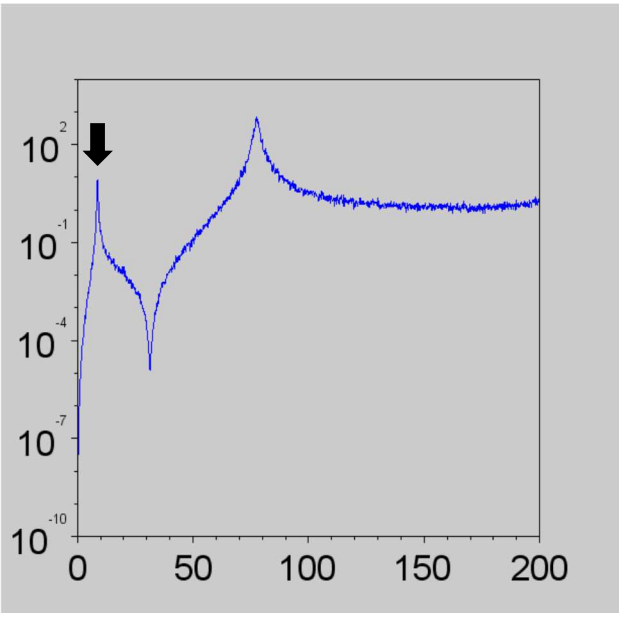

Picture 30: FRF of the displacement of a point at the centreline of the beam.

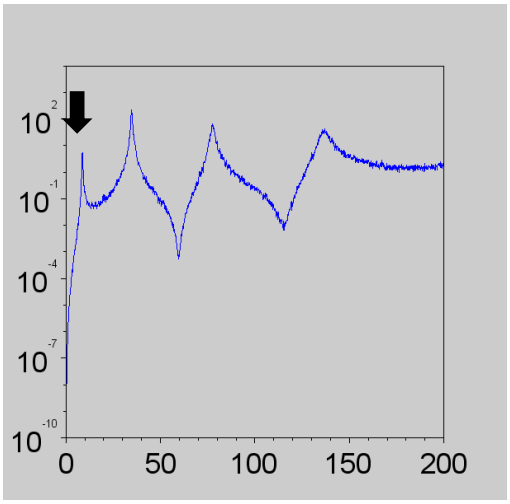

Picture 31: FRF of the displacement of a point at one quarter of the lenght of the beam.

5.2. Frequencies and mass participation factor for a bridge with one truck in cross section and one truck in the span

Picture 32 plots the values of $\frac{\omega}{\omega_2}$ for a bridge with $\bar{m} = 0.2,\ \bar{L} = 0.25$, one mass in in the span and one in the cross section. The blue line is relative to the fundamental circular frequency of the bridge and the orange line represents the second one, both have been identified with the FRF functions.

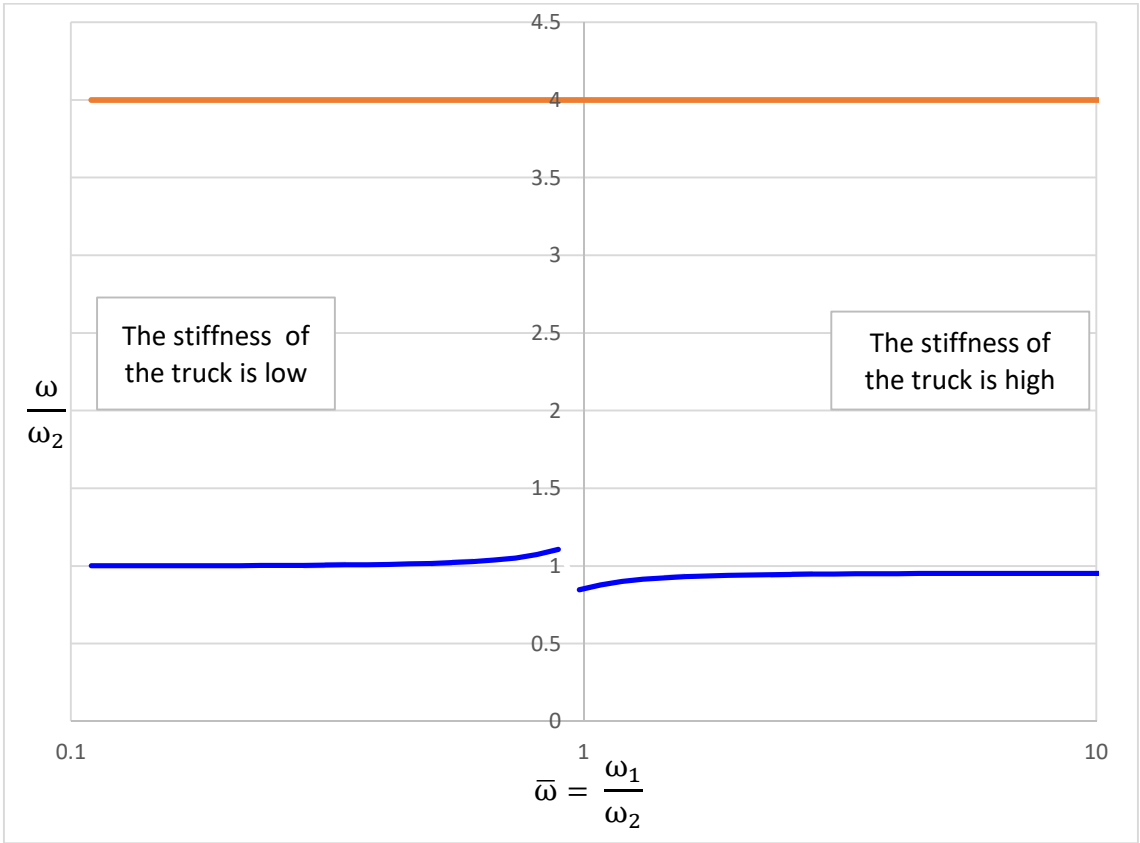

Picture 32: Frequencies for a bridge with a truck in the centreline. The blue curve is relative to the first frequency of the bridge, the orange curve is relative to the second one.

As for the case of the simply supported beam, the second frequency is four times the first one. This result is due to the position of the truck. In fact, this is exactly in the null point of the second mode of vibration. Therefore, it does not change its frequency.

For low values of $\bar{\omega}$, the value of the first circular frequency of the bridge approaches to one. In accordance with the observations for the 2DOF system, the trend of $\frac{\omega}{\omega_2}$ follows that of the second circular frequency of the 2DOF system. Pictures from Picture 33 to Picture 35 show the shape of the first three mode of vibration for low values of $\bar{\omega}$.

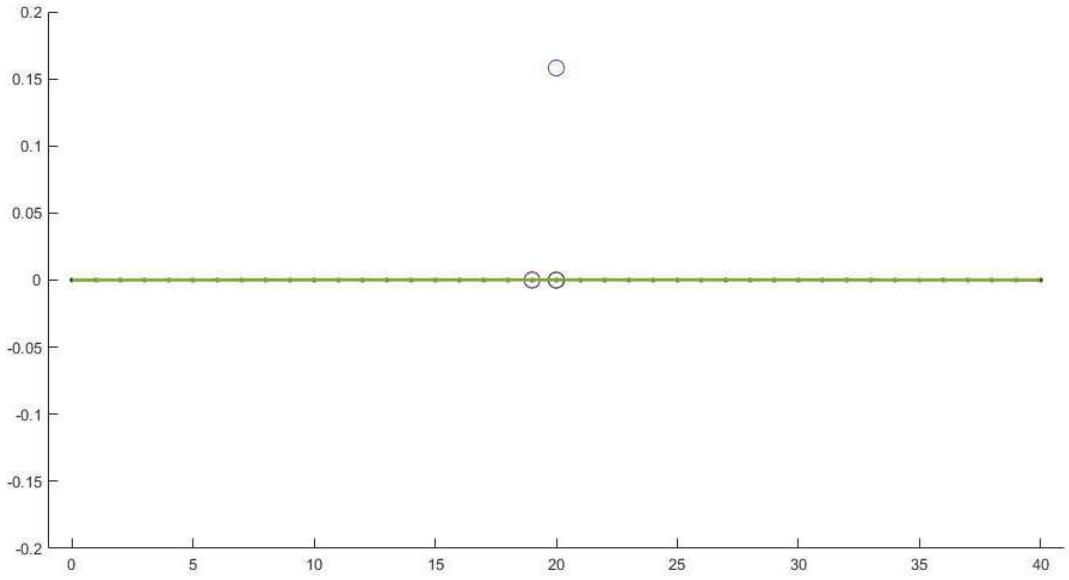

Picture 33: First mode of vibration for low values of $\bar{\omega}$.

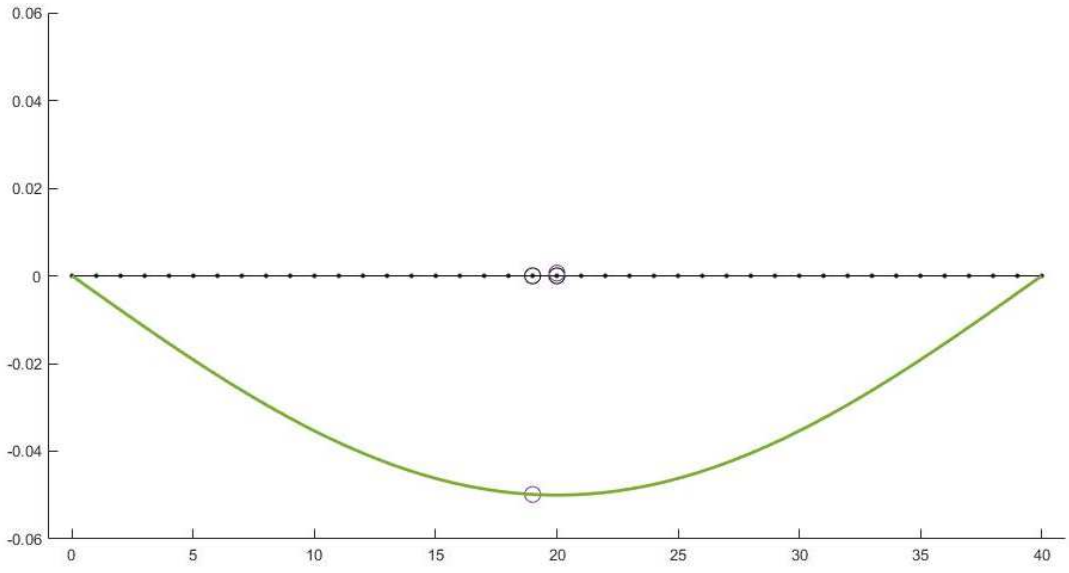

Picture 34: Second mode of vibration for low values of $\bar{\omega}$

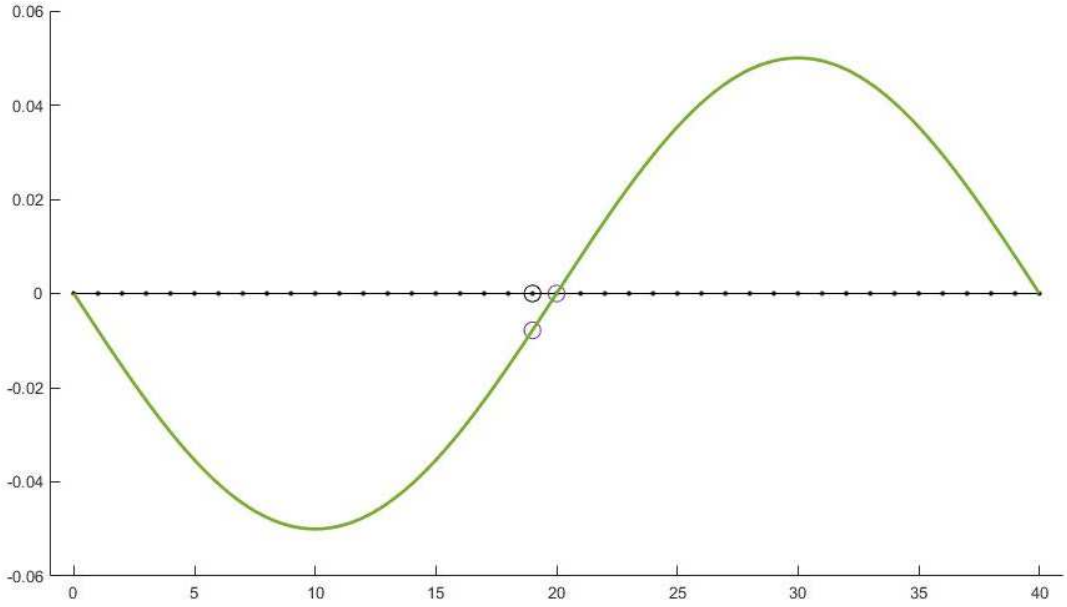

Picture 35: Third mode of vibration for low values of $\bar{\omega}$

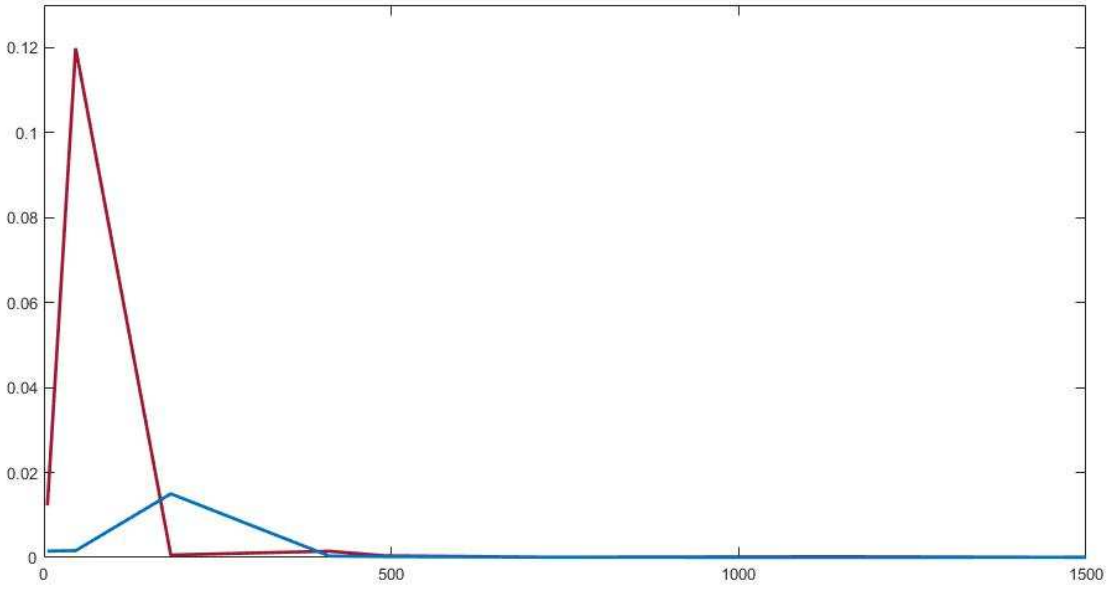

Picture 36: FRF of the displacement for low values of $\bar{\omega}$. The red line is measured for a point in the beam's centreline. The blue line is measured for a point at one quarter of the length of the beam.

Picture 36 and Picture 33 show that the first circular frequency of the system is not of interest for knowing the fundamental frequency of the bridge, since the peak of the FRF occurs for the second frequency of the system.

The curve relative to the first frequency of the bridge has a jump discontinuity for values of $\bar{\omega}$ close to 1. Up to the point where the jump occurs, the curve follows the same trend as the second circular frequency in the 2DOF case. From the jump onwards, the curve

follows the same trend of the first circular frequency of the 2DOF case. The jump discontinuity of the curve can be explained comparing the modes of vibration of the system just before and right after the jump.

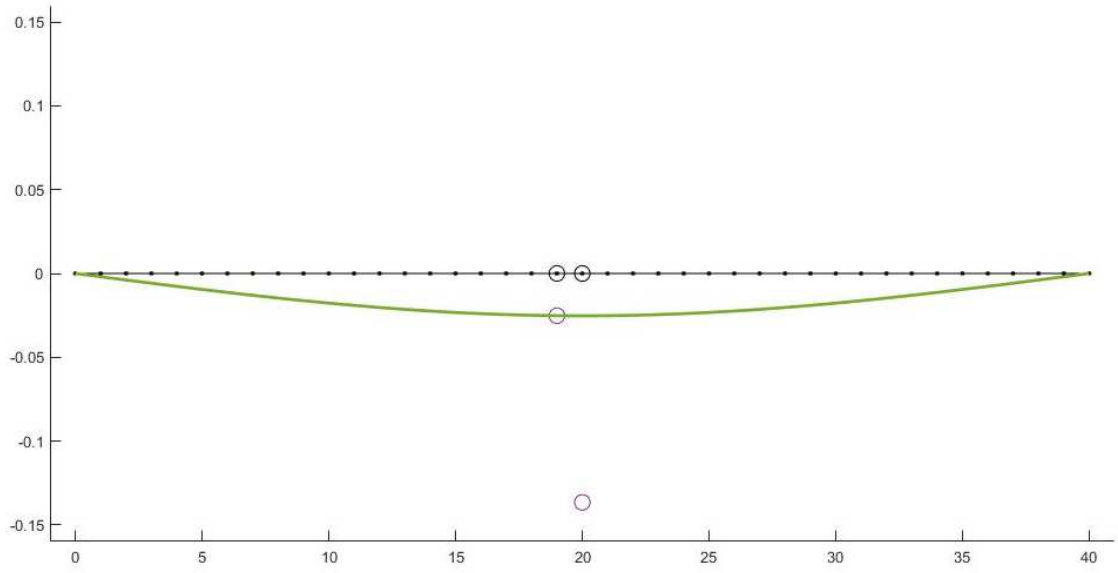

Picture 37: First mode of vibration before the jump discontinuity.

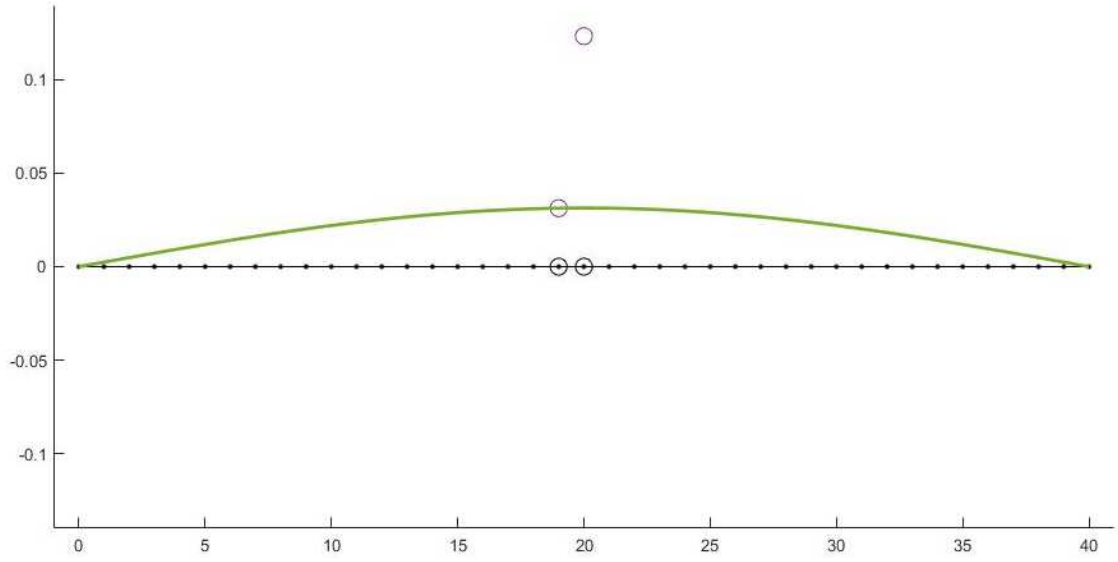

Picture 38: First mode of vibration right after the jump discontinuity.

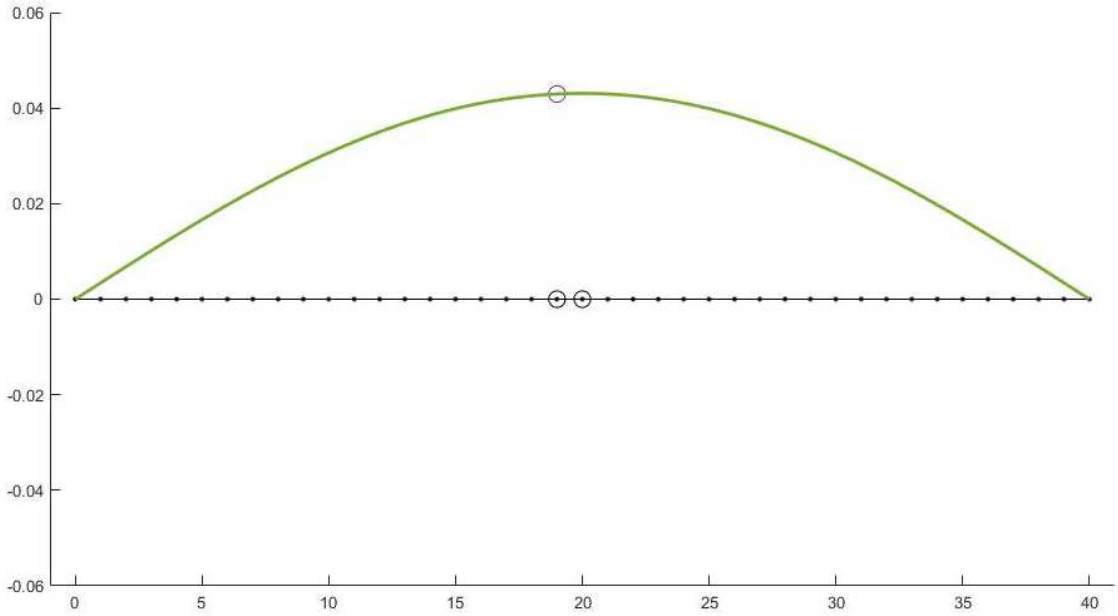

Picture 39: Second mode of vibration before the jump discontinuity.

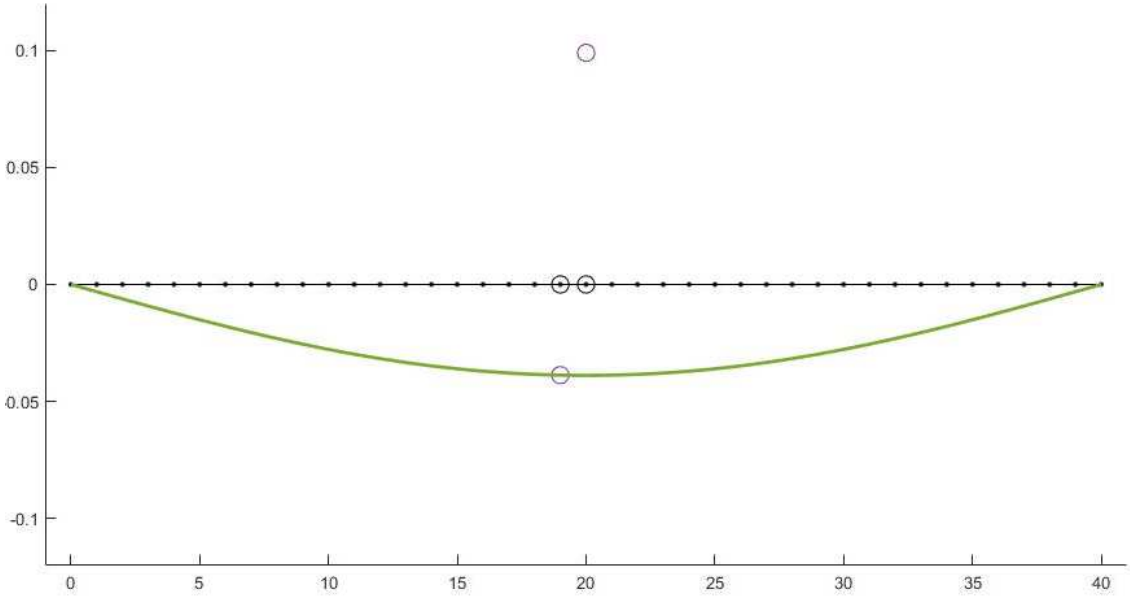

Picture 40: Second mode of vibration right after the jump discontinuity.

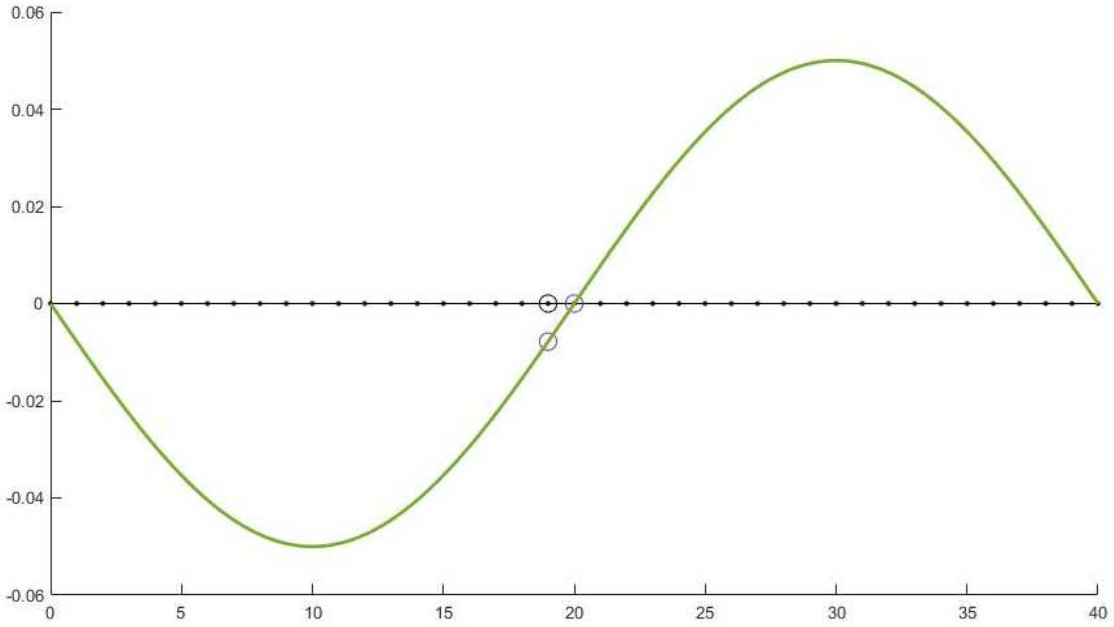

Picture 41: Third mode of vibration before the jump discontinuity.

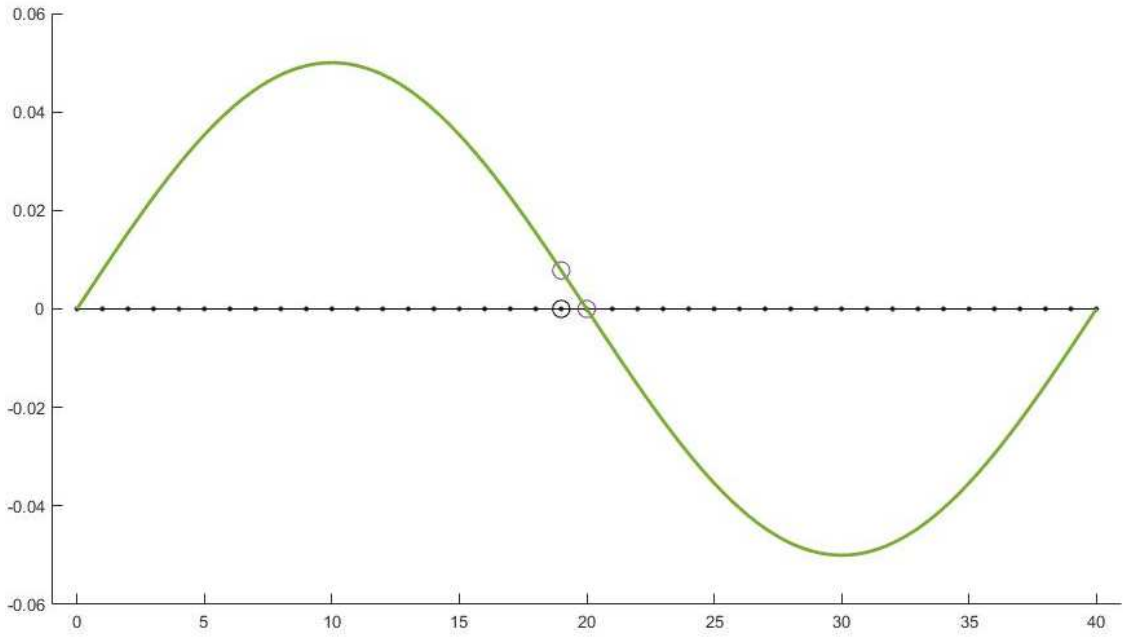

Picture 42: Third mode of vibration right after the jump discontinuity.

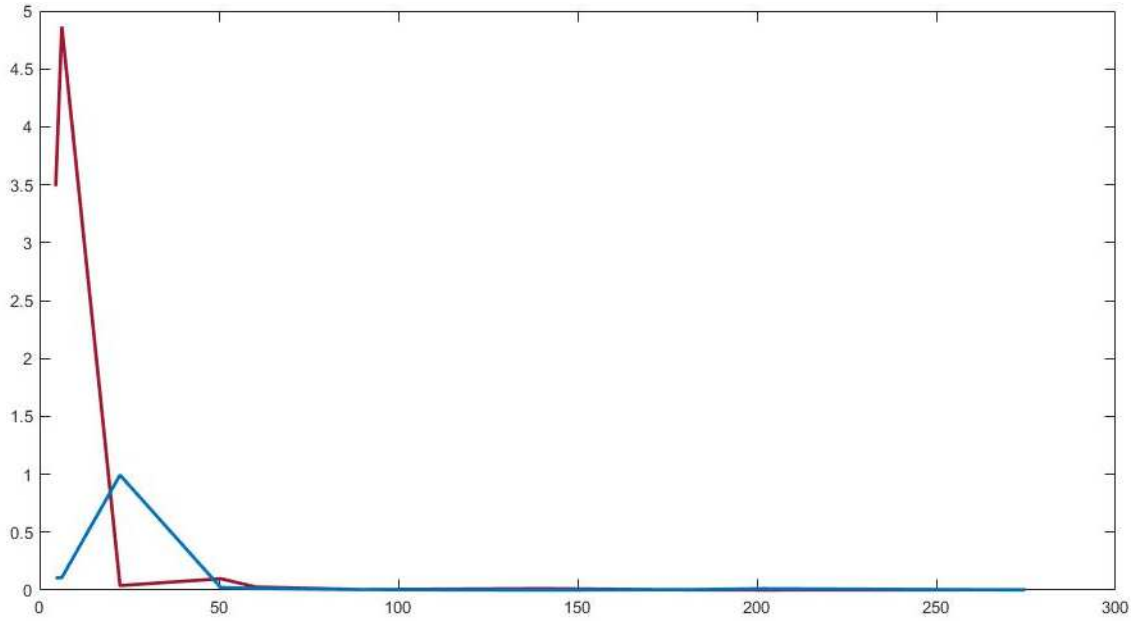

Picture 43: FRF of the displacement before the jump discontinuity. The red line is measured for a point in the beam's centreline. The blue line is measured for a point at one quarter of the length of the beam.

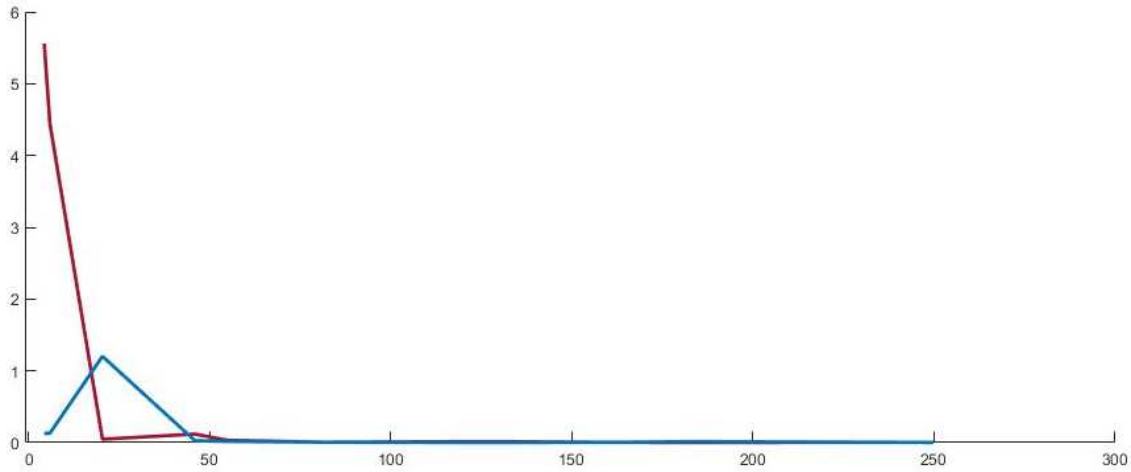

Picture 44: FRF of the displacement right after the jump discontinuity. The red line is measured for a point in the beam's centreline. The blue line is measured for a point at one quarter of the length of the beam.

Picture 43 and Picture 44 show the FRF of the displacement before and right after the jump discontinuity. The red lines are measured for a point in the beam's centreline, and identify the frequency of the first mode of vibration of the bridge. Right before the jump discontinuity, the highest peak of the curve occurs for the second frequency, while right after the jump the first peak of the red line is the highest one. In both cases, the third frequency of the system is the second frequency of the bridge.

For high values of $\bar{\omega}$, the value of the first circular frequency of the bridge approaches to a value smaller than one. This is again in accordance with the observations made from

the 2DOF system. The trend of $\frac{\omega}{\omega_2}$ follows that of the first circular frequency of the 2DOF system. In the case of very stiff truck, the first frequency of the system tends to the one of the truck modelled as an added mass. Pictures from Picture 45 to Picture 48 show the shapes of the first three mode of vibration and the FRFs for high values of $\bar{\omega}$.

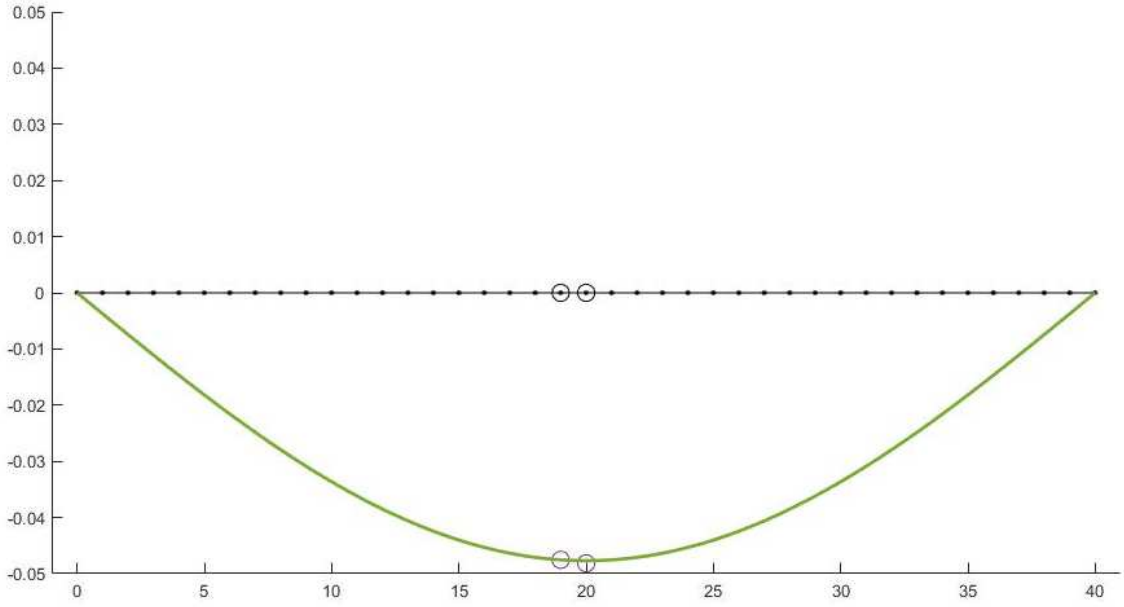

Picture 45: First mode of vibration for high values of $\bar{\omega}$.

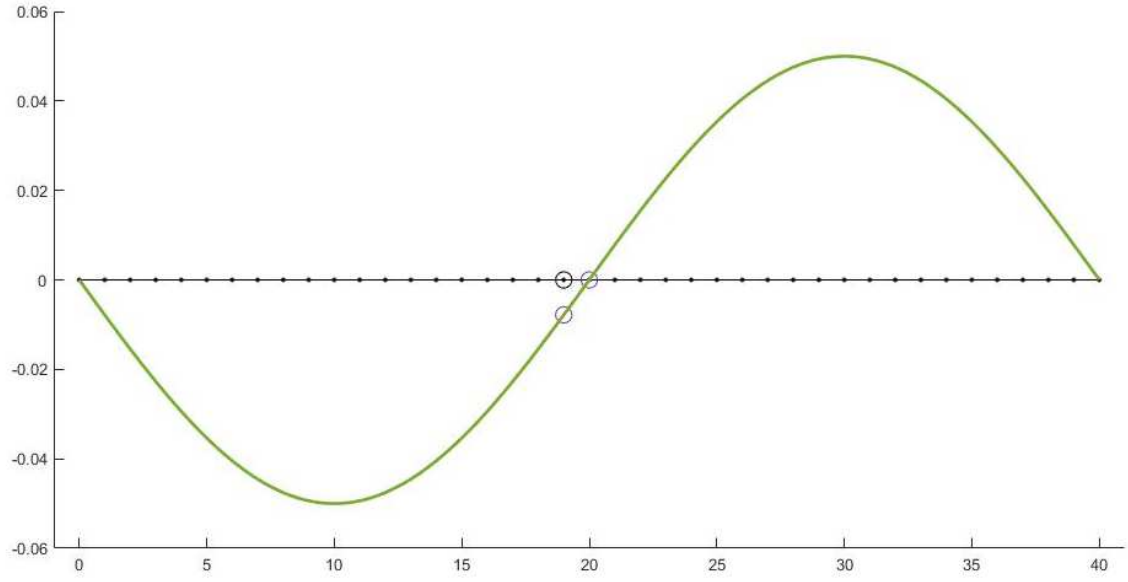

Picture 46: Second mode of vibration for high values of $\bar{\omega}$.

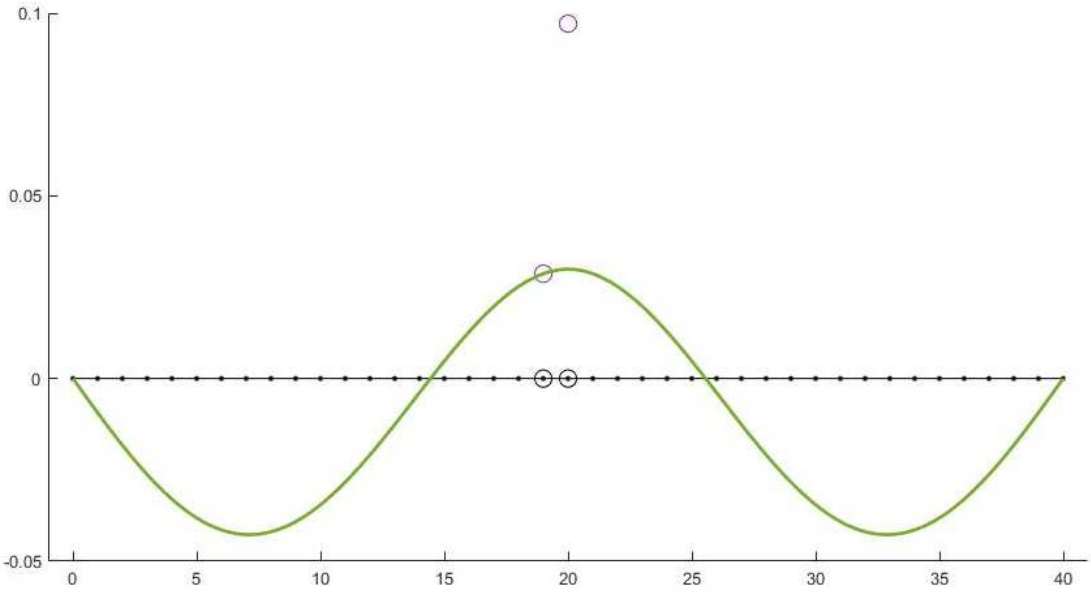

Picture 47: Third mode of vibration for high values of $\bar{\omega}$.

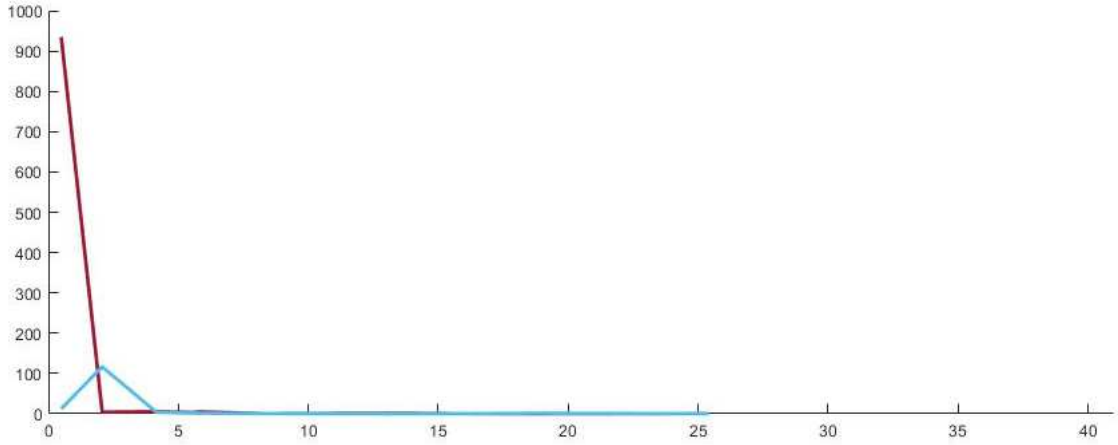

Picture 48: FRF of the displacement for high values of $\bar{\omega}$. The red line is measured for a point in the beam's centreline. The blue line is measured for a poin at one quarter of the length of the beam.

As the truck's stiffness becomes significant, the shapes of the system's mode of vibration coincide with those of the beam.

Lastly, Picture 49 shows the MPF of the first two mode of vibration of the bridge. The blue line is relative to the first mode of the bridge, the orange line to the second one. The MPF of the first mode decreases as $\bar{\omega}$ approaches to one. The curve has a jump discontinuity for the same values of $\bar{\omega}$ of the curve relative to the first frequency. The MPF of the second mode has a constant value equal to zero, which is the same value a beam in the unloaded configuration would have.

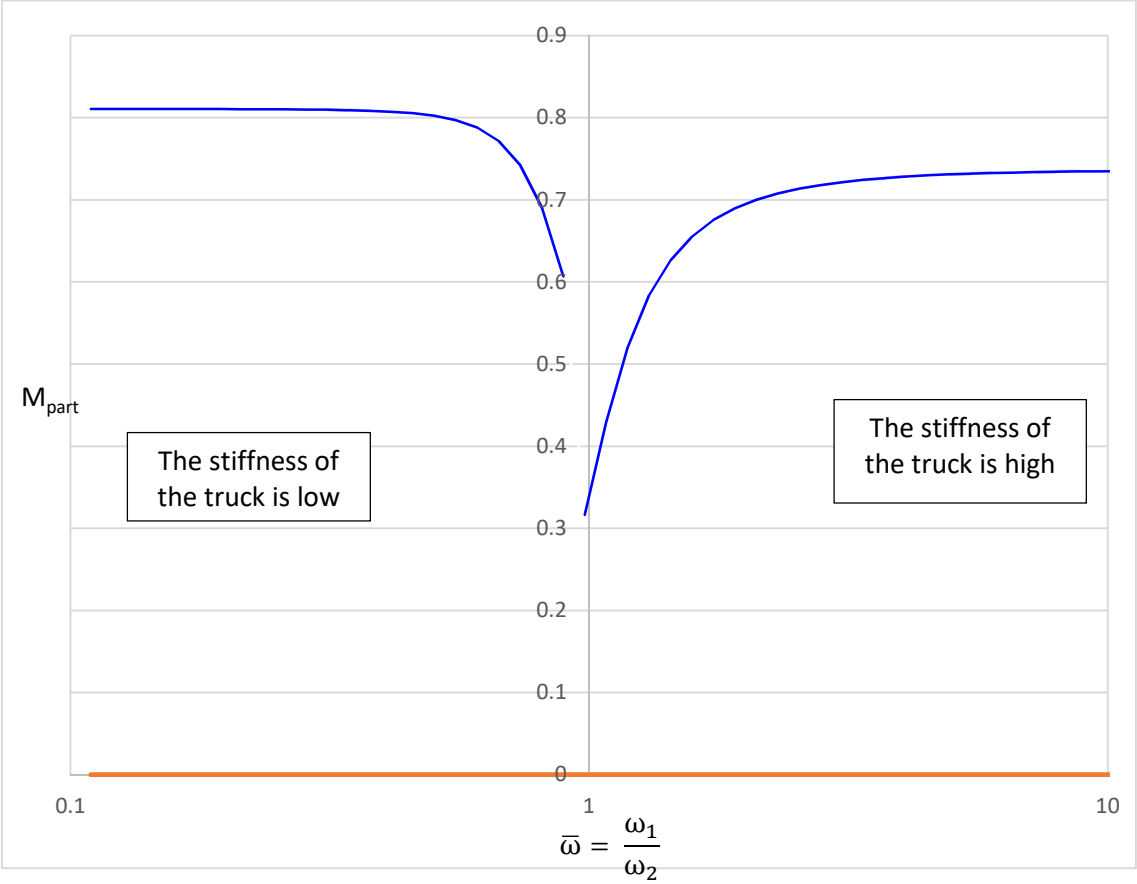

Picture 49: Mass participation factor for a bridge with a truck in the centreline. The blue line is relative to the first frequency of the bridge, the orange line is relative to the second one.

5.3. Influence of every parameters

To understand how every parameter can influence the results of the analysis, it is of use to analyse cases where only one parameter varies at a time. It is of interest to find out the influence of the mass ratio $\bar{m}$ – already observed in the 2DOF system –, the length ratio $\bar{L}$ and the load configuration – the number of trucks in the cross section and longitudinally.

5.3.1. The influence of $\bar{m}$

The influence of $\bar{m} = \frac{M_{truck}}{M_{loaded\ deck}}$ can be highlighted looking at Picture 50. It plots $\frac{\omega}{\omega_2}$ for different values of $\bar{m}$, for bridges with one truck in the cross section and longitudinally and a ratio $\bar{L} = 0{,}25$. The relative MPF are shown in Picture 51. It is possible to notice that:

- When the stiffness of the truck is low – left side of the graphs – as $\bar{m}$ increases, the value of $\frac{\omega}{\omega_2}$ increases as well;

- When the stiffness of the truck is high – right side of the graphs – as $\bar{m}$ increases, the value of $\frac{\omega}{\omega_2}$ decreases;
- Bridges with a higher ratio $\bar{m}$, have a lower mass participation factor;
- The position of the jump discontinuities depends on $\bar{m}$. It occurs for lower values of $\bar{\omega}$ for bridges with a higher $\bar{m}$.
- The height of the jump discontinuity in the frequency curve depends on $\bar{m}$. With respect to an unloaded bridge, one with an $\bar{m} = 0{,}2$ has a fundamental frequency that is 10% higher – on the left of the jump discontinuity – and 20% lower on the right of the jump discontinuity. These percentages become respectively 25% and 30% in case of a bridge with $\bar{m} = 1{,}4$
- The height of the jump discontinuity in the mass participation factor curve depends on $\bar{m}$. A bridge with an $\bar{m} = 0{,}2$ has an MPF that is 61% of the mass of the beam – on the left of the jump discontinuity – and 31% on the right of the jump discontinuity. These percentages become respectively 68% and 16% in case of a bridge with $\bar{m} = 1{,}4$.

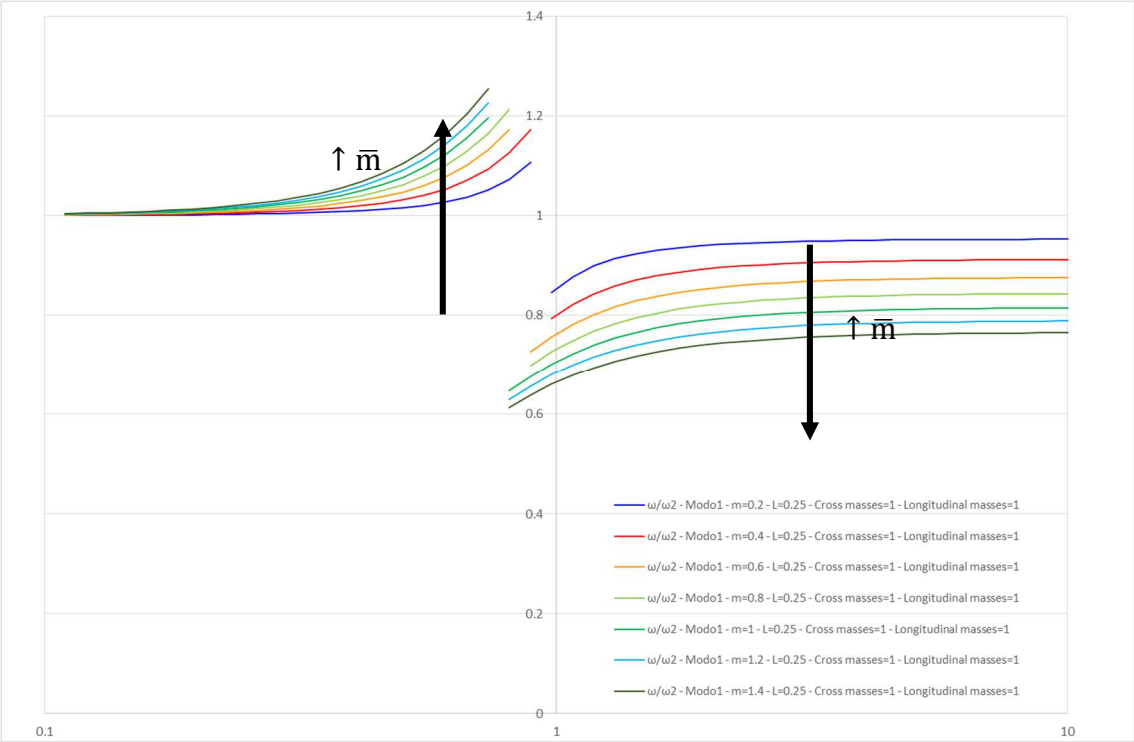

Picture 50: first circular frequencies for different values of $\overline{m}$ on bridges with a truck in the centreline.

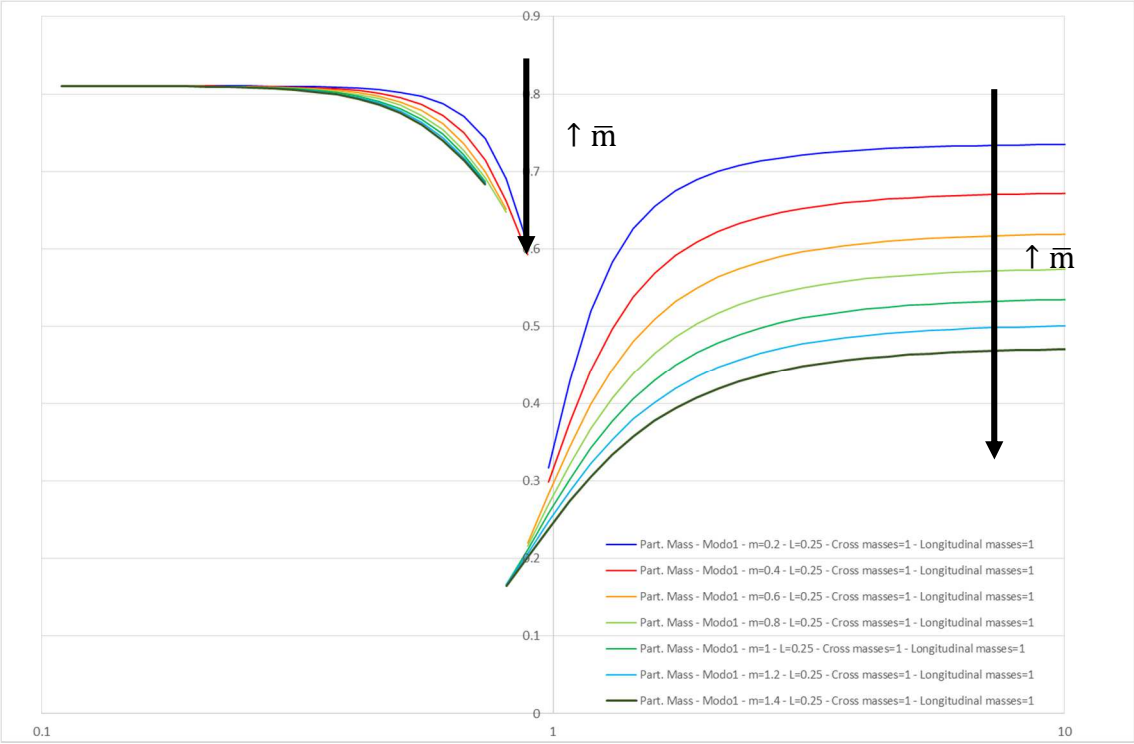

Picture 51: Mass participation factors for different values of $\overline{m}$ on bridges with a truck in the centreline.

5.4. Influence of the ratio $\bar{L}$

The influence of $\bar{L} = \frac{L_{loaded}}{L_{deck}}$ is studied comparing six different bridges. Picture 52 and Picture 53 show the curves of the first circular frequencies and the mass participation factors of bridges with $\bar{L} = 0{,}25$, $\bar{L} = 0{,}50$ and $\bar{L} = 0{,}75$. The orange curves are relative to bridges with an $\bar{m} = 1{,}4$ while the blue curves to ones with $\bar{m} = 0{,}2$. The load configuration is the one with one truck in the cross section and one in the deck span. From the graphs it is possible to observe that:

- When the stiffness of the truck is low – left side of the graphs – as $\bar{L}$ increases, the value of $\frac{\omega}{\omega_2}$ increases as well;
- When the stiffness of the truck is high – right side of the graphs – as $\bar{L}$ increases, the value of $\frac{\omega}{\omega_2}$ decreases;
- Bridges with a higher ratio $\bar{L}$, have a lower mass participation factor;
- The position of the jump discontinuities depends on $\bar{L}$. As $\bar{L}$ increases, it occurs for lower values of $\bar{\omega}$.
- The height of the jump discontinuity in the frequency curve depends on $\bar{L}$. With respect to an unloaded bridge, one with an $\bar{m} = 1{,}4$ and $\bar{L} = 0{,}25$ has a fundamental frequency that is 25% higher – on the left of the jump discontinuity – and 39% lower on the right of the jump discontinuity. These percentages become respectively 26% and 60% in case of a bridge with $\bar{L} = 0{,}75$
- The height of the jump discontinuity in the mass participation factor curve depends on $\bar{L}$. A bridge with an $\bar{m} = 1{,}4$ and $\bar{L} = 0{,}25$ has a MPF that is 70% of the mass of the beam – on the left of the jump discontinuity – and 16% on the right of the jump discontinuity. These percentages become respectively 76% and 7% in case of a bridge with $\bar{L} = 0{,}75$.

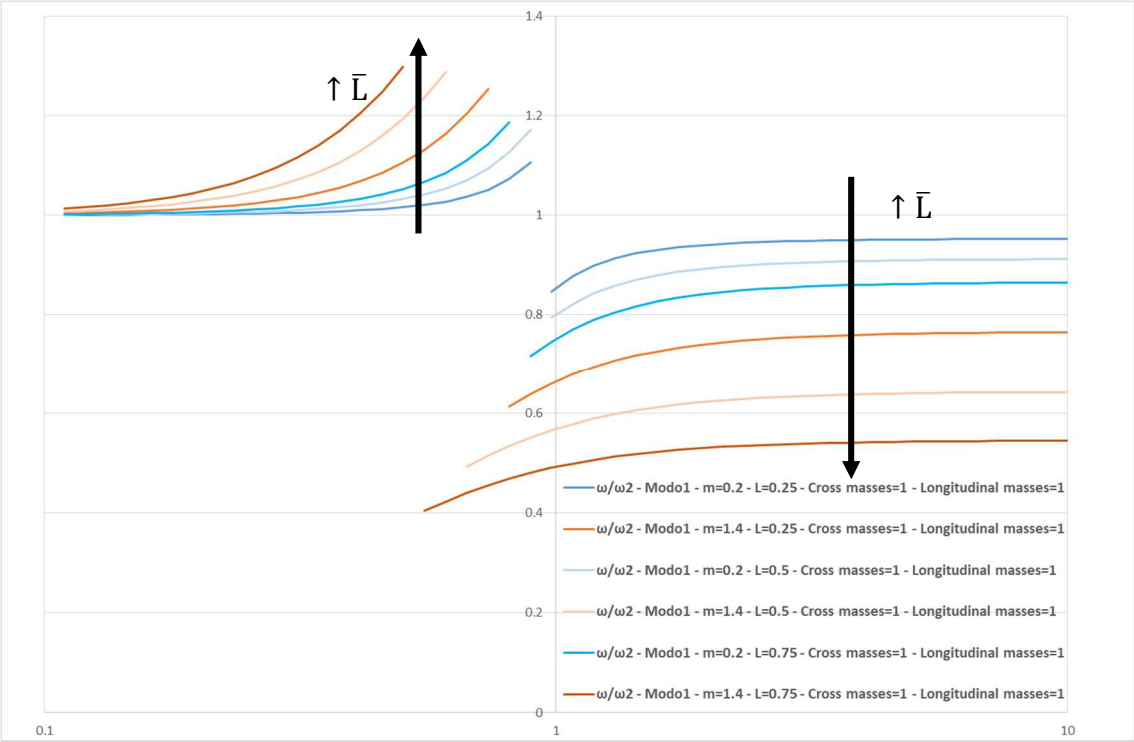

Picture 52: first circular frequencies for different values of $\bar{L}$ on bridges with a truck in the centreline

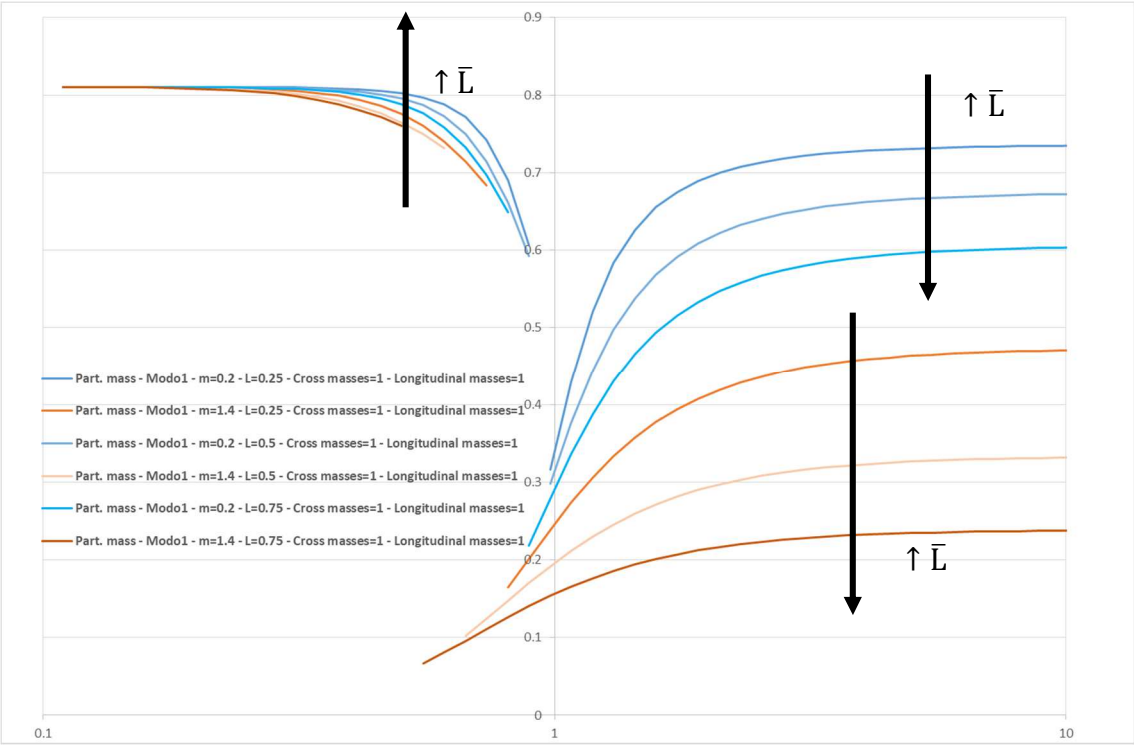

Picture 53: Mass participation factors for different values of $\bar{L}$ on bridges with a truck in the centreline

5.5. Influence of the number of trucks in the cross section

The influence of the number of trucks in the cross section can be highlighted looking at Picture 54 and Picture 55. They compare the first circular frequencies and the mass participation factors of bridges with $\bar{m} = 0{,}2$ or $\bar{m} = 1{,}4$ and $\bar{L} = 0{,}25$, with one, two or three masses in the cross section. It is possible to notice that:

- As the number of the masses in the cross section increases, the jump discontinuity occurs for higher values of $\bar{\omega}$.

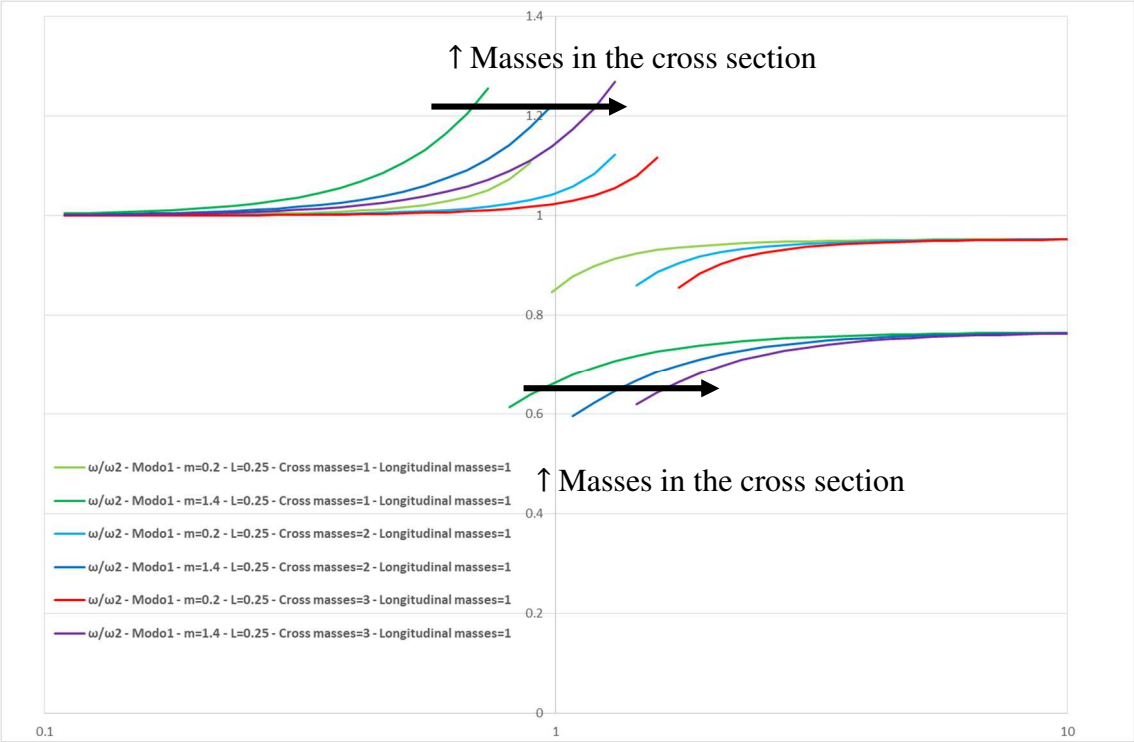

Picture 54: first circular frequencies for different values of $\overline{m}$ on bridges with one, two ore three truck in the cross section in the centreline.

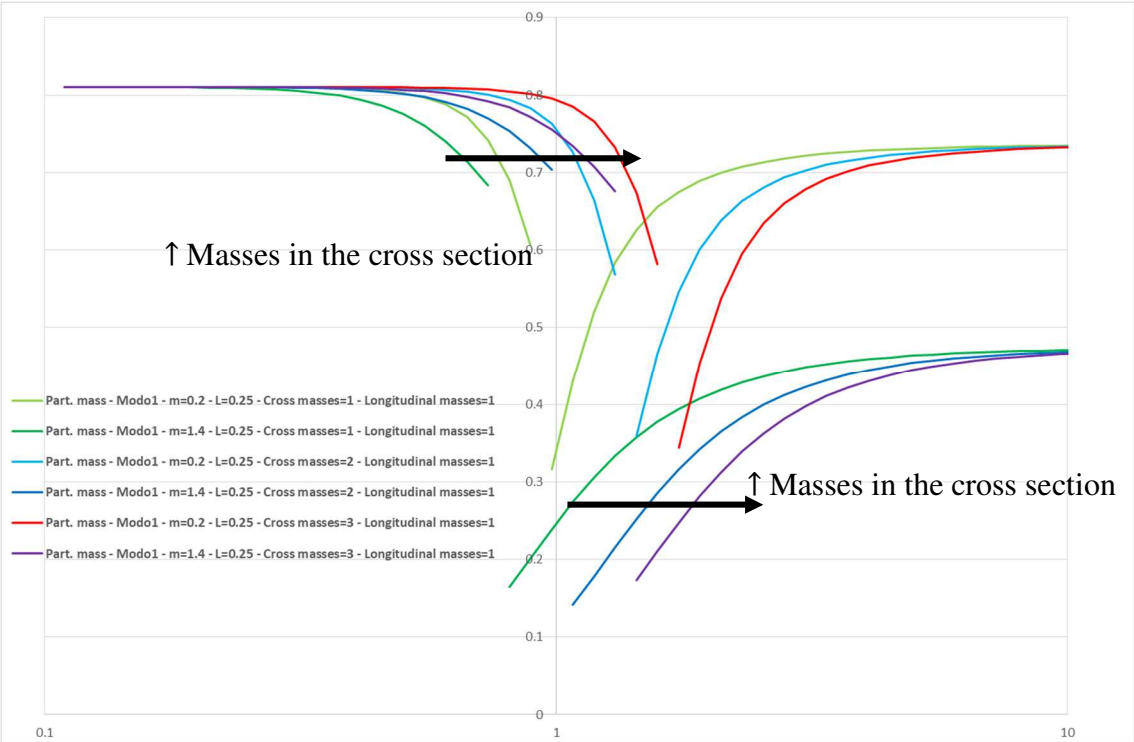

Picture 55: Mass participation factors for different values of $\overline{m}$ on bridges with one, two ore three truck in the cross section in the centreline.

5.6. Influence of the number of trucks in the deck span

The case of one truck in the centreline - which is the null point for the second mode of vibration - did not allow observations to be made on the second mode of vibration of a bridge. In the case of several longitudinal masses, the frequencies relative to the second mode also change. Picture 56 and Picture 57 show that the parameters considered previously – $\bar{L}$, $\bar{m}$ and masses in the cross section – have the same influence on the first and the second frequencies. For the second mode the MPF remains always zero.

The influence of the number of trucks in the deck span is studied comparing eight different bridges. Picture 58 and Picture 59 show the curves of the first circular frequencies and the mass participation factors of bridges with $\bar{L} = 0{,}25$, $\bar{L} = 0{,}50$ and $\bar{m} = 0{,}2$. The load configuration of the bridges sees one truck in the cross section and 2 or 4 trucks in the deck span. It is possible to observe that:

- The curves of $\frac{\omega}{\omega_2}$, for bridges with the same values of $\bar{L}$ and $\bar{m}$, and different load configuration, overlap. Therefore, the circular frequencies of the bridges do not depend on the number of longitudinal masses.
- The curves of the MPF, for bridges with the same values of $\bar{L}$ and $\bar{m}$, and different load configuration, overlap. Therefore, the participant mass factors of the bridges do not depend on the on the number of longitudinal masses.

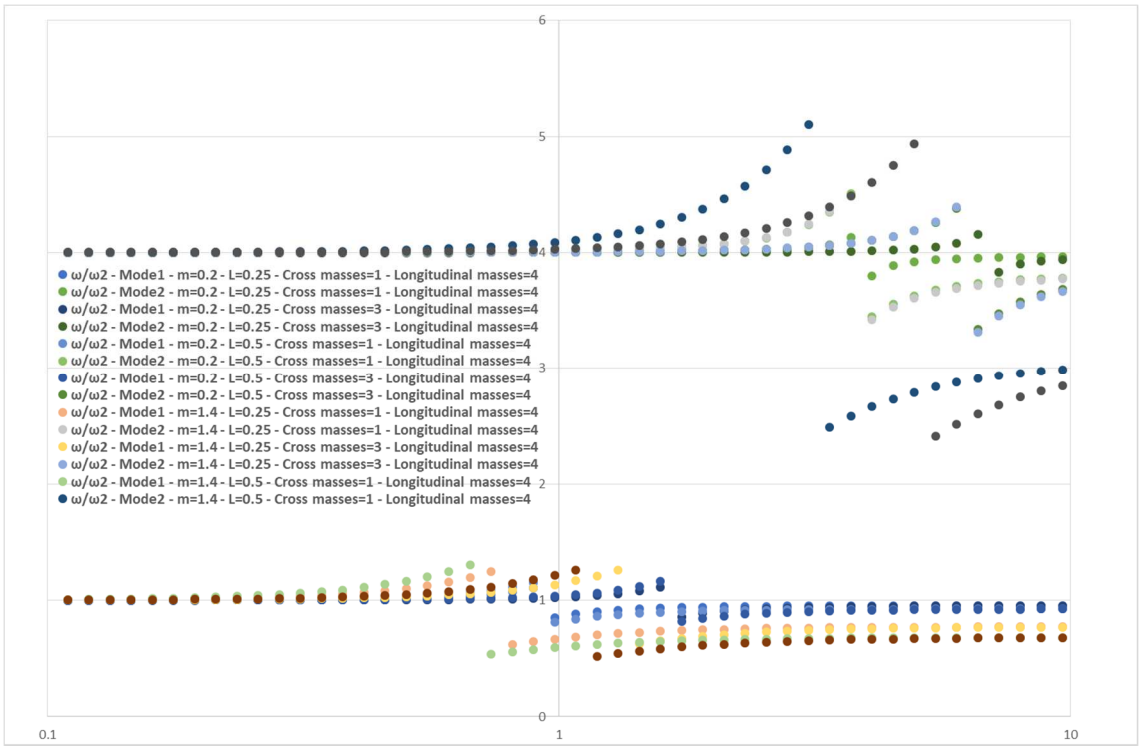

Picture 56: First and second circular frequencies for a set of bridges with $\bar{L} = 0{,}25$, $\bar{L} = 0{,}50$, $\bar{m} = 0{,}2$, $\bar{m} = 1{,}4$, 1 or 3 trucks in the cross section and four in the deck span.

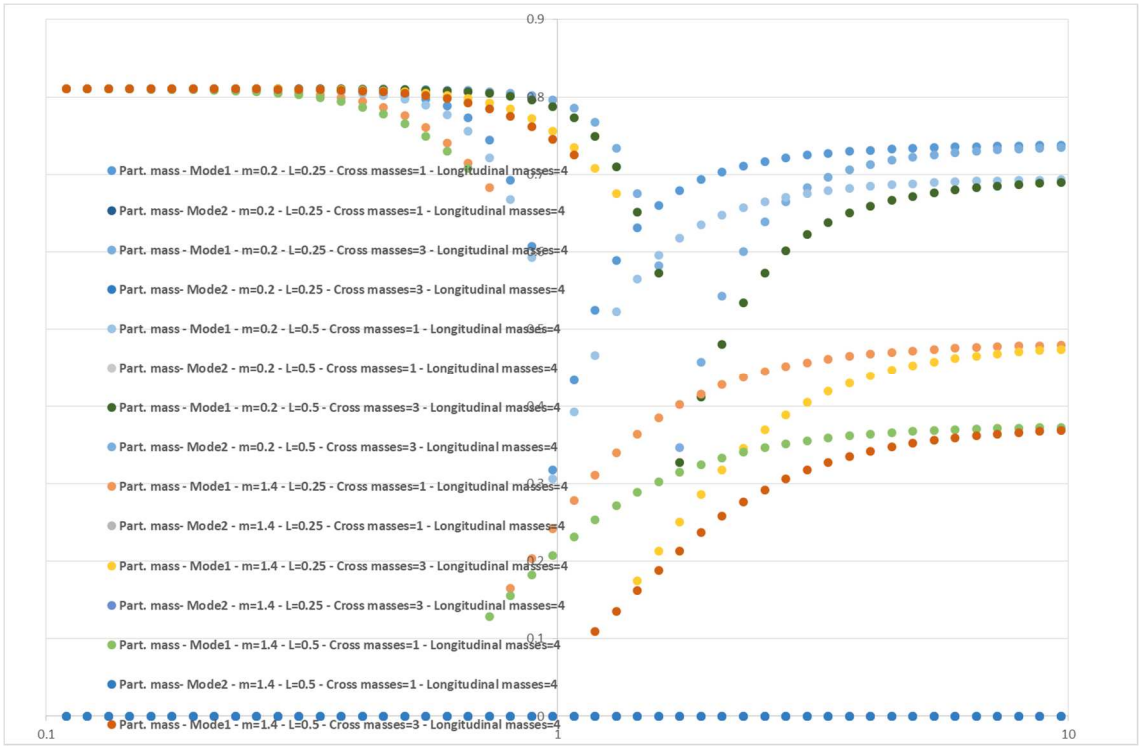

Picture 57: MPF for a set of bridges with $\bar{L} = 0{,}25$, $\bar{L} = 0{,}50$, $\bar{m} = 0{,}2$, $\bar{m} = 1{,}4$, 1 or 3 trucks in the cross section and four in the deck span.

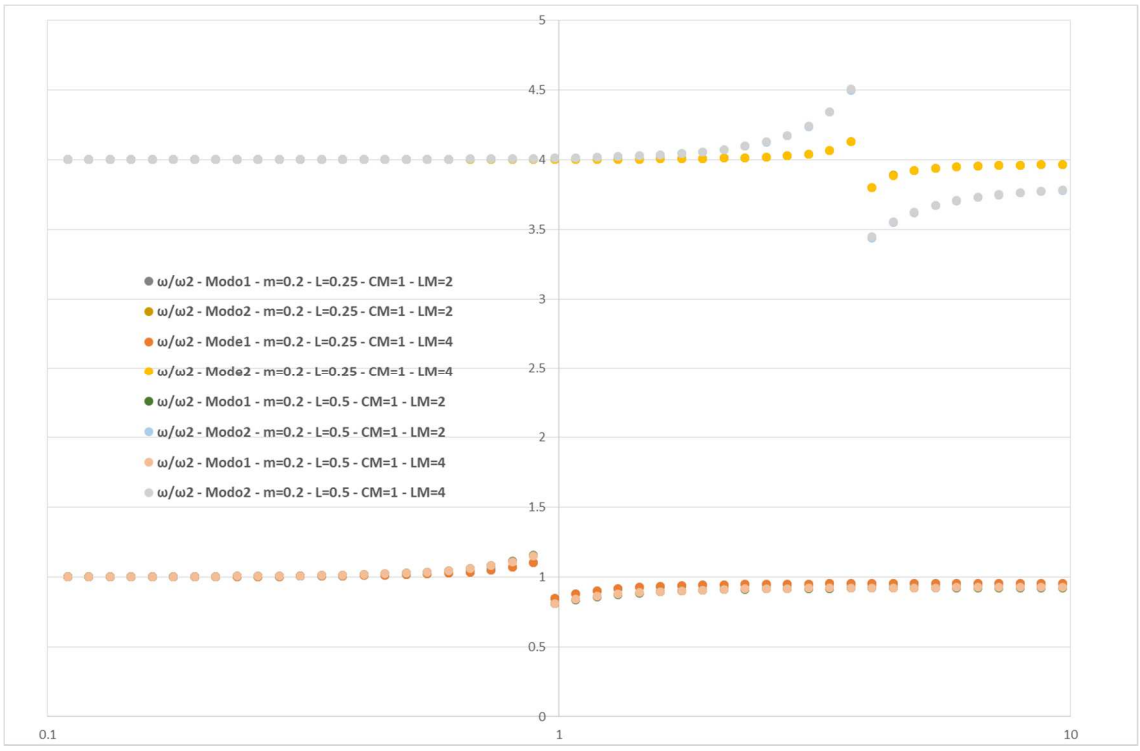

Picture 58: First circular frequencies for bridges with different ratios $\bar{L}$ and load configurations.

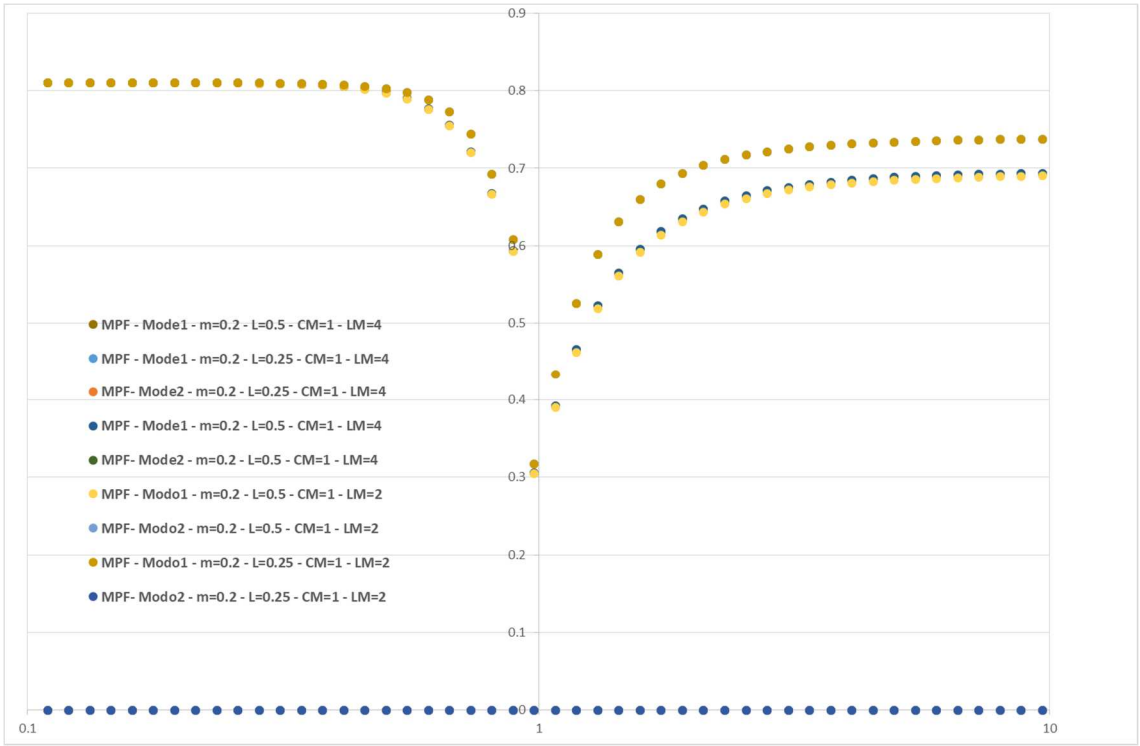

Picture 59 Mass participation factors for bridges with different ratios $\bar{L}$ and load configurations.

Conclusions

The mandatory Italian legislation provides for the execution of dynamic testing for road and railway bridges of significant importance. In particular, the fundamental period determined experimentally is required to be comparable with that foreseen in the design phase. To evaluate the real dynamic behaviour of the construction, the operational modal analysis is becoming increasingly important. This is carried out on the bridge in an unloaded condition and – to give consistency to the results and ensure the model validity – during the loading phases of the static proof test. As part of this thesis, the degree of complexity of an adequate modelling to evaluate the real dynamic behaviour of bridges during the loading phases was investigated. In the numerical model, trucks, used for static testing, are usually considered as simple increments of the mass of the bridge. Indeed, this method neglects the fact that they are complex dynamic systems themselves, whose interaction with the bridge can lead to significantly different results. For this reason, a more refined modelling has been proposed, which describes the trucks taking into account their flexibility.

At first the study was limited to simple analytical models, in which the bridge and the truck were reduced to a 1DOF system. The "increased masses" model consists of a spring whose stiffness is that of the bridge, and a mass whose value is the sum of the masses of the bridge and the truck. The more refined model is a 2DOF model in which the truck is coupled with the bridge with an in-series spring. The modal analysis, conducted on both systems (1DOF and 2DOF), allowed to derive the frequencies. These have been studied for changing truck stiffness.

Picture 60 shows, the value of the two natural frequencies of the 2DOF system – normalized with respect to the frequency of the unloaded bridge – for changing ratios of $\bar{\omega}$ – defined as the ratio between the frequency of the truck and the frequency of the bridge.

In the case of trucks with low stiffness, the fundamental period of the bridge is the second period of the 2DOF system, while when the stiffness of the truck is high, the first period of the 2DOF system is also the fundamental period of the bridge.

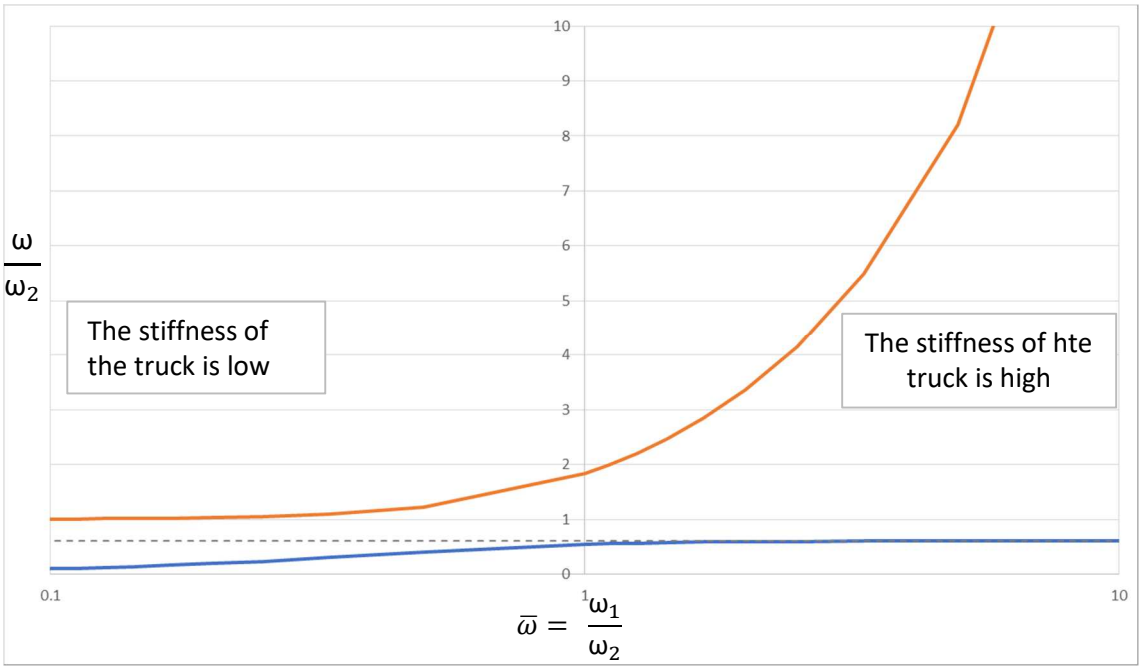

Picture 60: The two natural frequencies of the 2DOF system for changing values of $\bar{\omega}$.

The first natural frequency of the bridge obtained from the two models, is very different for those cases where the own frequencies of the bridge and the truck are similar. For these values of $\bar{\omega}$ – defined as the ratio between the frequency of the truck and the frequency of the bridge – a bridge-truck interaction was observed. The latter behaves like a tuned mass damper, modifying the dynamic behaviour of the bridge. In these cases, the use of an increased mass model – which cannot grasp this interaction – leads to a misinterpretation of the OMA.

Driven by the observations made on these simplified models, a finite element modelling of a bridge during the loading phases was performed. The study was conducted for single-span bridges of different lengths. The goal was to monitor the variation of the fundamental frequency of the bridge as various parameters vary, such as:

- The stiffness of the truck;
- The load configuration – intended as the number of trucks disposed longitudinally and in the cross section;
- The ratio $\bar{L} = \frac{L_{loaded}}{L_{deck}}$;
- The ratio $\bar{m} = \frac{M_{truck}}{M_{loaded\ deck}}$;

Picture 61 shows the frequencies of the first two modes of a bridge (which is under certain load conditions: $\bar{m} = 0{,}2$, $\bar{L} = 0{,}5$, there are 4 trucks longitudinally and one transversely), normalized with respect to the fundamental frequency of the unloading bridge. Picture 62 shows the relative participation mass factors.

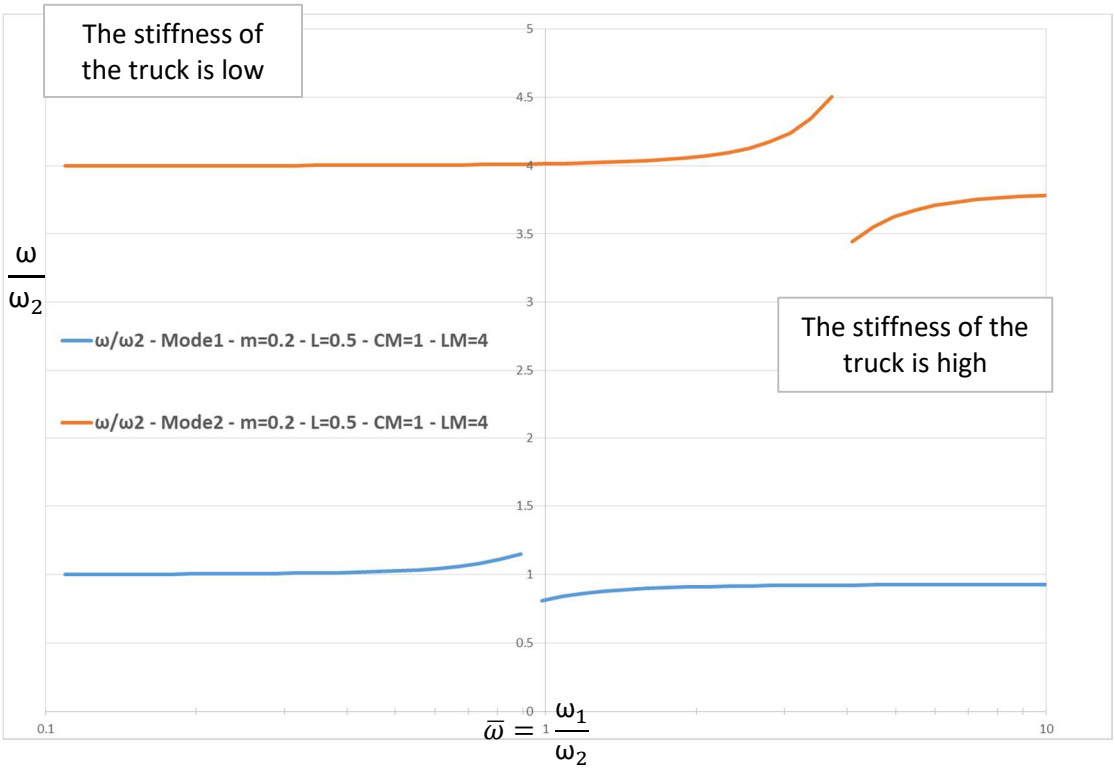

Picture 61: The first two natural frequencies of a bridge (under certain load conditions), for different values of $\bar{\omega}$.

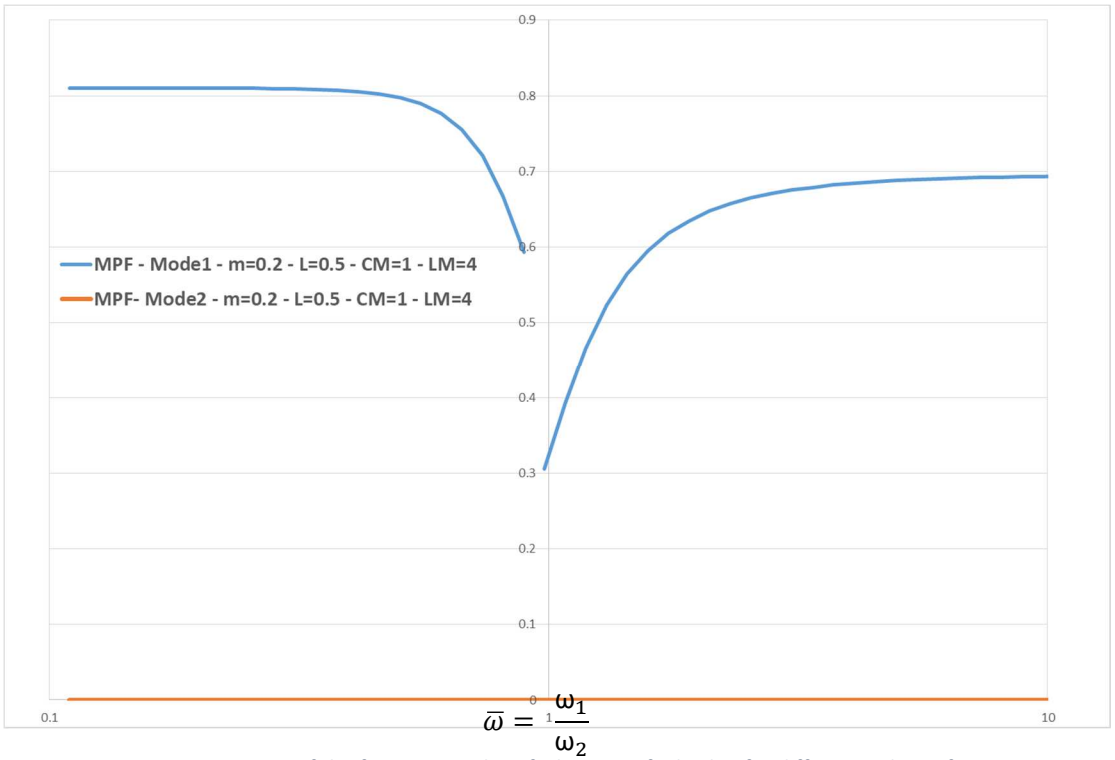

Picture 62: MPF of the first two modes of vibration of a bridge for different values of $\bar{\omega}$.

It has been observed that when trucks are very flexible, the fundamental frequencies of the loaded and unloaded bridges are similar. Conversely, when the trucks have a stiffness comparable to that of the bridge, the fundamental frequency of the loaded bridge changes considerably compared to that of the bridge in the unloaded configuration. In particular, where the jump discontinuity occurs, the ratio between these two frequencies reaches maximum values of about 1.3 and minimum values of about 0.5.

This difference is all the more pronounced the higher the ratio $\bar{L}$ and $\bar{m}$ are. Furthermore, as the value of these two parameters increases, the range of frequencies for which the truck behaves as a TMD is wider. It was found that increasing the number of masses in the cross section causes the truck to behave like a TMD for higher values of $\bar{\omega}$ – when the truck is stiffer than the bridge. Finally, the arrangement of several trucks along the bridge, if it occurs in a symmetrical way, has an effect limited to the frequencies of the second mode – for which all the previous conclusions are valid.

Bibliography

- Fabrizio Gara, Vanni Nicoletti, Sandro Carbonari, Laura Ragni, Andrea Dall'Asta, "*Dynamic monitoring of bridges during static load tests: influence of the dynamics of trucks on the modal parameters of the bridge"*, Journal of civil structural health monitoring 2020.
- UNI 10985, *"Vibrazioni su ponti e viadotti – linee guida per l'esecuzione di rilievi dinamici"*.
- Law n.1086 5.11.1971*, "Norma per la disciplina delle opere di conglomerato cementizio armato, normale, precompresso ed a struttura metallica"*.
- D.M. 17.01.2018, *"Nuove Norme Tecniche per le Costruzioni", (NTC'18).*
- D. J. Ewins, *"Modal Testing: Theory, Practice and Applications"*, 2002.
- Fabrizio Gara, "*Notes from the course Strutture Speciali*", Università Politecnica delle Marche, 2020.
- Giovanni Fabbrocino, C. Rainieri , G. M. Verderame, "*L'analisi dinamica sperimentale e il monitoraggio delle strutture esistenti",* Università degli Studi del Molise, Università degli Studi "Federico II" di Napoli, Consorzio ReLUIS.
- Mehdi Batel, Brüel & Kjær, Norcross, "*Operational Modal Analysis – Another Way of Doing Modal Testing",* Sound and vibration, august 2002.
- M. Danial A. Hasan, Z. A. B. Ahmad , M. Salman Leong , L. M. Hee, *"Enhanced frequency domain decomposition algorithm: a review of a recent development for unbiased damping ratio estimates",* Journal of Vibroengineering, Vol. 20, Issue 5, 2018, p. 1919-1936.

- S. Bolsunovsky, V. Vermel, G. Gubanov, A. Leontiev, "*Reduction of flexible workpiece vibrations with dynamic support realized as tuned mass damper*", 14th CIRP Conference on Modeling of Machining Operations(CIRP CMMO), 2013.
- Fabio Beni, *"Caratterizzazione dinamica e analisi dei segnali"*, capitolo 2, Università degli Studi di Genova, Facoltà di Ingegneria.
- Indapro, schede tecniche dei prodotti, Vibrodine elettro-meccaniche e Vibrodine elettro-idrauliche.
- Mola Elena, Mola Franco, Vanali Marcello e Cigada Alfredo *"Il collaudo dinamico di ponti autostradali come potente strumento di conoscenza e validazione ad integrazione del collaudo statico tradizionale",* Article on Ingenio-web.it, 2016.

Appendix

This appendix shows all the results of the analysis. For ensure readability they have been divided in sets. The graphs are first divided according to the number of longitudinal masses on the bridge, then according to the ratio $\bar{L}$ and finally according to the number of masses in the cross section. Every graph shows the curves for different ratios $\overline{m}$.

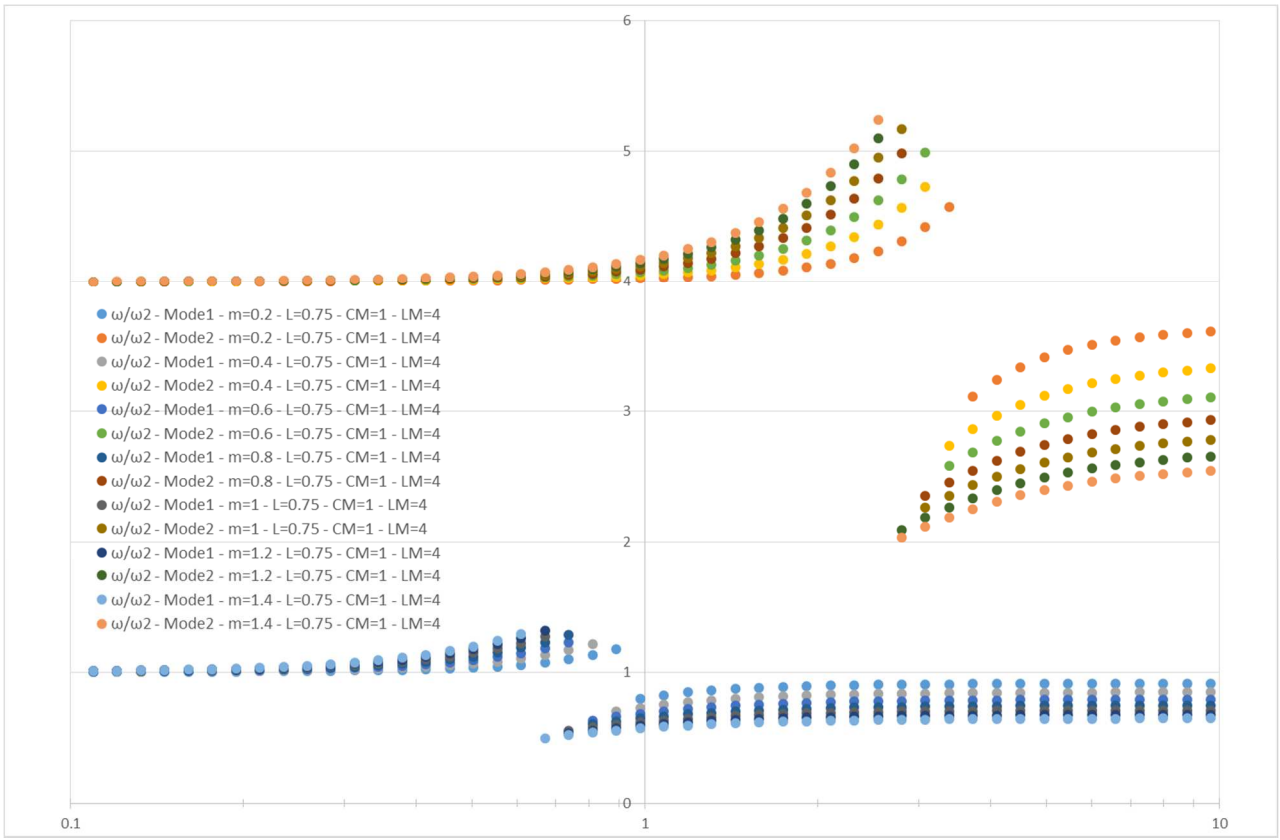

Picture 63: Circular frequencies of bridges with $\bar{L} = 0{,}75$; one truck in the cross section; fours truck in the span.

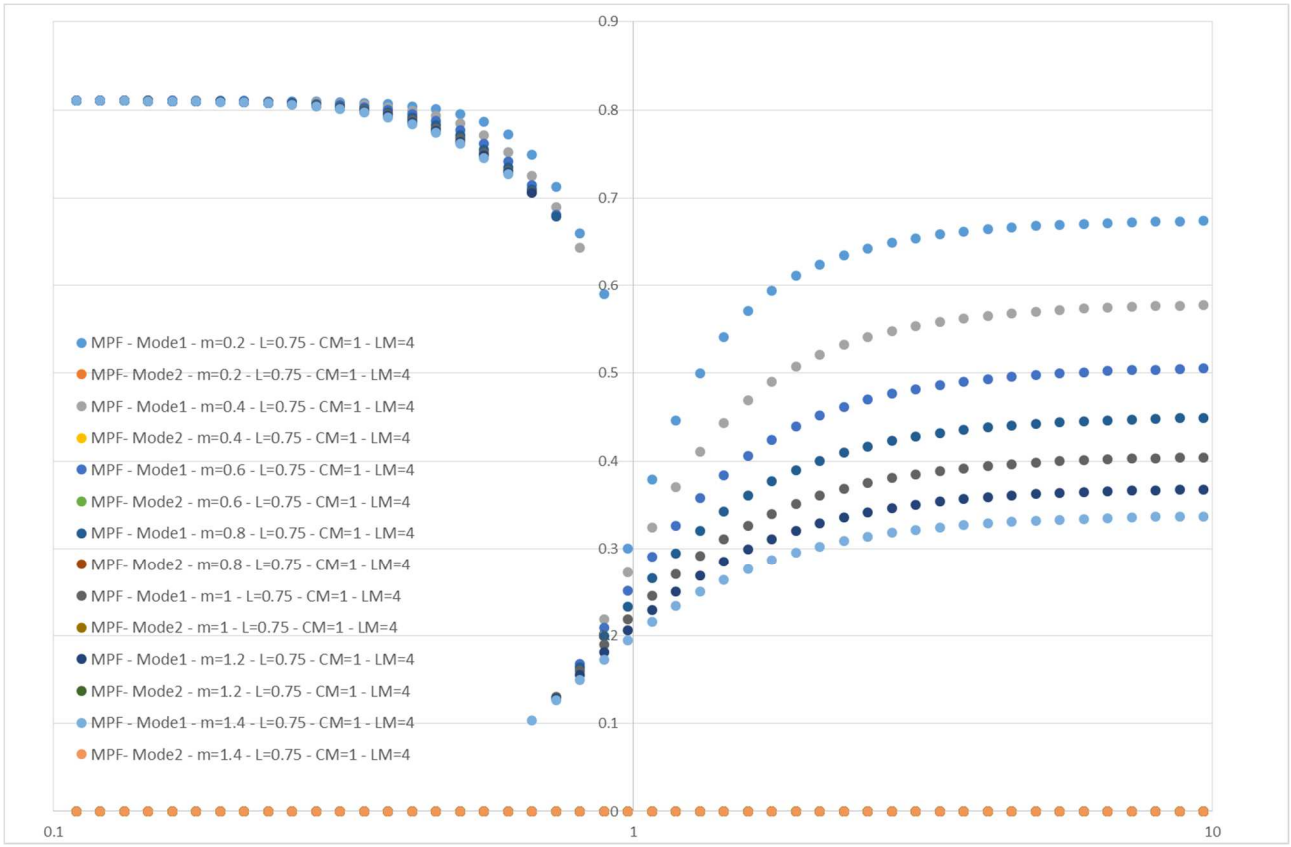

Picture 64: MPF of bridges with $\bar{L} = 0{,}75$; one truck in the cross section; four trucks in the span.

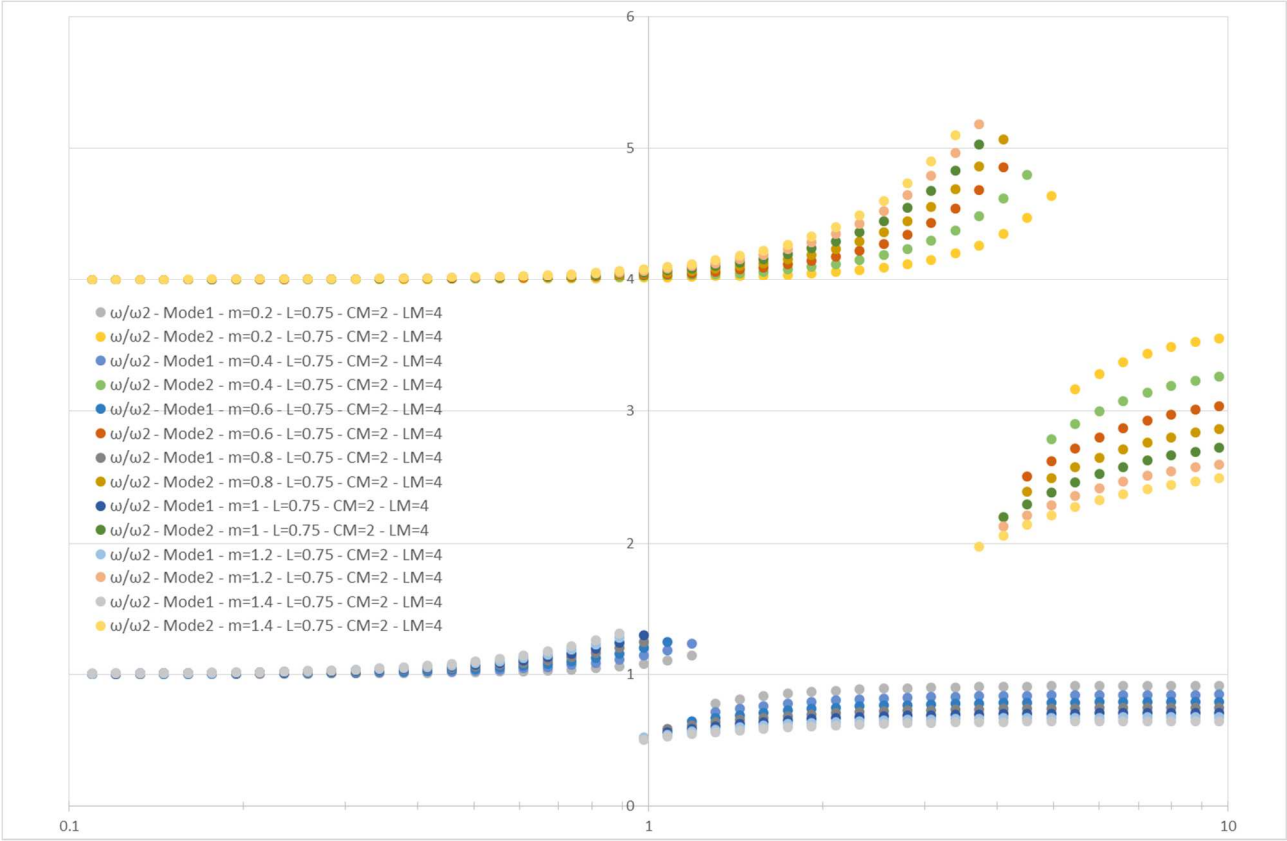

Picture 65: Circular frequencies of bridges with $\bar{L} = 0{,}75$; two trucks in the cross section; four trucks in the span.

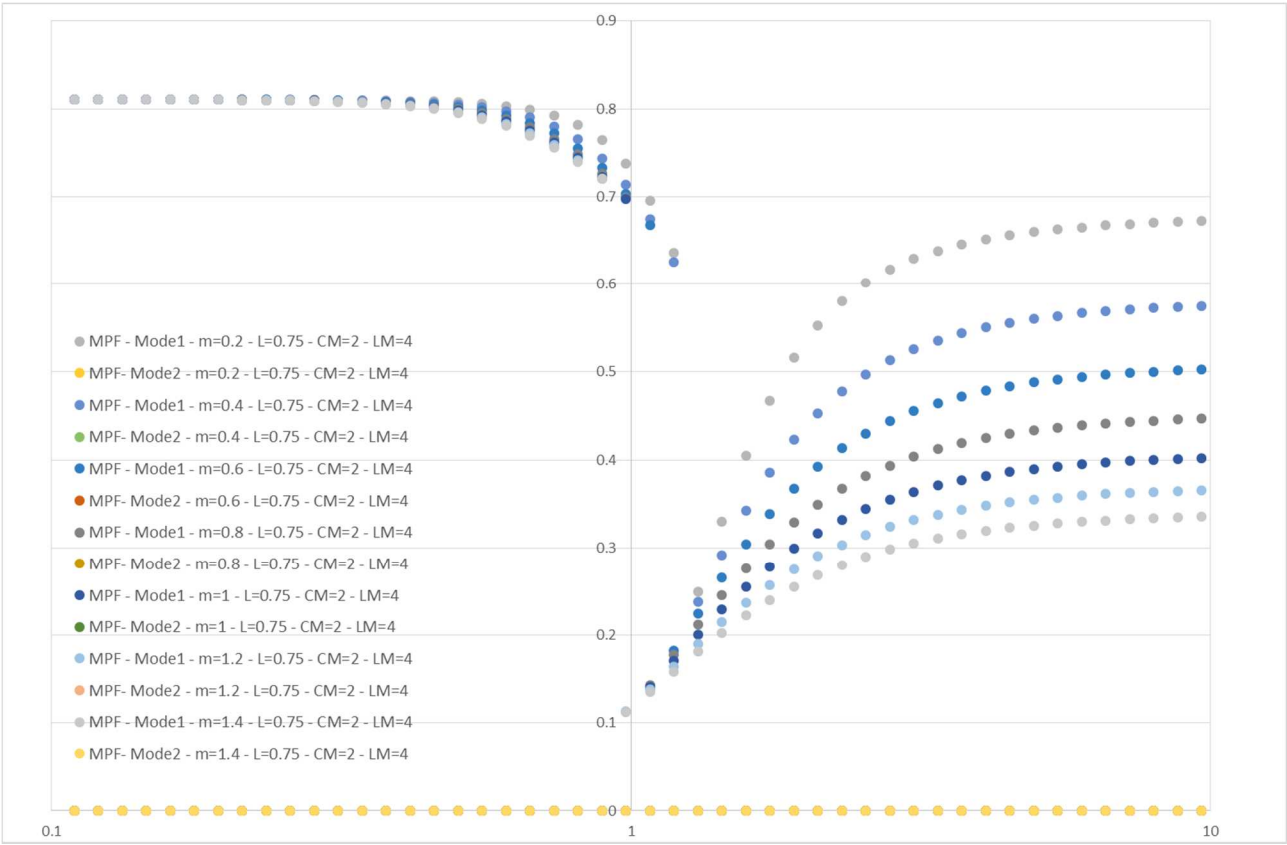

Picture 66: MPF of bridges with $\bar{L} = 0{,}75$; two trucks in the cross section; four trucks in the span.

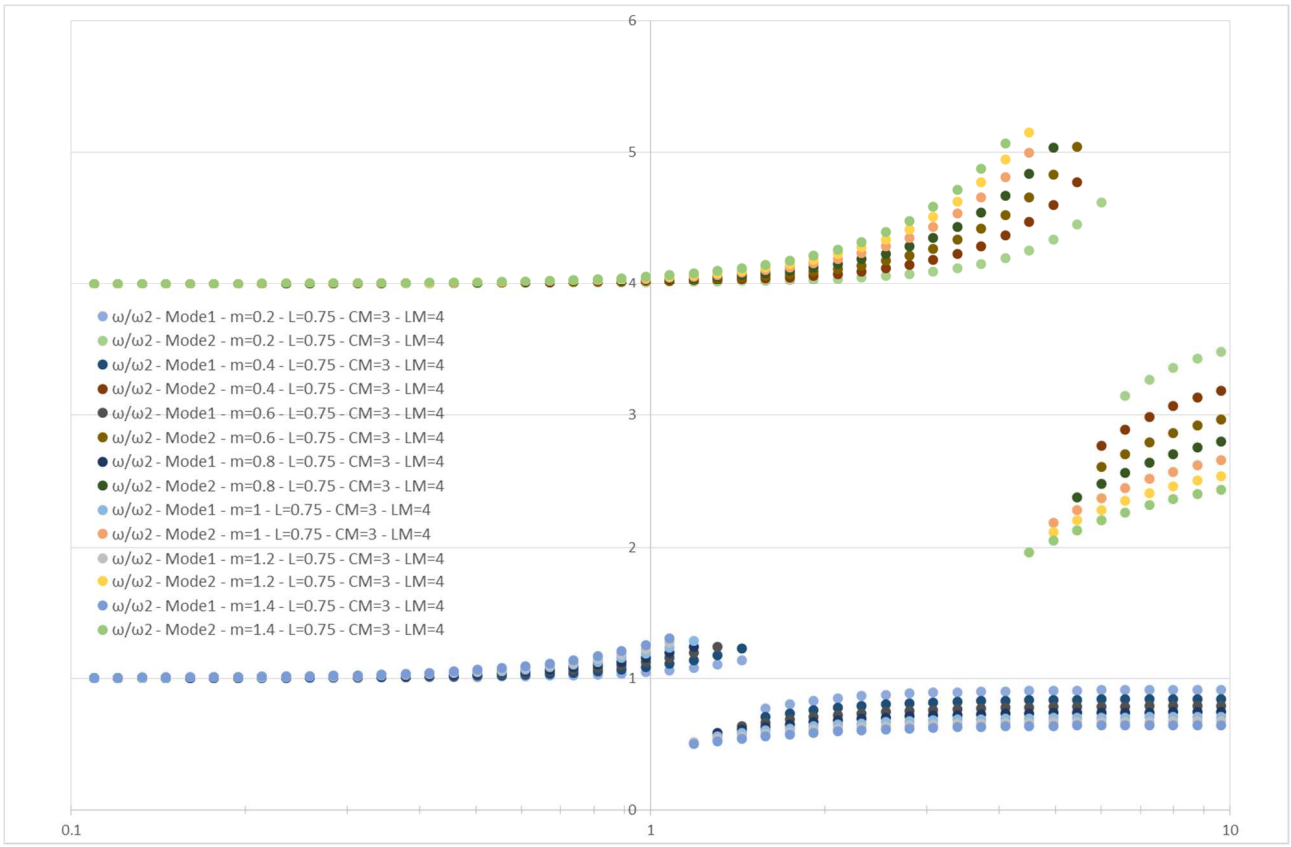

Picture 67: Circular frequencies of bridges with $\bar{L} = 0{,}75$; three trucks in the cross section; four trucks in the span.

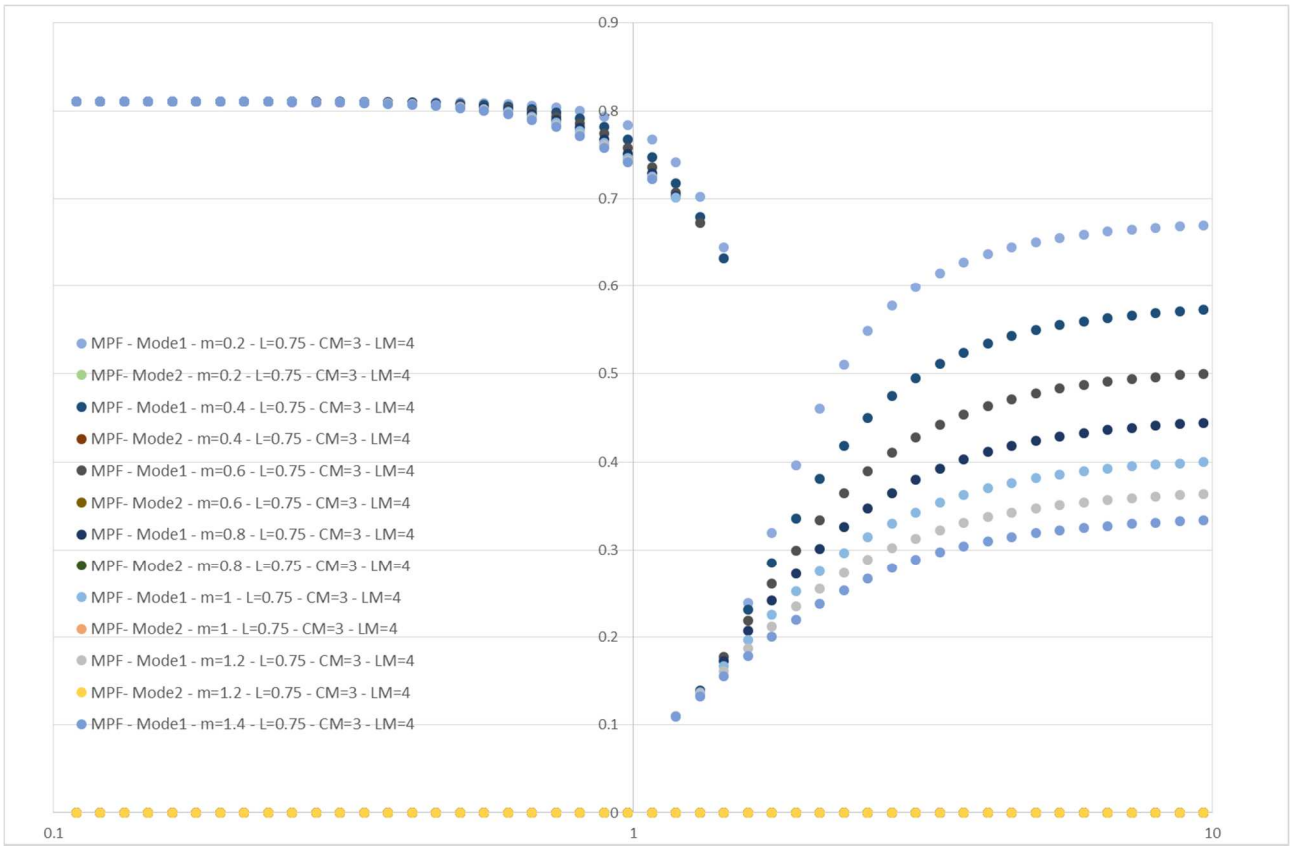

Picture 68: MPF of bridges with $\bar{L} = 0{,}75$; three trucks in the cross section; four trucks in the span.

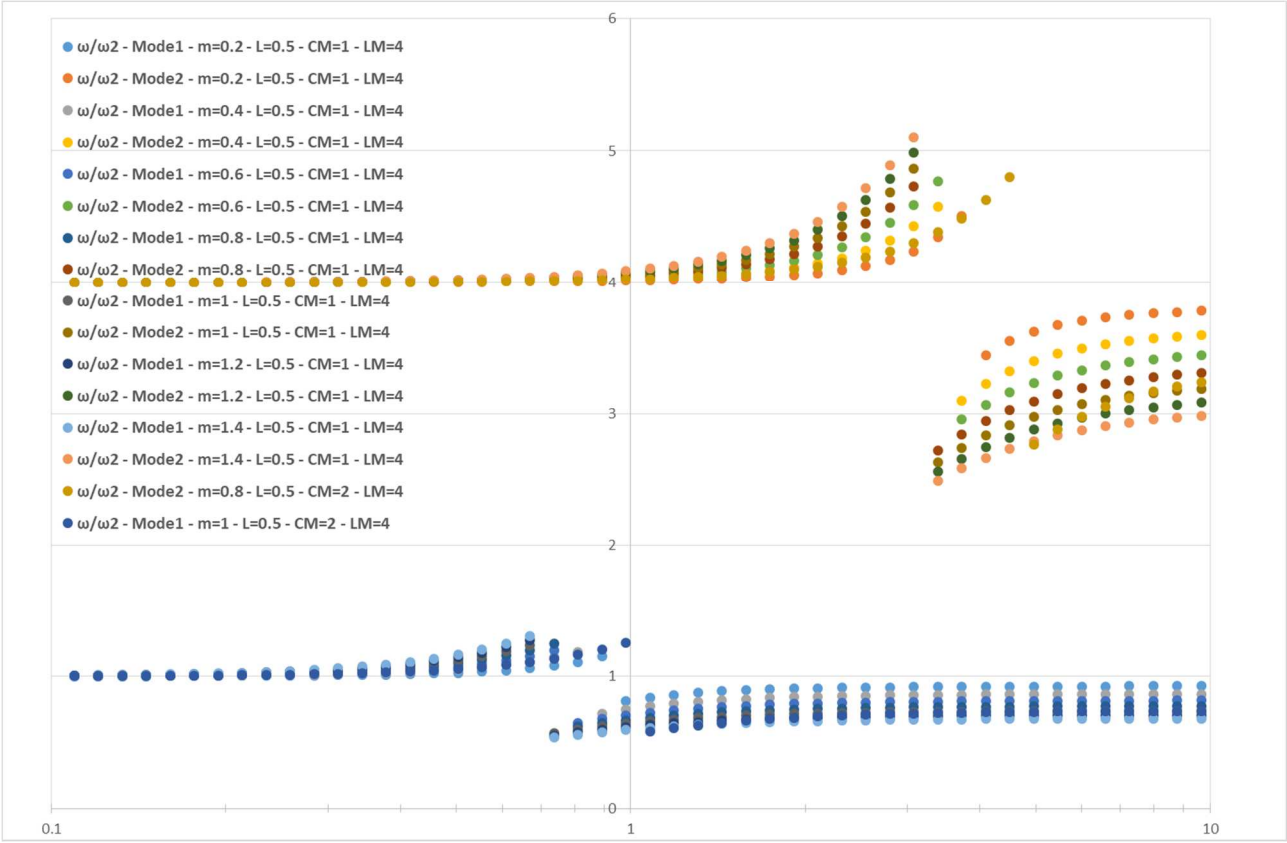

Picture 69: Circular frequencies of bridges with $\bar{L} = 0{,}50$; one truck in the cross section; four trucks in the span.

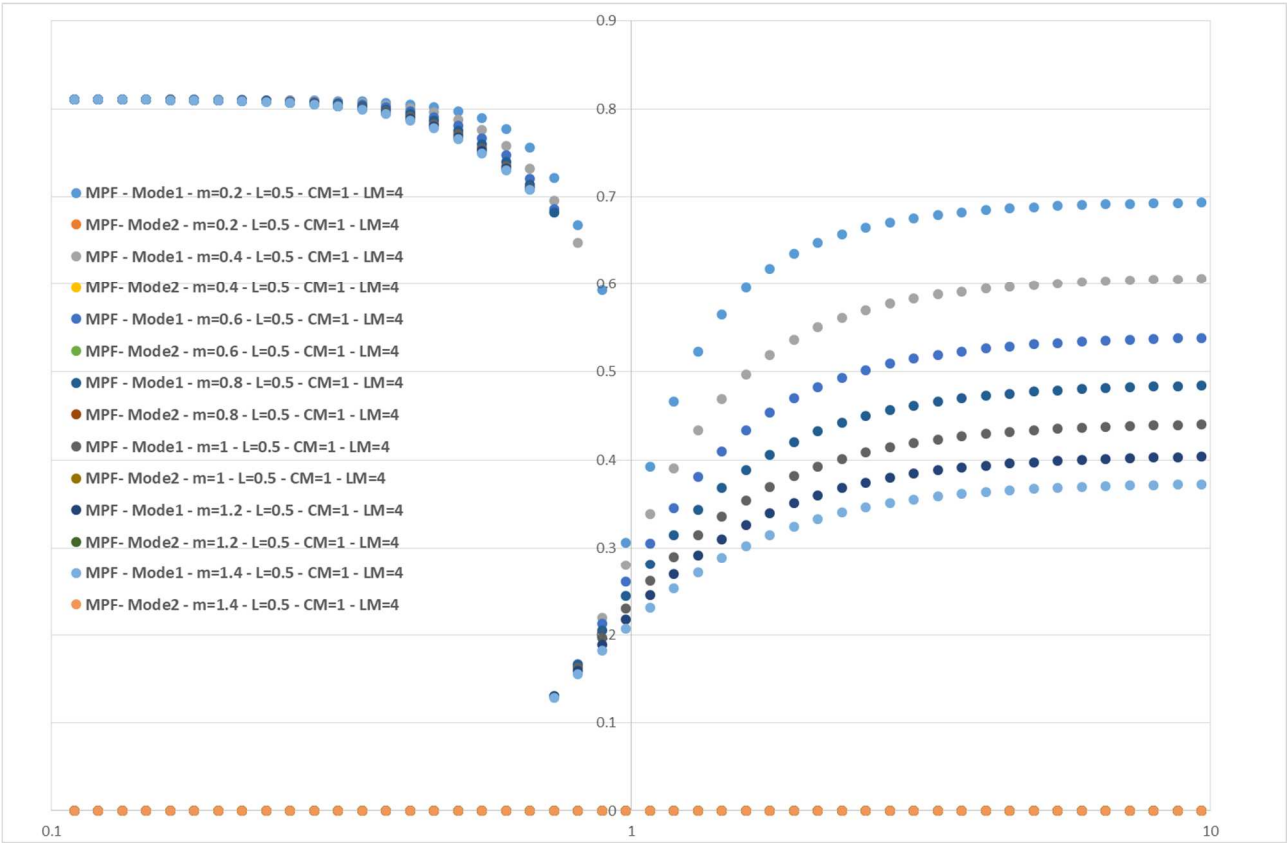

Picture 70: MPF of bridges with $\bar{L} = 0{,}50$; one truck in the cross section; four trucks in the span.

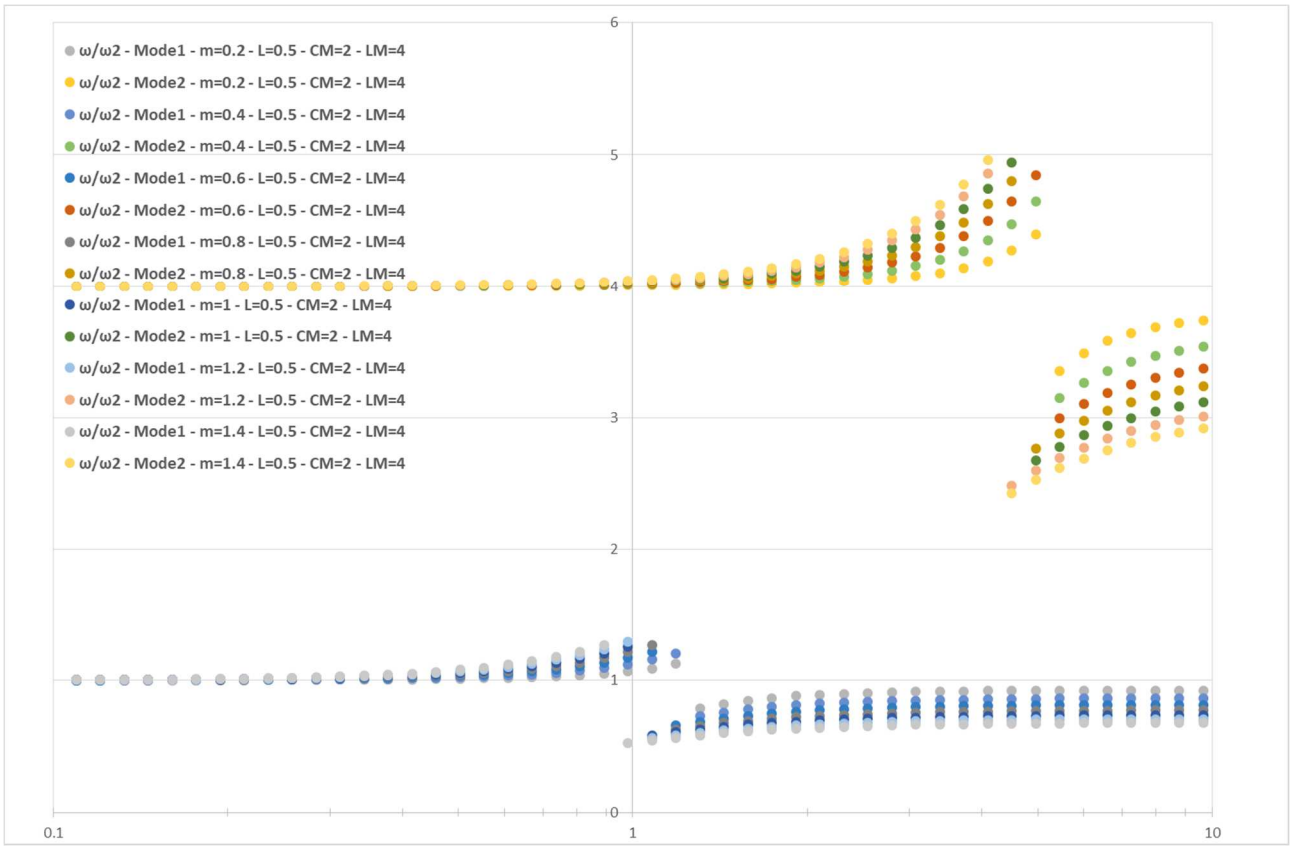

Picture 71: Circular frequencies of bridges with $\bar{L} = 0{,}50$; two trucks in the cross section; four trucks in the span.

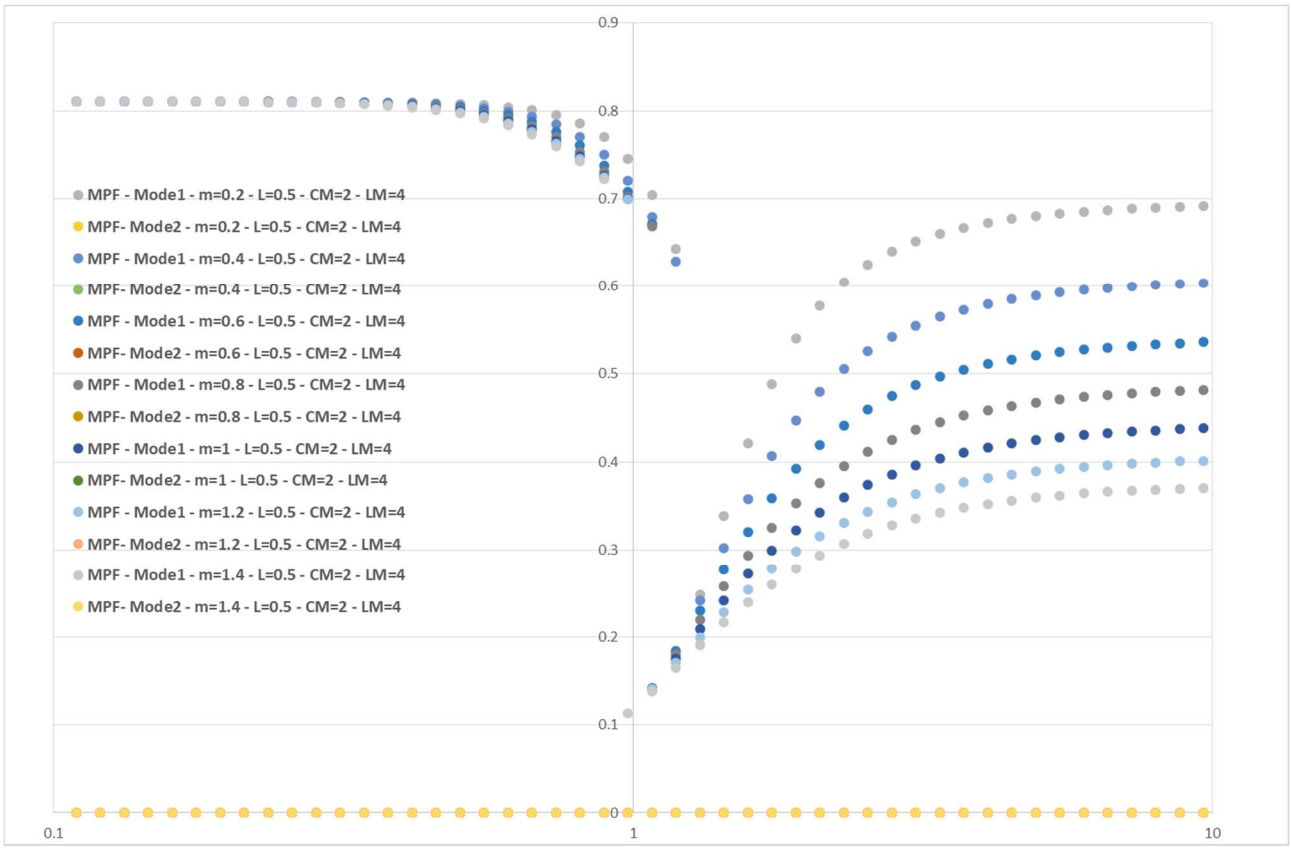

Picture 72: MPF of bridges with $\bar{L} = 0{,}50$; two trucks in the cross section; four trucks in the span.

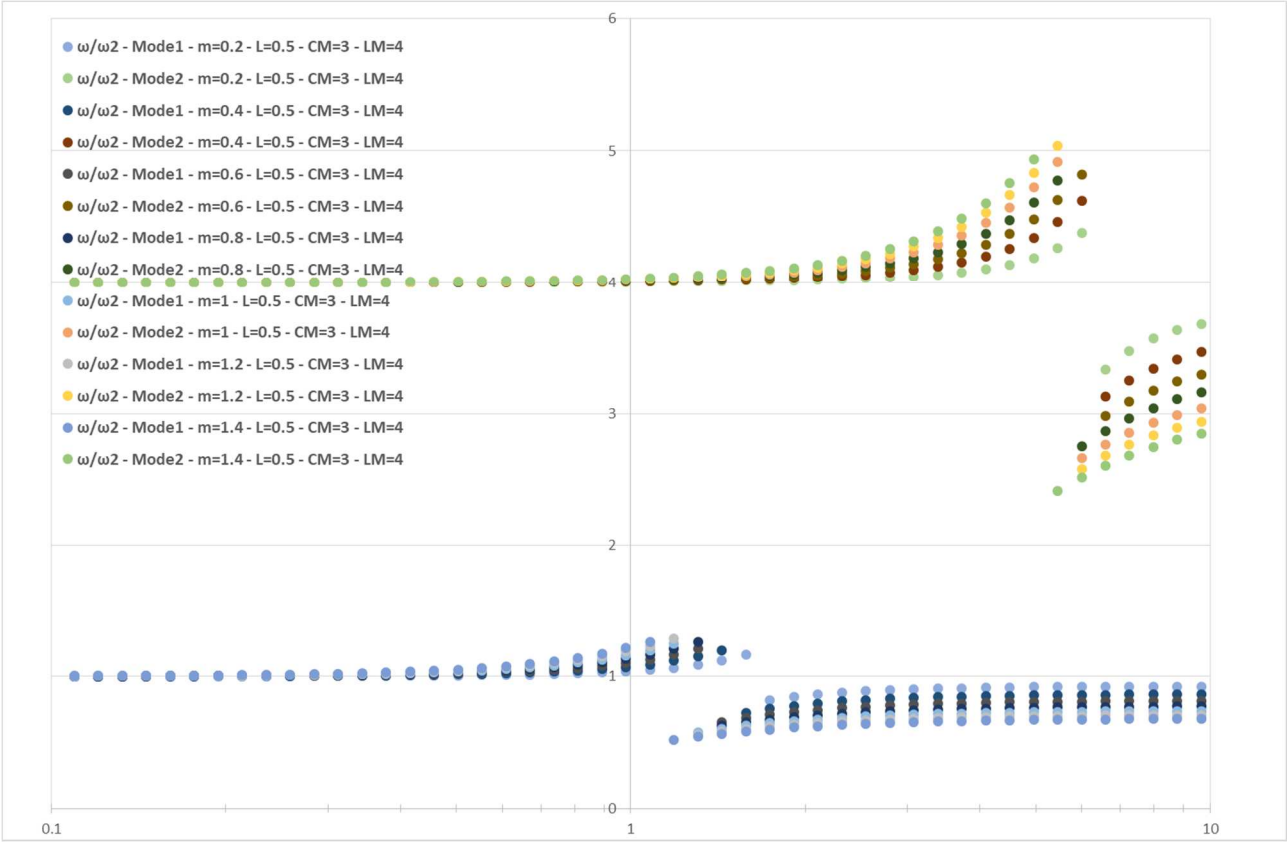

Picture 73: Circular frequencies of bridges with $\bar{L} = 0{,}50$; three trucks in the cross section; four trucks in the span.

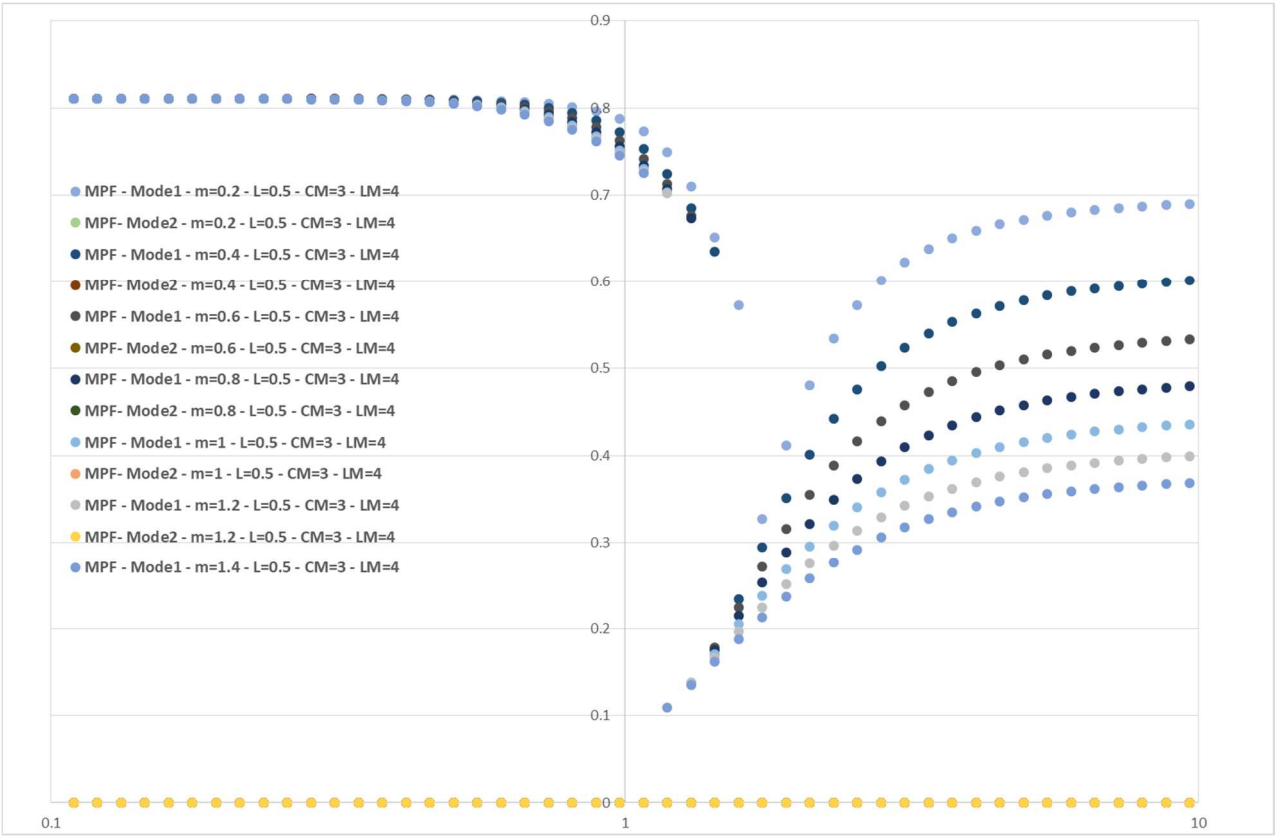

Picture 74: MPF of bridges with $\bar{L} = 0{,}50$; three trucks in the cross section; four trucks in the span.

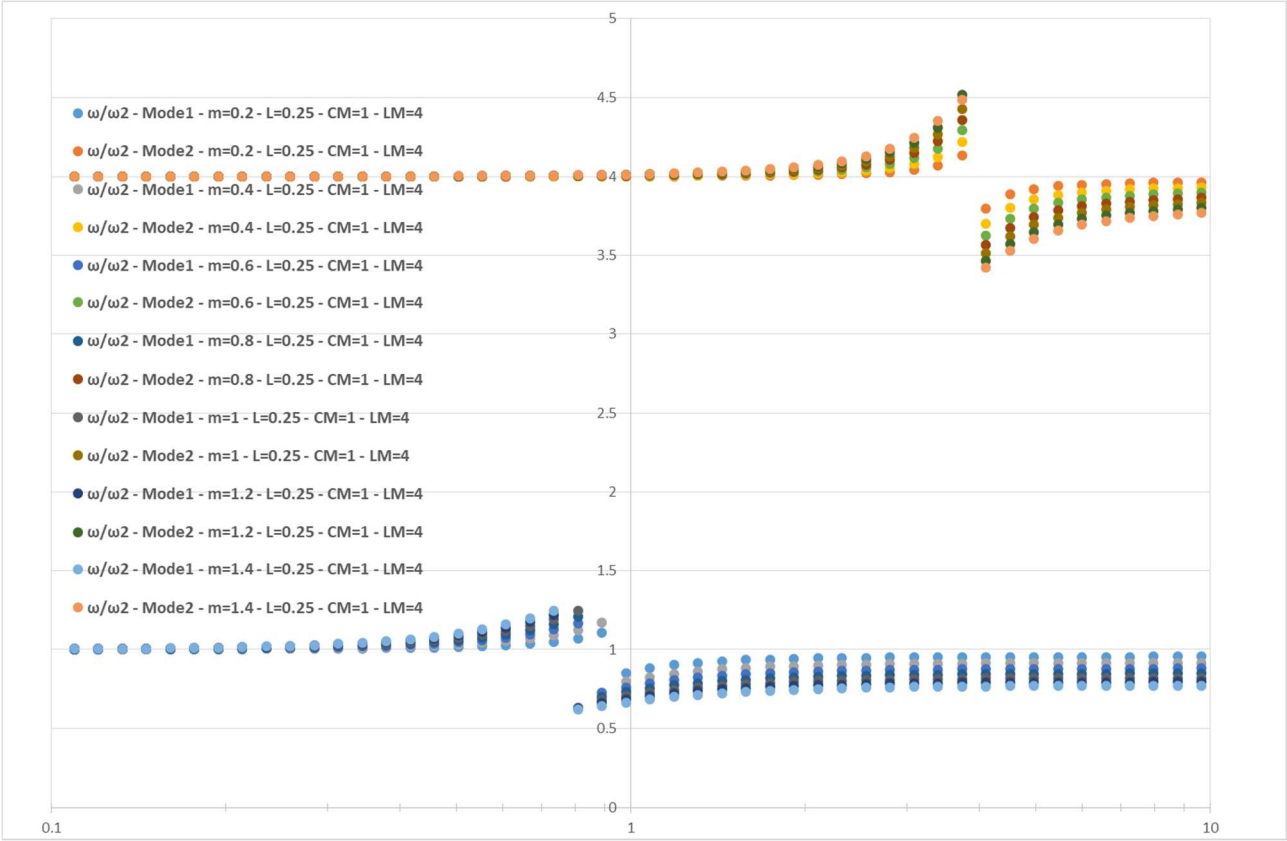

Picture 75: Circular frequencies of bridges with $\bar{L} = 0{,}25$; one truck in the cross section; four trucks in the span.

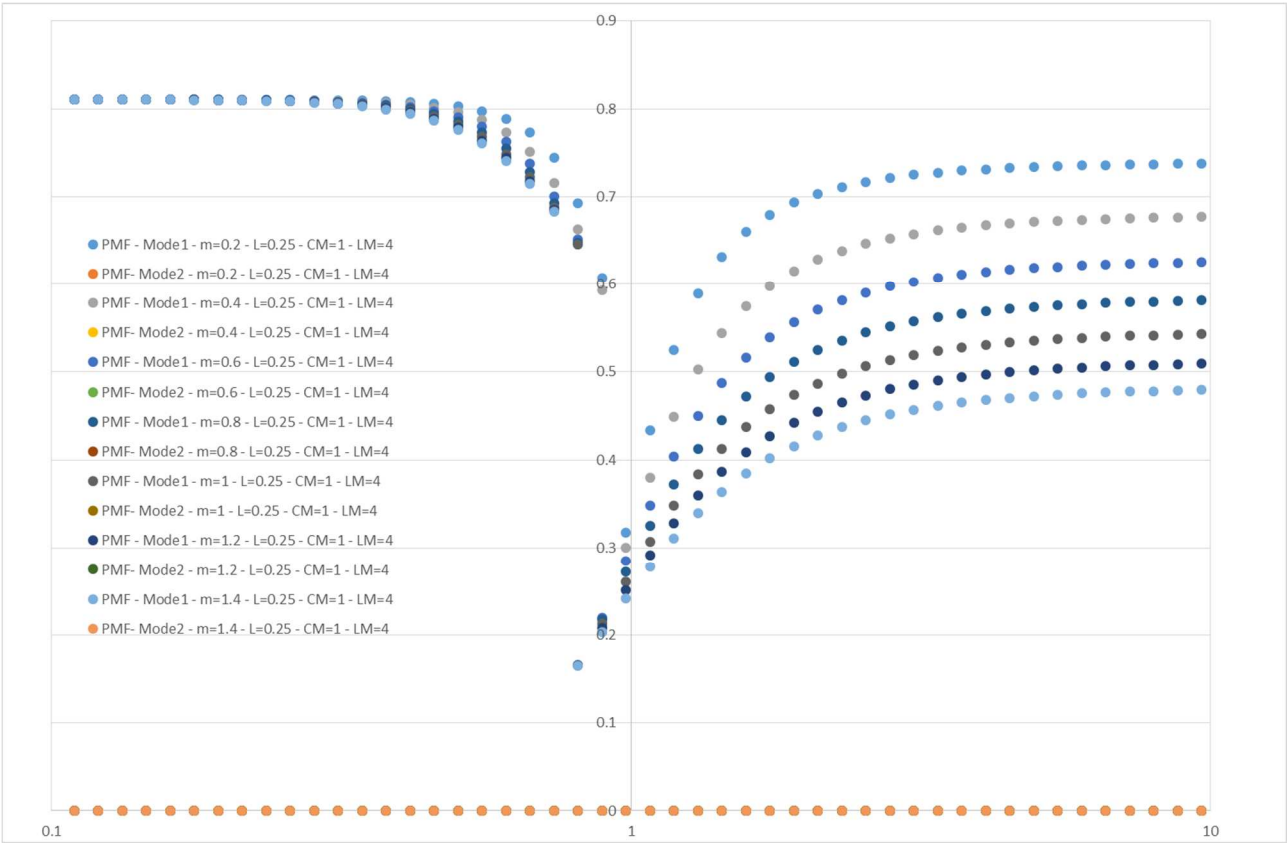

Picture 76: MPF of bridges with $\bar{L} = 0{,}25$; one truck in the cross section; four trucks in the span.

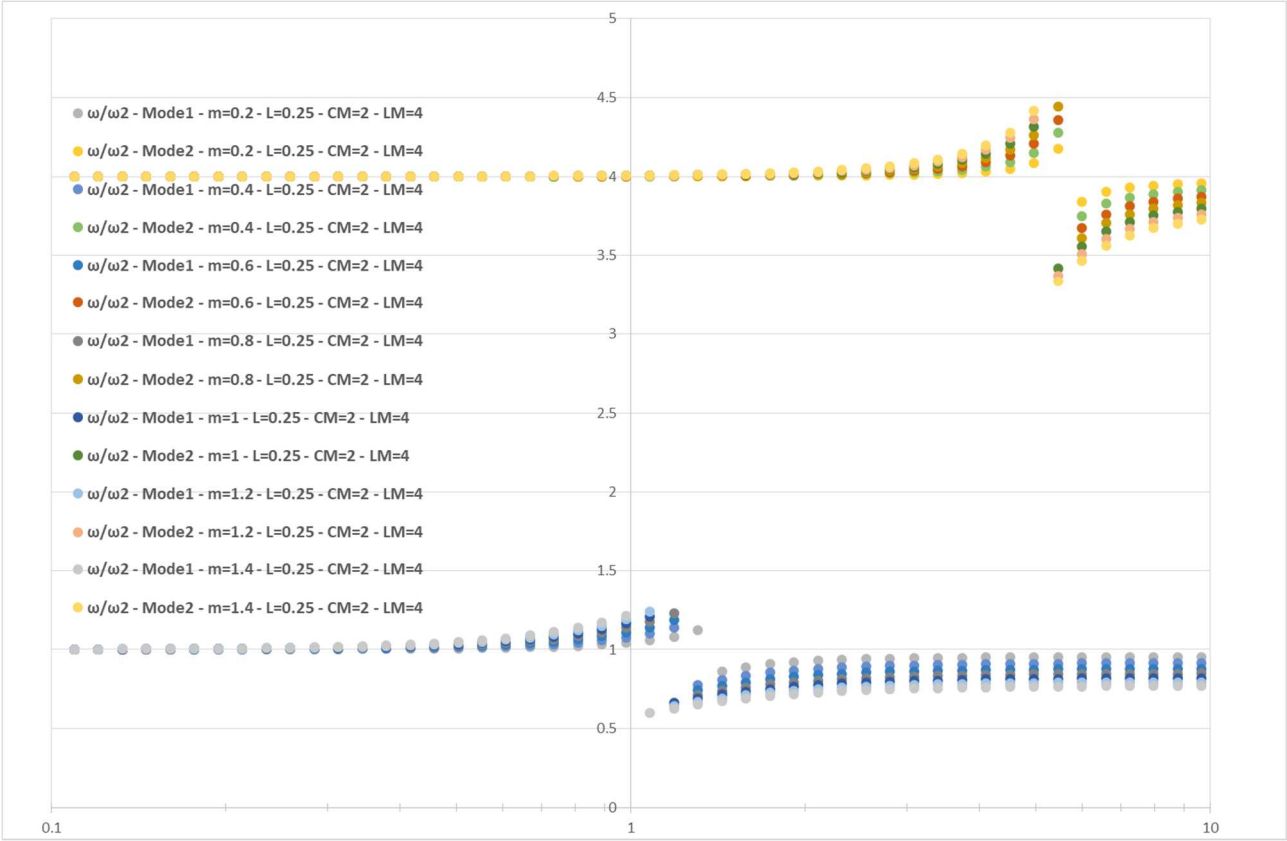

Picture 77: Circular frequencies of bridges with $\bar{L} = 0{,}25$; two trucks in the cross section; four trucks in the span.

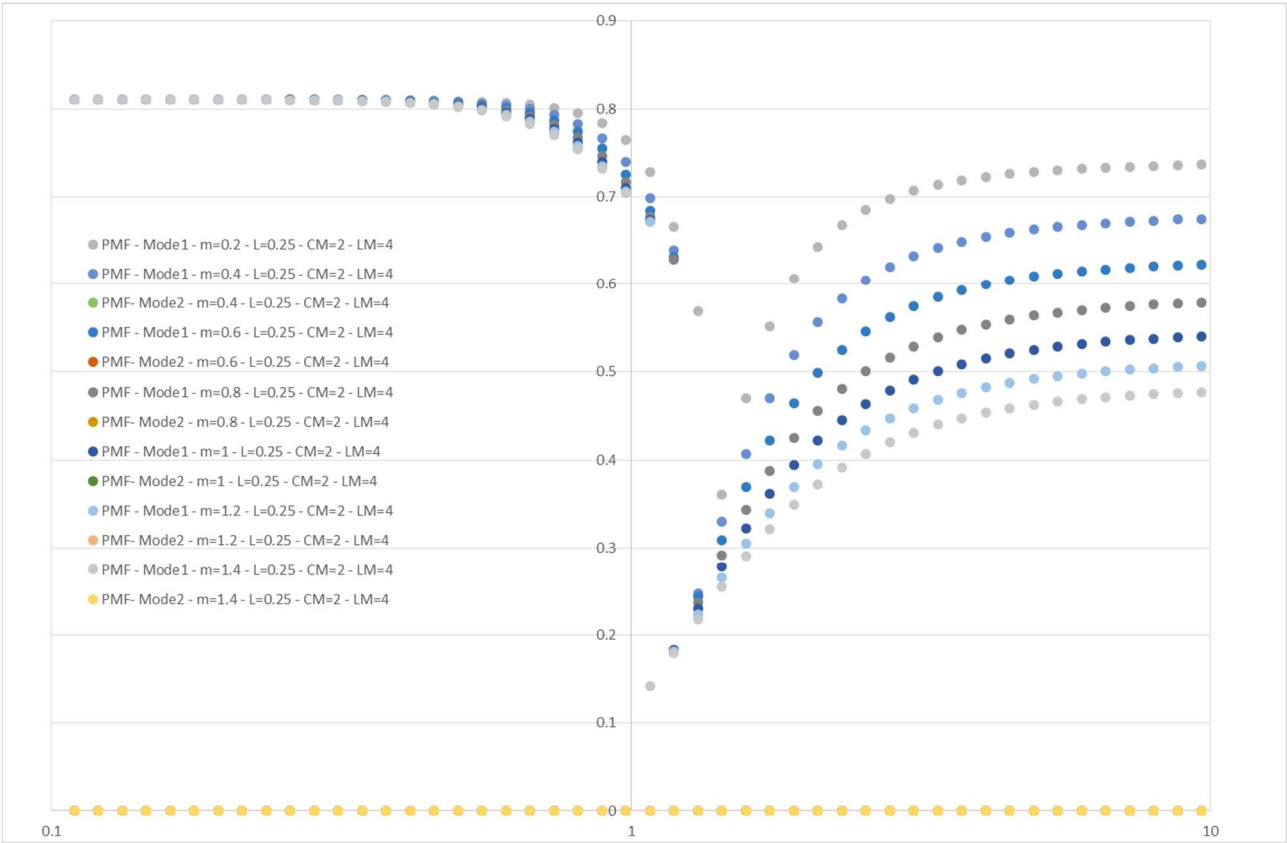

Picture 78: MPF of bridges with $\bar{L} = 0{,}25$; two trucks in the cross section; four trucks in the span.

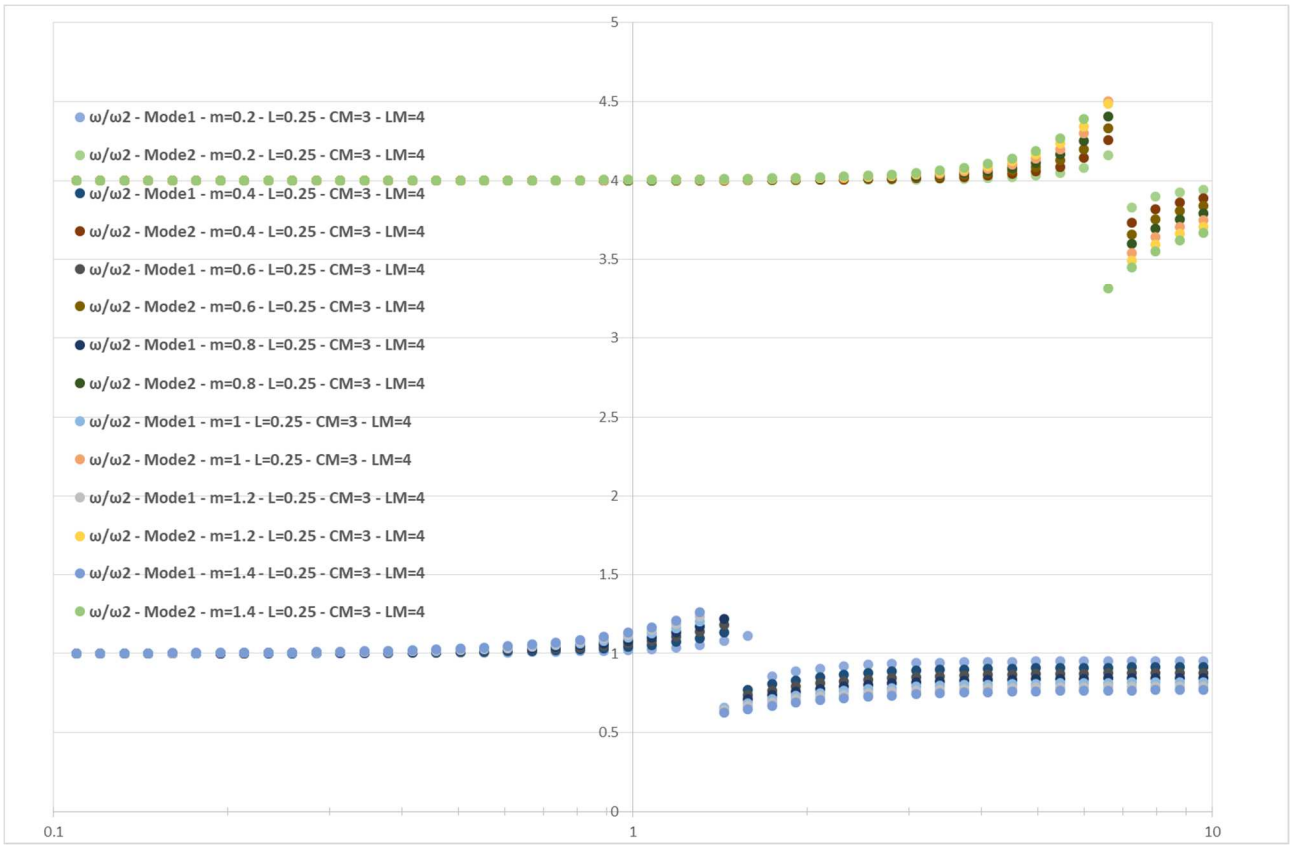

Picture 79: Circular frequencies of bridges with $\bar{L} = 0{,}25$; three trucks in the cross section; four trucks in the span.

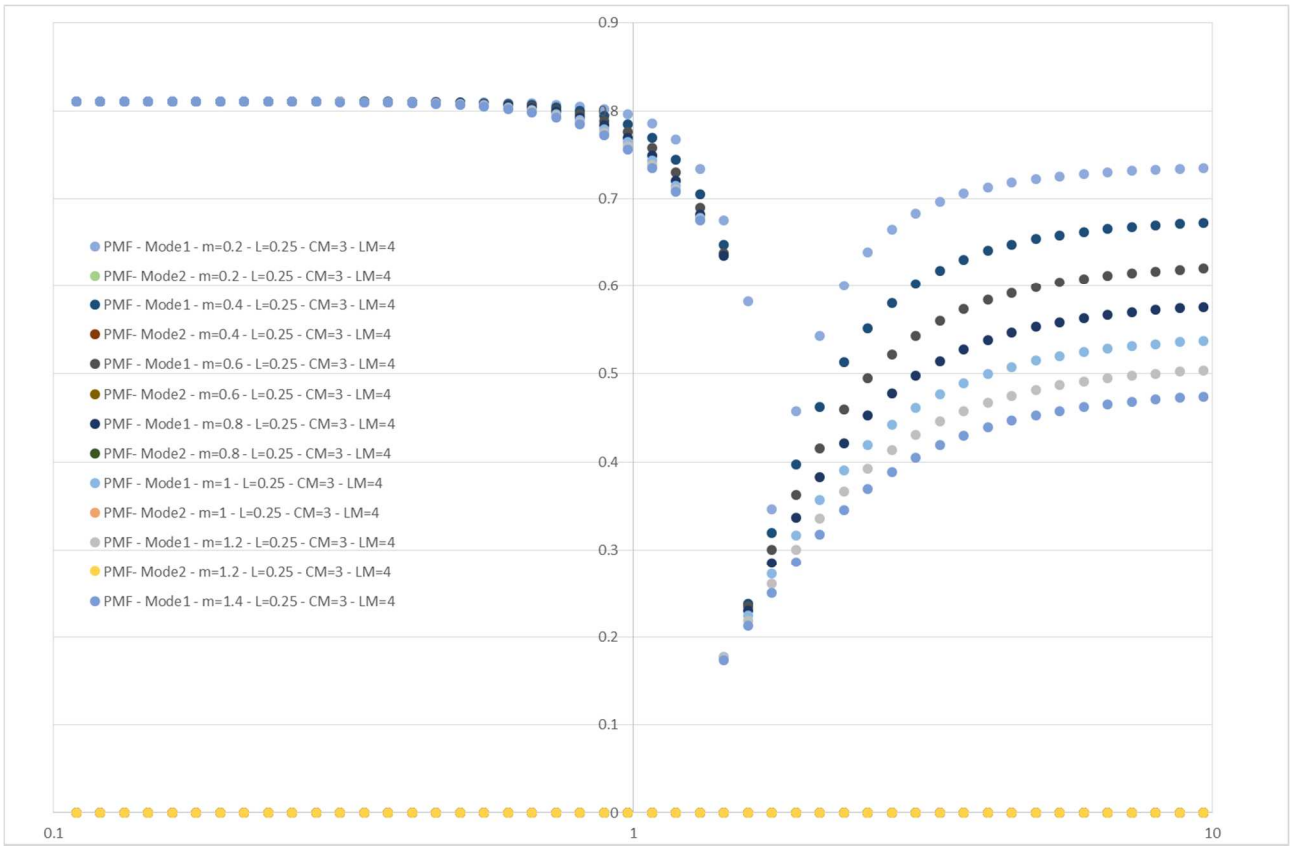

Picture 80: MPF of bridges with $\bar{L} = 0{,}25$; three trucks in the cross section; four trucks in the span.

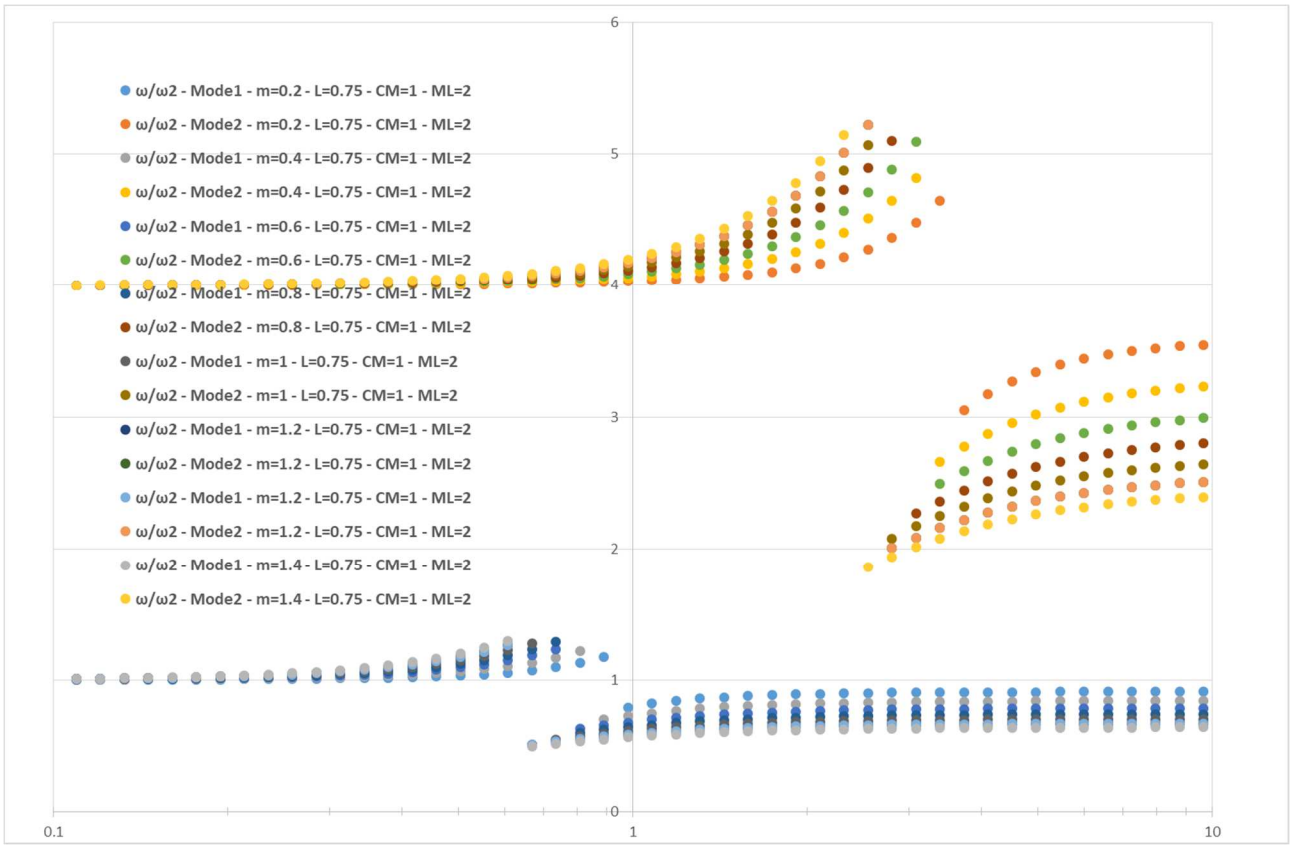

Picture 81: Circular frequencies of bridges with $\bar{L} = 0{,}75$; one truck in the cross section; two trucks in the span.

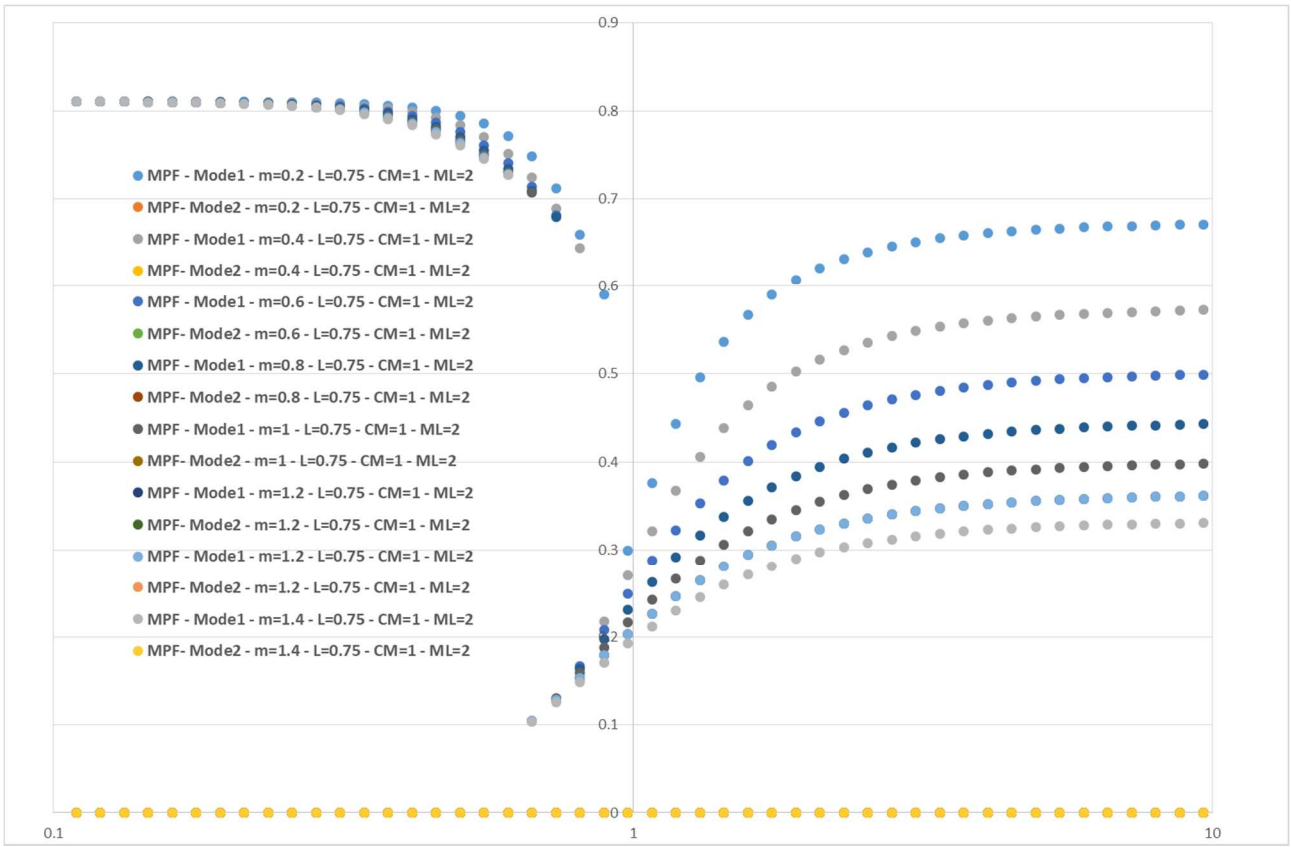

Picture 82: MPF of bridges with $\bar{L} = 0{,}75$; one truck in the cross section; two trucks in the span.

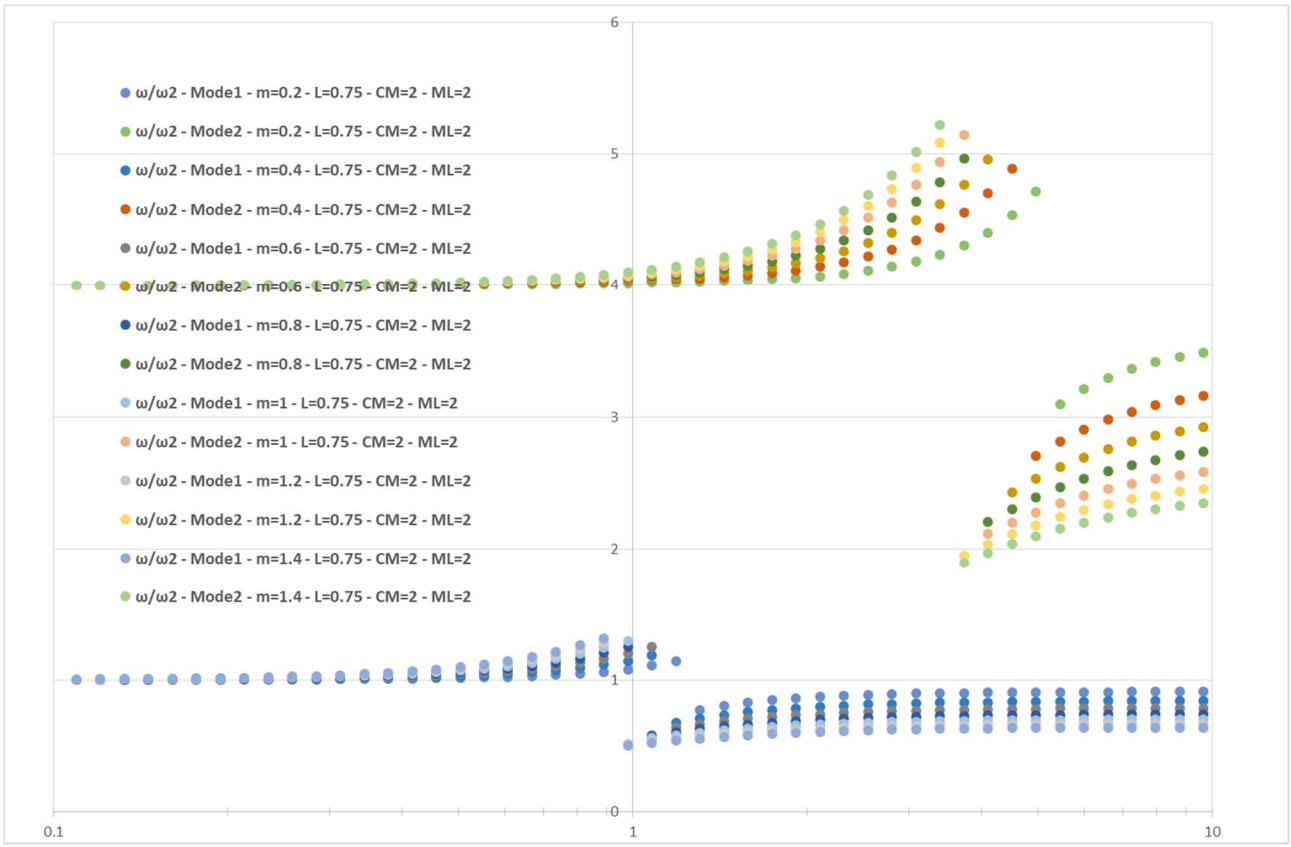

Picture 83: Circular frequencies of bridges with $\bar{L} = 0{,}75$; two trucks in the cross section; two trucks in the span.

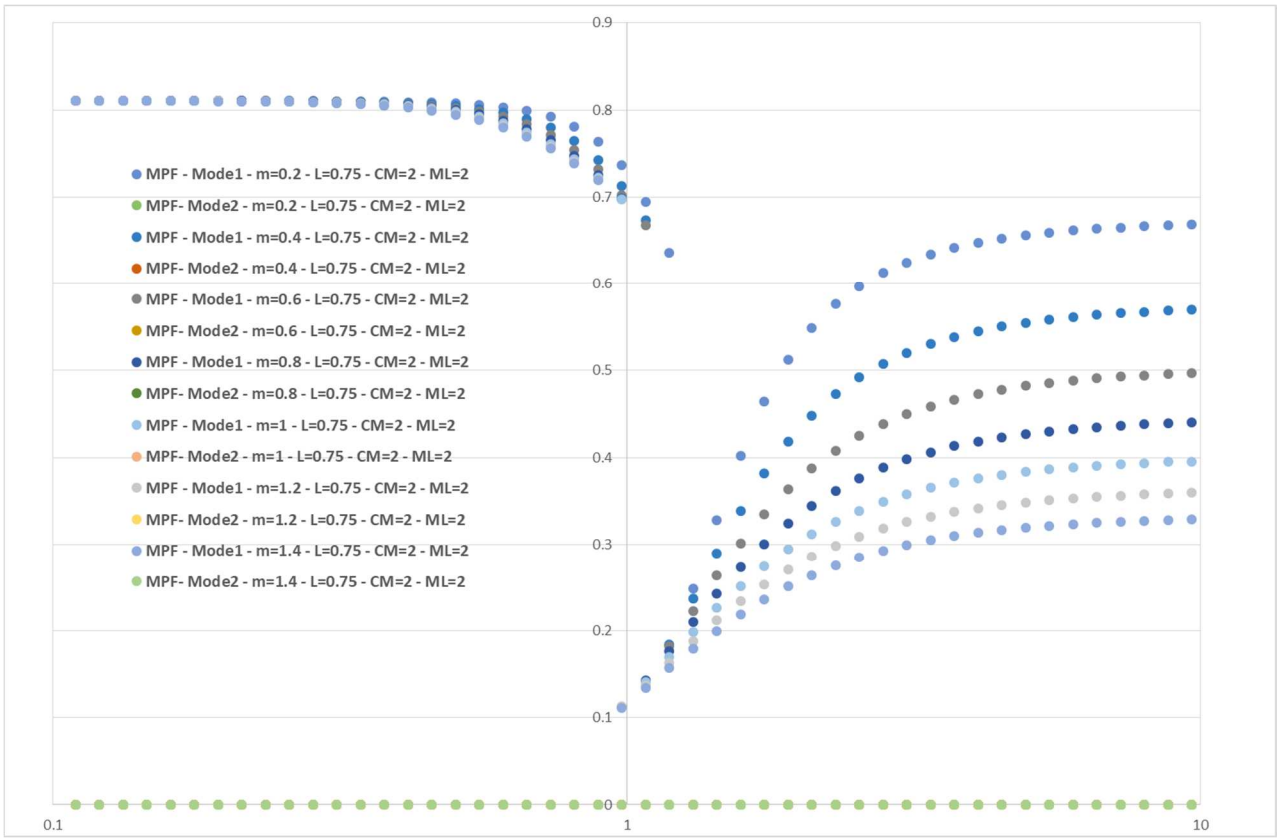

Picture 84: MPF of bridges with $\bar{L} = 0{,}75$; two trucks in the cross section; two trucks in the span.

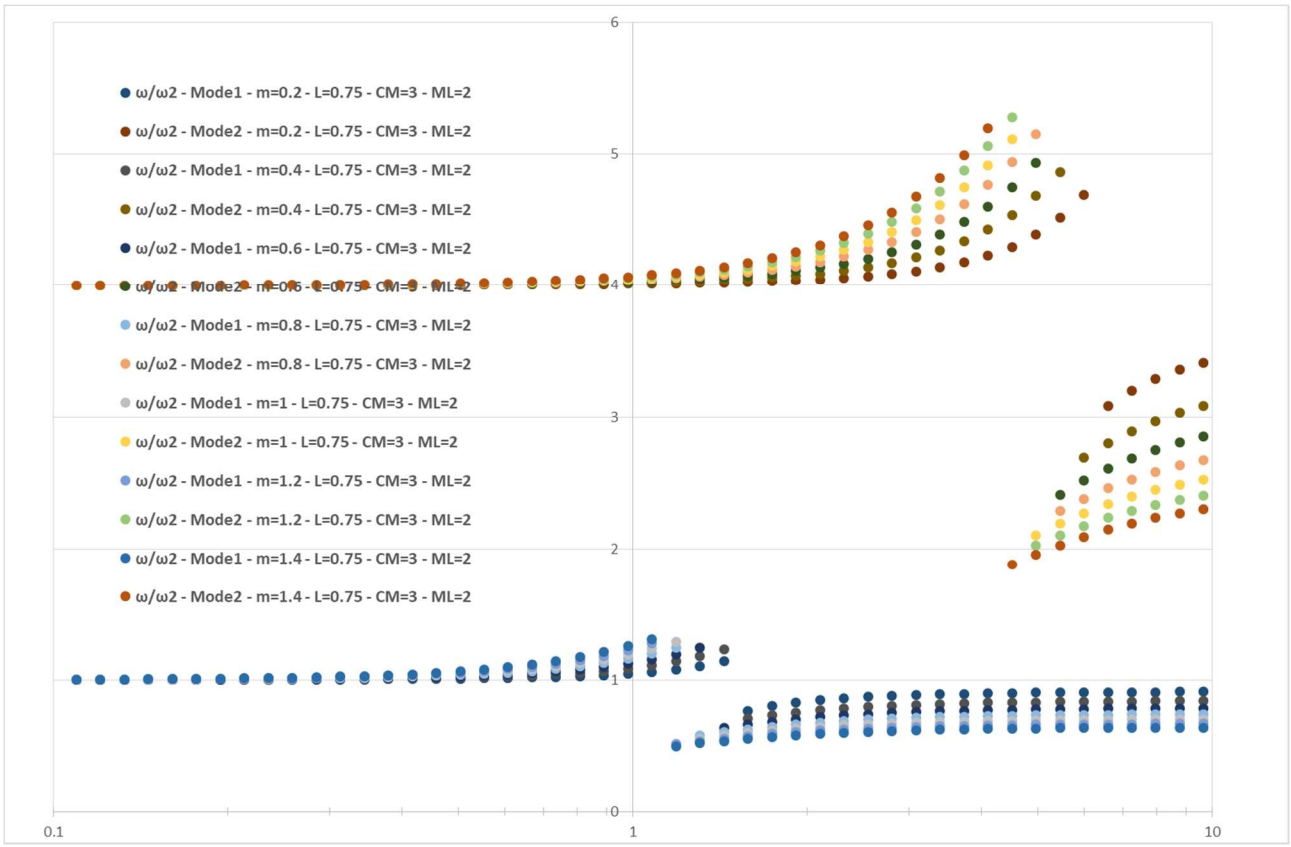

Picture 85: Circular frequencies of bridges with $\bar{L} = 0{,}75$; three trucks in the cross section; two trucks in the span.

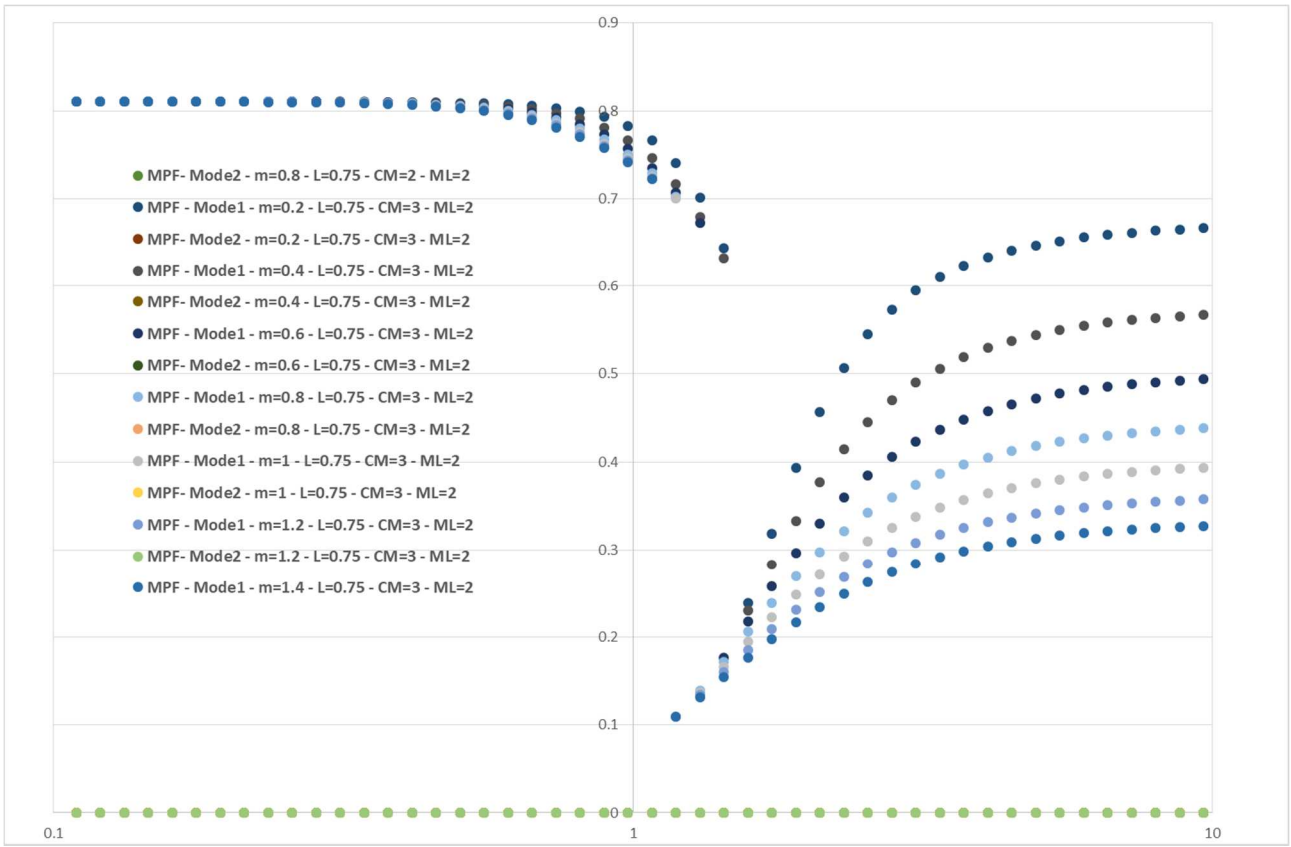

Picture 86: of bridges with $\bar{L} = 0{,}75$; three trucks in the cross section; two trucks in the span.

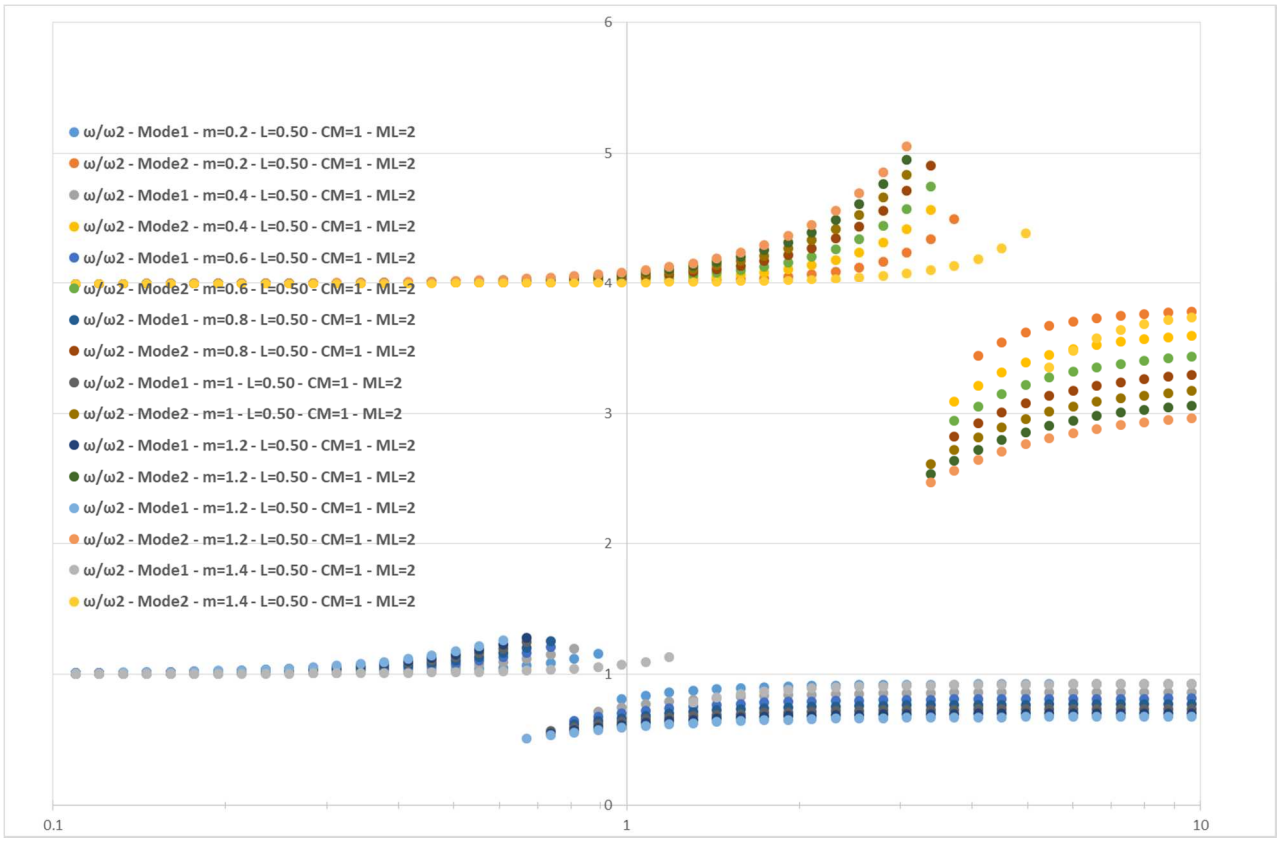

Picture 87: Circular frequencies of bridges with $\bar{L} = 0{,}50$; one truck in the cross section; two trucks in the span.

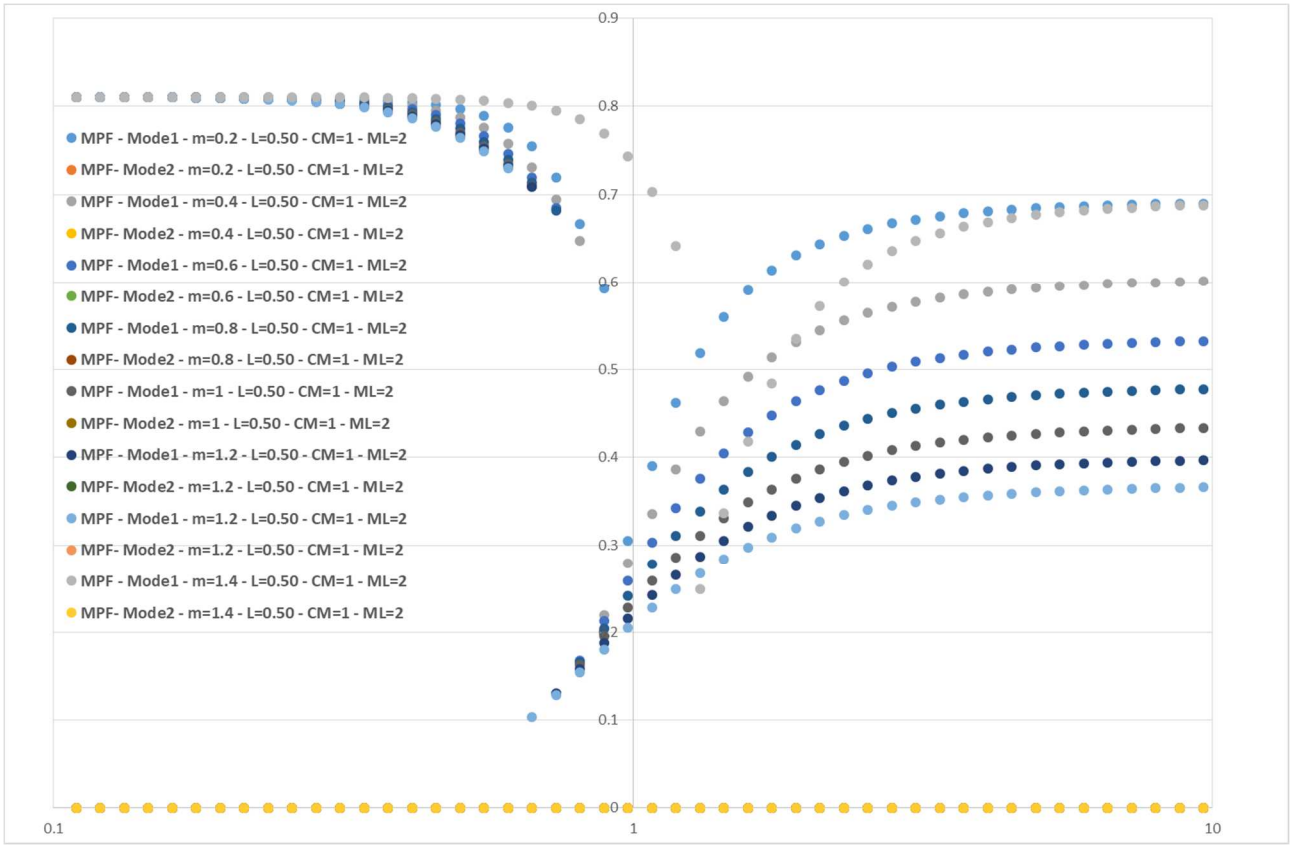

Picture 88: of bridges with $\bar{L} = 0{,}50$; one truck in the cross section; two trucks in the span

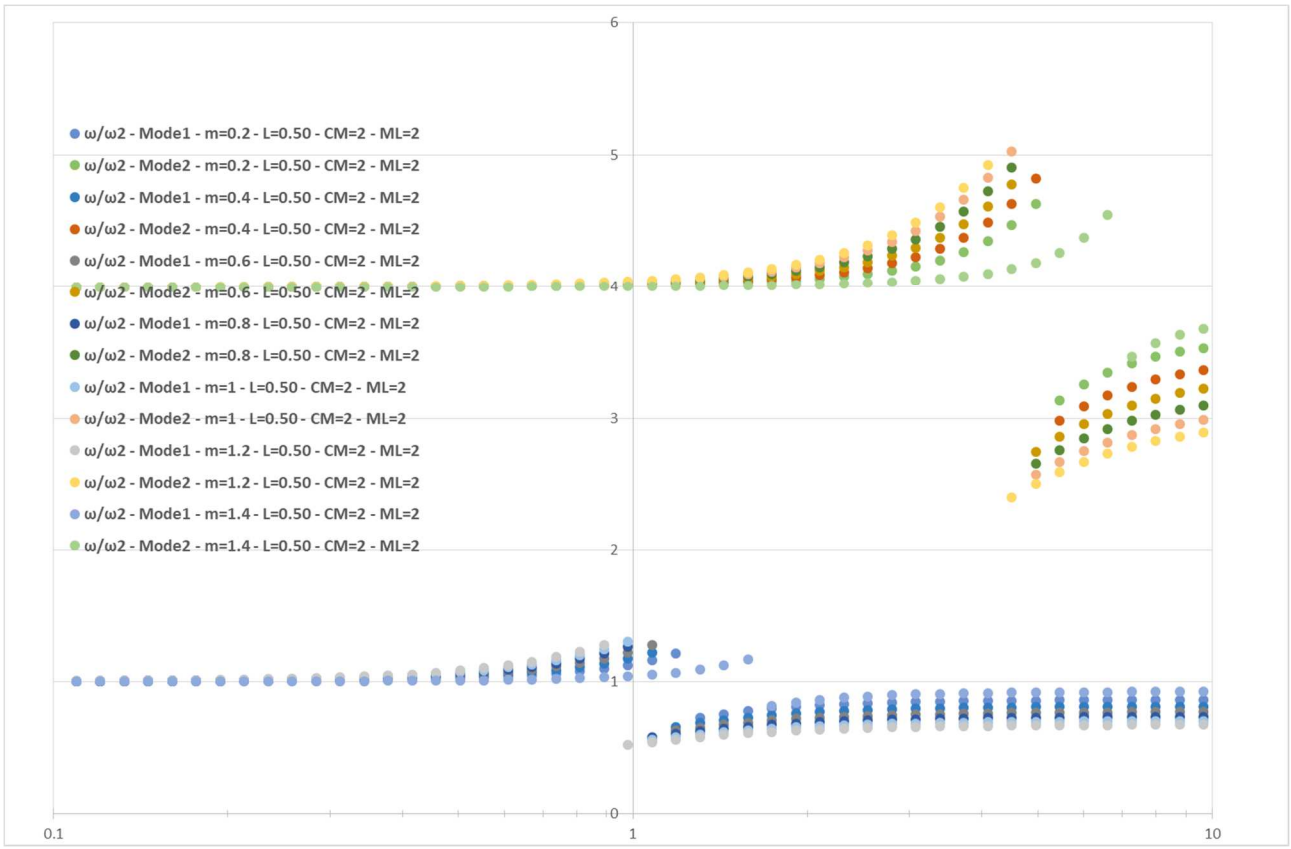

Picture 89: Circular frequencies of bridges with $\bar{L} = 0{,}50$; two trucks in the cross section; two trucks in the span.

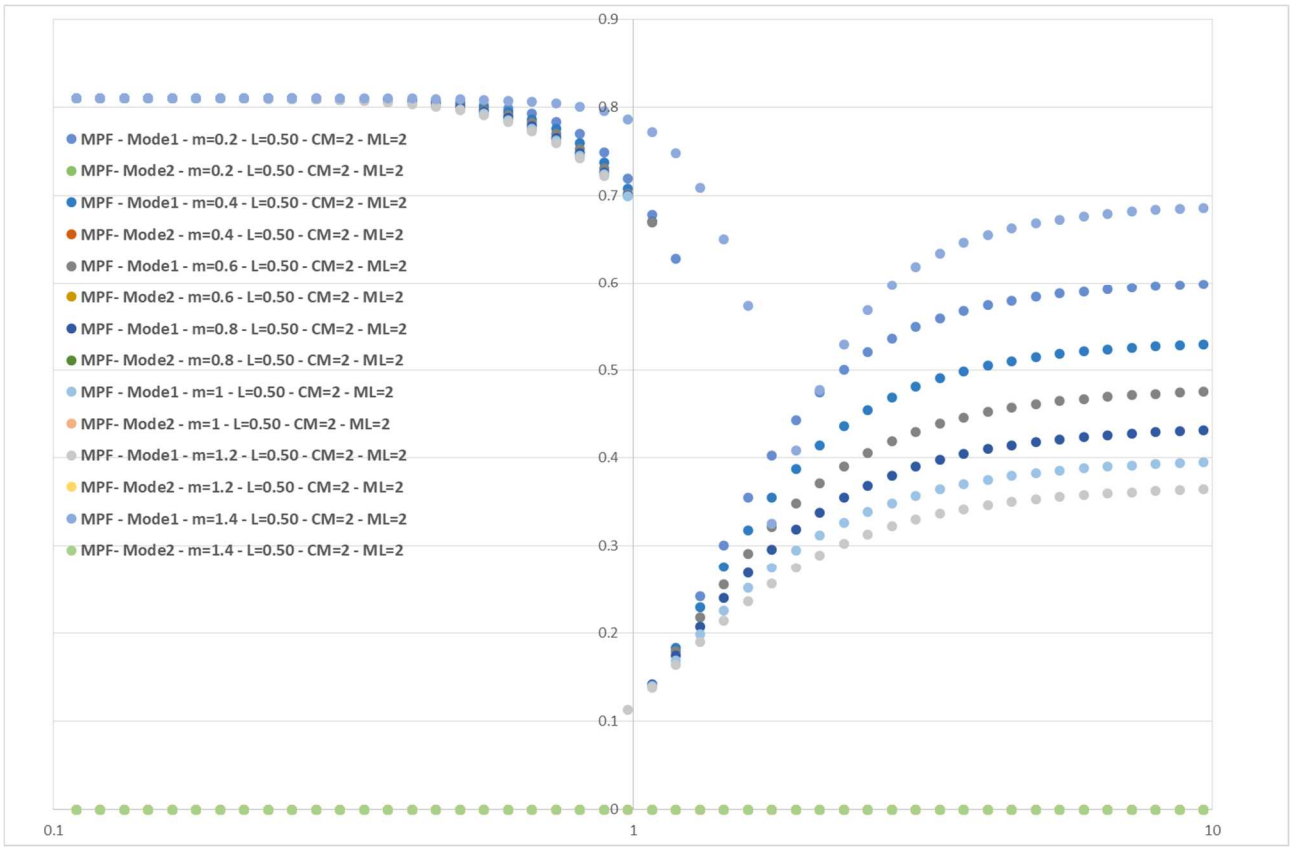

Picture 90: MPF of bridges with $\bar{L} = 0{,}50$; two trucks in the cross section; two trucks in the span.

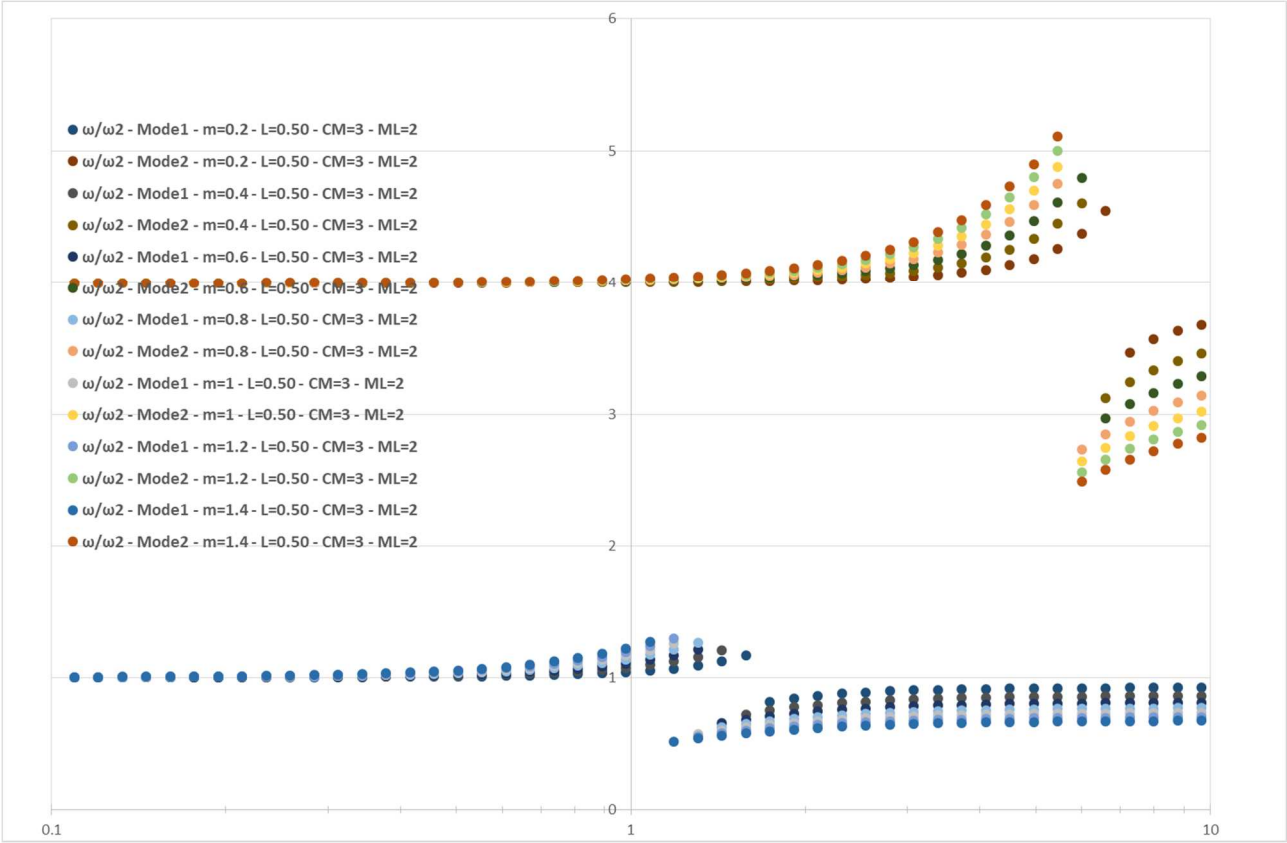

Picture 91: Circular frequencies of bridges with $\bar{L} = 0{,}50$; three trucks in the cross section; two trucks in the span.

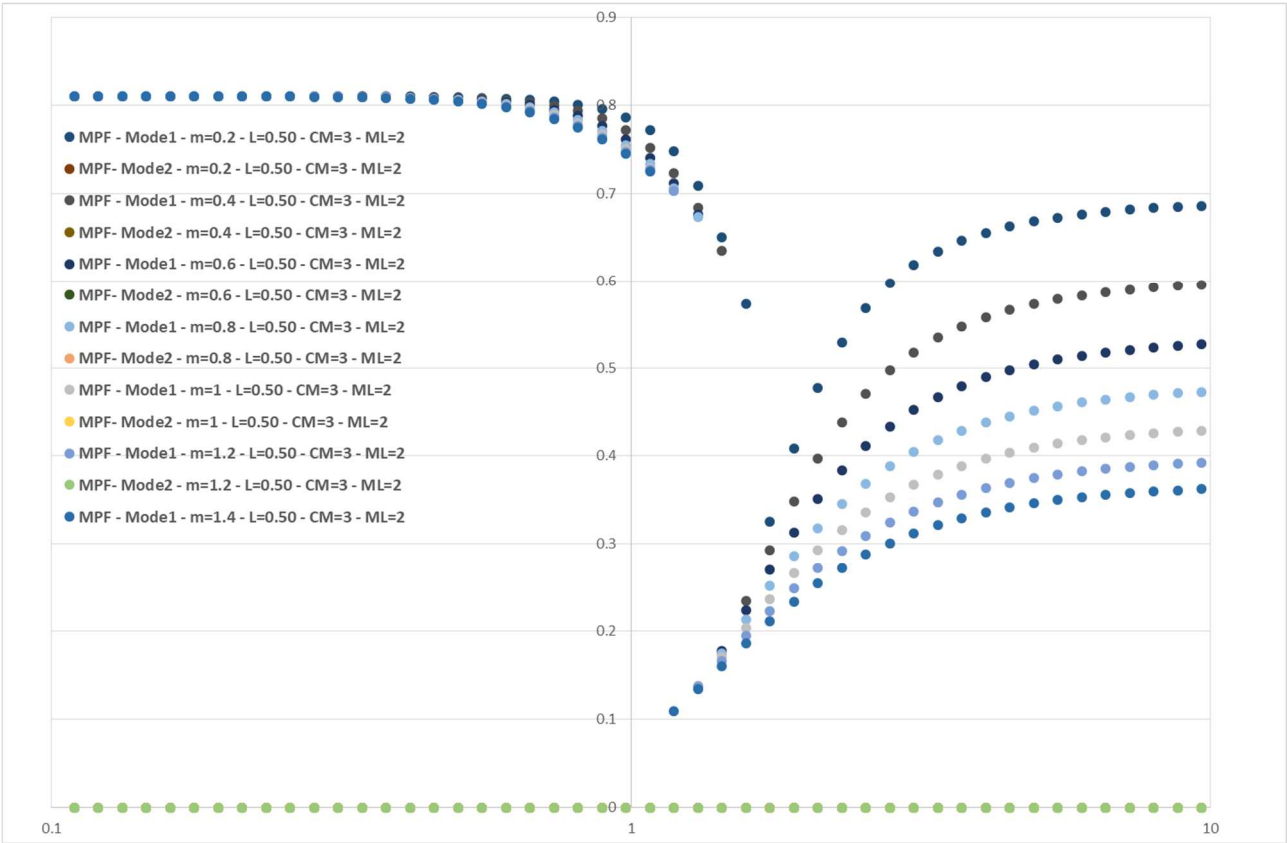

Picture 92: MPF of bridges with $\bar{L} = 0{,}50$; three trucks in the cross section; two trucks in the span.

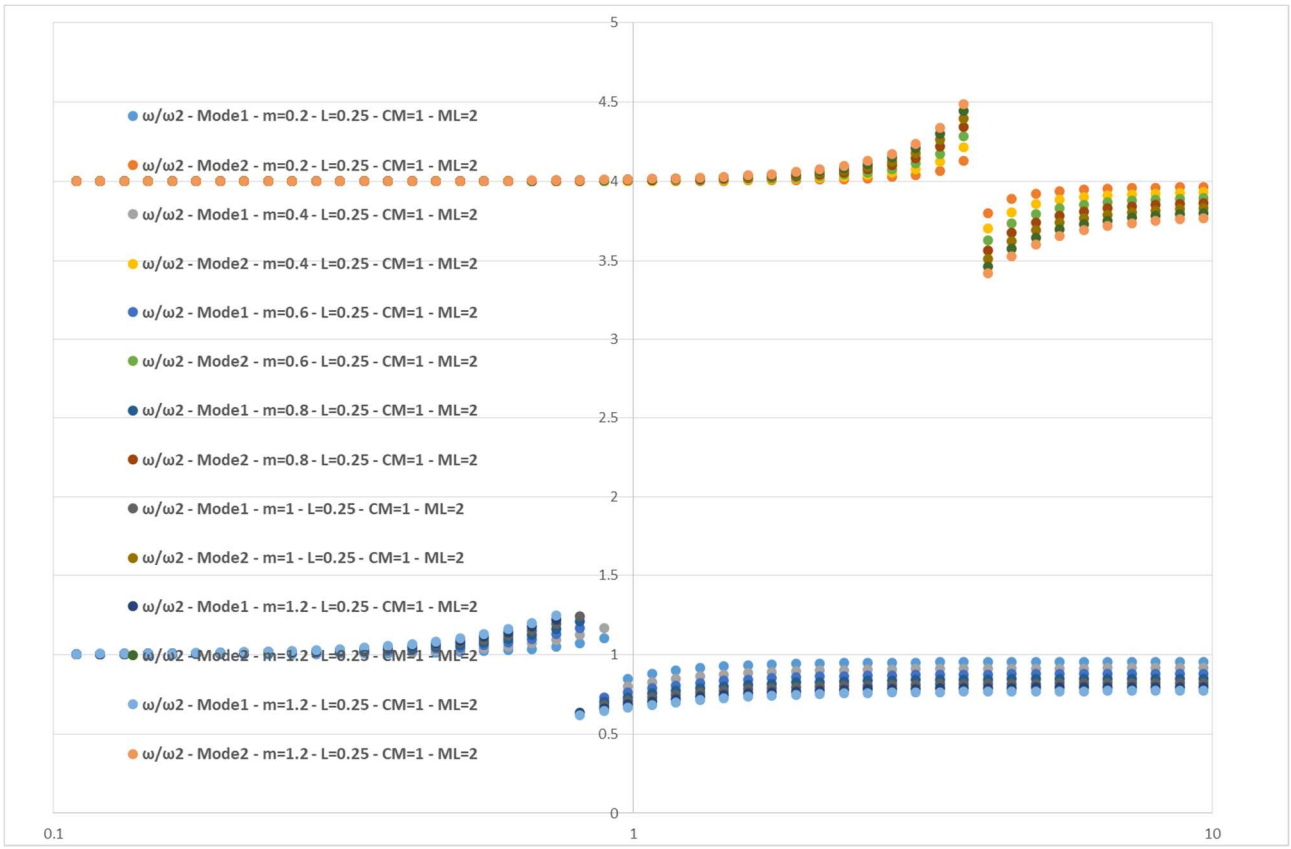

Picture 93: Circular frequencies of bridges with $\bar{L} = 0{,}25$; one truck in the cross section; two trucks in the span.

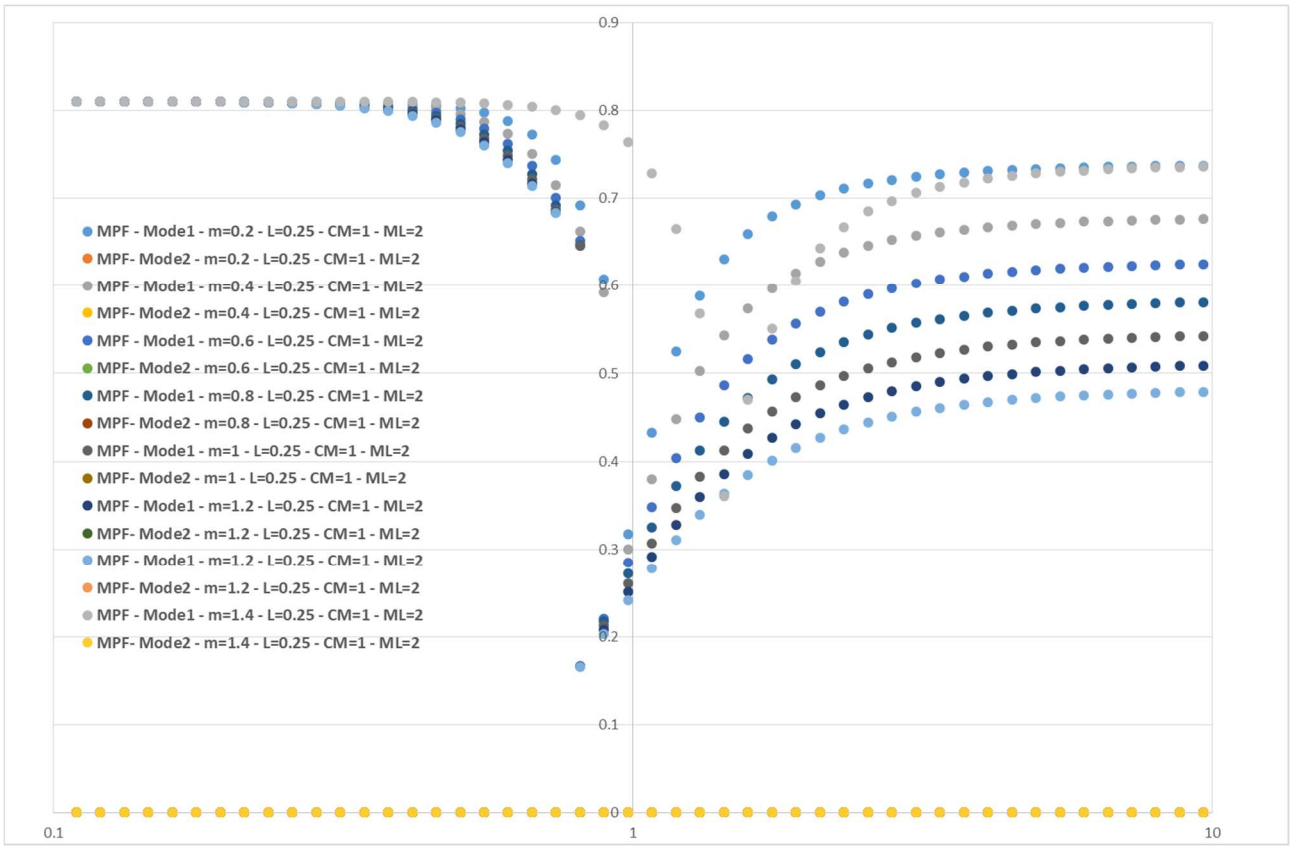

Picture 94: MPF of bridges with $\bar{L} = 0{,}25$; one truck in the cross section; two trucks in the span.

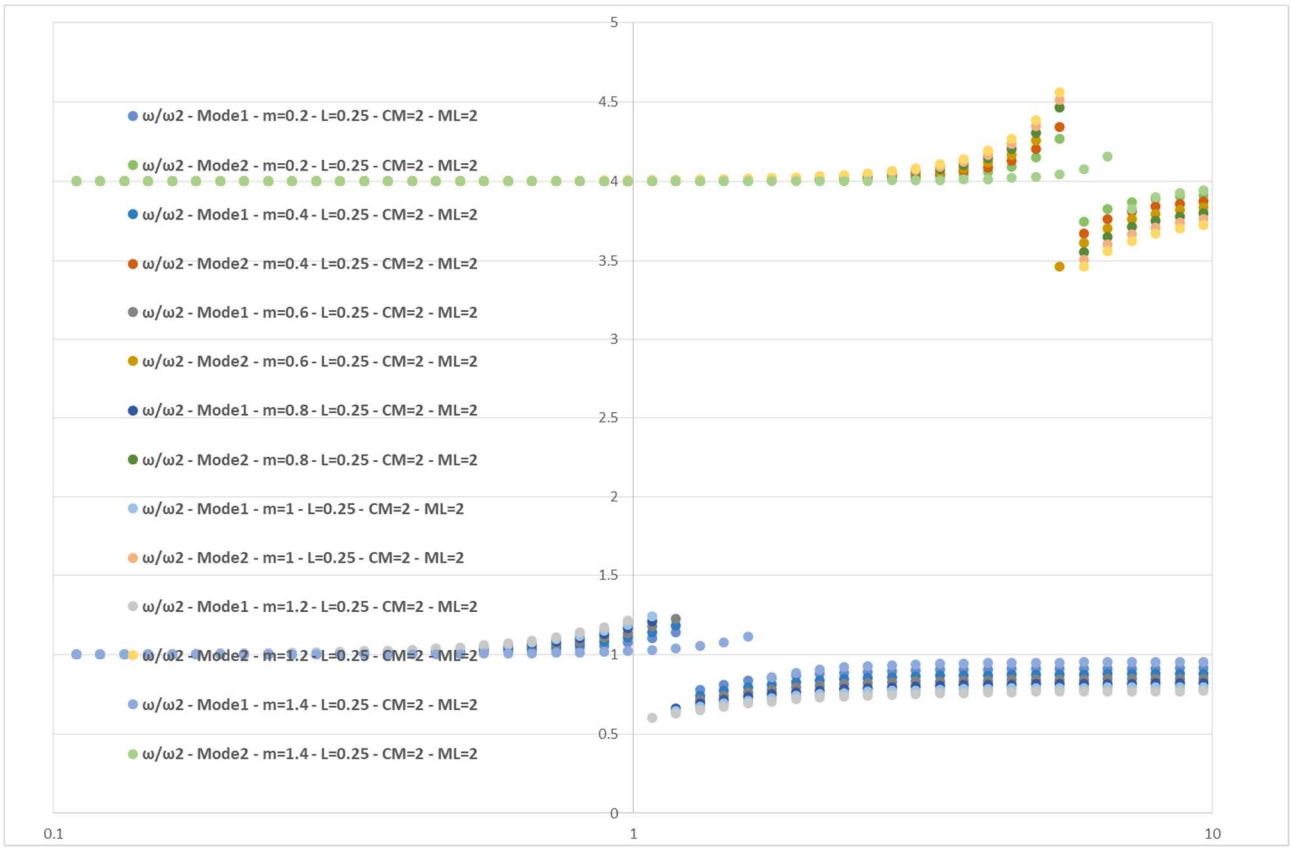

Picture 95: Circular frequencies of bridges with $\bar{L} = 0{,}25$; two trucks in the cross section; two trucks in the span.

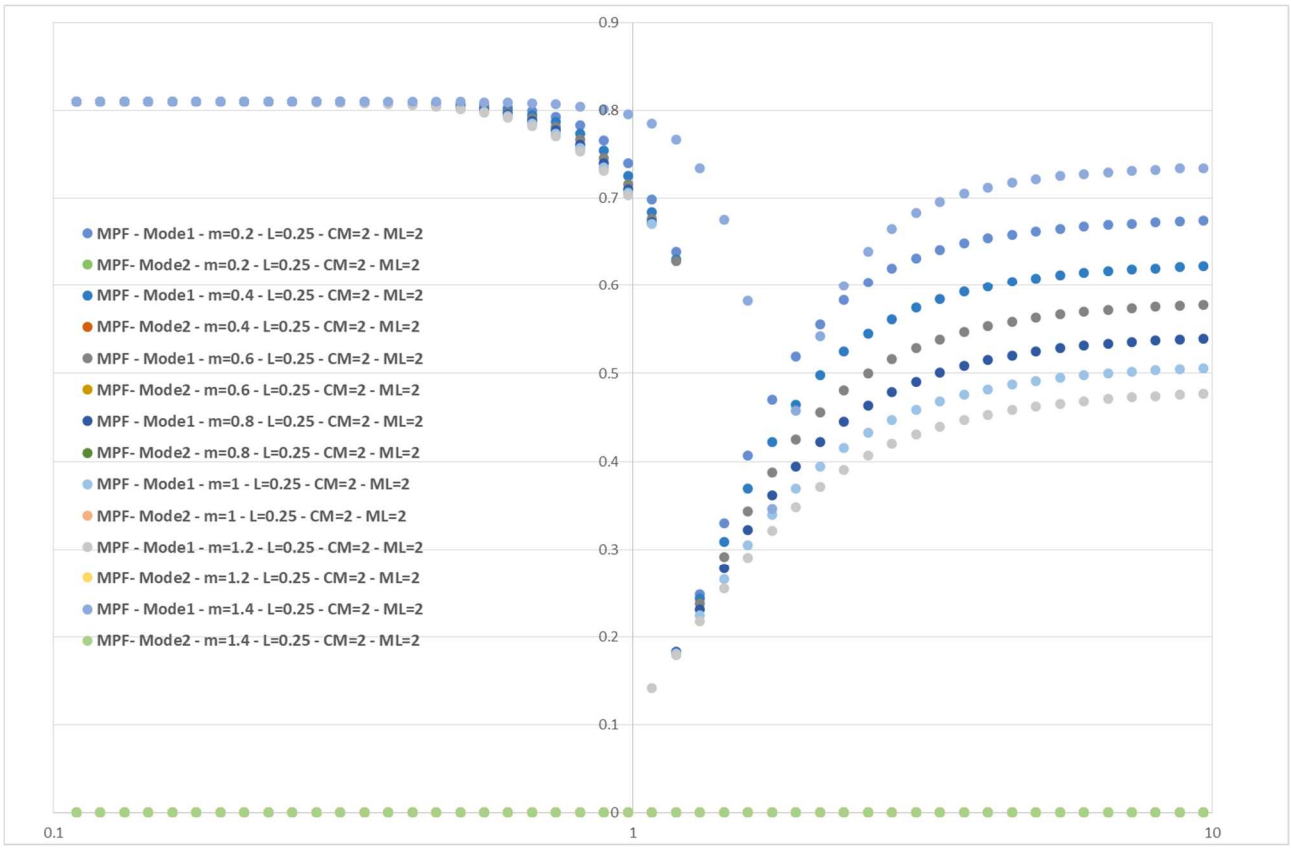

Picture 96: MPF of bridges with $\bar{L} = 0{,}25$; two trucks in the cross section; two trucks in the span.

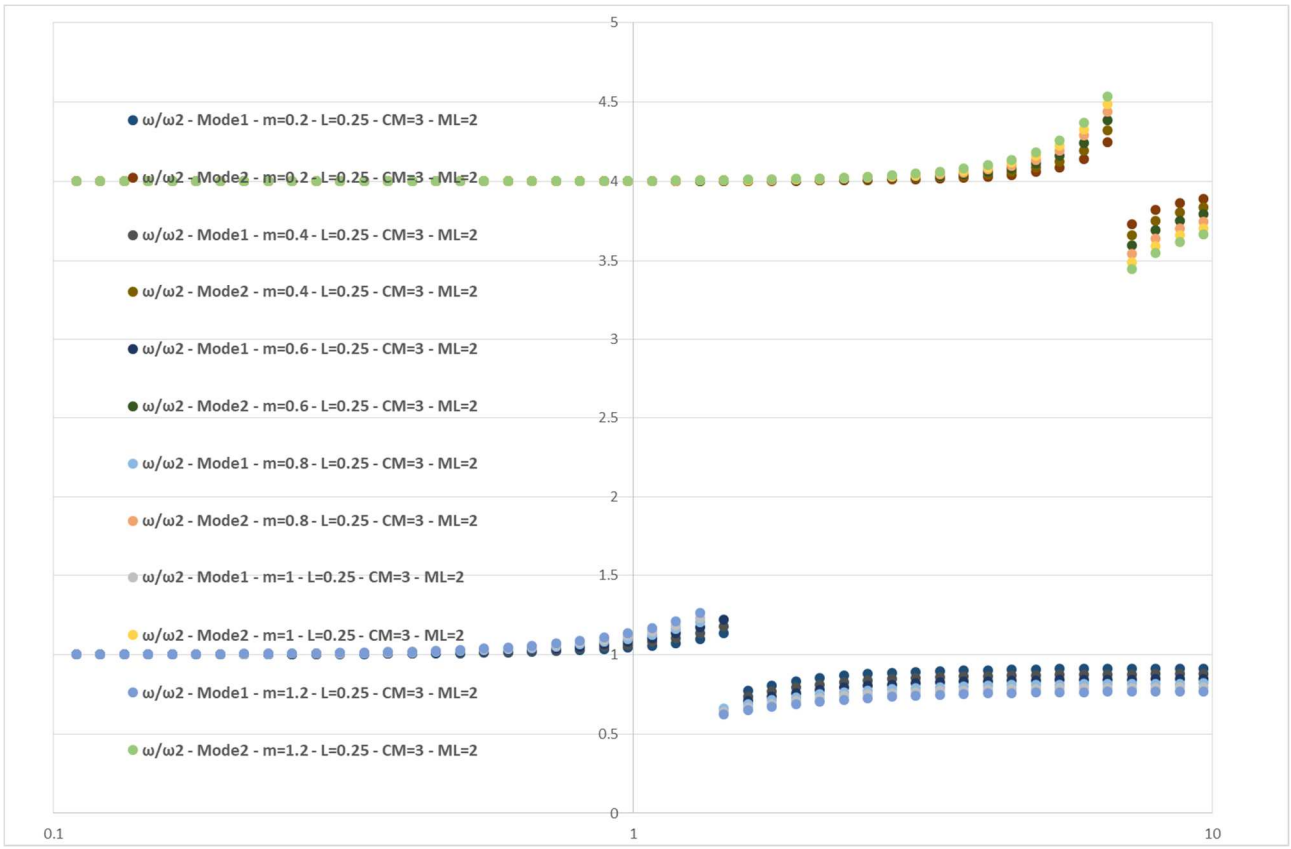

Picture 97: Circular frequencies of bridges with $\bar{L} = 0{,}25$; three trucks in the cross section; two trucks in the span.

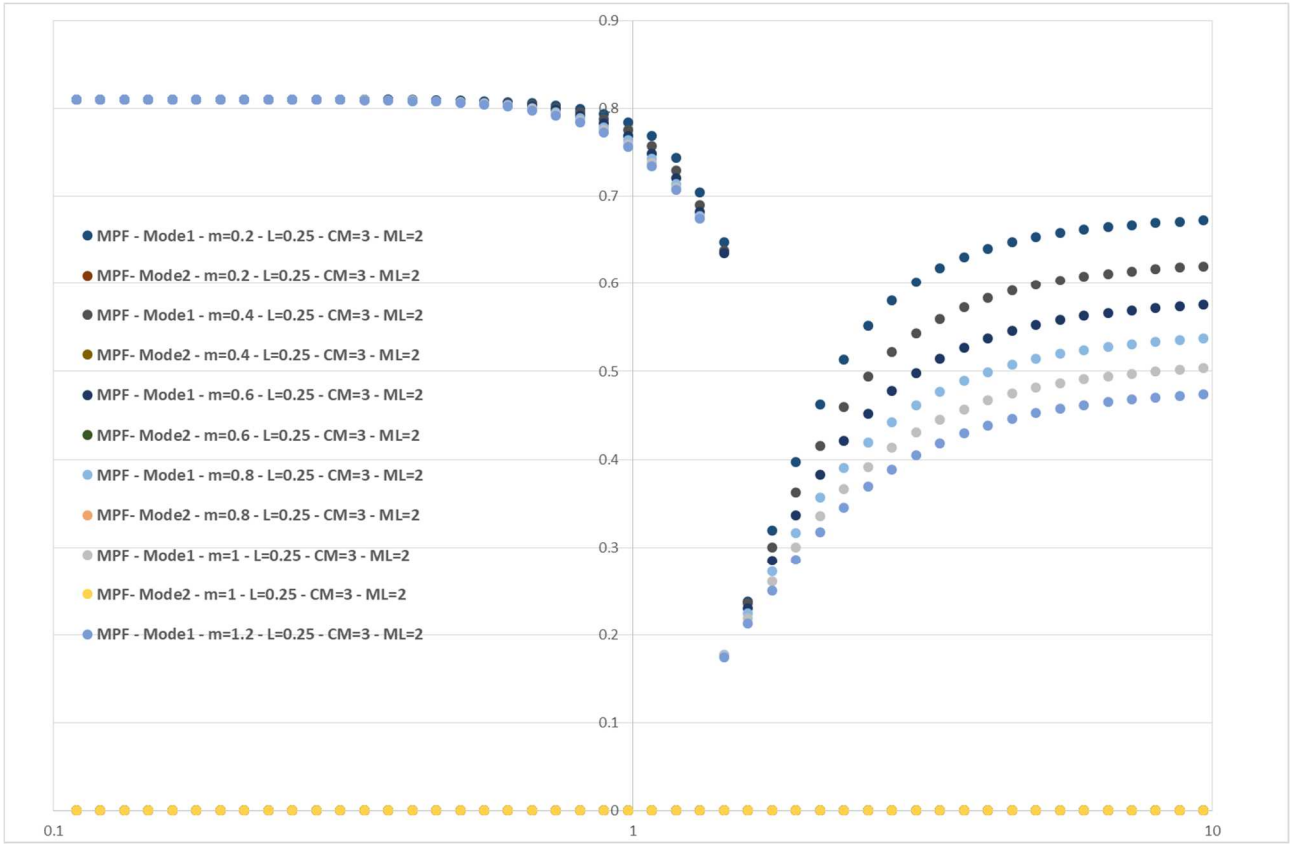

Picture 98: MPF of bridges with $\bar{L} = 0{,}25$; three trucks in the cross section; two trucks in the span.

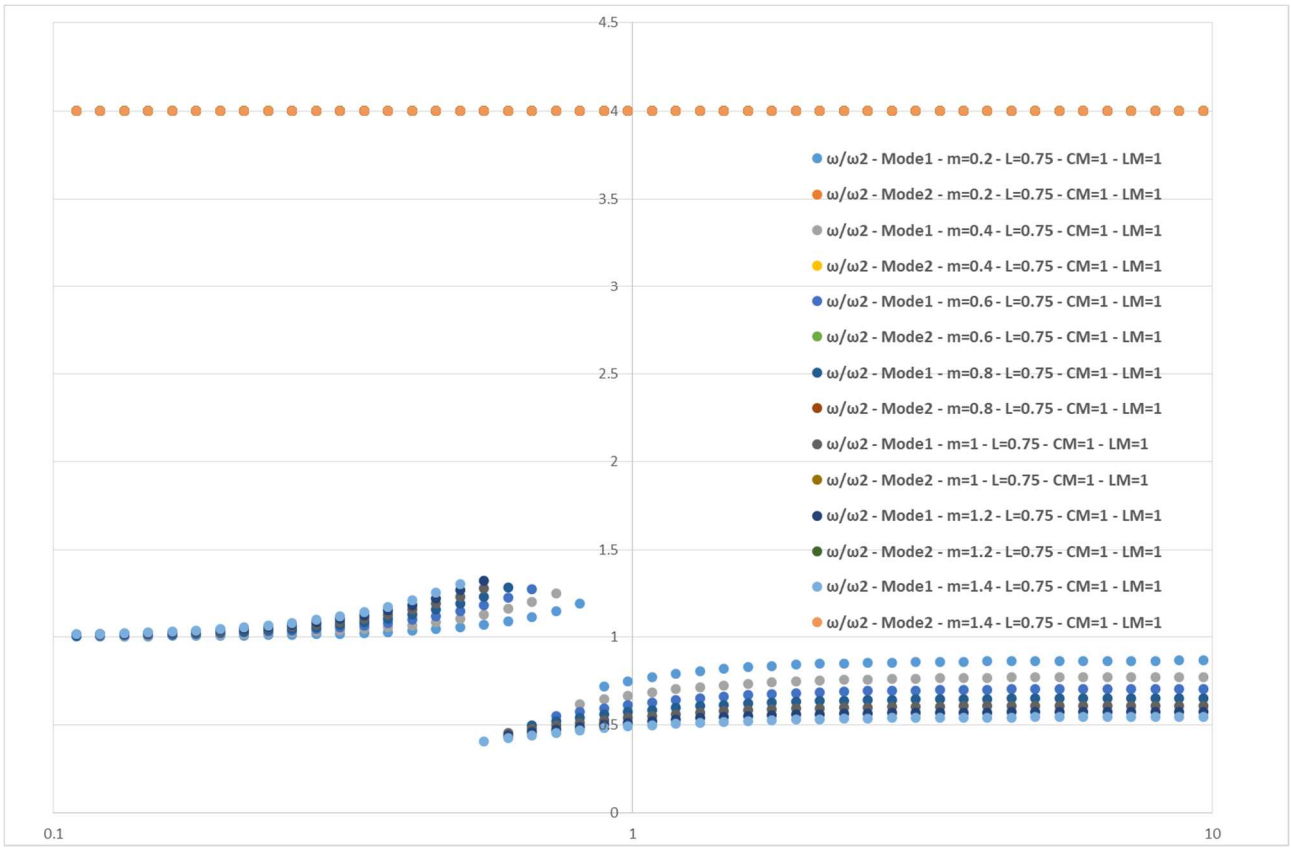

Picture 99: Circular frequencies of bridges with $\bar{L} = 0{,}75$; one truck in the cross section; one truck in the span.

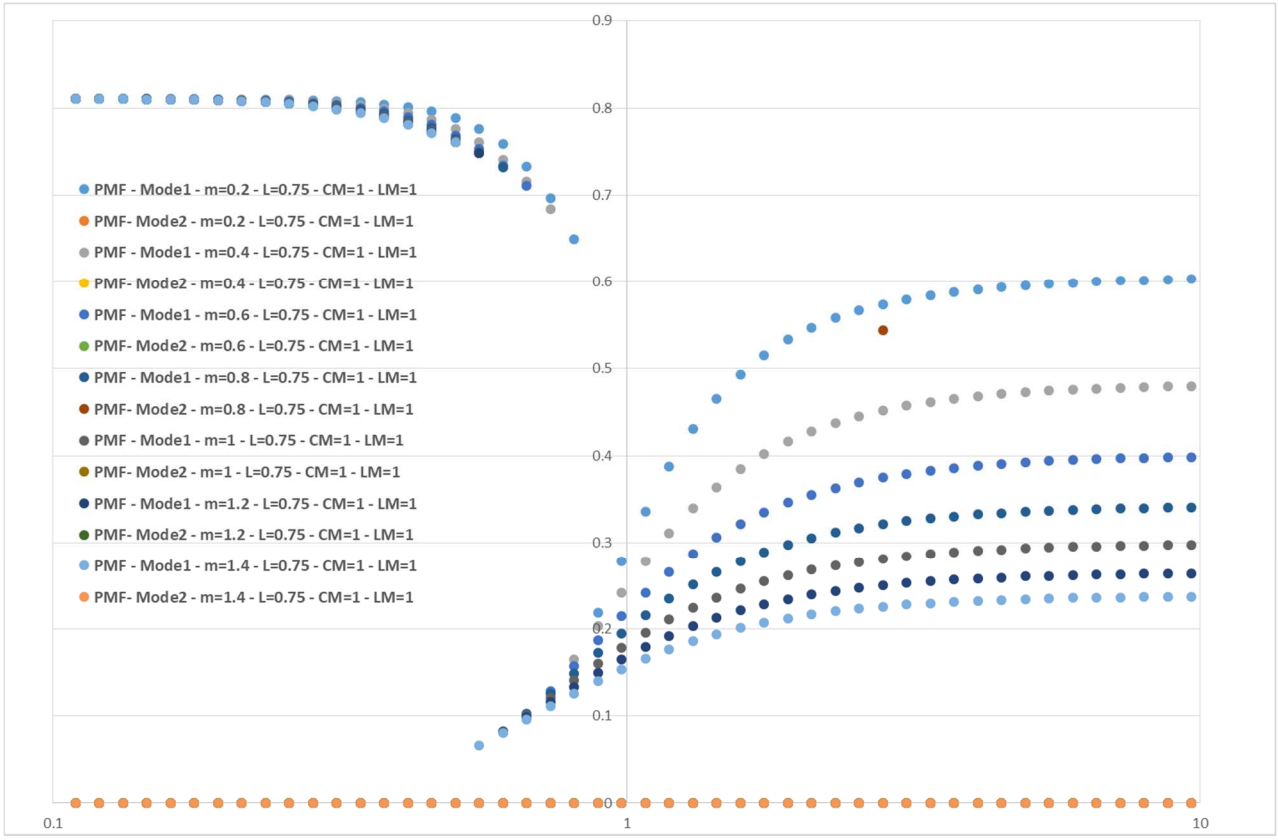

Picture 100: MPF of bridges with $\bar{L} = 0{,}75$; one truck in the cross section; one truck in the span.

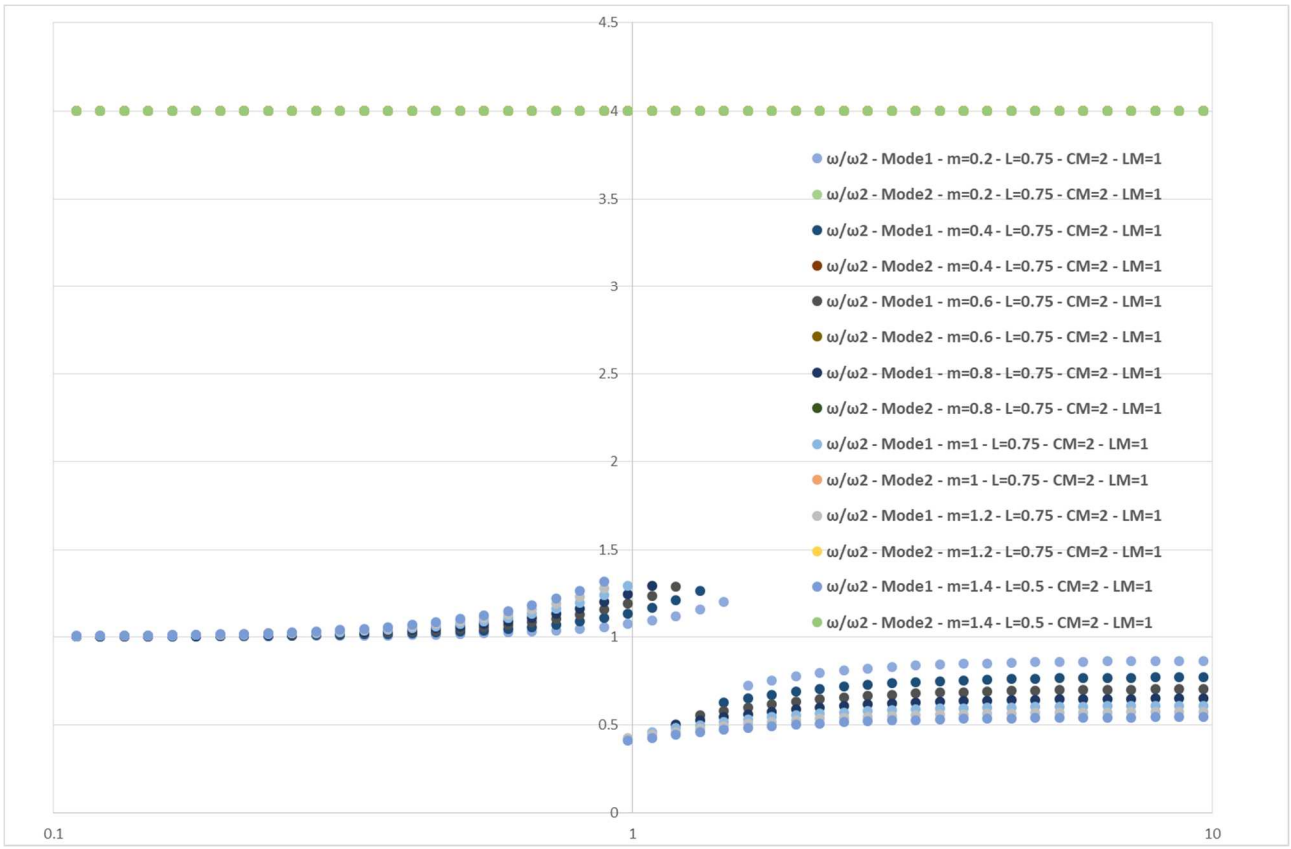

Picture 101: Circular frequencies of bridges with $\bar{L} = 0{,}75$; two trucks in the cross section; one truck in the span.

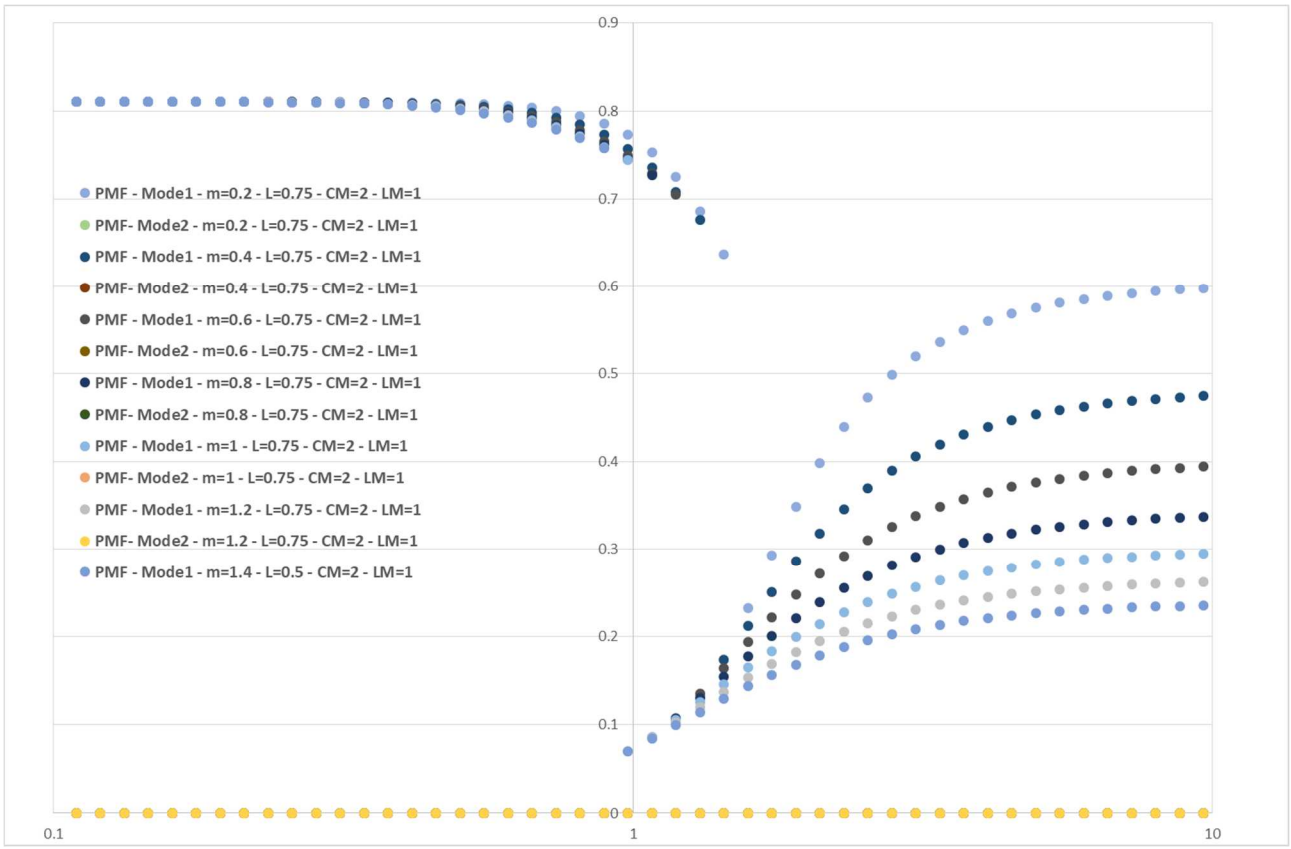

Picture 102: MPF of bridges with $\bar{L} = 0{,}75$; two trucks in the cross section; one truck in the span.

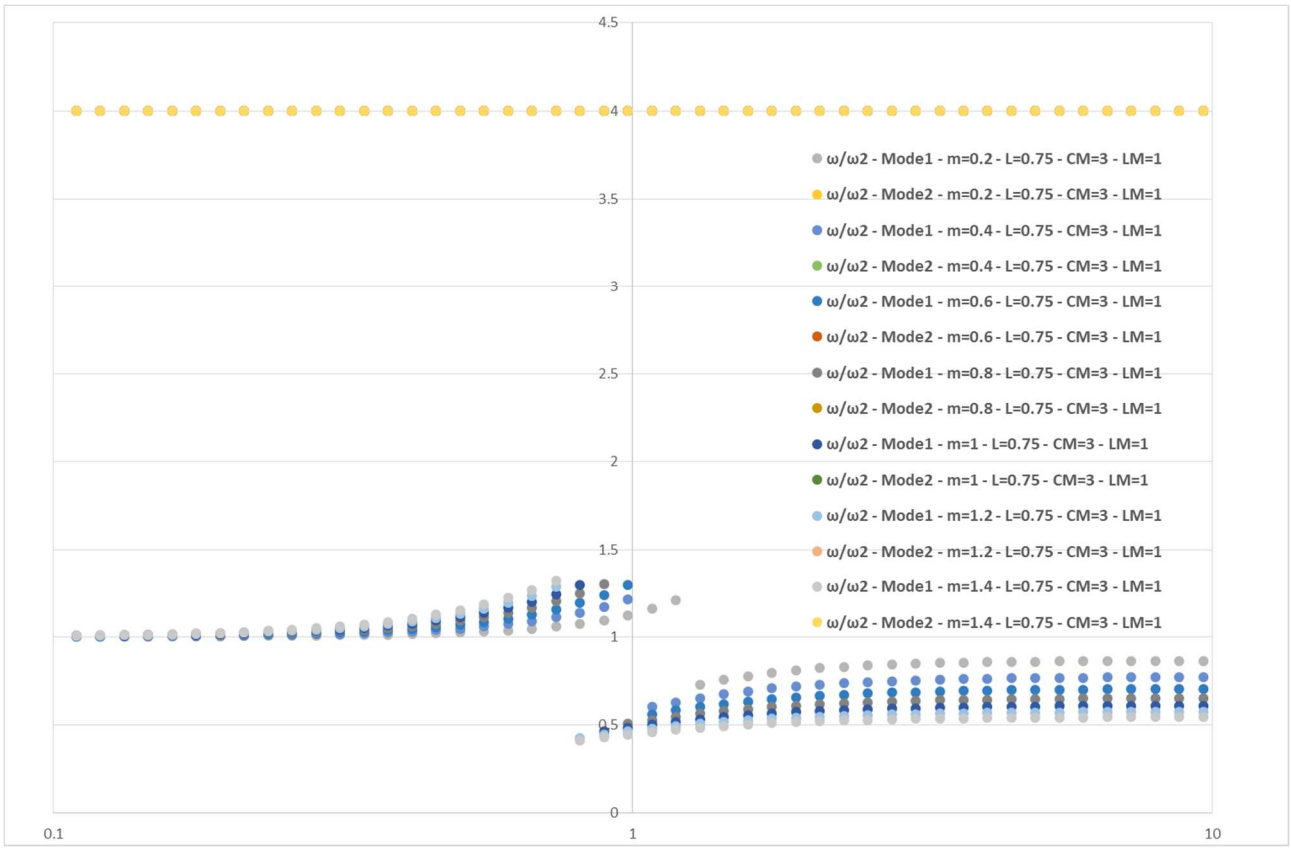

Picture 103: Circular frequencies of bridges with $\bar{L} = 0{,}75$; three trucks in the cross section; one truck in the span.

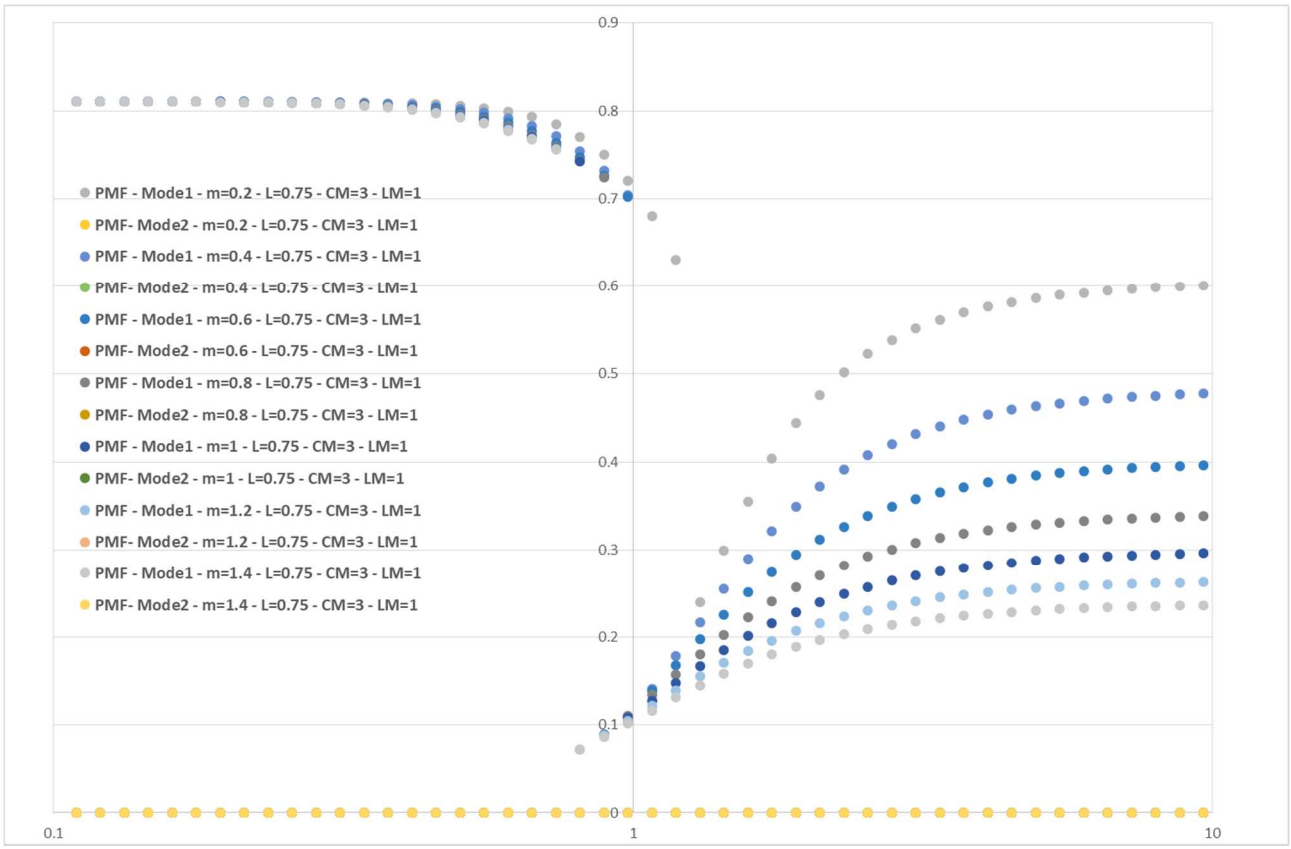

Picture 104: MPF of bridges with $\bar{L} = 0{,}75$; three trucks in the cross section; one truck in the span.

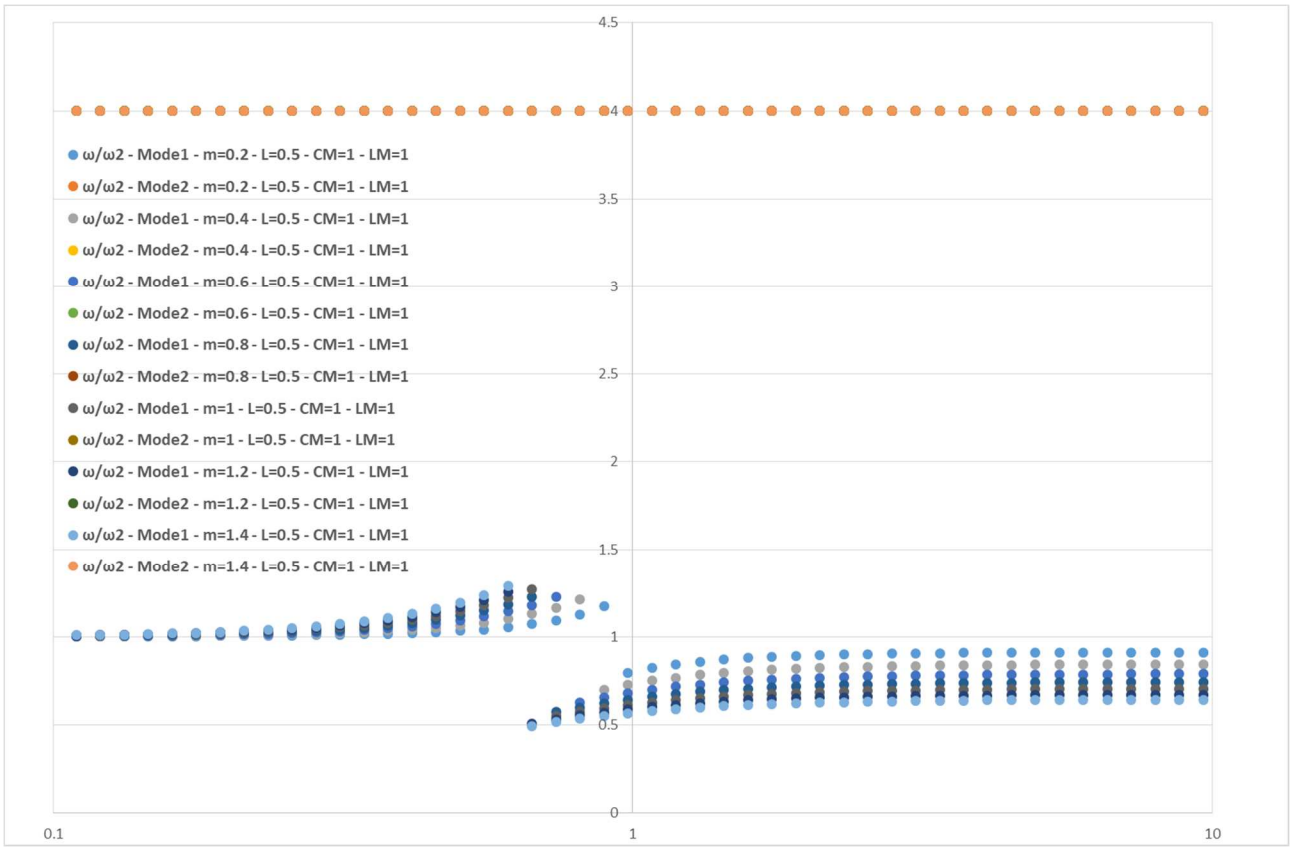

Picture 105: Circular frequencies of bridges with $\bar{L} = 0{,}50$; one truck in the cross section; one truck in the span.

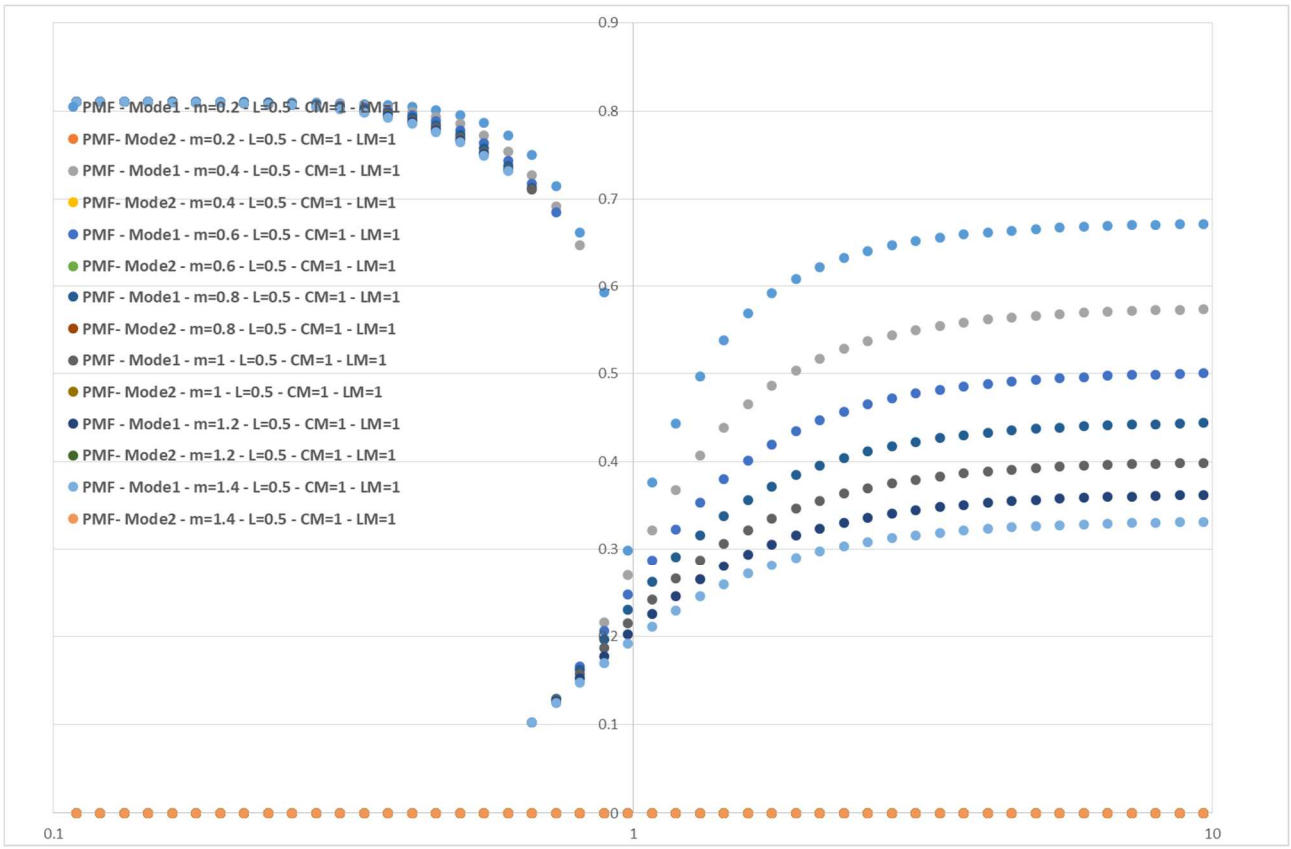

Picture 106: MPF of bridges with $\bar{L} = 0{,}50$; one truck in the cross section; one truck in the span.

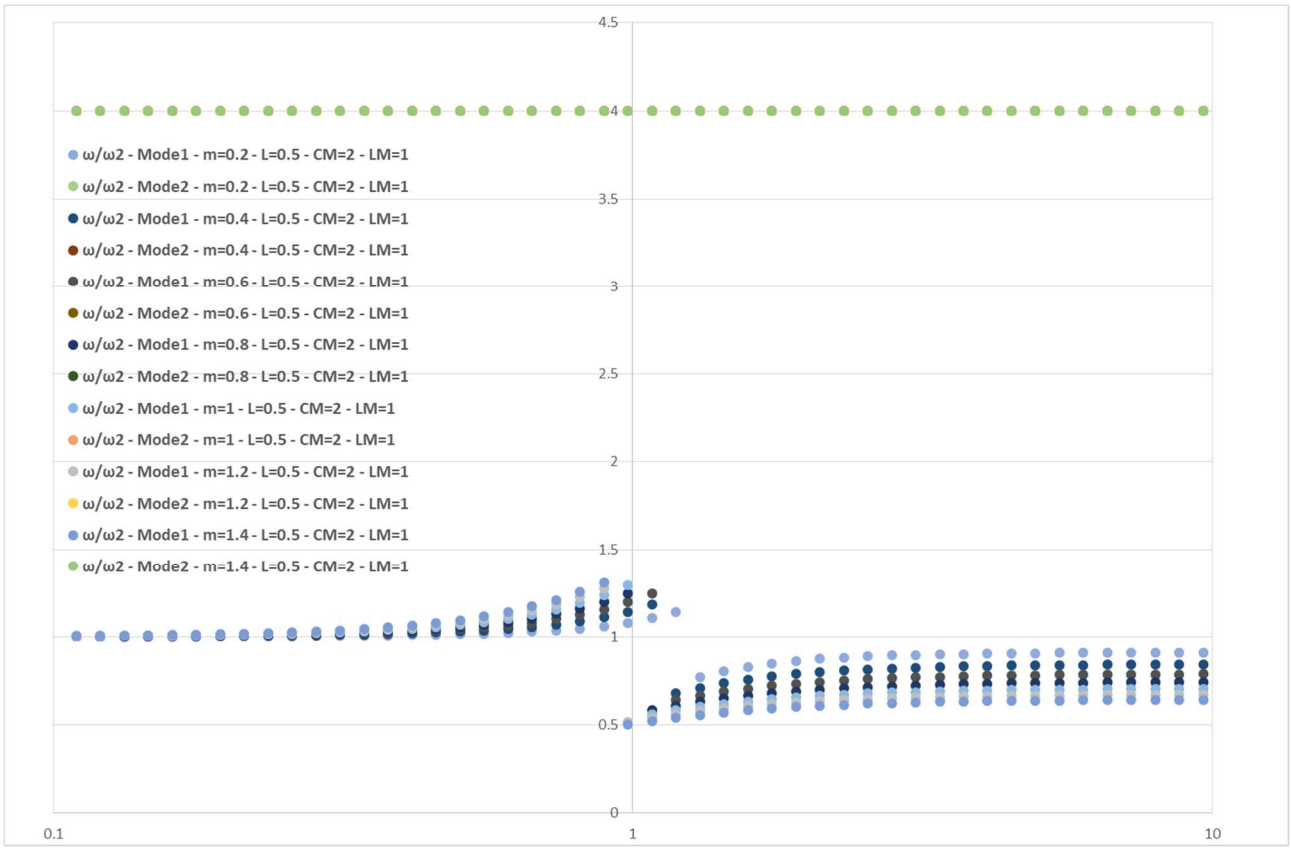

Picture 107: Circular frequencies of bridges with $\bar{L} = 0{,}50$; two trucks in the cross section; one truck in the span.

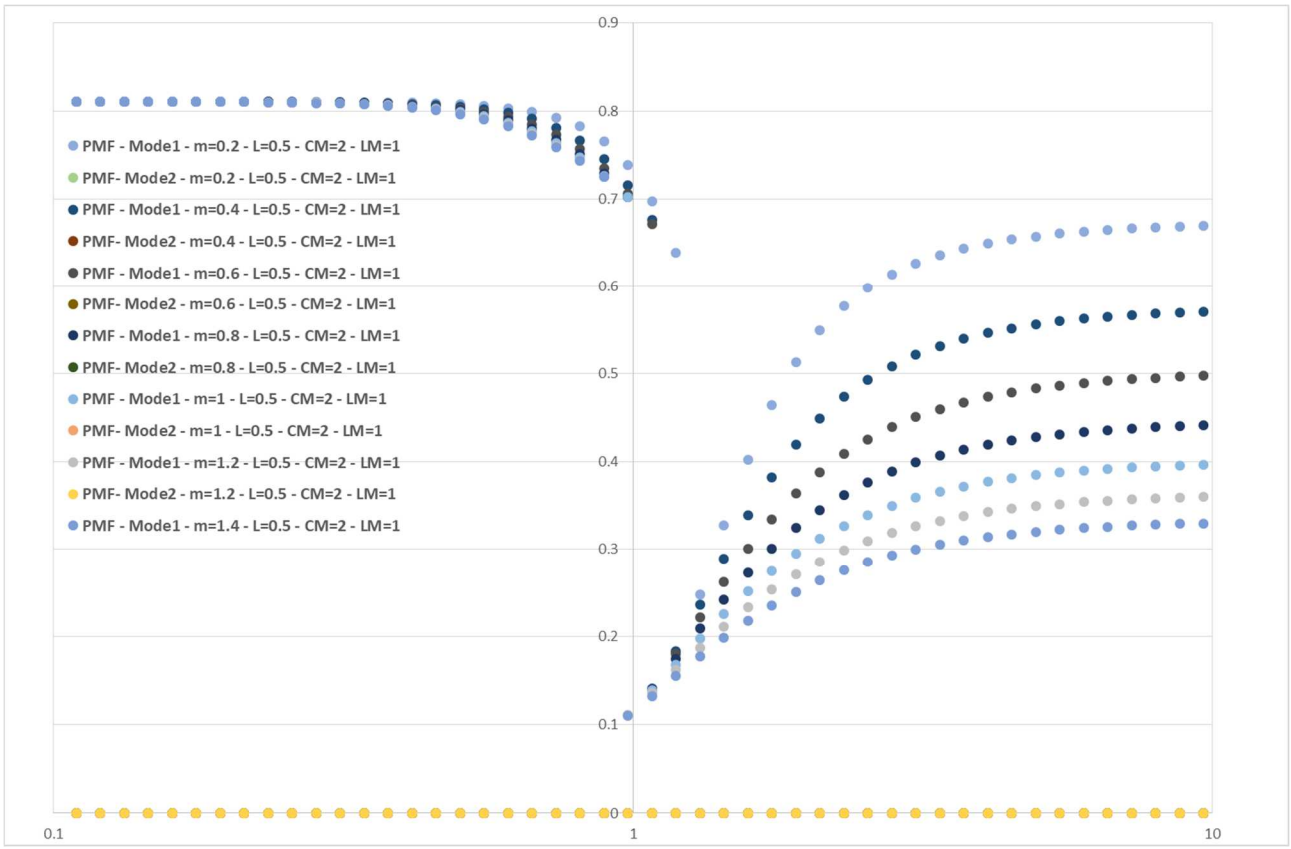

Picture 108: MPF of bridges with $\bar{L} = 0{,}50$; two trucks in the cross section; one truck in the span.

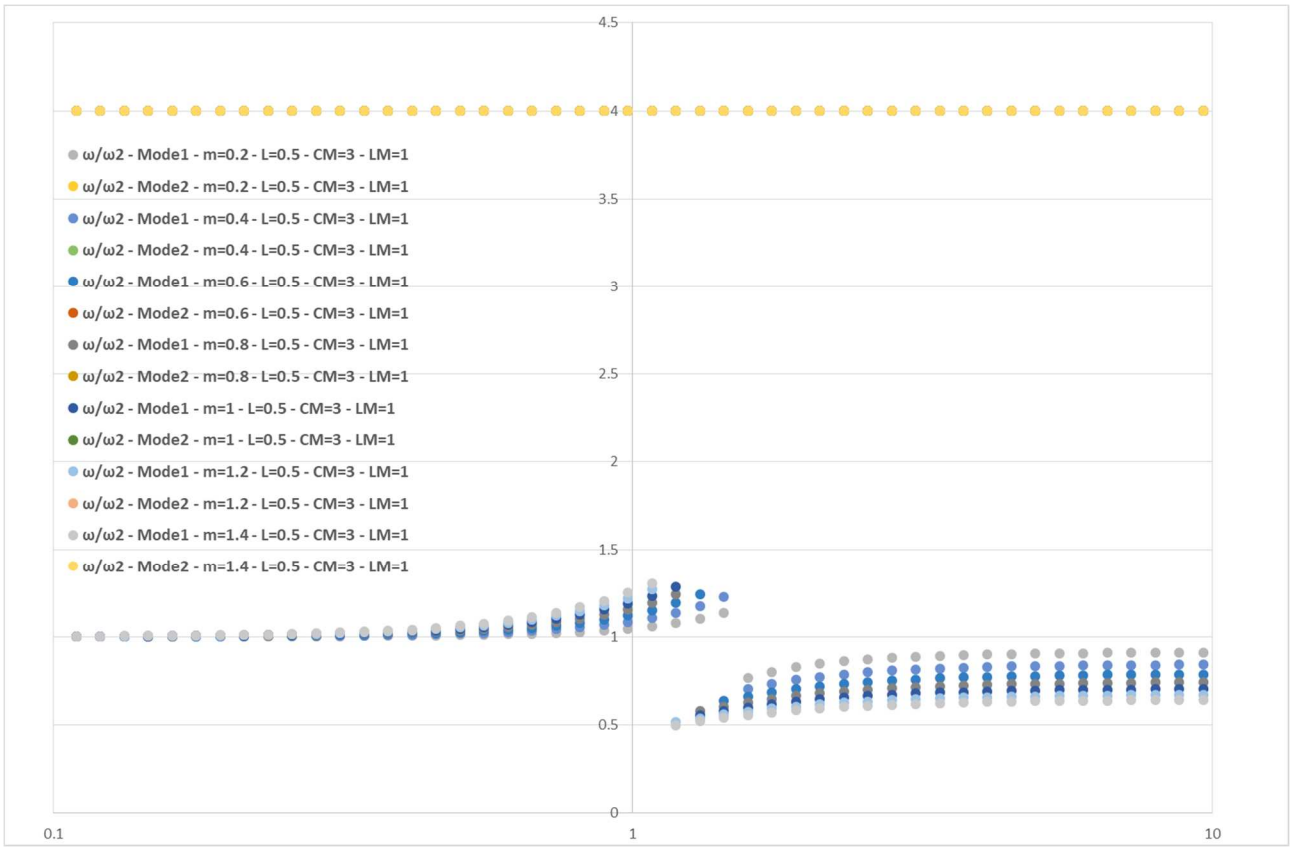

Picture 109: Circular frequencies of bridges with $\bar{L} = 0{,}50$; three trucks in the cross section; one truck in the span.

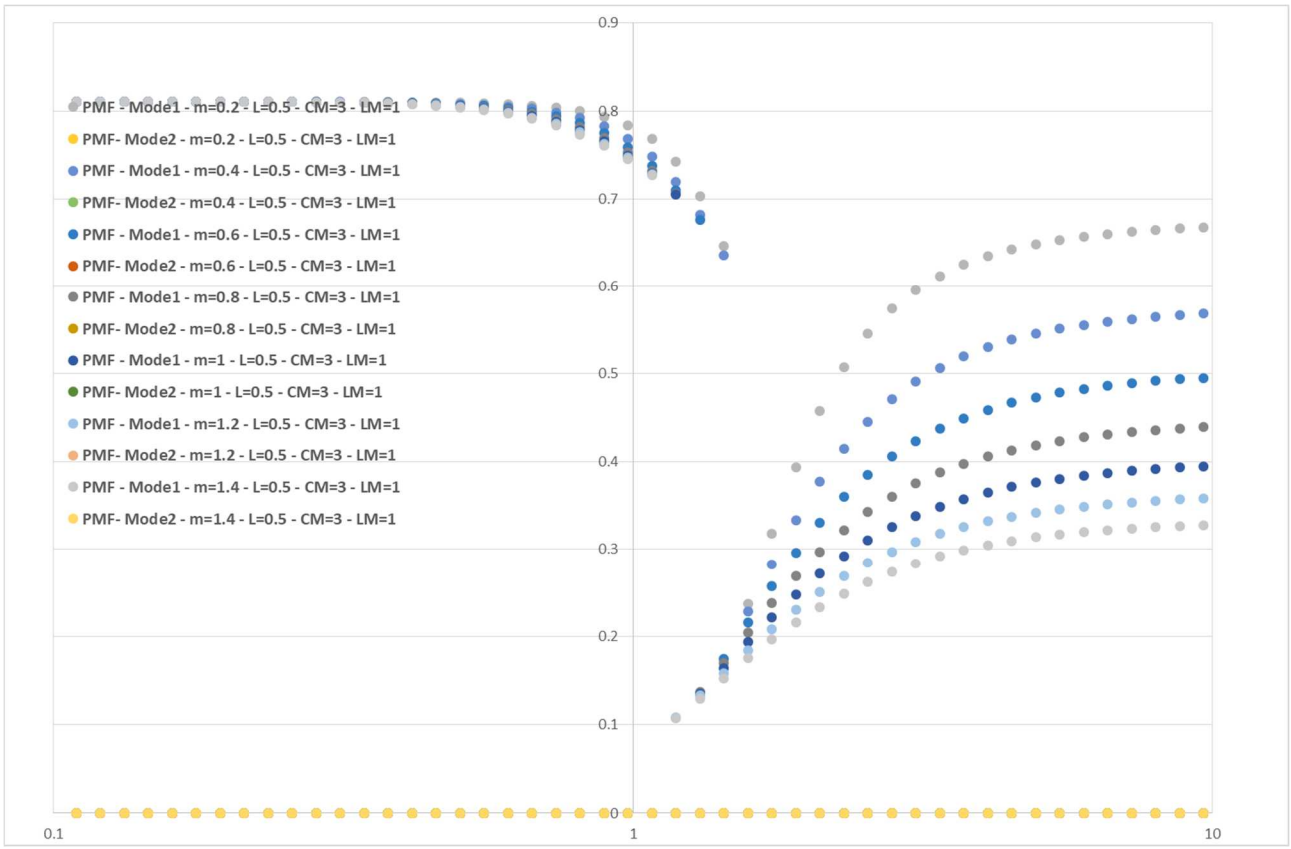

Picture 110: MPF of bridges with $\bar{L} = 0{,}50$; three trucks in the cross section; one truck in the span.

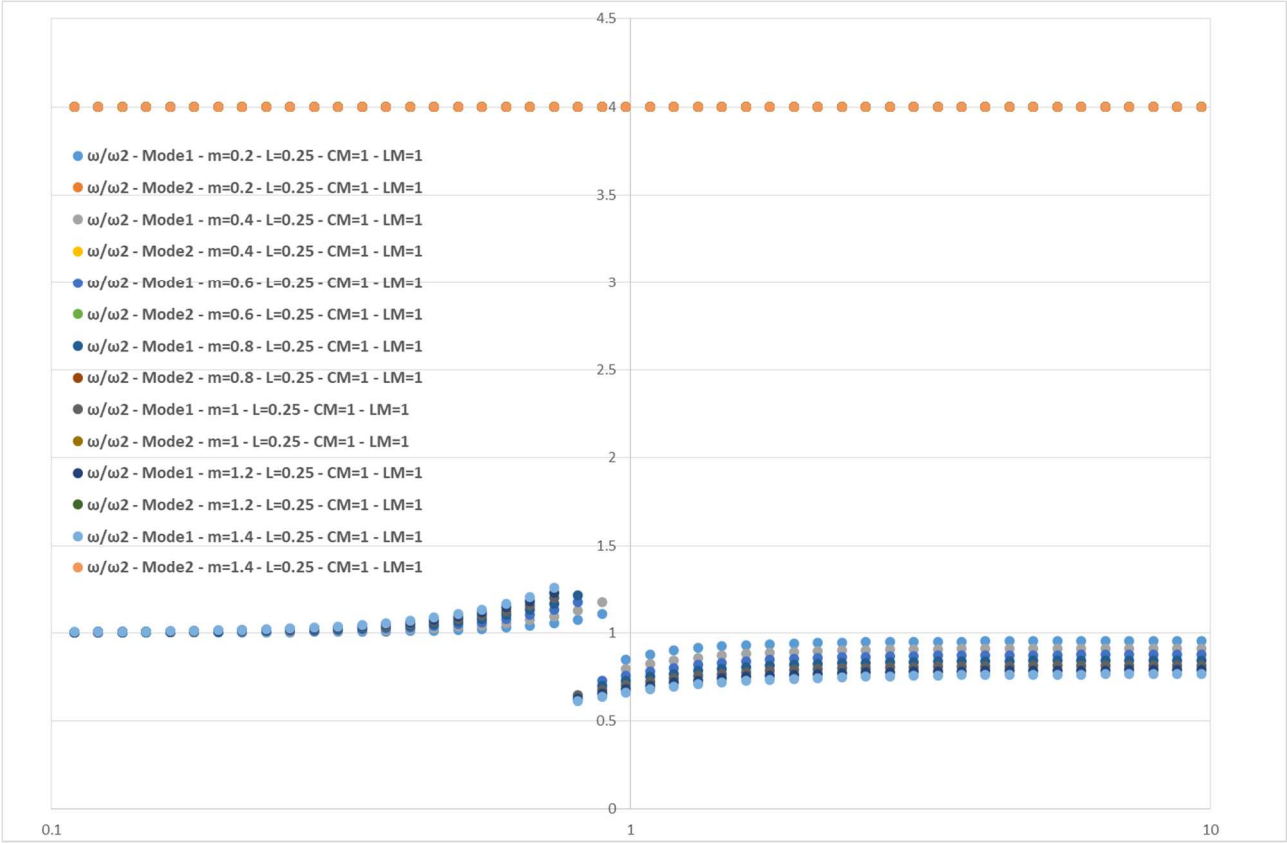

Picture 111: Circular frequencies of bridges with $\bar{L} = 0{,}25$; one truck in the cross section; one truck in the span.

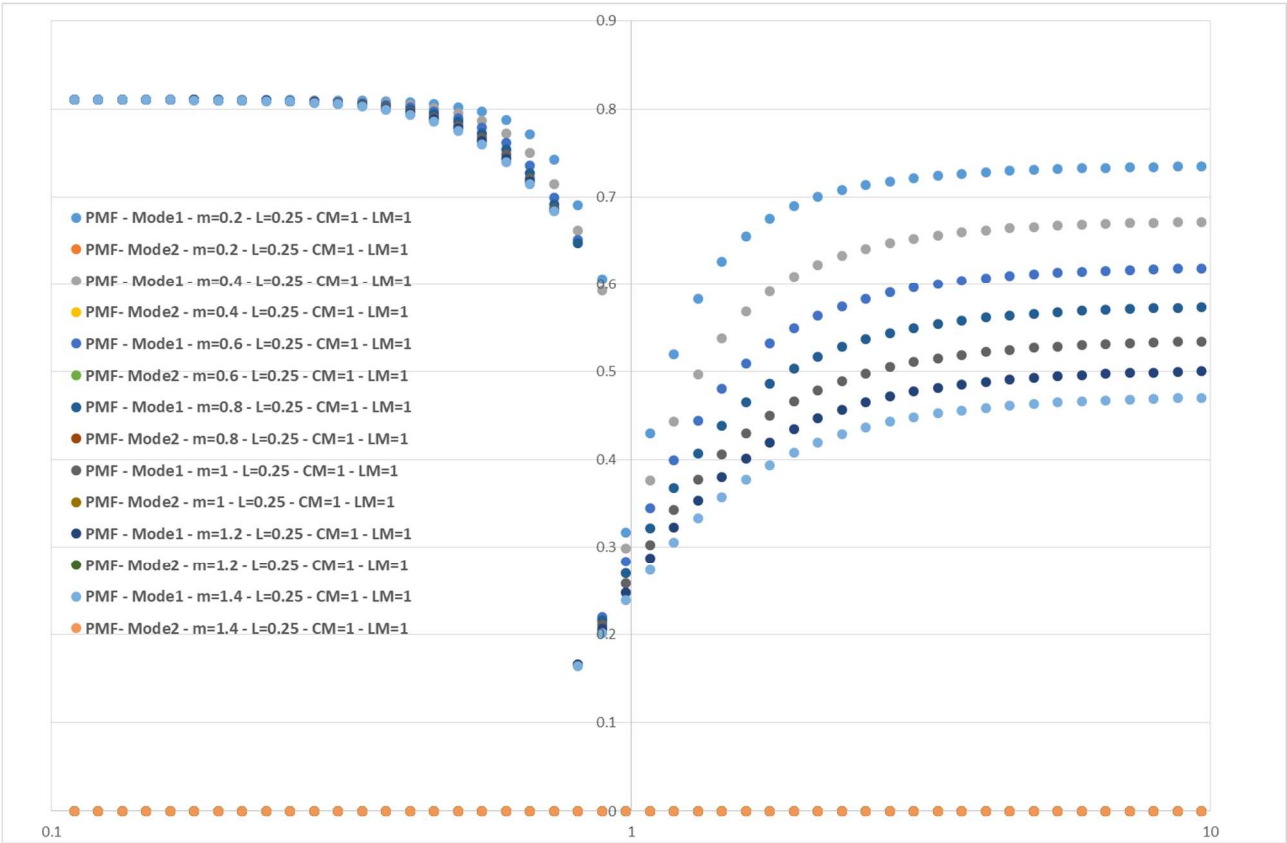

Picture 112: MPF of bridges with $\bar{L} = 0{,}25$; one truck in the cross section; one truck in the span.

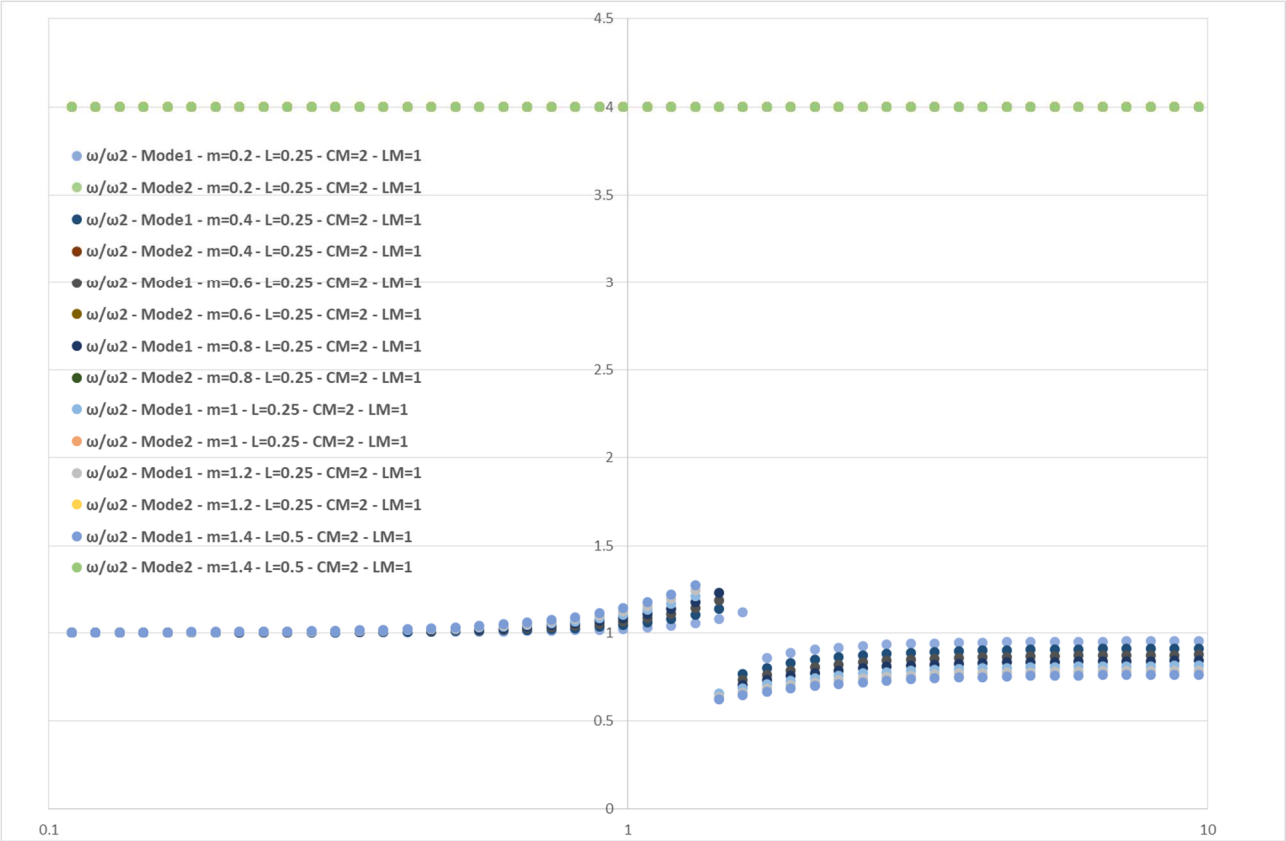

Picture 113: Circular frequencies of bridges with $\bar{L} = 0{,}25$; two trucks in the cross section; one truck in the span.

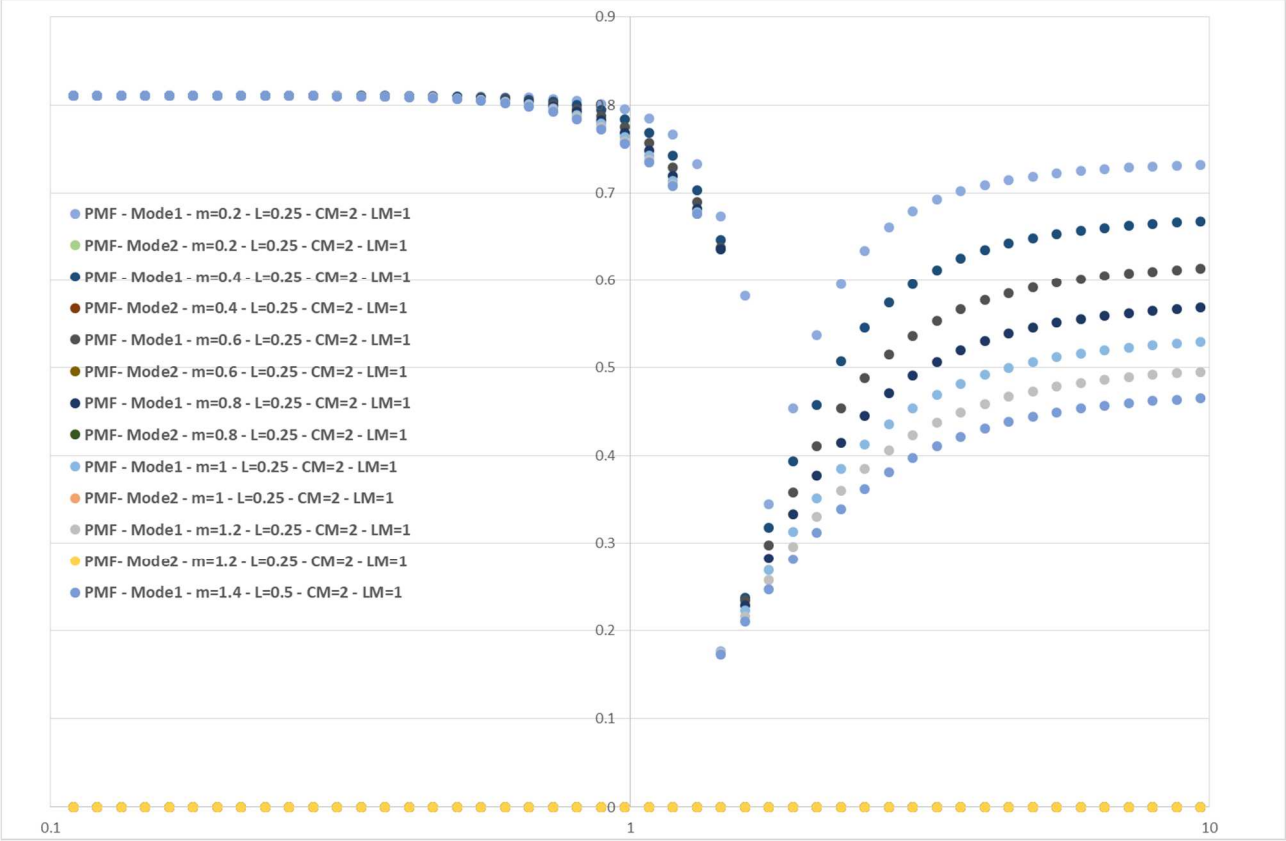

Picture 114: MPF of bridges with $\bar{L} = 0{,}25$; two trucks in the cross section; one truck in the span.

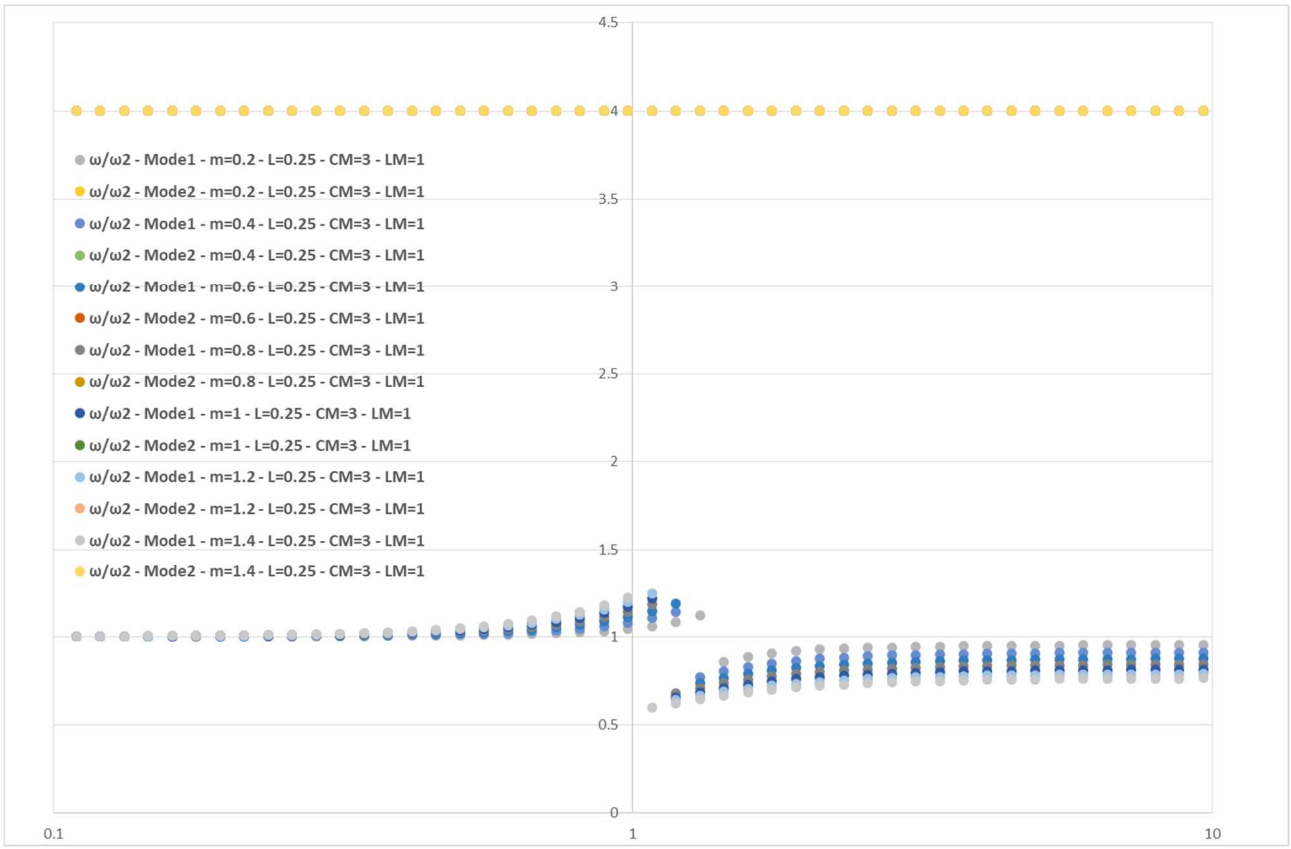

Picture 115: Circular frequencies of bridges with $\bar{L} = 0{,}25$; three trucks in the cross section; one truck in the span.

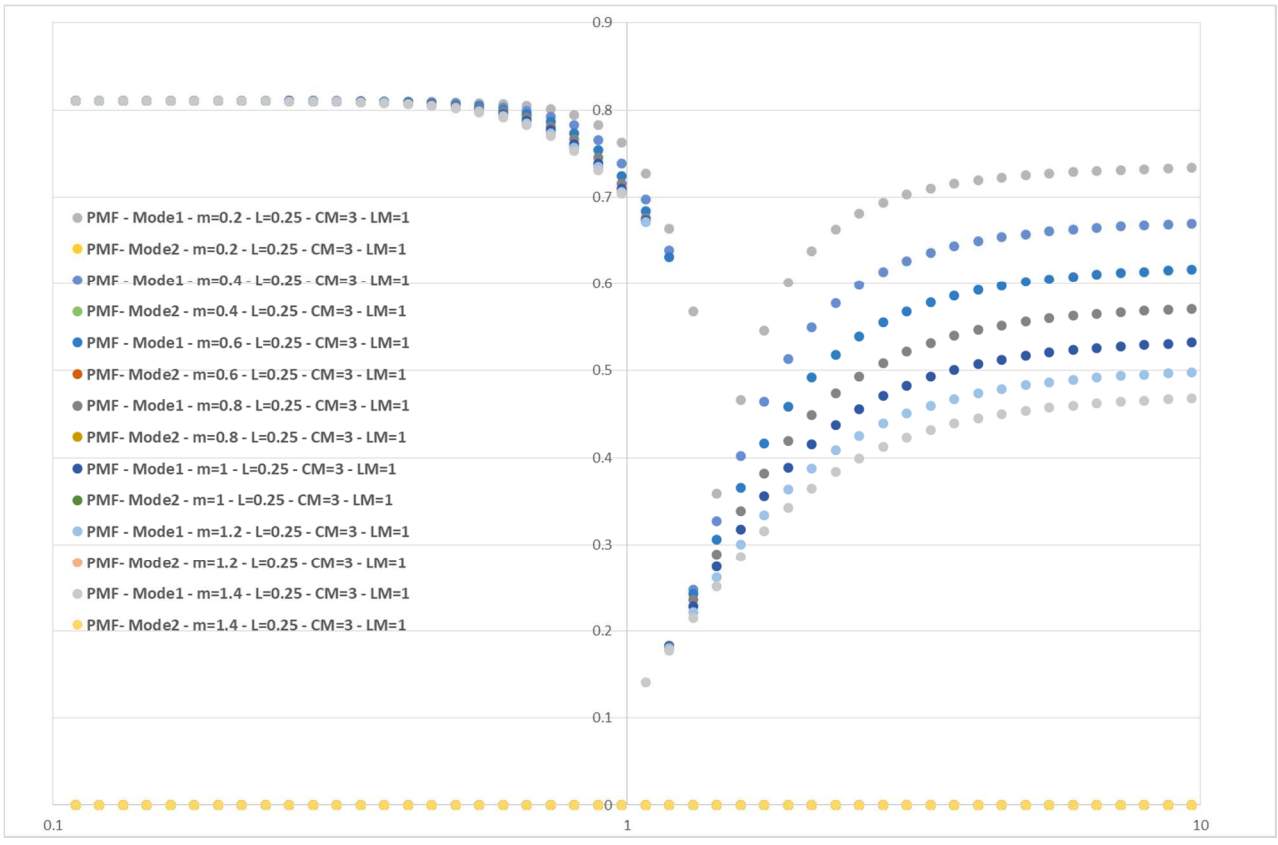

Picture 116: MPF of bridges with $\bar{L} = 0{,}25$; three trucks in the cross section; one truck in the span.